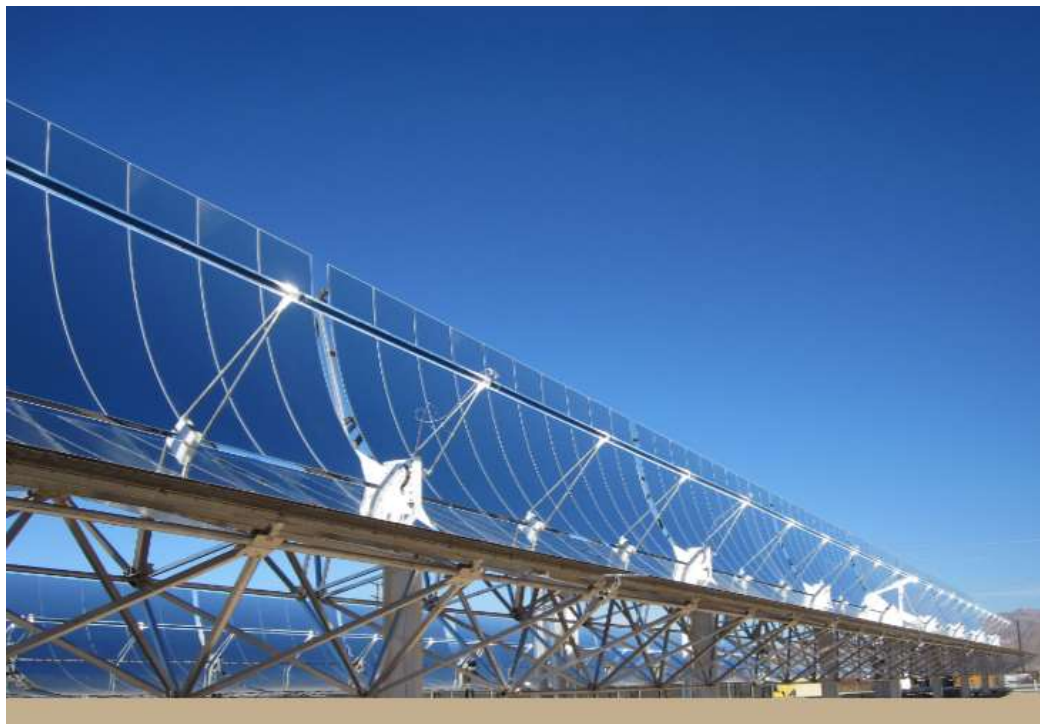


SENSITIVITY ANALYSIS OF THE EFFICIENCY OF A PARABOLIC-TROUGH SOLAR COLLECTOR



Nombre del Alumno: Eduardo Ubieta Astigarraga

Director del Trabajo Fin de Master: Jose María Pedro Sala Lizarraga

Co-director del Trabajo Fin de Master: Víctor de la Peña Aranguren

Curso académico: 2015-2016

INDEX

1. ABSTRACT	12
1. RESUMEN	13
1. LABURPENA	14
2. MEMORY	15
2.1. Objectives, scope and benefits of the project	15
2.2. Benefits of the project.....	16
2.3. State of the art	17
2.3.1. Recent history of the Parabolic-Trough solar Collectors	17
2.3.2. Theory of the Parabolic-Trough solar Collectors.....	20
2.3.2.1. Principal components of the PTCs.....	21
Foundation and metal structure	21
Parabolic shape reflector	21
Absorber tube	22
Transmission.....	23
Solar tracking system	23
Connexions between collectors	24
Heat transfer fluid	24
2.3.2.2. Collectors types.....	25
2.3.2.3. Design parameters	25
2.3.2.4. Energy losses	26
Optical losses.....	26
Geometric losses	26
2.3.3. Energy balance of a PTC	28
2.3.3.1. Thermal performance of a solar collector.....	28
2.3.3.2. Solar irradiance of a PTC	28
2.3.3.3. Optical efficiency, η_{opt}	29
2.3.3.4. Heat transport mechanisms.....	30
Radiation	30
Conduction	30
Convection.....	30
2.3.3.5. Overall loss ratio of a PTC.....	31
Overall energy balance.....	31
2.3.3.6. Efficiency factors	32
2.3.4. STAGE project.....	32
2.3.5. Introduction to the PSA.....	33

2.3.6. Experimental test of the Parabolic-trough solar Collectors.....	35
2.3.6.1 Methodology.....	36
Heat losses	37
Peak optical efficiency ($\eta_{opt, 0^\circ}$)	37
Incidence angle modifier ($K(\theta)$)	38
Overall efficiency (η)	39
2.3.7. DYMOLA	40
2.3.7.1. Modelling and simulation tools.....	40
Transient Systems Simulation Program (TRNSYS).....	40
System Advisor Model (SAM).....	40
IPSEpro	40
PCTrough	41
Matlab-Simulink	41
Renovetec solar thermal simulator.....	41
Modelica.....	41
2.3.7.2. Introduction to the program	42
2.3.7.3. Introduction to the model.....	43
Collector	44
SolarPower4Loop	55
EndIn and EndOut	55
Constant:	58
PrescribedTemperature:	58
Sensors:	59
MassFlowSource_T:.....	59
FixedBoundary:	60
System:	60
2.4. Risk analysis.....	62
3. METHODOLOGY	63
3.1. Initial problems with the model.....	63
3.2. Sensitivity analysis.....	72
3.2.1. The emittance of the glass cover.	72
3.2.2. The emittance of the absorber.	73
3.2.3. The emittance of the shield.	74
3.2.4. All cases together	74
3.3. Validation of the model.....	75
3.3.1. Heat losses test validation	79

3.3.2. Peak optical efficiency test validation.....	79
3.3.3. Dynamic efficiency test validation	80
4. CALCULATIONS	82
4.1. Sensitivity analysis.....	82
4.1.1. Reflectivity of the mirror	83
4.1.2. Transmittance of the glass cover	84
4.1.3. Infiltration of hydrogen	85
ConvConcentricCylindHydrogen	85
4.1.4. Infiltration of air	89
ConvConcentricCylindP	89
4.1.5. Degradation of the HTF.	91
4.1.6. Absorptance of the absorber tube	93
4.1.7. Emittance of the absorber tube	93
4.1.8. Emittance of the glass cover	94
4.1.9. Emittance of the shield	95
4.1.10. Interception factor	96
5. FUTURE WORKS.....	98
6. ECONOMICS	100
6.1. Internal hours.....	100
6.2. Amortizations.....	100
6.3. Costs.....	100
6.4. Budget summary	101
7. CONCLUSIONS	102
8. REFERENCES	104
9. ANNEX I: TABLES AND GRAPHS	105
Model Validation.....	105
Sensitivity analysis.....	106
Reflectivity of the mirror.....	106
Transmittance of the glass cover	116
Infiltration of hydrogen.....	126
Infiltration of air	155
Degradation of the HTF.....	160
Absorptance of the absorber tube.....	173
Emittance of the absorber tube	180
Emittance of the glass cover	198
Emittance of the shield	208

Interception factor 218

FIGURE INDEX

Figure 1. The battle of Syracuse and the invention of Archimedes 17

Figure 2. Solar collector designed by Leonardo Da Vinci 17

Figure 3. Solar concentrator made by Georges-Louis Leclerc (left) and solar furnace of Antoine Lavoisier (right)..... 17

Figure 4. "Hot box" designed by Horace de Saussure..... 18

Figure 5. Solar motor invented by Auguste Mouchout..... 18

Figure 6. PTC plant designed and build by Frank Shuman in Meadi..... 19

Figure 7. PSA Almería 19

Figure 8. Current Solar Thermal Energy market situation. 20

Figure 9. Typical absorber tube of a PTC..... 22

Figure 10. Collectors with one and two axes solar tracking..... 25

Figure 11. Dimensions of a collector..... 25

Figure 12. Acceptance and aperture angles of a solar collector..... 26

Figure 13. Shaded area when the distance between the collectors is not enough. 27

Figure 14. Losses due to incidence angle..... 27

Figure 15. Section of an absorber tube..... 31

Figure 16. Diagram of the PSA "HTF Test Loop". Source from the PSA Annual Report 2014. 35

Figure 17. Libraries from Modelica. 43

Figure 18. Complete model in Dymola..... 44

Figure 19. Complete model with the collector submodel rounded..... 44

Figure 20. SimpleRing Dymola (left) and its representation in the simulator (right). 45

Figure 21. SimpleCylinder in Dymola (top-left) and its representation in the simulator (top-right).Also the MultipleCylinder (down-left) and its representation (down-right)..... 46

Figure 22. BaseReceiverTest in Dymola (left) and its representation in the simulator (right). .. 46

Figure 23. Component of the radiation in the interior of the collector..... 47

Figure 24. Component of the convection in the interior of the collector..... 48

Figure 25. ReceiverSchottPSATest in Dymola (left) and its representation in the simulator (right)..... 49

Figure 26. radiationOnTube in Dymola (left) and its representation in the simulator (right). ... 49

Figure 27. The three NaturalConvAbsorberAmb components. 50

Figure 28. NaturalConvReceiverAmb component (left) and one of the NaturalConvectionHorizontalCylinder (right). 50

Figure 29. The six RadAbsorberAmb components..... 52

Figure 30. RadReceiverAmb component (left) and one of the BodyRadiation (right)..... 52

Figure 31. ModulePSATest in Dymola (left) and its representation in the simulator (right). 53

Figure 32. ModuleOptics in Dymola (above) and its representation in the simulator (down)... 54

Figure 33. SemiCollector in Dymola 54

Figure 34. Representation of the SemiCollector in Dymola..... 54

Figure 35. Complete model with the SolarPower4Loop submodel rounded. 55

Figure 36. Representation of the SolarPower4Loop in Dymola..... 55

Figure 37. Complete model with the EndIn and EndOut submodels rounded. 55

Figure 38. EndIn (top) and EndOut (down) in Dymola and their representation in the simulator. 56

Figure 39. Hose in Dymola (right) and its representation in the simulator (left). 57

Figure 40. SharedPipe in Dymola (right) and its representation in the simulator (left). 57

Figure 41. Location of different Constant components (left) and shape of the component (right)..... 58

Figure 42. Location of different PrescribeTemperature components (left) and shape of the component (right). 58

Figure 43. Location of different Pressure, Enthalpy and Temperature sensors components 59

Figure 44. Pressure sensor. 59

Figure 45. Enthalpy sensor. 59

Figure 46. Temperature sensor. 59

Figure 47. Location of the MassFlowSource_T component (left) and shape of the component (right)..... 60

Figure 48. Location of the FixedBoundary component (left) and shape of the component (right)..... 60

Figure 49. Location of the System component (left) and shape of the component (right)..... 61

Figure 50. Model CollectorPSAwithMeteoDataTest. 61

Figure 51. Model CollectorPSAwithMeteoDataTest with the new components marked..... 62

Figure 52. Model of the semicollector without HTF flowing through it. 63

Figure 53. Submodels of SemiCollectorNoFluid (above) and the ModulePSATestNoFluid (below). 64

Figure 54. Model of the semicollector without endIn and endOut. 65

Figure 55. Results of the simulation of the model without HTF. 65

Figure 56. Real Shape of the collector, with the considered parts numbered. 66

Figure 57. Scheme of the Cross String Method..... 67

Figure 58. Results of the simulation of the model with new from factors. Total losses (left) and HTF’s outlet temperature (right)..... 69

Figure 59. Model of the semicollector without heat transfer through radiation to the mirror. 70

Figure 60. Submodel ModulePSATestNoMirror..... 70

Figure 61. Results of the simulation of the model without considering the radiation with the mirror. Total Losses (left) and HTF’s outlet temperature (right). 71

Figure 62. Model of the semicollector without neither HTF flowing through it, nor heat transfer through radiation to the mirror. 71

Figure 63. Results of the simulation of the model without considering neither the fluid, nor the radiation with the mirror. 72

Figure 64. Results of simulating the heat losses test for different values of the glass cover’s emittance. 73

Figure 65. Results of simulating the heat losses test for different values of the absorber’s emittance. 73

Figure 66. Results of simulating the heat losses test for different values of the shield’s emittance. 74

Figure 67. Summary of the results of the 3 cases. 75

Figure 68. Real heat losses depending on the temperature difference between the HTF medium T and the ambient T..... 76

Figure 69. Real emittance and its fitting curve 78

Figure 70. Results for the efficiency when the reflectivity varies from 0,1 to 1. 83

Figure 71. Results of the efficiency (real value and percentage) when the reflectivity varies from 0,83 to 0,93..... 84

Figure 72. Results of the efficiency when the transmittance of the collector varies from 0,8 to 1..... 85

Figure 73. Component of the convection in the interior of the collector when there is hydrogen.	85
Figure 74. Results of the efficiency when there is hydrogen infiltration.	88
Figure 75. Results of the heat losses when there is hydrogen infiltration.	89
Figure 76. Component of the convection in the interior of the collector when there is air inside.	89
Figure 77. Results for the efficiency when there is air infiltration.	91
Figure 78. Results of the heat losses when there is air infiltration.	91
Figure 79. Results of the tests carried out to analyze the degradation of the Heat Transfer Fluid.	92
Figure 80. Results of the efficiency when the absorptance of the absorber varies from 0,8 to 1.	93
Figure 81. Results of the heat losses when the emittance of the receiver varies.	94
Figure 82. Results of the efficiency test when the interception factor varies.	96

TABLES INDEX

Table 1. Comparison of the different simulation tools.	42
Table 2. Results of the simulation of the model without HTF.	65
Table 3. Results of the simulation of the model with the new Form Factors.	69
Table 4. Results of the simulation of the model without considering the radiation with the mirror.	70
Table 5. Results of the simulation of the model without considering neither the fluid, nor the radiation with the mirror.	71
Table 6. Results of simulating the heat losses test for different values of the glass cover's emittance.	72
Table 7. Results of simulating the heat losses test for different values of the absorber's emittance.	73
Table 8. Results of simulating the heat losses test for different values of the shield's emittance.	74
Table 9. Summary of the results of the 3 cases.	74
Table 10. Real heat losses	76
Table 11. Summary of model heat losses depending on the emittance and the HTF medium T.	77
Table 12. Interpolated emittance values.	77
Table 13. Fit equation of the emittance and the error committed.	78
Table 14. Heat losses test results.	79
Table 15. Peak optical efficiency test data.	79
Table 16. Peak optical efficiency test results.	79
Table 17. Dynamic efficiency test data.	80
Table 18. Dynamic efficiency data for introducing in the model.	80
Table 19. Dynamic efficiency test results.	81
Table 20. Data for the dynamic efficiency test.	82
Table 21. Data for the Heat losses test.	83
Table 22. Form factors of the glass cover for different values of its emittance.	95
Table 23. Form factors of the shield for different values of its emittance.	95
Table 24. Summary of the internal hours.	100

Table 25. Summary of the amortization.	100
Table 26. Summary of the costs.	100
Table 27. Budget summary.	101

INDEX OF THE TABLES IN THE ANNEX I

Table A 1. Model heat losses depending on the emittance and the HTF medium T.	105
Table A 2. Data for the dynamic efficiency test.	106
Table A 3. Data for the Heat losses test.	106
Table A 4. Results for the dynamic efficiency test when the reflectivity of the collector varies from 0,1 to 1.	106
Table A 5. Results from the dynamic efficiency test expressed in percentages when the reflectivity of the collector varies from 0,1 to 1.	109
Table A 6. Results for the dynamic efficiency test when the reflectivity of the collector varies from 0,84 to 0,93.	111
Table A 7. Results from the dynamic efficiency test expressed in percentages for different values of the reflectivity.	114
Table A 8. Results for the dynamic efficiency test when the transmittance of the glass cover varies from 0,1 to 1.	116
Table A 9. Results from the dynamic efficiency test expressed in percentages for different values of the transmittance of the glass cover from 0,1 to 1.	119
Table A 10. Results for the dynamic efficiency test when the transmittance of the collector varies from 0,8 to 1.	121
Table A 11. Results from the dynamic efficiency test expressed in percentages for different values of the transmittance of the glass cover from 0,8 to 1.	124
Table A 12. Results for the dynamic efficiency test when there is infiltration of hydrogen, and its pressure varies from 0,01 Pa to 5065 Pa.	126
Table A 13. Results from the dynamic efficiency test expressed in percentages when there is infiltration of hydrogen, and its pressure varies from 0,01 Pa to 5065 Pa.	129
Table A 14. Results for the dynamic efficiency test when there is infiltration of hydrogen, and its pressure varies from 0,00001 Pa to 8 Pa.	131
Table A 15. Results from the dynamic efficiency test expressed in percentages for different values of hydrogen's pressure from 0,0001 Pa to 8 Pa.	134
Table A 16. Results from the heat losses test at 40°C for different values of hydrogen's pressure.	137
Table A 17. Results from the heat losses test at 90°C for different values of hydrogen's pressure.	140
Table A 18. Results from the heat losses test at 140°C for different values of hydrogen's pressure.	142
Table A 19. Results from the heat losses test at 40°C expressed in percentages for different values of hydrogen's pressure.	146
Table A 20. Results from the heat losses test at 90°C expressed in percentages for different values of hydrogen's pressure.	149
Table A 21. Results from the heat losses test at 140°C expressed in percentages for different values of hydrogen's pressure.	151
Table A 22. Results of the dynamic efficiency test when air enters the gap between the glass cover and the absorber.	155

Table A 23. Results from the dynamic efficiency test when air enters the space between the glass cover and the metal tube expressed in percentages.	158
Table A 24. Results from the heat losses test when air enters the space between the glass cover and the metal tube.	158
Table A 25. Results from the heat losses test when air enters the space between the glass cover and the metal tube.	160
Table A 26. Results for the dynamic efficiency test when there is degradation of the HTF.	160
Table A 27. Results from the dynamic efficiency test expressed in percentages when the HTF degrades.	163
Table A 28. Results from the heat losses test at 40°C when HTF degrades.	165
Table A 29. Results from the heat losses test at 90°C when HTF degrades.	167
Table A 30. Results from the heat losses test at 140°C when HTF degrades.	169
Table A 31. Results for the dynamic efficiency test for different values of the absorptance of the metal tube from 0,1 to 1.	173
Table A 32. Results for the dynamic efficiency test for different values of the absorptance of the metal tube from 0,8 to 1.	175
Table A 33. Results from the dynamic efficiency test expressed in percentages when the absorptance of the receive varies from 0,8 to 1.	178
Table A 34. Results for the dynamic efficiency test for different values of the emittance of the metal tube.	180
Table A 35. Results from the heat losses test at 40°C for different values of absorber's emittance.	183
Table A 36. Results from the heat losses test at 90°C for different values of absorber's emittance.	185
Table A 37. Results from the heat losses test at 140°C for different values of absorber's emittance.	187
Table A 38. Results from the heat losses test at 40°C expressed in percentages for different absorber's emittance.	190
Table A 39. Results from the heat losses test at 90°C expressed in percentages for different absorber's emittance.	192
Table A 40. Results from the heat losses test at 140°C expressed in percentages for different absorber's emittance.	194
Table A 41. Results for the dynamic efficiency test for different values of the emittance of the glass cover.	198
Table A 42. Results from the heat losses test at 40°C for different values of glass cover's emittance.	200
Table A 43. Results from the heat losses test at 90°C for different values of glass cover's emittance.	202
Table A 44. Results from the heat losses test at 140°C for different values of glass cover's emittance.	204
Table A 45. Results for the dynamic efficiency test for different values of the emittance of the shield.	208
Table A 46. Results from the heat losses test at 40°C for different values of shield's emittance.	210
Table A 47. Results from the heat losses test at 90°C for different values of shield's emittance.	212
Table A 48. Results from the heat losses test at 140°C for different values of shield's emittance.	214

Table A 49. Results for the dynamic efficiency test when the interception factor of the collector varies from 0 to 1. 218

Table A 50. Results for the dynamic efficiency test when the interception factor of the collector varies from 0,8 to 1. 220

Table A 51. Results from the dynamic efficiency test expressed in percentages when the interception factor of the collector varies from 0,8 to 1. 223

INDEX OF THE FIGURES IN THE ANNEX I

Figure-A 1. Graphs of the results for the dynamic efficiency test when the reflectivity of the collector varies from 0,1 to 1. 108

Figure-A 2. Graphs of the results from the dynamic efficiency test expressed in percentages when the reflectivity of the collector varies from 0,1 to 1. 111

Figure-A 3. Graphs of the results for the dynamic efficiency test when the reflectivity of the collector varies from 0,84 to 0,93. 113

Figure-A 4. Graphs of the results for the dynamic efficiency test expressed in percentages for different values of the reflectivity from 0,84 to 0,93..... 116

Figure-A 5. Graphs of the results for the dynamic efficiency test when the transmittance of the glass cover varies from 0,1 to 1..... 118

Figure-A 6. Graphs of the results for the dynamic efficiency test expressed in percentages for different values of the transmittance from 0,84 to 0,93. 121

Figure-A 7. Graphs of the results for the dynamic efficiency test when the transmittance of the glass cover varies from 0,8 to 1..... 123

Figure-A 8. Graphs of the results for the dynamic efficiency test expressed in percentages for different values of the transmittance of the glass cover from 0,8 to 1. 126

Figure-A 9. Graphs of the results for the dynamic efficiency test when there is infiltration of hydrogen, and its pressure varies from 0,01 Pa to 5065 Pa. 128

Figure-A 10. Graphs of the results for the dynamic efficiency test expressed in percentages when there is infiltration of hydrogen, and its pressure varies from 0,01 Pa to 5065 Pa. 131

Figure-A 11. Graphs of the results for the dynamic efficiency test when there is infiltration of hydrogen, and its pressure varies from 0,0001 Pa to 8 Pa. 134

Figure-A 12. Graphs of the results for the dynamic efficiency test expressed in percentages for different values of the hydrogen’s pressure..... 137

Figure-A 13. Graphs of the results for the heat losses test at 40°C for different values of hydrogen’s pressure..... 139

Figure-A 14. Graphs of the results for the heat losses test at 90°C for different values of hydrogen’s pressure..... 142

Figure-A 15. Graphs of the results for the heat losses test at 140°C for different values of hydrogen’s pressure..... 144

Figure-A 16. Graphs of the results for the heat losses test for the three cases for different values of hydrogen’s pressure. 146

Figure-A 17. Graphs of the results for the heat losses test at 40°C expressed in percentages for different values of hydrogen’s pressure. 148

Figure-A 18. Graphs of the results for the heat losses test at 90°C expressed in percentages for different values of hydrogen’s pressure. 151

Figure-A 19. Graphs of the results for the heat losses test at 140°C expressed in percentages for different values of hydrogen’s pressure. 153

Figure-A 20. Graphs of the results for the heat losses test for the three cases expressed in percentages for different values of hydrogen’s pressure..... 155

Figure-A 21. Graphs of the results of the dynamic efficiency test when air enters the space between the glass cover and the metal tube..... 157

Figure-A 22. Graphs of the results of the heat losses test when air enters the space between the glass cover and the metal tube..... 159

Figure-A 23. Graphs of the results for the dynamic efficiency test when there is degradation of the HTF. 162

Figure-A 24. Graphs of the results for the dynamic efficiency test expressed in percentages when the HTF degrades. 165

Figure-A 25. Graphs of the results for the heat losses test at 40°C when the HTF degrades. . 167

Figure-A 26. Graphs of the results for the heat losses test at 90°C when the HTF degrades. . 169

Figure-A 27. Graphs of the results for the heat losses test at 140°C when the HTF degrades. 171

Figure-A 28. Graphs of the results for the heat losses when the HTF degrades. 172

Figure-A 29. Graphs of the results for the dynamic efficiency test when the absorptance of the receive varies from 0,1 to 1..... 175

Figure-A 30. Graphs of the results for the dynamic efficiency test when the absorptance of the receive varies from 0,8 to 1..... 177

Figure-A 31. Graphs of the results for the dynamic efficiency test expressed in percentages when absorptance of the absorber varies from 0,8 to 1. 180

Figure-A 32. Graphs of the results for the dynamic efficiency test when the emittance of the absorber varies..... 182

Figure-A 33. Graphs of the results for the heat losses test at 40°C for different values of absorber’s emittance. 184

Figure-A 34. Graphs of the results for the heat losses test at 90°C for different values of absorber’s emittance. 186

Figure-A 35. Graphs of the results for the heat losses test at 140°C for different values of absorber’s emittance. 188

Figure-A 36. Graphs of the results for the heat losses test for different values of absorber’s emittance. 190

Figure-A 37. Graphs of the results for the heat losses test at 40°C expressed in percentages for different absorber’s emittance. 192

Figure-A 38. Graphs of the results for the heat losses test at 90°C expressed in percentages for different absorber’s emittance. 194

Figure-A 39. Graphs of the results for the heat losses test at 140°C expressed in percentages for different absorber’s emittance. 196

Figure-A 40. Graphs of the results for the heat losses test expressed in percentages for different absorber’s emittance. 197

Figure-A 41. Graphs of the results for the dynamic efficiency test when the emittance of the glass cover varies..... 200

Figure-A 42. Graphs of the results for the heat losses test at 40°C for different values of glass cover’s emittance..... 202

Figure-A 43. Graphs of the results for the heat losses test at 90°C for different values of glass cover’s emittance..... 204

Figure-A 44. Graphs of the results for the heat losses test at 140°C for different values of glass cover’s emittance..... 206

Figure-A 45. Graphs of the results for the heat losses for different values of glass cover’s emittance. 207

Figure-A 46. Graphs of the results for the dynamic efficiency test when the emittance of the shield varies..... 210

Figure-A 47. Graphs of the results for the heat losses test at 40°C for different values of shield’s emittance. 212

Figure-A 48. Graphs of the results for the heat losses test at 90°C for different values of shield’s emittance. 214

Figure-A 49. Graphs of the results for the heat losses test at 140°C for different values of shield’s emittance. 216

Figure-A 50. Graphs of the results for the heat losses test for different values of shield’s emittance. 217

Figure-A 51. Graphs of the results for the dynamic efficiency test when the interception factor of the collector varies from 0 to 1..... 220

Figure-A 52. Graphs of the results for the dynamic efficiency test when the interception factor of the collector varies from 0,8 to 1..... 222

Figure-A 53. Graphs of the results for the dynamic efficiency test expressed in percentages when the interception factor of the collector varies from 0,8 to 1. 225

1. ABSTRACT

The text presented below analyses the variation of the performance of a parabolic trough solar collector, when some of the parameters that govern its operation vary due to dirty mirror, degradation etc.

In order to reach that point, it will be seen how the human has made use of solar energy with different purposes, through history until it has been reached the point where solar technology has the widespread use and in such a variety of technologies as it has today. As in this project, the technology analysed is the solar collectors, it is going to make more emphasis on solar thermal technology.

They will be explained in detail how the parabolic trough collectors are, analysing from its different components, to its thermal performance. Once acquainted with this technology, it will be seen which tests will be carried out.

Finally it is going to be explained how the model, used for the simulation and implementation of the relevant tests, has been developed. It will also be explained how the model has been validated, for once validated, proceed to the sensitivity analysis of the collectors.

1. RESUMEN

El texto presentado a continuación analiza la variación del rendimiento de los colectores solares cilindro-parabólicos, cuando alguno de los parámetros que rigen su funcionamiento varía debido a la suciedad, degradación etc.

Para llegar a ese punto, primero se verá como a lo largo de la historia el ser humano ha hecho uso de la energía solar con diferentes fines, hasta que tener el uso tan extendido y en tanta variedad de tecnologías como la que se tiene hoy en día. Se hará gran hincapié en la energía solar térmica, por ser la más relacionada con este trabajo.

Se explicaran de forma detallada como son los colectores cilindro-parabólicos, analizando desde sus diferentes componentes, hasta su funcionamiento térmico. Una vez familiarizados con esta tecnología, se verá cuáles son los ensayos que se realizan de cara a analizar su funcionamiento.

Por último se explicara cómo se ha desarrollado el modelo que se utiliza para la simulación y realización de los ensayos pertinentes. También se explicará cómo se ha validado el modelo, para una vez validado, proceder al análisis de sensibilidad de los colectores.

1. LABURPENA

Ondoren aurkeztutako testua, zilindro-paraboliko forma duen eguzki kolektoreak aztertzen ditu, bere funtzionamendua arautzen duten parametroak batzuk aldatu egiten direnean, ala nola, ispiluetan zikinkeria agertzeak, degradazioa etc.

Puntu horretara heltzeko, lehenengo historian zehar, gizakiak eguzki teknologiarri eman dion erabilera ezberdinak ikusiko dira. Análisi hau ezagutzen diren lehenengo eguzki erabileretatik, gaur egun existitzen diren horrenbeste teknologia arte doa.

Zehatz-mehatz azalduko dira, nolakoak dira kolektore zilindro-parabolikoak, osatzen duten osagai ezberdinetatik, bere eragiketa termiko arte ikusiko da. Teknologia hau ezagutzean, hauen errendimendua aztertzeke egiten diren probak ikusiko dira.

Azkenik, simulaziorako eta probak garatzeko eraikitako modeloa azalduko da. Ondoren, modeloa nola baieztatu egin den azalduko da, sentzibilitate analisiarekin jarraitzeko.

2. MEMORY

2.1. Objectives, scope and benefits of the project

The purpose of this project is to understand how parabolic-trough solar collectors (PTCs) work. In order to archive this objective, this text may introduce some important aspects of the PTCs, such as their components, their energy balance, which and why the most important losses that they have are, etc.

Once acquainted with the collectors, they are going to be explained the different experimental tests that the Plataforma Solar de Almería does in order to measure some important parameters that will be necessary to quantify the collector's behaviour.

A simulation tool, called *Dymola*, will be used to represent the collector's behaviour and see what happens in different situations. So first it is going to be explained what *Dymola* is and how it works. In order to get an idea of how this simulator approximates to the reality, the results obtained from the simulation are going to be compared to those obtained in the tests made in the reality.

The main objective of this project is to analyse how different parameters affect to the behaviour of the efficiency of this collectors with the help of this simulator. So once validated the model with the real results from the mentioned tests, it will be seen the influence of some parameters in the collector's behaviour.

2.2. Benefits of the project

The use of Thermal Solar technologies is increasing every day. This project will introduce and help to deeply comprehend a kind of technology which belongs to this group, the Parabolic Trough solar Collectors (PTS from now on).

During PTC's operation in plants the efficiency of these can decrease for multiple reasons. In this project they are going to be studied the influence of different parameters of the collectors. With the obtained results it will be seen how each affect, so when in the reality a change in the collector's behaviour happens can be easily recognised which parameters could be the responsible for this change. This will help to easily recognise and correct problems a PTC could have.

In order to archive the results mentioned in the previous paragraph a model which imitates the behaviour of the collectors is used. The use of these kinds of models will also be usable during the planning and design of new solar plants. These models will help to get an idea of how the plant should be, or which are going to be the expected results during its operation once build.

2.3. State of the art

2.3.1. Recent history of the Parabolic-Trough solar Collectors

The idea of using the solar energy for human's benefits comes from ancient times. At the beginning, around the seventh century B.C., the sun heat was concentrated with glass and mirrors to light fires. In the Third century B.C. the Greek, Archimedes defended the Syracuse coast from the Roman invaders by setting fire to their boats, using mirrors to reflect the sun light on them.



Figure 1. The battle of Syracuse and the invention of Archimedes.

Some manuscripts from the first century A.C. showed how the Chinese used different methods in order to concentrate sun heat to light torches in religious acts. Lots of years later, in the 16th century, Leonardo Da Vinci also thought about a system of concentrating the sun light. His idea was to build a concentrator, with a diameter of 6 km, using concave mirrors so it produced vapor and industrial heat. But his idea, as many he had, never took place.

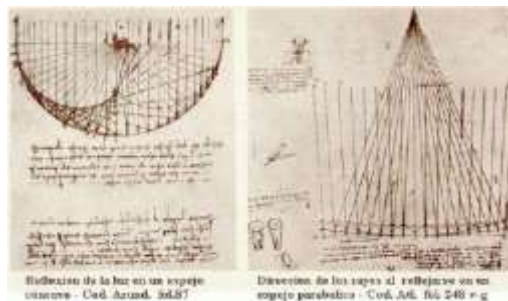


Figure 2. Solar collector designed by Leonardo Da Vinci.

In 18th Century Georges-Louis Leclerc, earl of Buffon used the Sun power in order to set fire to firewood and melt lead; also in the 18th Century the French Antoine Lavoisier built the first solar furnace which was capable of melting platinum.

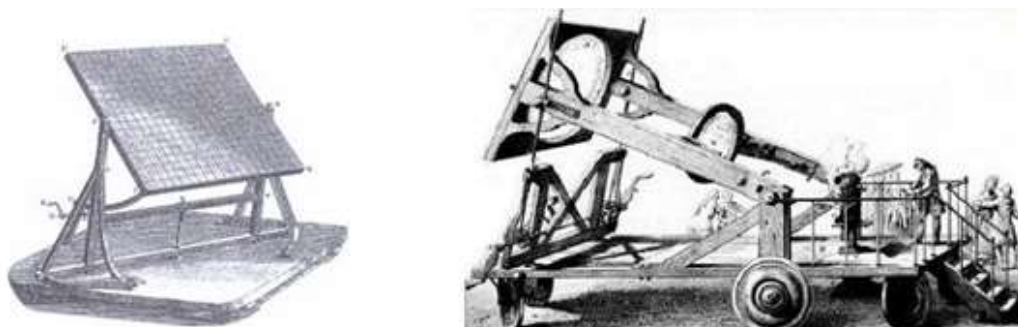
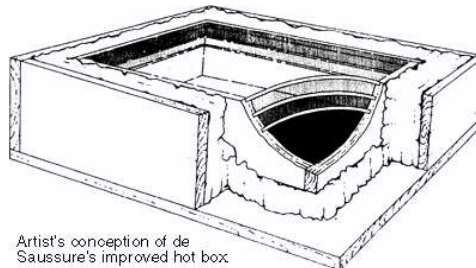


Figure 3. Solar concentrator made by Georges-Louis Leclerc (left) and solar furnace of Antoine Lavoisier (right).

A key event in the history of solar thermal energy was started by the Swiss naturalist Horace de Saussure in 1767 when he invented what he called "hot box". Saussure was aware of the greenhouse effect that occurs in an enclosed space which has a glazed opening to allow the entrance of the solar radiation, and decided to maximize the effect to check until which temperatures it could reach. He used a glazed box with its interior painted in black. All faces except the glazed one had an insulation layer, so the heat was kept inside. The result was that his hot-box managed to reach temperatures up to 109 °C.



Artist's conception of de Saussure's improved hot box.

Figure 4. "Hot box" designed by Horace de Saussure.

In 1861 Auguste Mouchout patented the first solar motor, which used solar heat to evaporate water at low pressure. In the following two decades, he and his assistant, Abel Pifre, constructed the first solar powered engines and used them for a variety of applications. These engines became the predecessors of modern parabolic dish collectors.

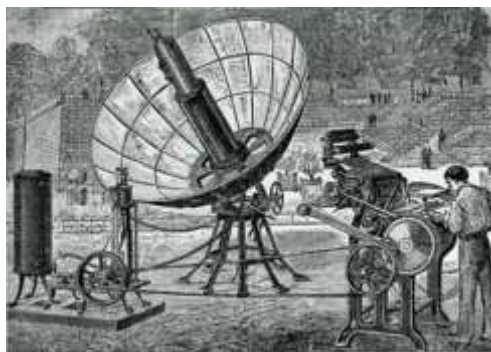


Figure 5. Solar motor invented by Auguste Mouchout.

In the 20th Century the U.S Frank Shuman designed and build a plant of 5 parabolic-trough collectors in Meadi, Egypt. Each collector had 4 metres aperture and 60 metres length, with a solar tracking mechanism. The function of this plant was to evaporate water in order to move some pumps which would water the desert lands of the surroundings with water from the Nile River.



Figure 6. PTC plant designed and build by Frank Shuman in Meadi.

Unfortunately, the First World War came on the scene, and stopped the development of the solar technology. After the war, the discovery of some big quantities of cheap oil were found. This made the solar technology to be put aside for the next 50-60 years.

In 1973 the *First Oil Crisis* appeared, because of it, the production of ways of generating energy from other sources begun to be considered, one of the other sources was the solar energy. When the *Second Oil Crisis* happened this considerations were ratified.

The International Energy Agency planed building a rehearsing platform with two different philosophies for energy producing plants, one using the solar power tower technology and the other ones using the distributed parabolic trough collectors (PTC from now on). The place selected for the construction of both platforms was the Tabernas dessert, in Almeria, Spain. The first contract for this project was signed in 1978 and the capacity of each power plant was of 0.5 MW_e.



Figure 7. PSA Almería.

The development of this technology has continued since then. All around the world different PTC plants have been set, with different type of collectors and uses; most of them for the generation of vapour for the industry. In 1984 the first out of nine SEGS plants for the power generation from PTCs was built in California, US. The ninth and last one was built in 1990. They have a capacity of generating a net total power of 354 MW_e. This has been the largest solar

thermal energy generating facility, until the commissioning of the even larger Ivanpah facility in 2014.

Since then many Solar Thermal Energy (STE) plants have been built. In the 2015, the total solar thermal power installed in the world was of 5 GW. Around the 61% of the STE plants in operation worldwide, are located in Spain, and around the 18% in the US.

But in the last years, the market interests has changed from its traditional markets of Spain and the US, to emerging markets such as South Africa, Morocco or Chile, where there are higher solar resources and political commitment to solar energy.

In the next image it is shown the present and future of the installed power of STE plants around the world.

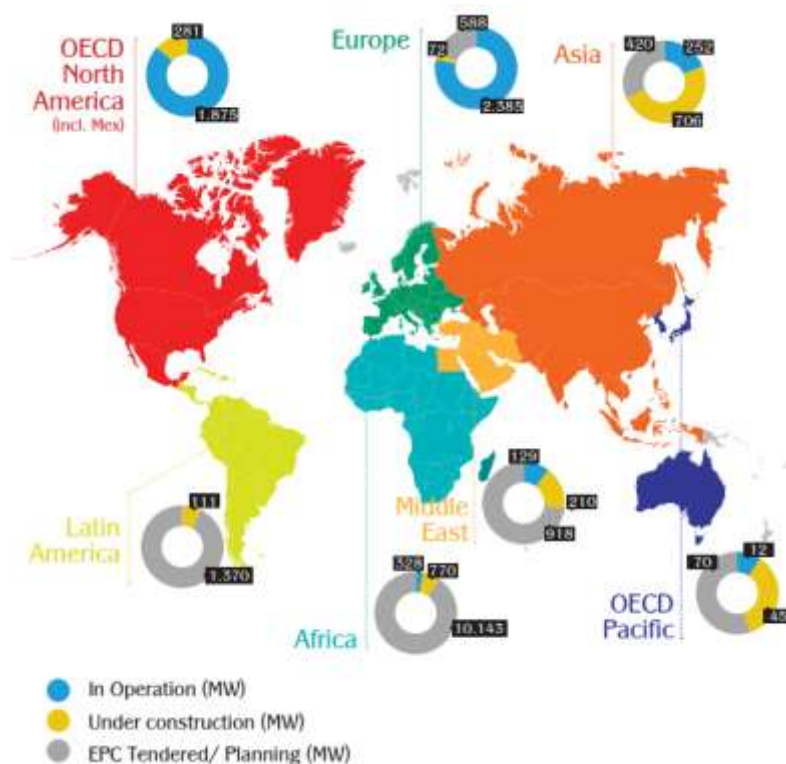


Figure 8. Current Solar Thermal Energy market situation.

2.3.2. Theory of the Parabolic-Trough solar Collectors

As it has been said the first appearance of the PTCs as we know today, was at the beginning of the 20th Century and it has developed into what we nowadays know.

A Parabolic Trough Collector consists in a long half tube reflector with a parabolic shape, which has a solar tracking system to follow the sun during operation. The reflector concentrates the solar radiation on a lineal receptor located at the focus of the parabola. Thanks to the parabolic contour of the reflector, the concentrated energy in the focus is from 30 to 100 times the solar radiation. This concentrated energy is used to heat a fluid that flows through the collector's tube, transforming the solar radiation energy into thermal energy which can be used for different objectives.

When it comes to the solar concentration technology, just the direct solar radiation is usable, so it is required that the collector follows continuously the sun's path every day. Usually the tracking is made on one axis, which can be in East-West direction or in North-South direction.

The reflective portion is formed by a parabolic mirror set on a structure previously build on a determined direction. This way the direct radiation is focused in the focal line of the parabola.

2.3.2.1. Principal components of the PTCs

The main components of a Parabolic Trough Collector are:

- Foundations and metal structure.
- Parabolic shape reflector.
- Absorber tube.
- Transmission.
- Solar tracking.
- Connexions between collectors.
- Heat transfer fluid.

Foundation and metal structure

The foundation is the part that holds up the collectors and fixes them into the ground, so the metal structure stands the forces which may appear. Its form and composition depends on the dimensions of the collectors, as well as its physical attributes, which is translated into weight and wind forces; it's also important the kind of ground where it's going to be build.

The collectors can be settled in a horizontal position, or taking advantage of the natural inclination of the ground. When the orientation on the collectors is East-West they must be settled in horizontal, on the other hand, when their orientation is North-South both possibilities are available, always with the inclination in South direction.

It's very important to build the foundation exactly as designed, so the orientation is perfect; and the separation between lines must be enough not to appear shadows, but not too much that space is wasted.

The mission of the metal structure is to give rigidity to the whole system of collectors. Also when thin mirrors are used, the structure is the one that gives the parabolic shape to the collector. In these cases it is really important that the structure has the exact dimensions, so all the irradiation is reflected on the focus line.

Parabolic shape reflector

This is one of the most important parts of the collector. Its aim is to concentrate the solar power that strikes on it, and concentrate that power, by reflexing it into the focal line. The reflectors are mirrors, which can have different forms and can be made from different materials depending on the chosen configuration.

There are two different ways of obtaining the reflectors. By depositing aluminium and silver, forming a very thin layer, on a rigid parabolic supporter. The other way is using polished plates.

In this last case is the plate itself the one which acts as supporter. The main advantage of this type of mirror is its low cost; but it has a low durability, because the reflectance of the aluminium decreases quite quickly when it is outside.

On the other hand there are the silver or aluminium layers on a glass supporter. The advantage of the silver over the aluminium it is its higher reflectance (>92% for the silver; <86% for the aluminium) with a similar cost. For this reason nowadays it is mainly used the silver.

Depending on the thickness of the glass layer, two types of mirrors can be differentiated, the thick ones (thickness>3mm), or the thin ones (thickness<1.5 mm; this ones are easily broken). The thick glass mirrors can be directly mounted on the structure. In order to get the parabolic shape, they are hot bended after depositing the silver.

The thin glass mirrors, do not have the enough rigidity to be directly mounted, they need another supporter. This mirror, if it has been template, has the enough flexibility to be mounted on the supporter, which has the necessary parabolic contour.

Absorber tube

The absorber tube (also called receiver tube) is the part of the collector whose aim is to transform the concentrated solar light into the thermal energy needed to heat the fluid. As it has been previously said, the absorber tube is located in the focal line or the parabolic mirror, so the reflected sun rays collide with it.

It is one of the most important parts of a PTC. The global efficiency of the system depends to a large degree on this part.

The absorber tube consists basically of two concentric cylinders, the outer one made of glass, and the other one made of metal, covered by some selective paintings that increase its absorptance, and durability, and decreases its emittance.

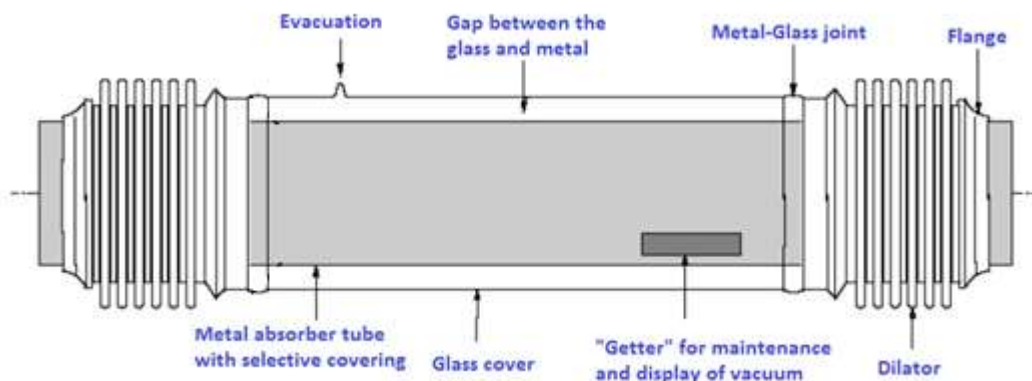


Figure 9. Typical absorber tube of a PTC.

The components that form an absorber tube vary depending on the manufacturer, the design and the working temperature. One example for the group off components that comprehend an absorber tube can be the next one (this is the one that attains this project):

- Set of the metal tube composed of several welded units.
- Glass tube concentric to the metal one.
- Union between both tubes.
- Support rings for the metal tube.
- Supports for the glass tube.

Depending in the working temperatures, the metal tube can be covered with different types of selective painting; this paintings have a high absorptivity (Over 90%) and a low emittance

(below 30%). This kind of coverings, go from a deposition of black chromium or cobalt, to different compounds of cermet (it is a mixture of metal and ceramic products). The first ones have better properties under 200°C, and degrade over 300°C. Meanwhile, the second ones, when the temperature is over 300°C have to use selective coverings obtained by sputtering or PVD (Physical Vapour Deposition), this way values of absorptivity over 95% and values of emittance below 15% can be reached at 400°C. The main problem of the PVD coverings or the sputtering is that they deteriorate in contact with air when they are working at high temperatures. For this reason it is necessary that the gap between the glass tube and the metal tube remains in a vacuum atmosphere. On this case it is necessary to close the set of tubes. The procedure to make the gap watertight is to make a metal-glass welding, placing some dilators at the extremes of the tubes. The function of this dilator is to absorb the differential dilatations that happen between the metal tube and the glass tube when the system is working under high temperatures.

In order to avoid, external air or particles enter the gap, getters are used. They are made from a special compound capable of absorbing the particles of the different substances, which over time could penetrate the interior space.

In order to increase the transmittance and the optical efficiency of the glass cover, an anti-reflexive treatment is carried out.

Transmission

It is important that the PTC is able to follow the sun's path, in order to catch as much direct solar radiation as possible and the best efficiency as possible is obtained. The transmission is the component in charge of making the tracking movement possible.

Usually the transmission avails the movement of the collector in one axis (almost always in East-West or North-South direction). The transmission system can be either electric or hydraulic; and at the same time it can be distributed for a single collector unit or for an entire row.

It also exists the possibility of a transmission system, with the capacity of tracking in 2 axes, but the more energy it can generate does not compensate the higher cost and the higher amount of thermal losses.

Solar tracking system

The solar collectors whose acceptance semi angle is less than 10° need a solar tracking system, so the efficiency of the collector is maximum.

There are two types of tracking systems, ones that use photocells and the other ones that use the calculation of the solar position to program the movement of the motor.

When it comes to photocells, two types of sensors are used, photocells with a shadow band and photocells of flux line.

The first kind are formed by two photocells on a flat surface. The cells are separated by a thin wall located between both, and the group is placed in the PTC in a direction perpendicular to the sun's rays and the band of shadow is in the same direction as the axis of the collector. In such a way, when the sun moves the shadow of the band touches one of the photocells. This causes the imbalance between the cells. The imbalance is processed by an electronic comparator which depending on the polarity and magnitude of it, orders to the motor to move

the collector on the correct direction until the shadow disappears and the signal is again balanced.

The flux line sensors are placed directly on the absorber tube. It comprises two photocells located in both parts of the tube so they can detect the concentrated flux on the absorber tube. The collector is in the right position when both cells are equally illuminated, and send the same signal. If the signals are imbalanced, the collector moves in the right direction till the signal is balanced again.

The other way of solar tracking, as it has been said, is through mathematic algorithms that tell accurately what the position of the sun is at any time and date. With an angular encoder connected to the collector, the position of it to the sun is known. So when the position of the collector is not the one it should be, the motor moves it. This tracking system is not yet commercially available and is being tested in the PSA.

Connexions between collectors

In the PTC plants, various collectors are joined in series forming rows. This rows are parallel blinded till it is reached the necessary catchment area in order to reach the desired power. An important aspects to take into account is how the collectors are joined ones with others. This joints should allow the independent movement of the collector of one row, at the same time it has to absorb the possible dilatation that could appear in the absorber tubes. This joints also allow the heat transfer fluid flow between the modules, mobile pieces, and the circulation pipes, fixed parts.

There are two types of joints, rotary joints, which allow the rotation of the collector as well as, longitudinal expansions; and flexible pipes, which can be bended as much as necessary to allow the rotation of the collector and absorb the longitudinal dilatations.

Heat transfer fluid

The kind of Heat Transfer Fluid (HTF) depends on the temperature it is going to reach. The most common ones are water or thermal oils, but in some cases it is also used glycol or molten salt.

Water is used for low temperatures, bellow 200°C. When overheated vapor is needed (temperatures of 200-300°C) it can be obtained directly, using distilled water as HTF. The drawback of using water is that the system needs to be under much more pressure than when thermal oil is used, and therefore the cost of the equipment is much higher.

There are many types of thermal oils. The most typical ones, determined by the desired working temperature are:

- *Caloria® HT-43* and *Solutia-Therminol® 55*, they can reach 300°C and have an economic cost.
- *Solutia®-VP-1*, it can reach 400°C. It has the disadvantage that its freezing point is of 12°C, which means that in winter is going to be needed an auxiliary heating system.
- *Dow Chemical- Syltherm® 800*. This one also can reach 400°C and its freezing point is of -40°C, so there is no problem. The disadvantage of this one is its high cost. (This HTF is the one used along this project).

2.3.2.2. Collectors types

When it comes to Parabolic-Trough Collector there are two types, differentiated on their movement; movement in one axis or in two axes.



Figure 10. Collectors with one and two axes solar tracking.

Nowadays the collectors with two axes solar tracking are scarcely used, because the more energy they are capable of generate, don't compensate their higher cost and amount of energy losses. Also they are more fragile to high wind.

2.3.2.3. Design parameters

Two principal parameters of a PTC are the *Concentration ratio* and *Acceptance angle*.

The *Concentration ratio*, C , is the ratio between the aperture area of the collector and the total area of the absorber tube.

$$C = \frac{A}{\pi \cdot D \cdot L}$$

Where:

- A: Aperture of the collector.
- D: Diameter of the absorber tube.
- L: Length of the absorber tube.

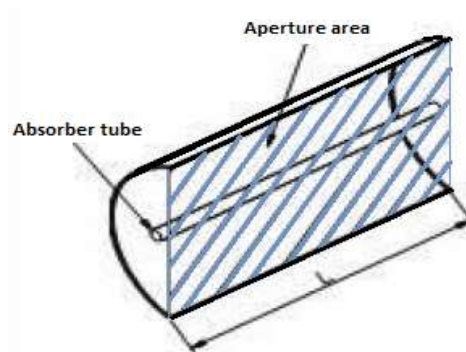


Figure 11. Dimensions of a collector.

The Acceptance angle is the maximum angle that two sun's rays on a cross plane to the collector's aperture can have, so they impact against the absorber tube after they are reflected. The precision of the solar tracking system must be higher than the acceptance angle.

Nowadays the collectors have an acceptance angle around the 2° , so they need a precise tracking system.

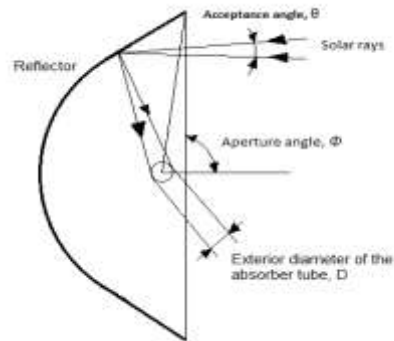


Figure 12. Acceptance and aperture angles of a solar collector.

2.3.2.4. Energy losses

When the solar radiation reaches the collector, an important amount of energy is lost due to three main reasons, geometric, thermal and optic reasons. The thermal losses will be explained in detail later in the present test.

Optical losses

The reason for the presence of this losses is that neither the reflexive surface is a perfect reflector, nor the glass cover is totally transparent, nor the absorber tube is an ideal absorber, nor the geometric of the parabolic reflector is excellent.

- Reflectance, ρ

This parameter indicate which rate of the incident radiation is reflected from the mirrors, when these are perfectly clean. Common values for this parameter are around 90%, but this value decreases as the time goes by.

- Interception factor, γ

This parameter expresses the percentage of solar radiation reflected by the mirrors that reaches the absorber tube. This parameter's value is usually around 95%.

- Transmittance, τ

This parameter quantifies the amount of radiation that crosses the glass cover out of the radiation that reaches it. Common values for this parameter are around 90-95%.

- Absorptance, α

Quantifies the amount of radiation absorbed of the total radiation that arrives the absorber tube.

Geometric losses

These losses are the ones that appear due to the reduction of the effective area. They can be inherent to each collector, or because of the relative position of collector between each other.

- Losses due to shadows

They are from the second group, and appear when a collector overshadows part of the one behind.

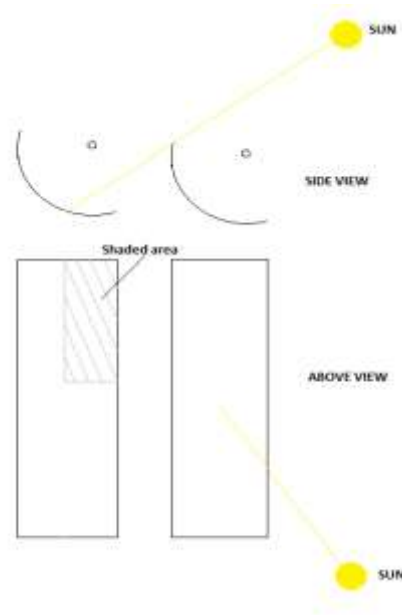


Figure 13. Shaded area when the distance between the collectors is not enough.

- Losses due to the incidence angle

These kind of losses are inherent to each collector. The cause for their appearance is that when the collectors just have a one axis tracking system (in most cases), appears the *angle of incidence*, φ , this angle is the one between the direct solar irradiance that reaches the aperture surface and the normal to that surface. It depends on the time and the date, because it's directly related to the Sun's position.

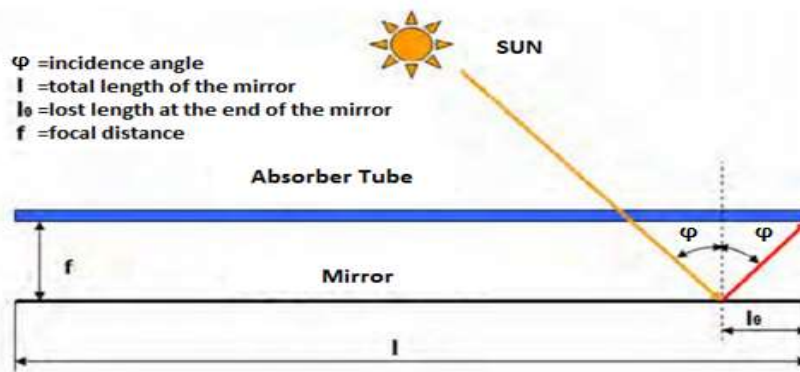


Figure 14. Losses due to incidence angle.

In the top figure we can see how there is a not useful area, l_0 , because the solar radiation that it reflects does not reach the absorber tube. The lost area of the collector, A_f , is:

$$A_f = W \cdot ED = W \cdot F \cdot \tan(\varphi)$$

Where

- W =Aperture of the collector.
- L =Length of the collector.
- F =Focal distance
- φ =Incidence angle.

2.3.3. Energy balance of a PTC

2.3.3.1. Thermal performance of a solar collector

The parameter which determines the thermal performance of any solar collector is the *Global efficiency*, η . This parameter represents the amount of power is obtained from the collector, or useful power, P_{useful} out of the total solar power that reaches the area of the collector, P_{solar} .

$$\eta = \frac{P_{useful}}{P_{solar}}$$

The reference solar power, P_{solar} is the product of the *aperture area*, A_c and the *reference solar irradiance*, E_C .

$$P_{solar} = A_c \cdot E_C$$

In steady state the *useful power*, P_{useful} is the result of the balance between the *absorbed power*, $P_{absorbed}$ and the *lost power*, P_{lost} .

$$P_{useful} = P_{absorbed} - P_{losses}$$

Just a part of the total solar power can be absorbed by the receptor, this absorbed power is given by the *optical efficiency*, η_{opt} .

$$P_{absorbed} = \eta_{opt} \cdot P_{solar} = \eta_{opt} \cdot A_c \cdot E_C$$

The lost power is due to the higher temperature of the absorber compared to the ambient temperature. Calling T_A to the temperature of the absorber and T_{∞} , to the temperature of the surroundings. And A_A to the area of the absorber, we have that the lost power is

$$P_{losses} = U_L \cdot A_A \cdot (T_A - T_{\infty})$$

So the useful power can also be expressed as

$$P_{useful} = P_{absorbed} - P_{losses} = \eta_{opt} \cdot A_c \cdot E_C - U_L \cdot A_A \cdot (T_A - T_{\infty})$$

And the Global efficiency

$$\eta = \frac{P_{useful}}{P_{solar}} = \eta_{opt} - \frac{U_L}{C} \cdot \frac{(T_A - T_{\infty})}{E_C}$$

$$\text{Where: } C = \frac{A_c}{A_A}$$

2.3.3.2. Solar irradiance of a PTC

The global irradiance of any horizontal surface, E_g that only sees the sky, is given by the component of direct irradiance, E_b and the component of diffuse irradiance, E_d .

$$E_g = E_b \cdot \cos(\varphi) + factor \cdot E_d = E_b \cdot \cos(\varphi) + \frac{1}{C} \cdot E_d$$

Where φ is the angle between the solar radiation and the surface (incidence angle), and "factor" is the amount of diffuse irradiance that reach the surface.

$$factor = \frac{A_A}{A_c} = \frac{1}{C} \quad \text{So: } E_g = E_b \cdot \cos(\varphi) + \frac{1}{C} \cdot E_d$$

When the value of the parameter C is between 13 and 30, the second part of the expression can be neglected over the first one.

$$\frac{1}{C} \cdot E_d \ll E_b \cdot \cos(\varphi) \quad \text{So:} \quad = E_b \cdot \cos(\varphi)$$

Considering that the reference solar irradiance is the global irradiance, the efficiency of a PTC is

$$\eta|_{E_b \cdot \cos(\varphi)} = \eta_{opt}|_{E_b \cdot \cos(\varphi)} - \frac{U_L}{C} \cdot \frac{(T_A - T_\infty)}{E_b \cdot \cos(\varphi)}$$

Many authors, prefer to use the direct irradiance (E_b) as the reference solar radiation (E_c), for the collectors with solar tracking, so the efficiency is expressed as

$$\eta|_{E_b} = \eta_{opt}|_{E_b} - \frac{U_L}{C} \cdot \frac{(T_A - T_\infty)}{E_b}$$

2.3.3.3. Optical efficiency, η_{opt}

The optical efficiency, η_{opt} is defined as the factor that considers the energy difference between the reference solar power (P_{solar}) and the absorbed power ($P_{absorbed}$). This difference is due to energy losses, which take into account both the optical and the geometrical ones.

Considering the different losses that have been mentioned before, the absorbed power can be expressed as

$$P_{absorbed} = E_b \cdot \cos(\varphi) \cdot r(\varphi) \cdot \tau_{solar,c}(\varphi, \lambda) \cdot \alpha_{solar,A}(\varphi, \lambda) \cdot \gamma_A(\varphi)$$

Where:

- r : *Specular reflectance*. Represents the quantity of energy reflected by the mirrors out of the energy that reach them. Depends on the incidence angle (φ).
- $\tau_{solar,c}$: *Transmittance*. This parameter expresses the percentage of solar radiation that passes the glass cover. Depends on the incidence angle (φ) and on the range of wavelengths (λ).
- $\alpha_{solar,A}$: *Absorptance*. Quantifies the amount of radiation absorbed of the total radiation that arrives the absorber tube. Depends on the incidence angle (φ) and on the range of wavelengths (λ).
- γ_A : *Interception factor*. This parameter expresses the percentage of solar radiation reflected by the mirrors that reaches the absorber tube. Depends on the incidence angle (φ).

The expression of the absorbed power, can be simplified without considering λ to

$$P_{absorbida} = E_b \cdot \cos(\varphi) \cdot r(\varphi) \cdot \tau_{solar,c}(\varphi) \cdot \alpha_{solar,A}(\varphi) \cdot \gamma_A(\varphi)$$

So the optical efficiency can now be expressed as

$$\eta_{opt} = \frac{P_{absorbida}}{P_{solar}} \begin{cases} \text{Si } P_{solar} = A_c \cdot E_b \cdot \cos(\varphi) \rightarrow \eta_{opt}|_{E_b \cdot \cos(\varphi)} = r(\varphi) \cdot \tau_{solar,c}(\varphi) \cdot \alpha_{solar,A}(\varphi) \cdot \gamma_A(\varphi) \\ \text{Si } P_{solar} = A_c \cdot E_b \rightarrow \eta_{opt}|_{E_b} = r(\varphi) \cdot \tau_{solar,c}(\varphi) \cdot \alpha_{solar,A}(\varphi) \cdot \gamma_A(\varphi) \cdot \cos(\varphi) \end{cases}$$

From now on it is going to use the second equation.

It is called *incidence angle modifier* to the factor that takes into account all the geometric and optical losses because of the radiation reaching with a an incidence angle

$$K(\varphi) = \frac{\eta_{opt}(\varphi)}{\eta_{opt}(\varphi = 0^\circ)} = \frac{\eta_{opt}}{\eta_{opt,0^\circ}}$$

Where:

- $\eta_{opt,0^\circ}$: *Peak optical efficiency*. Is the efficiency when the incidence angle is equal to 0 ($\varphi = 0^\circ$)

The optical efficiency can be expressed as

$$\eta_{opt} = K(\varphi) \cdot \eta_{opt,0^\circ}$$

Where:

$$\eta_{opt,0^\circ} = r_{0^\circ} \cdot \tau_{0^\circ} \cdot \alpha_{solar,A,0^\circ} \cdot \gamma_{A,0^\circ}$$

So

$$K(\varphi) = \frac{r(\varphi) \cdot \tau_{solar,C}(\varphi) \cdot \alpha_{solar,A}(\varphi) \cdot \gamma_A(\varphi)}{r_{0^\circ} \cdot \tau_{0^\circ} \cdot \alpha_{solar,A,0^\circ} \cdot \gamma_{A,0^\circ}} \cdot \cos(\varphi)$$

2.3.3.4. Heat transport mechanisms

The thermal energy is transferred from hot places to places with lower temperatures. The main way of energy transfer are conduction, convection and radiation. When it comes to reality, the energy transfer happens in more than one of these mechanisms acting at the same time.

Radiation

Thermal radiation is electromagnetic radiation generated by the thermal motion of charged particles in matter. All matter with a temperature greater than absolute zero emits thermal radiation. When the temperature of the body is greater than absolute zero, inter-atomic collisions cause the kinetic energy of the atoms or molecules to change. This results in charge-acceleration and/or dipole oscillation which produces electromagnetic radiation, and the wide spectrum of radiation reflects the wide spectrum of energies and accelerations that occur even at a single temperature. So, the radiation of any body is the electromagnetic emitted radiation due to its temperature and at the expense of its internal energy.

In the case of the PTCs the main heat transport mechanism is radiation; most of the heat losses that happen to a collector are through this mechanism.

Conduction

It is the mechanism of energy transfer between two bodies which are in physical contact. The conduction phenomenon takes place at a molecular level, when the molecules with higher energy transfer energy to those with lower energy.

Convection

This is the mechanism of energy transfer that takes place between a solid body and a fluid due to the macroscopic movement of the fluid. In the case of the PTCs heat transfer through this mechanism will happen between the glass cover and the ambient, in that same direction.

This phenomenon will also happen in the gap between the glass cover and the absorber, cause although it is supposed that there is vacuum in that gap, in reality there is air at a very low pressure, but enough so convection occurs.

2.3.3.5. Overall loss ratio of a PTC

The absorber tube of a PTC is a metallic tube whose external layer is prepared for the absorption of the solar radiation; that is the reason why it is called absorber tube. Inside the tube circulates a fluid, called Heat Transfer Fluid, which is going to be used to make usable the solar radiation.

Around the absorber tube there is a glass cover, which protects and isolates the absorber tube from the external ambient.

Overall energy balance

When considering a PTC the next energy transfers happen:

- Energy transfer between absorber and glass cover.
- Energy transfer through the glass cover.
- Energy transfer from the glass cover to the ambient.
- Energy transfer from the absorber to the ambient through the supports and braces of the receptor.

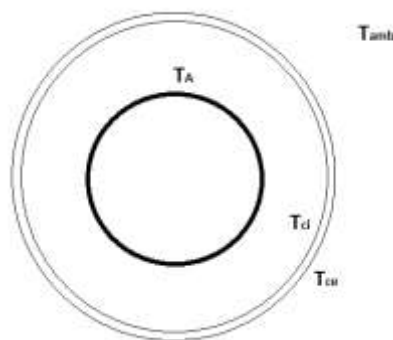


Figure 15. Section of an absorber tube.

On stationary state there is an energy balance. It can be expressed as follows

$$P_{A,rad} + P_{A,conv} = P_{C,conv} = P_{A,lost}$$

$$P_{C,abs} + P_{C,cond} = P_{ext,conv} + P_{ext,rad}$$

Where

- $P_{A,rad}$: Lost energy from the absorber tube to the glass cover through radiation.
- $P_{A,conv}$: Lost energy from the absorber tube to the glass cover through convection.
- $P_{C,conv}$: Transmitted energy through the glass cover by conduction.
- $P_{C,abs}$: Absorbed radiation by the external layer of the glass cover.
- $P_{ext,conv}$: Lost energy from the glass cover to the ambient through convection.
- $P_{ext,rad}$: Lost energy from the glass cover to the ambient through radiation.
- $P_{A,lost}$: Lost energy from the absorber tube to the ambient through the glass cover. $P_{A,lost} = U_{LA} \cdot A_A \cdot (T_A - T_\infty)$.

The total heat losses of the collector, and so, the overall loss ratio, U_L has to take into account the energy losses through the braces and the supports of the absorber, $P_{supp,lost}$:

$$P_{lost} = P_{A,lost} + P_{supp,lost} = U_L \cdot A_A \cdot (T_A - T_\infty)$$

2.3.3.6. Efficiency factors

In order to quantify the experimental behaviour of the collector, it is useful to use the temperature of the HTF that flows through the absorber. When talking about the temperature of the fluid, the inlet temperature (T_{in}) can be used, but it is more common to use the medium temperature (T_m) between the inlet and the outlet (T_{out}) temperatures.

$$T_m = \frac{1}{2} \cdot (T_{out} + T_{in})$$

So, the overall efficiency can be expressed, depending on the medium temperature as:

$$\eta = F_m \left\{ \eta_{opt} - \frac{U_L}{C} \cdot \frac{(T_m - T_\infty)}{E_C} \right\}$$

Where:

- F_m : Collector's efficiency factor or heat transfer factor.

This factor is given by the energy transfer between the absorber and the HTF. It can be expressed as

$$F_m = \frac{U_{HTF}}{U_L}$$

When instead of the medium temperature of the fluid, it is used the inlet temperature, the equation for the overall efficiency is:

$$\eta = F_R \left\{ \eta_{opt} - \frac{U_L}{C} \cdot \frac{(T_{in} - T_\infty)}{E_C} \right\}$$

Where:

- F_R : Collector heat renewal factor. It is the ratio between the real energy transfer and the maximum possible energy transfer.

2.3.4. STAGE project

The STAGE project is an Integrated Research Program (IRP) that includes the major European research institutes and companies, as well as some others worldwide, that work in relation to the Concentration Solar Energy.

The Concentration Solar Energy encompasses Solar Thermal Energy (STE), Solar Fuels, Solar Process Heat and Solar Desalination which will play a major role in the near future due to their unique features such as:

- The solar energy offers the highest renewable energy potential of the Earth.
- Solar Thermal Energy can be provided in a technically and economically viable way.

However, research is necessary to attain this goal. That's why some European research institutes have joined in order to accomplish different objectives. The main one is to get together the main European research organizations, and set that consortium as a reference

institution for Concentrating Solar Energy in Europe. In addition to defining priorities, spotlights and research agenda in the coming years, it should achieve aligning the existing funds at European level with those of the various countries concerned in the development of related technologies. Industrial participants in the consortium will define the involvement of industry in the whole process of generation and transfer of acquired knowledge and international organizations will provide their vision and collaboration in specific developments necessary for the effective implementation of technology in different regions with important solar potential.

2.3.5. Introduction to the PSA

In the wake of the oil crisis, it was decided to seek and promote alternative means of power generation. Among these alternative it was located solar energy.

In this context, the International Energy Agency proposed the construction of a platform for testing the technologies of solar power tower and parabolic trough collector. The place chosen to implement the platform was the Tabernas desert in Almeria, leading to the formation of the Plataforma Solar de Almeria. The first contract for the execution of this project was signed in 1978.

The PSA is part of the Centro de Investigaciones Energéticas, Medioambientales y Tecnológicas (CIEMAT). It is the largest concentrating solar energy research, development and test centre in Europe.

The objective of the PSA is the research and development of new ways for the exploitation of the solar energy in the industry of the concentration Solar Thermal Energy and the solar photochemistry. On this sense the work the PSA realizes is divided in three different R&D units.

- *Solar concentrating system*: this unit looks for new and better ways of producing electricity from solar power.
- *Water desalination*: its objective is to develop the way seawater and brackish water is desalinated through solar power.
- *Solar treatment of water*: this unit investigates the chemical possibilities of solar power, especially with regards to its potential for water detoxification and disinfection.

Due to its location, the PSA receives a direct annual irradiation over 1900kWh/(m²·year) and the medium annual temperature is around the 17°C. This location and climate condition make the PSA a prime plant in order to test, demonstrate and transfer solar technologies.

Nowadays, the available testing facilities are:

- CESA-1 and SSPS-CRS central collector systems, of 5 and 2.5 MW_{th} each.
- DISS experimental test loop with a 2.5 MW_{th} capacity. This system is used for the research of the two-phase flow and the direct steam generation for the electricity production.
- TCP-100 2.3 MW_{th} parabolic-trough collector field with associated 115 m³ thermal oil storage system.
- HTF test loop, for the experimentation of new heat transfer fluids for the parabolic-trough collectors.
- The FREDESMO “linear Fresnel” technology loop.
- The Parabolic Trough Test Loop (PTTL) facility.

- A parabolic-trough collector test facility with thermal oil (the so-called HTF Test loop) for qualification of components and complete collectors.
- 4-unit dish/Stirling facility, called DISTAL, and 2 EuroDish units.
- A group of three solar furnaces, 2 of them with horizontal axis 60 kW_{th} and 40 kW_{th}; and the third one with vertical axis 5kW_{th}.
- A test stand for small evaluation and qualification of parabolic trough collectors, named CAPSOL.

The facility that attains this project is the HTF Test Loop. It was built in 1997 and it is ideal for the qualifying and monitoring of the following components:

- New designs of parabolic-trough collectors (up to 75 m long).
- Parabolic-trough collector mirrors
- Parabolic-trough collector absorber tubes
- New designs of ball-joints or flex-hoses for connecting parabolic-trough collectors in the solar fields.
- Solar tracking systems.

This system consist in a closed thermal loop connected to three semi-collectors of 75 metres long connected in parallel. Due to the fluid pump, it is only possible to operate one of them at a time. The direction of this collectors is East-West. This orientation increases the number of hours during a year time in which the angle of incidence is less than 5°, which makes this system appropriate for the test of *Peak optical efficiency* and *Incidence angle modifier* (these will be explained later).

The system has different elements to enable the flow of the heat thermal fluid through it in some conditions established by the user. The thermal fluid used in this system is Syltherm® 800 which thanks to its thermal properties (maximum working temperature of 420°C and freezing point of -40°C) makes it appropriate for this system. The oil circuit has a maximum working pressure of 18 bar. The main elements that enable the functioning of this circuit are:

- Centrifugal oil pump with a maximum capacity of pumping 30 m³/h.
- Two oil heaters of 40 kW used to set the fluid in the operation conditions required.
- One air-cooler of 400kW with air speed control. It is also used to set the fluid in the operation conditions.
- One expansion tank of 1 m³ to set the pressure of the fluid in the system. It has an automatic nitrogen inertisation.
- Manual valves to operate in emergency cases.
- Temperature, flow and pressure sensors; also Wind sensor (at 5 metres and 10 metres high)

As it has been said the HTF system is formed by three Semi-collectors: EuroTrough, UrssaTrough and AlbiassaTrough. Each semi-collector is formed by six modules, each formed by three absorber tubes (this makes a total of 18 absorber tubes and a total length of 75 metres). During this project it going to be analysed the behaviour of the UrssaTrough, manufactured by the company URSSA Energy Corporation. The absorber tubes this collector has used are the model PTR®70 manufactured by the German company Schott.

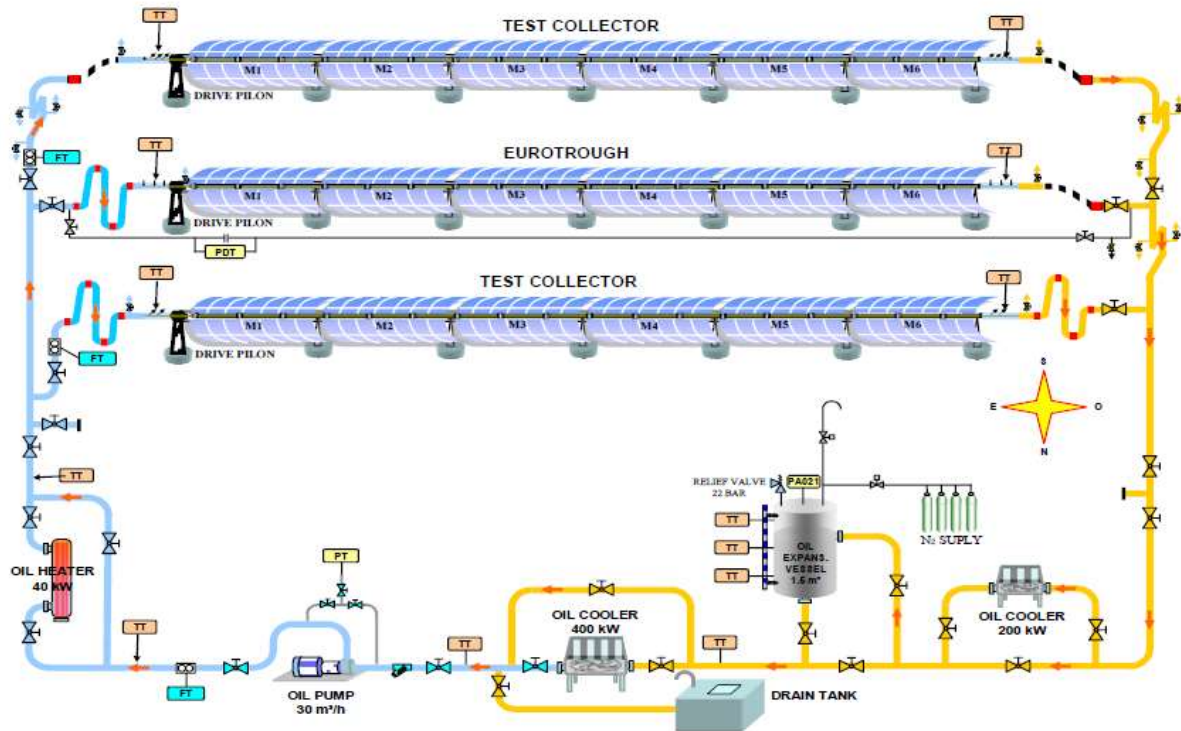


Figure 16. Diagram of the PSA "HTF Test Loop". Source from the PSA Annual Report 2014.

2.3.6. Experimental test of the Parabolic-trough solar Collectors

To see how good a parabolic trough collector is it is necessary to test some parameters that define its behaviour. As it has been said in the previous paragraphs according to (L. Valenzuela, R. López-Martín, & E. Zarza, 2014) there are various types of tests, depending on what it's going to be measured. For each test there is a different procedure, with some different initial parameters.

The main parameters that describe the performance of line-focus tracking collectors are:

- Peak optical efficiency.
- Longitudinal and transversal incidence angle modifier.
- Heat loss curve.

The standard methods used to determine the thermal performance of the concentrating solar collectors are *ASHRAE standard*, *ASTM standard E905-87*, and *SRCC Standard 600*. But this test are not applicable to qualify large parabolic trough collectors.

Although there are some standard methods for determining the thermal performance of the concentrating solar collectors as *ASHRAE standard*, *ASTM standard E905-87*, and *SRCC Standard 600*, the procedures described later are not directly applicable to qualify large parabolic-trough collectors that work at high temperatures.

The reason for the standard methods not been applicable in these cases is that during the test, as the working temperatures are high, some components of the collector will expand and change their position. This makes that the position of the absorber could not be exactly the focal plane. This has to be taken into account when performing the tests, and mechanical corrections must be made so the position of the absorber is the correct one for all the working temperature range.

It is going to be explained a test method for evaluating the optical and the thermal performance of large-size parabolic-trough solar collectors (≥ 100 m). This test method has different procedures in order to measure the optical and thermal performance for some specified conditions. It is important to be capable of measuring the parameters that represent both performances (peak optical efficiency, incidence angle modifiers and heat loss curve), so the global performance of this collectors is known.

Peak optical efficiency and the incidence angle modifiers are both obtained from an outdoor testing of a collector with heat transfer fluid temperatures close to ambient temperatures. Meanwhile, heat losses are determined indirectly from collector's global efficiency data, which are obtained from test performed in steady state conditions at various working fluid temperatures with the incidence angle of solar radiation equal to 0° .

2.3.6.1 Methodology

There are two different stages in the testing of the large- size PTCs:

- *Measurement of the optical performance of the collector.* First step is to carry out the tests to measure the peak optical efficiency and the incidence angle modifier. They are also measured the heat losses at low temperatures, so their effect is quantified.
- *Measurement of the thermal performance of the collector.* The temperatures of the HTF during this test are between 293°C and 393°C . Tests are carried out at different average fluid temperatures within this range to measure the thermal efficiency when the angle of incidence of solar radiation is equal to 0° .

The useful radiant solar power in the aperture area of the collector (\dot{Q}_s , in W) can be calculated as:

$$\dot{Q}_s = A_c \cdot E_d \cdot \cos \theta$$

Where:

- A_c : Net collecting area in m^2 .
- E_d : Direct solar irradiance in W/m^2 .
- θ : Incidence angle of the solar radiation in the collector aperture plane in $^\circ$.

Since the pressure is maintained constant through the all collector, it is an isobaric process, so thermodynamically it can be demonstrated that the useful thermal power transferred in the absorber to the HTF in heat power form (\dot{Q}_u , in W) is determined by the enthalpy difference between the entrance and the exit of the collector.

$$\dot{Q}_u = m \cdot \Delta h$$

Where:

- m : Mass flow in kg/s .
- Δh : Increase in the specific enthalpy of the fluid in J/kg .

And finally the thermal power balance of the collector is:

$$\dot{Q}_{s,a} = \dot{Q}_u + \dot{Q}_1$$

Where:

- $\dot{Q}_{s,a}$: Incident radiant solar power absorbed by the absorber in W.

- \dot{Q}_1 : Heat loss power in the collector in W.

Heat losses

The thermal fluid is heated while crossing the absorber tube. As its temperature is higher than the environment temperature, there is a heat transference from the fluid to the ambient. This heat transfer is no longer exploitable for another usage, so it is lost energy. They are called energy losses and are mainly due to radiation with the environment, and through convection in less extent.

The heat losses must be quantified during the testing of any PTC prototype. In practice in order to quantify this losses, it is much easier to measure the temperature of the HTF than the temperature of the absorber's surface. Therefore the heat losses are calculated by means of the HTF's inlet and outlet temperatures. As the pressure is also known, with those temperatures, the enthalpy at the entrance and at the exit can be established. So, if incidence of direct and concentrated solar radiation is avoided, the $\dot{Q}_{s,a}$ is equal to 0 and heat losses can be determined by the HTF's enthalpy difference between the entry and the exit of the absorber as:

$$\dot{Q}_1 = -m \cdot \Delta h$$

The heat losses during the collector's optical performance test (with a range of low temperatures), are very low, however they must be quantified to enhance the accuracy of the measurements of peak optical efficiency and incident angle modifier.

During the experimental determination of the heat losses the PTC has to be positioned to avoid the incident solar radiation on the absorber tube. The inlet temperature of the HTF that circulates through the collector must be kept constant for different temperature levels within the whole working range. These test must be done during night or during very cloudy days to reduce the effect of diffuse solar radiation.

The heat loss curve fit depends on the temperature difference (ΔT) between the average fluid temperature in the absorber and the ambient temperature. Considering the heat loss mechanism that can appear in the absorber tubes, the curve takes the form:

$$\dot{Q}_1 = a_1 \cdot \Delta T + a_2 \cdot \Delta T^4$$

Where:

- a_1 : Fitting parameter related mainly to convection and conduction heat losses in W/K.
- a_2 : Fitting parameter related to radiation heat losses in W/K⁴.

Peak optical efficiency ($\eta_{opt, 0^\circ}$)

This parameter determines the maximum performance that can be obtained from a solar collector. Its value can be obtained multiplying the mirror reflectance ρ , the overall intercept factor γ_T , which is the product of the intercept factor of the solar concentrator γ_C and the effective length factor of the absorber tubes installed in the PTC γ_R , the absorptance of the absorber tube α , and the transmittance of the absorber glass cover τ .

When it comes to practice, the optical efficiency has to be determined by testing a complete PTC so all the factors that affect the theoretical efficiency are considered. This factor are i.e. twisting deformation, bad performance of the sun tracking system, etc.

Conditions required to perform the tests and to reach this maximum performance are unique, i.e. the solar collector must be completely clean; the angle of incidence of radiation must be 0° to avoid the effects of the incident angle, which is achieved at solar noon for PTCs oriented in East-West direction; and the temperature of the HTF has to be close to ambient temperature or at least below 125°C , so the heat losses are minimum.

The optical efficiency, as it has been previously said, can be calculated as:

$$\eta_{\text{opt}} = \frac{\dot{Q}_{s,a}}{\dot{Q}_s}$$

The followed procedure to determine the maximum value of this parameter is to perform test circulating the HTF through the absorber with the collector in sun-tracking position, and keeping steady state conditions during a period of at least 4 times the mean fluid residence time when angle of incidence is zero or very close to zero.

As $\cos \theta$ must be 1 or very close ($\theta \cong 0$), the peak optical efficiency can be calculated as:

$$\eta_{\text{opt},0^\circ} = \frac{\dot{m} \cdot \Delta h + \dot{Q}_1}{A_c \cdot E_d}$$

To ensure the repeatability of the measurements, it is recommended to repeat at least three times the peak optical efficiency measuring test. This recommendation is general for all the parameters.

Incidence angle modifier ($K(\theta)$)

This parameter refers to the longitudinal incidence angle modifier, which is a factor lower than 1 as incidence angle increases from 0° . As the PTCs are equipped with sun-tracking systems the transversal incidence angle is equal to zero, so the transversal incidence angle modifier is always assumed to be 1.

Therefore, on now on the longitudinal incidence angle modifier will be referred to as just incidence angle modifier. This parameter considers the degradation of the collector optical performance due to the incidence angle of the solar radiation, and can be obtained as:

$$K(\theta) = \frac{\dot{m} \cdot \Delta h + \dot{Q}_1}{\eta_{\text{opt},0^\circ} \cdot A_c \cdot E_d \cdot \cos \theta}$$

The steps followed to obtain the incidence angle modifier of a PTC consists on running the tests from nearly sunrise to sunset, with the collector tracking the sun. The mass flow of HTF circulating the collector should remain as constant as possible, as well as the inlet temperature of the fluid which also has to be close to ambient temperature.

Transient conditions are avoided in this test by reducing as much as possible the variation in the HTF's inlet temperature and mass flow during the complete test. Also the data obtained when the direct solar irradiance varies a lot is removed.

The test should be carried out at HTF's temperatures as low as possible and close to the ambient temperature, in order to minimize the effect of the heat losses. The values of the direct solar irradiance should be over 650 W/m^2 and its changes less than 15 W/m^2 .

Data should be measured during periods of approximately 3-4 times the residence time of the HTF in the collector, and every 20 or 30 minutes.

The best-fit curve to the experimental data of incidence angle modifier in large-sized PTCs has the form:

$$K(\theta) = 1 + \frac{b_1 \cdot \theta + b_2 \cdot \theta^2}{\cos \theta}$$

Where:

- b_1 and b_2 : Best-fitting parameters of the curve.

Overall efficiency (η)

This parameter measures how much useful radiant solar power is transformed into useful heat power in the absorber, so:

$$\eta = \frac{\dot{Q}_u}{\dot{Q}_s}$$

The procedure followed to determine the global efficiency of a PTC consists of running tests for the condition of maximum optical response. Different tests are done by circulating HTF through the collector absorber at different HTF temperature levels, which are defined within the working temperature range of the collector. Test must be performed maintaining steady conditions and for a minimum of four temperature levels selected from the typical working temperature range in a solar plant. Although the recommended test duration is from 10 to 20 min around the time when the incidence angle is zero, the system has to be heated up at least 1 h before running the test to up period is defined depending on the fluid temperature defined for the test, the higher the temperature the more the time is needed to heat the system.

When $\cos \theta$ is nearly 1:

$$\eta = \frac{\dot{m} \cdot \Delta h}{A_c \cdot E_d}$$

Another way of expressing the overall efficiency could be:

$$\eta = \eta_{\text{opt},0^\circ} \cdot K(\theta) \cdot F_c - \frac{\dot{Q}_1}{A_c \cdot E_d \cdot \cos \theta}$$

Where the F_c factor represents the ratio between the product of the mirrors reflectance and glass covers transmittance measured during the test and the maximum values for this parameters measured when the mirror is perfectly clean (usually $0.95 < F_c < 1$).

In summary the procedure suggested to measure the overall efficiency of a PTC oriented East-West direction by outdoor experiments is to carry out tests at solar noon, when the incidence angle is zero or very close to zero and consequently the incidence angle modifier and the $\cos \theta$ are equal to 1. The collector must be clean ($F_c > 0.99$). Taking these testing conditions into consideration, experimental data obtained depend on the temperature difference between the average HTF temperature in the absorber and the ambient temperature, the direct normal irradiance and the measured peak optical efficiency. As a result, the curve fitting the overall efficiency data has the form:

$$\eta = \eta_{\text{opt},0^\circ} - \frac{a_1' \cdot \Delta T + a_2' \cdot \Delta T^4}{A_c \cdot E_d}$$

Where:

- a_1' : Fitting parameter related mainly to convection and conduction heat losses in W/K.
- a_2' : Fitting parameter related to radiation heat losses in W/K⁴.

2.3.7. DYMOLA

As it has been said at the beginning of this text the objective of this project is to see how different parameters affect to the efficiency of a PTC. In order to achieve this objective it is necessary the help of a simulation tool, so the different situations are brought out. The simulation tool used in this case is “Dymola”. First it is going to be introduced some simulation tools in order to get an idea of why has Dymola been selected, then Dymola will be introduced and finally it is going to be described the model that has been used during this project.

2.3.7.1. Modelling and simulation tools

In this paragraphs they are going to be presented the different simulation tools that can be used for the modelling of the PTCs.

Transient Systems Simulation Program (TRNSYS)

TRNSYS is a transient systems simulation program, widely used in the simulation of solar systems and buildings, with a modular structure. It recognizes a system description language in which the user specifies the components that constitute the system and the manner in which they are connected. The TRNSYS library includes many of the components commonly found in thermal and electrical energy systems, as well as component routines to handle input of weather data or other time-dependent forcing functions and output of simulation results. The modular nature of TRNSYS gives the program tremendous flexibility, and facilitates the addition to the program of mathematical models not included in the standard TRNSYS library. TRNSYS is well suited to detailed analyses of any system whose behaviour is dependent on the passage of time. TRNSYS has become reference software for researchers and engineers around the world. Main applications include: solar systems (solar thermal and photovoltaic systems), low energy buildings and HVAC systems, renewable energy systems, cogeneration, fuel cells.

However the paradigm of object-oriented models is partially developed and often there are problems of convergence due to the inability of the program to allocate computational causality.

System Advisor Model (SAM)

It is a software developed by the National Renewable Energy Laboratory USA (NREL). It is free to access and has a broad base of meteorological data in a variety of locations. Beside the parabolic trough CSP module, has other modules of other solar technologies such as photovoltaic, thermal tower, Fresnel technology or Stirling dishes; and other renewable energies such as wind, geothermal and hydropower.

It is especially specified for general feasibility study of a plant, making predictions of performance and associated energy costs. It has a very powerful financial models encompassing different scenarios designed to facilitate decision-making from project managers, energy policy analysts, technology developers and researchers. However it lacks the capacity of a detailed performance analysis, limiting it to low-resolution annual studies.

IPSEpro

It is a modular software developed by SimTech. It aims to give solutions to plants throughout its life, from design to operation through the verification of the actual measurements in acceptance testing. Among its uses are those of calculating energy balances and predicting by design the preliminary performance, verify and validate instrumental measurements during

acceptance testing of plants, monitoring and optimizing the performance of the on-line plant and plan modifications and improvements for existing plants. In addition to solar thermal parabolic trough collector plants, IPSEpro also offers modelling and simulation solutions for thermal plants with fossil energy, geothermal energy, desalination, refrigeration, washing emission gases and biomass gasification plants.

It is structured in libraries and has great flexibility to develop new models through a development package of new models for the user. The library has well-developed solar thermal models although there is no pre-assembly of these in macrosystems characteristic of Concentrated Solar Plants (CSP), resulting tedious and complicated their composition from the primary elements. The problem with this software is also the high cost of licenses.

PCTrough

This particular model was developed by Flabeg and is specified for customers of CSP plants to take it as a standard against which measure the annual operation of the operating companies, who must defeat him after a year. The model is a black box in which is calculated the result of electricity produced from the introduction of meteorological data. The operating range in which the model is accurate is limited and flexibility of modification is void because of the protection that the developer submits and intransigence of customers and operators to have a fixed pattern in which compare their annual efficiency.

Matlab-Simulink

The famous Mathworks tool for modelling and simulation has also been used for some studies, developing models for CSP plants on a commercial basis and CSP plants for innovative research centres. Simulink is very powerful to model and simulate blocks so it is very useful for the control systems. However the modelling paradigm is not linked to objects so the flexibility to study new cases is low, the physical sense of the plants are disfiguring and modification of the models is tedious and induces great potential for error during modelling.

Renovetec solar thermal simulator

This solar thermal simulator uses SCADA LabVIEW program and is primarily developed to serve as a training platform for operators although you can also check the status of each of the major equipment that make up the plant simulator comparing the result with the actual values. In addition to solar thermal power plants of parabolic trough collector, Renovetec has developed so far of this work four more simulators for the following applications: biomass plants, combined cycle plants, cogeneration plants and coal thermal power plants.

Although the *termosolare* simulator has been compared with a real plant located in Ciudad Real and small deviations are achieved, the low flexibility to change settings for other types of plants and operating procedures makes the simulator limited for more complex applications.

Modelica

Modelica is a free language object-oriented modelling specially designed for modelling complex multiphysics systems and whose standard library and other accessible libraries contain a large amount of mechanical, electrical, electronic, thermal, control components... with open code and they have great potential for modification, reuse and adaptability.

The language can be supported by multiple modelling environments both free and commercial. Among free are the following:

- JModelica.org

- Modelicac, Scicos
- OpenModelica

Dymola is a commercial simulation environment developed by Dassault Systemes and its main feature is that it has a graphical editor, plus utilities for communication from the models with Simulink.

Table 1. Comparison of the different simulation tools.

Simulation tool	Modular	Easy to use	Possible to daily analysis	Flexible and adaptable	Free modelling environments
TRNSYS	YES	NO	YES	YES	NO
SAM	NO	YES	NO	NO	YES
Renovetec	NO	YES	YES	NO	NO
IPSEPro	YES	YES	YES	YES	NO
PCTrough	NO	YES	YES	NO	NO
Matlab-Simulink	NO	NO	YES	YES	NO
Renovetec	NO	YES	YES	NO	NO
Modelica	YES	YES	YES	YES	YES

The selected model in order to achieve the objectives described at the beginning of the present document is the Modelica language in the Dymola environment.

2.3.7.2. Introduction to the program

Dymola (Dynamic Modelling Laboratory) is a commercial modelling and simulation environment based on the open *Modelica* modelling language. The first version of Dymola was initially designed in 1978 by Hilding Elmqvist, for his PhD thesis at Lund University (in 1978 called Lund Institute of Technology). This first version was based on the *Dymola modelling* language and was implemented in *Simula 68*. Later it was re-implemented in C++.

In 1991, Elmqvist created the Swedish company *Dynasim AB* to continue the development of Dymola. In 1996, he initiated the Modelica design effort. The goal was to develop an object-oriented language for modelling of technical systems to reuse and exchange dynamic system models in a standardized format. Modelica is based on the Dymola language, but the experience with the Dymola language and with other modelling languages have been taken into account. In September 1997, version 1.0 of the Modelica specification was released which was the basis for a prototype implementation within Dymola. In the year 2000, the non-profit *Modelica Association* was formed to manage the continually evolving Modelica language and the development of the free *Modelica Standard Library*. For some transition period, the Dymola software supported both the Dymola and the Modelica language. Since 2002, only the Modelica language is supported.

In 2006, *Dassault Systèmes* acquired Dynasim and started to integrate Dymola in *CATIA*. In 2010, *Dassault Systèmes AB*, Sweden was created and *Dynasim AB* is now part of this subsidiary of *Dassault Systèmes*.

Dymola is suitable for modelling of various kinds of physical systems. It supports hierarchical model composition, libraries of truly reusable components, connectors and composite casual connections. These model libraries are available in many engineering domains. Dymola uses a modelling methodology based on object orientation and equations. The usual need for manual conversion of equations to a block diagram is removed by the use of automatic formula manipulation. Other highlights of Dymola are:

- Handling of large, complex multi-engineering models.
- Faster modelling by graphical model composition.
- Faster simulation symbolic pre-processing.
- Open for user defined model components.
- Open interface to other programs.
- 3D Animation.
- Real-time simulation.

2.3.7.3. Introduction to the model

In order to build the model, there have been used the next libraries:

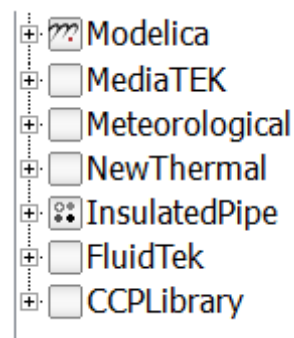


Figure 17. Libraries from Modelica.

- **Modelica:** This is the standard library from Modelica. It has many different models, from simple ones such as units from the International System or constants, to complex ones like thermal, mechanical or electric components. These basic components will be used to make more complex components.
- **MediaTEK:** This library contains different fluids that doesn't have Modelica, such as Heat Thermal Fluids. This Library contains the Syltherm® 800 fluid which is the one that will be used during this project.
- **Meteorological:** Contains the different components needed to establish the ambient conditions.
- **NewThermal:** This model encloses distinct models of different materials and heat transfer materials, which are not in the *Modelica* standard library.
- **InsulatedPipe:** It contains different models for the insulated pipes used to join the collectors.
- **FluidTEK:** This library is the same as the library "Fluid" of *Modelica*, but has some new medium models that don't appear in it.
- **CCPLibrary:** On this library there are the main components used to build the model.

To build the final model, the one created for the simulation, different components have been used, this components have been made by simpler components, and at the same time this components have been built from simpler ones, and so on until ultimately basic components from the *Modelica* standard library are reached.

Now the components that really have interest for the understanding of the model that concerns us will be explained. To do this, the explanation will start from the final model and will go down until the basic components.

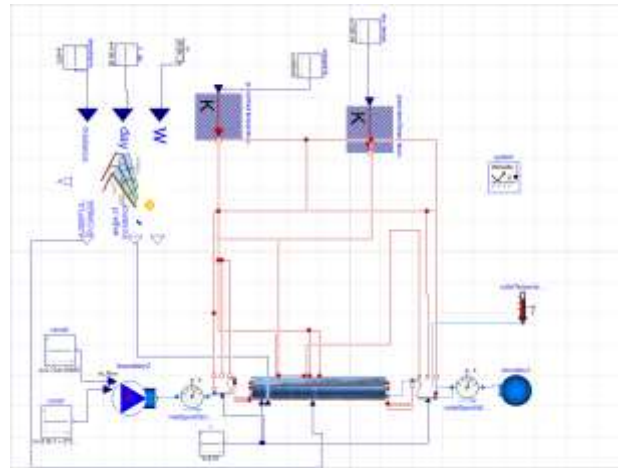


Figure 18. Complete model in Dymola.

The final model is the one presented in the picture above. It is formed by the next submodels:

- *Collector.*
- *SolarPower4Loop.*
- *Endin and EndOut.*

This submodels have been formed in a modular way, i.e. starting from basic and simple models, claspig each other are formed more complex models, till this submodels are reached.

Some of the models also used are from the *Modelica* standard library.

Collector

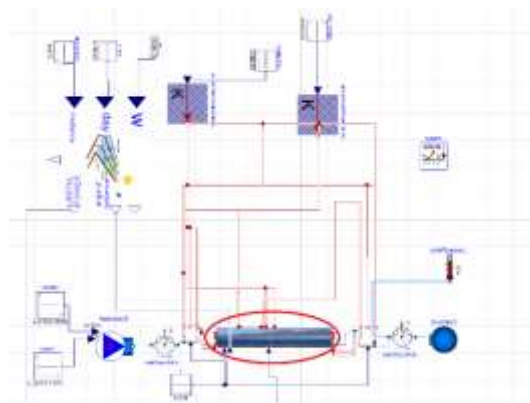


Figure 19. Complete model with the collector submodel rounded.

This is the most important part of the model, it represents the behaviour of the collector, which in the reality might be the absorber tube and the glass envelope, formed by six modules (SCAs) of 12 m length, and 18 units of the PTR®70 absorber.

As it has been previously said, this model has been formed from some simple basic models. In this case the smallest base model is, the *SimpleRing*, it represents the heat transfer in a piece of tube. It can be used for the glass cover or for the absorber metal tube. This base model is formed by a component of inertia, to illustrate the heat storage of the material; it's also formed by 4 conduction heat transfer components, which describe the longitudinal and the transversal heat transfer through the model, this components have been taken from the *Modelica* standard library.

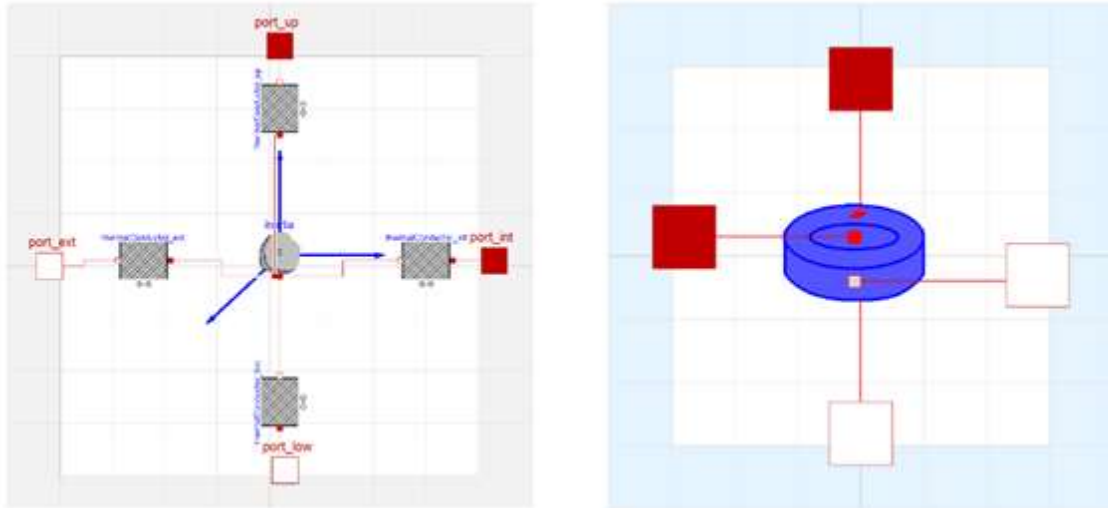


Figure 20. *SimpleRing* Dymola (left) and its representation in the simulator (right).

As it can be seen in the picture above there are also four ports, this are used to represent the entrance and exit of heat flows. There will be this kind of ports in all the collectors, they are also contained in the *Modelica* standard library.

The next step in the formation of the model, is the *SimpleCylinder* and the *MultipleCylinder*. The first is formed by a group of *SimpleRings* and is used to illustrate the glass cover. The second one is formed by a group of *SimpleCylinders* concentric relative to each other and it represents the metal absorber tube (it is formed by a group of *SimpleCylinders* so the different layers of the tube are displayed).

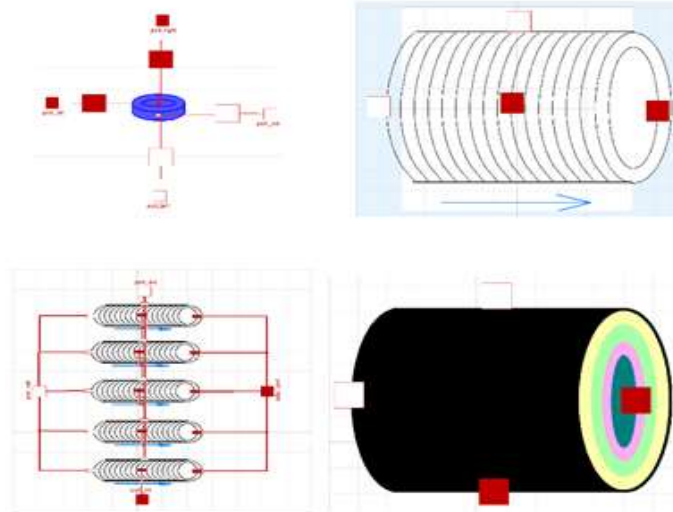


Figure 21. *SimpleCylinder* in Dymola (top-left) and its representation in the simulator (top-right). Also the *MultipleCylinder* (down-left) and its representation (down-right).

The group of the *SimpleCylinder* and the *MultipleCylinder*, joined by two components of heat transfer, one to represent the radiation between the two cylinders and the other one to represent the convection heat transfer in a vacuum ambient (contained in the *NewThermal* library; they are explained below), form the model called *BaseReceiverTest*.

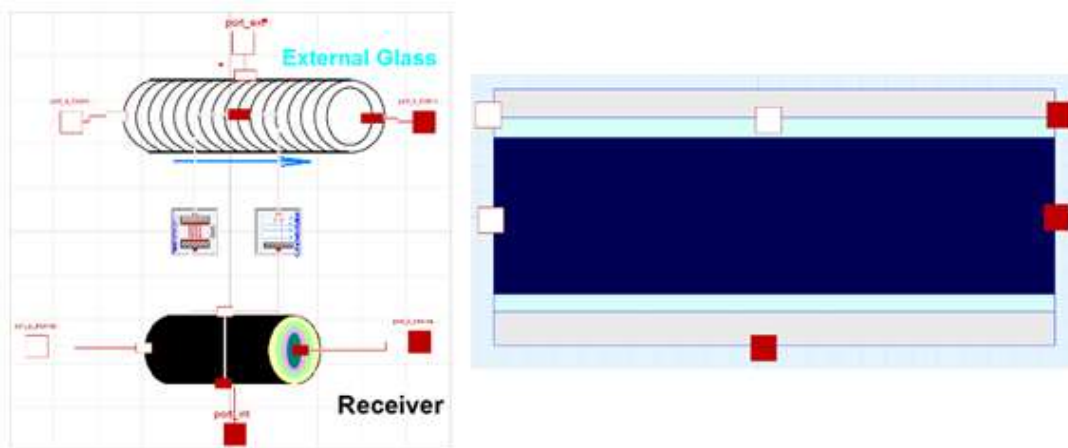


Figure 22. *BaseReceiverTest* in Dymola (left) and its representation in the simulator (right).

Next they will be explained the different possible components that are used to represent the heat transfer between the absorber and the glass cover; and which are the equation and correlations that dictate the behaviour of the mentioned components.

- RadiationConcentricCylindersSchott

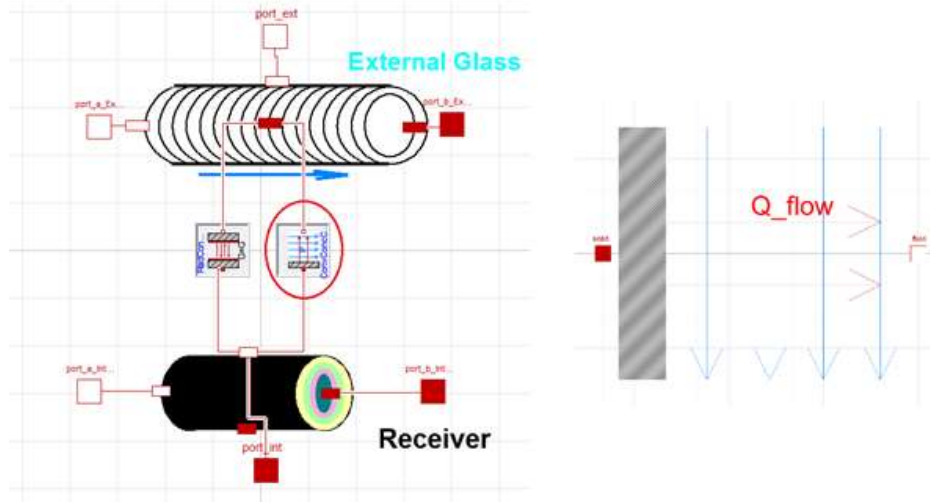


Figure 23. Component of the radiation in the interior of the collector.

It is used to quantify the heat transference from the metal tube to the glass cover, through the radiation mechanism. This model is used once the model is validated.

The equations that express the heat transference are which follow:

$$Q = Gr \cdot \sigma \cdot \Delta T$$

- $\Delta T = ABS(T_{solid} - T_{fluid})$.
- σ : Stefan – Boltzmann constant.
- $Gr = \frac{2 \cdot \pi \cdot \frac{D_i}{2} \cdot L}{\left\{ \frac{1}{\varepsilon_i} + \left[\left(\frac{1}{\varepsilon_o} + 1 \right) \cdot \frac{D_i}{D_o} \right] \right\}}$
- D_i : outer diameter of the receiver.
- D_o : internal diameter of the glass cover.
- ε_o : emittance of the glass cover.
- ε_i : emittance of the receiver.

$$\varepsilon_i = -3,821 \cdot 10^{-9} \cdot T^3 + 4,702 \cdot 10^{-6} \cdot T^2 - 1,634 \cdot 10^{-3} \cdot T^2 + 0,3044$$

- RadiationConcentricCylindersConstantEmittance

It works the same way as the previous one, but in this one the emittance of the absorber is set by the user. This model is used to find the equation which governs the behaviour of the absorber's emittance once validated.

- RadiationConcentricCylindersSchott

This model is the one used at the beginning of this project, before the validation of the entire model is done. The only difference with the RadiationConcentricCylindersSchott model is the equation that governs the behaviour of the absorber's emittance.

- ε_i : emittance of the receiver. $\varepsilon_i = 3,88145 \cdot 10^{-2} \cdot e^{1.43491 \cdot 10^{-3} \cdot T}$

• ConvConcentricCylindVacuum

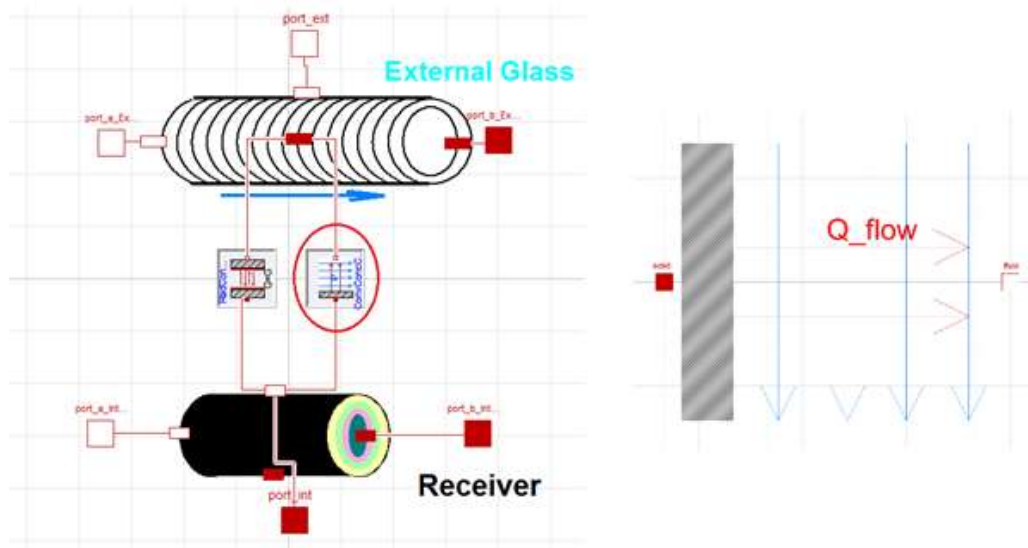


Figure 24. Component of the convection in the interior of the collector

This model is used to represent the heat transfer due to convection between the metallic tube and the glass cover. In the gap there is a vacuum atmosphere (in reality there is air at a very low pressure). The equations for the calculation of the heat flow are obtained from the next correlations.

$$Q = Gc \cdot \Delta T$$

- $\Delta T = ABS(T_{solid} - T_{fluid})$.
- $Gc = A \cdot h$.
- $A = \text{convection surface}$.
- $$h = \frac{k}{\{2 \cdot Di \cdot \log(\frac{Do}{Di}) + [b \cdot \lambda \cdot (\frac{Di}{Do} + 1)]\}}$$
- k : Thermal conductivity of the gas between the two concentric cylinders at standard temperature and pressure.
 $k = 0.02551$
- Di : outer diameter of the receiver.
- Do : internal diameter of the glass cover.
- b : interaction coefficient $b = 1,571$:
- λ : mean free path between collisions of molecule [cm].
$$\lambda = \frac{2,31 \cdot 10^{-20} \cdot T_m}{Pa \cdot \sigma^2}$$
- $T_m = \frac{T_{solid} + T_{fluid}}{2}$
- Pa : pressure in the gap.
- σ : molecular diameter of the gas [cm]. $\sigma = 3,53 \cdot 10^{-8}$

The next step is the *AbsorberSchottPSATest*, it is composed by the *BaseAbsorberTest* previously explained, four *SimpleRings*, to represent the heat transfer through the shields of the glass cover and the absorber tube; and a component called *radiatonOnTube*, this

component has as entrances the solar radiation and the angle of incidence, and as exit the real radiation that reaches the collector.

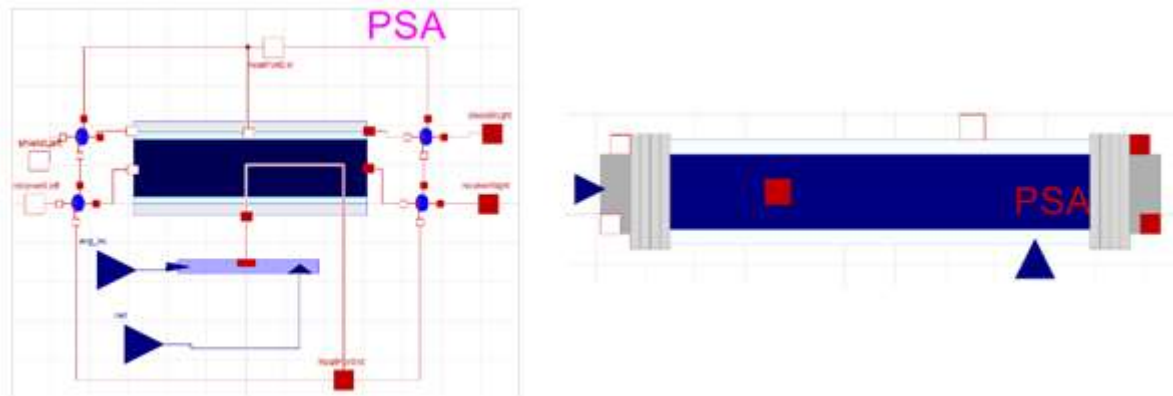


Figure 25. ReceiverSchottPSATest in Dymola (left) and its representation in the simulator (right).

The *radiatonOnTube* component is formed by a *product* component from the modelica library, which multiplies the solar radiation and the absortance of the absorber. There is also an *Absortance* component from the *CCPLibrary* that calculate the absortance from the incidence angle. The last component used is the on called *PrescribedHeatFlow* from the *Modelica* standard library.

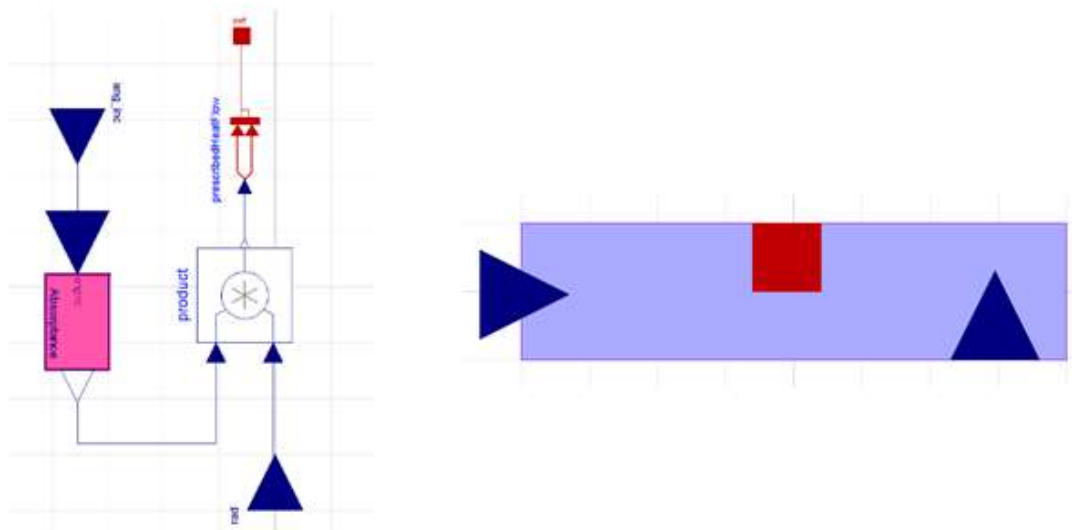


Figure 26. radiationOnTube in Dymola (left) and its representation in the simulator (right).

The next level is the *ModulePSATest*. It is formed by three *AbsorberSchottPSATest*, each has its exit heat port (*HeatPortExt*) connected to three heat transfer components, one which represents the radiation with the ambient (*radAbsorberAmb*), another one the radiation with the mirror (*radAbsorberMirror*), and the last one displays the convection with the ambient (*convAbsorberAmb*). This three components are explained below, explaining also the equation and correlations used for the formation of those components.

- NaturalConvAbsorberAmb:

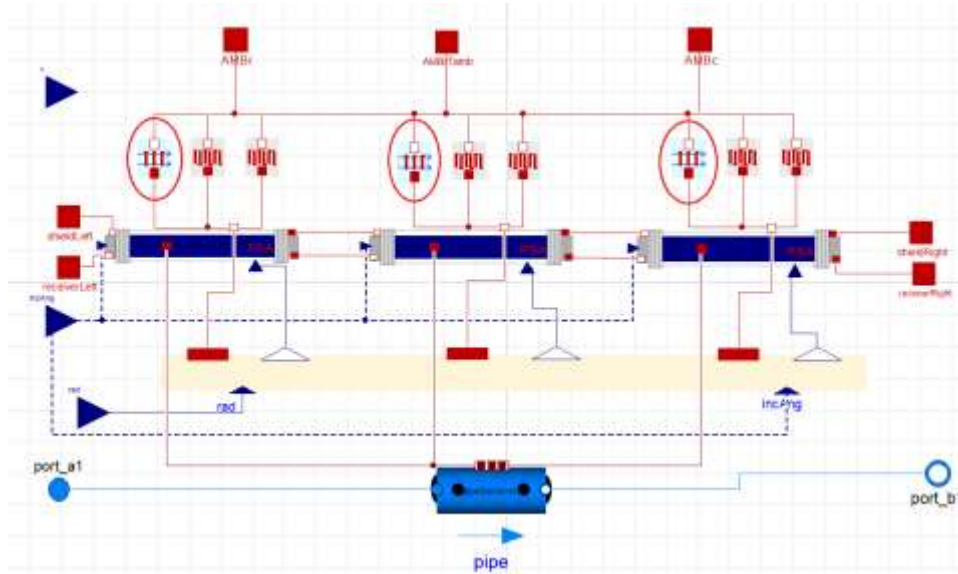


Figure 27. The three NaturalConvAbsorberAmb components.

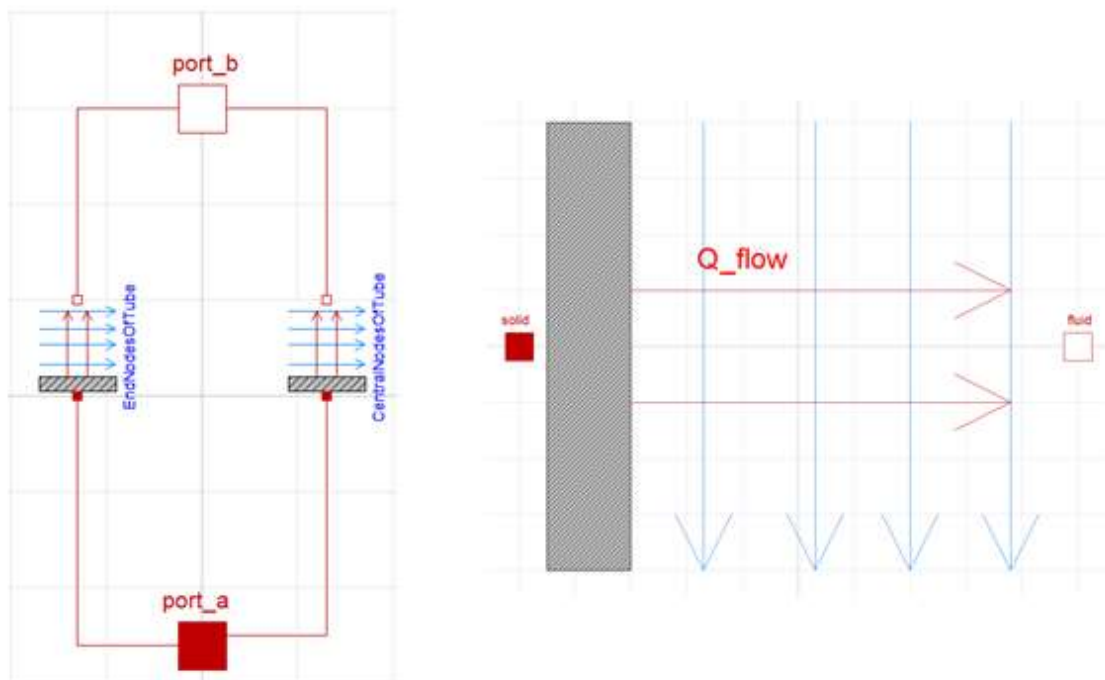


Figure 28. NaturalConvReceiverAmb component (left) and one of the NaturalConvectionHorizontalCylinder (right).

On its interior it has two convection components, one for the radiation of the middle sections of the tube, and the other for the end sections. Both are the same type of component, called NaturalConvectionHorizontalCylinder.

This model calculates the heat transfer through natural convection from a horizontal cylinder to the ambient. To implement the convection model there have been necessary some correlations. In the coming paragraphs there are explained the different correlations used.

Volumetric coefficient of expansion (β):

$$\beta = \frac{1}{V} \left(\frac{dV}{dT} \right)_P \rightarrow \text{assuming the fluid behaves as ideal gas (air)} \rightarrow \beta = \frac{1}{T}$$

Where: $T = \frac{T_{solid} + T_{fluid}}{2}$

Grashof number (Gr):

$$Gr = \frac{g \cdot \beta \cdot \Delta T \cdot D^3}{\nu^2}$$

Where:

- g : gravity acceleration, $9,81 \text{ m/s}^2$.
- $\Delta T = ABS(T_{solid} - T_{fluid})$.
- D : diameter of the cylinder.
- ν : cinematic viscosity. $\nu = \frac{\mu(P,T)}{\rho(P,T)}$
- μ : dynamic viscosity.
- ρ : density of the fluid.

Raileigh number (Ra):

$$Ra = Gr \cdot Pr$$

Where:

- Gr : Grashof number.
- Pr : Prandtl number. $Pr = \frac{c_p(P,T) \cdot \mu(P,T)}{k(P,T)}$
- c_p : Heat capacity at constant pressure.
- k : Thermal conductivity.

Nusselt number (Nu_D):

$$Nu_D = \left\{ 0,60 + 0,387 \cdot \left[\frac{Ra}{\left[1 + \left(\frac{0,559}{Pr} \right)^{\frac{9}{16}} \right]^{\frac{16}{9}}} \right]^{\frac{1}{4}} \right\}^2$$

And finally, the convection coefficient (h):

$$h = \frac{Nu_D \cdot k(P,T)}{D}$$

Once the convection coefficient is known, the heat transfer can be easily calculated by:

$$Gc = A \cdot h$$

$$Q = Gc \cdot \Delta T$$

Where:

- $\Delta T = ABS(T_{solid} - T_{fluid})$.
 - $A = \text{convection surface. } A = 2 \cdot \pi \cdot R \cdot L$.
 - R : External radius of the glass cover.
 - L : Length of the glass cover.
- RadAbsorberAmb:

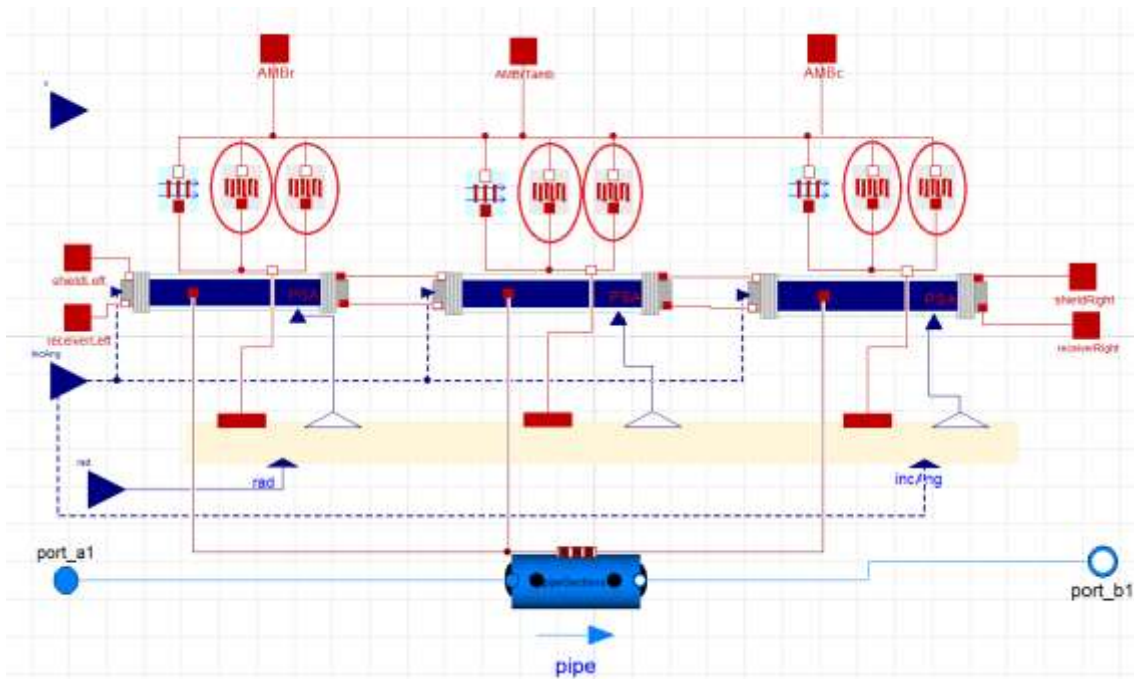


Figure 29. The six RadAbsorberAmb components.

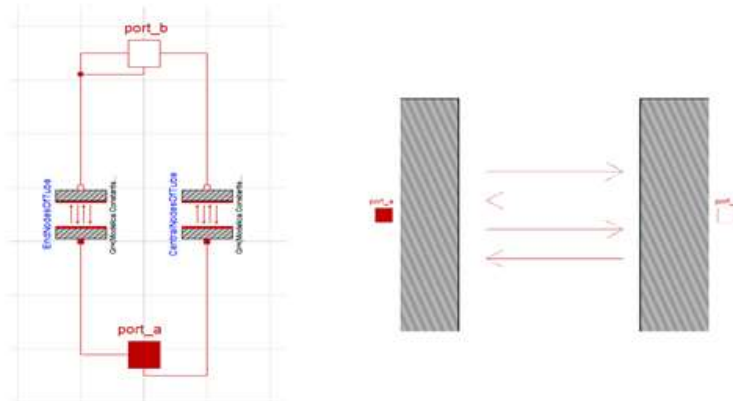


Figure 30. RadReceiverAmb component (left) and one of the BodyRadiation (right).

Is used to represent the heat transfer through radiation from the collector to the ambient. On its interior it has two radiation components, one for the middle sections and the other for the end sections. These radiation components are both the same and called BodyRadiation.

The formulation used to obtain the heat transfer is which continues.

$$Gr = A \cdot FF$$

Where:

- FF : form factor of the body which is transferin heat through radiation.
- A = interaction surface. $A = 2 \cdot \pi \cdot R \cdot L$.
- R : External radium of the glass cover.
- L : Length of the glass cover.

Finally the Heat flux is:

$$Q = Gr \cdot \sigma \cdot \Delta T$$

Where:

- $\Delta T = ABS(T_{solid} - T_{fluid})$.
- σ : Stefan – Boltzmann constant. $\sigma = 5,670367 \cdot 10^{-8} \frac{W}{m^2 K^4}$

The Form factors have been calculated outside the model. For their calculation some simplification has taken into account. The collector has been considered as a half- cylinder shaped system, with the absorber tube on its centre. Then all the form factors are calculated from the equations proposed by (R. Forristal, 2003), with the exception of the forma factor F_{31} which is obtained apling the *Cross Strings Theorem*.

Another component used to build the *ModulePSATest* is the *ModuleOptics*. This component generates the value of the incidence power due to solar radiation.

The last component that conforms the model is a *DynamicPipe* from the *Modelica* standard library.

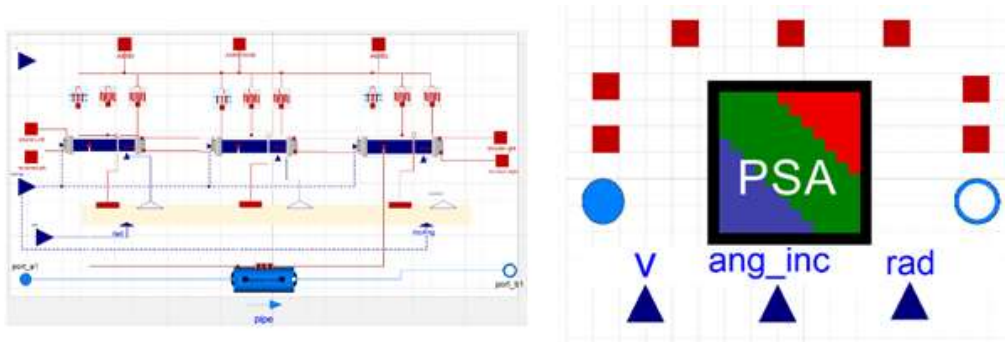


Figure 31. *ModulePSATest* in *Dymola* (left) and its representation in the simulator (right).

This pipe is trough which the HTF flows and gets heated or cooled. As it can be seen in the picture below, there are two blue ports (*port_a1* and *port_b1* from the *Modelica* standard library), they represent the entrance and exit of fluid flows.

The *Moduleoptics* component is composed by six gains from *Modelica* standard library, this will multiply te solar radiation and the absortance of the right and left shield of each receiver, to obtain the heat that those shilds will absorb. There are also three *AbsorberOptics* which calculate the radiation and the heat that will reach each absorber. It also has nine *PrescribedHeatFlow* components from the *Modelica* standard library.

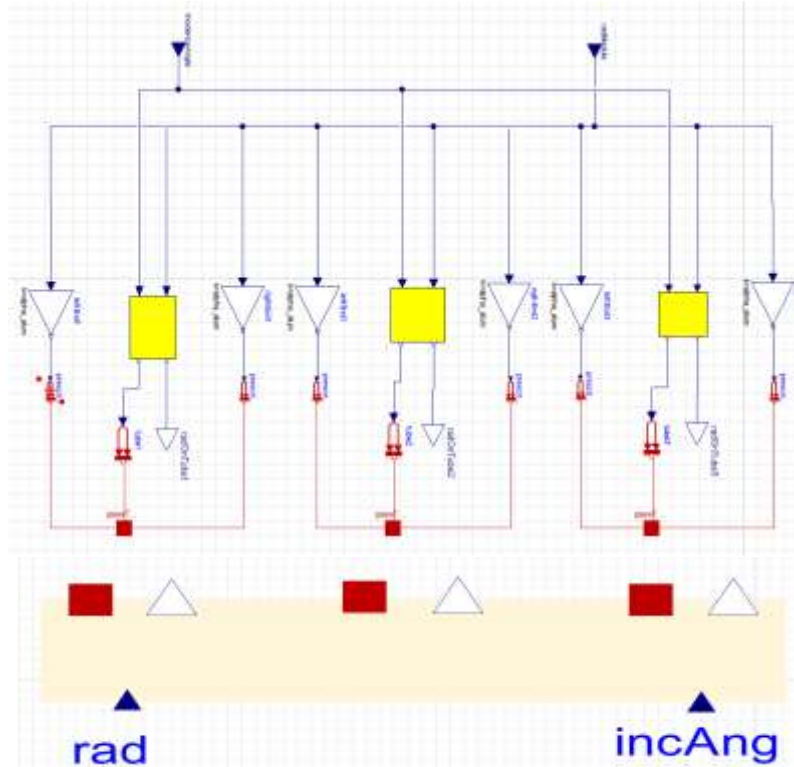


Figure 32. ModuleOptics in Dymola (above) and its representation in the simulator (down).

The last step in the formation of the collector is the SemiCollector model. It is formed by six *ModulePSATest* and one *Drive*. This last component represents the final part of the collector, where the last heat losses happen. This losses are due to convection and radiation, and a *MultipleCylinder* is used to display the the drive.

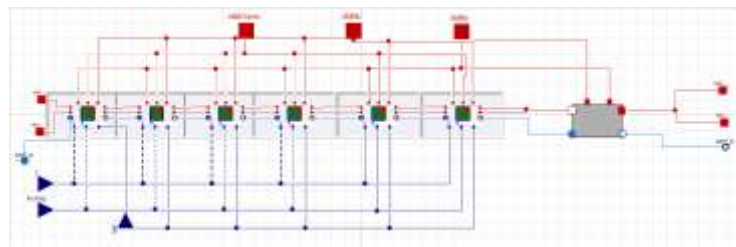


Figure 33. SemiCollector in Dymola

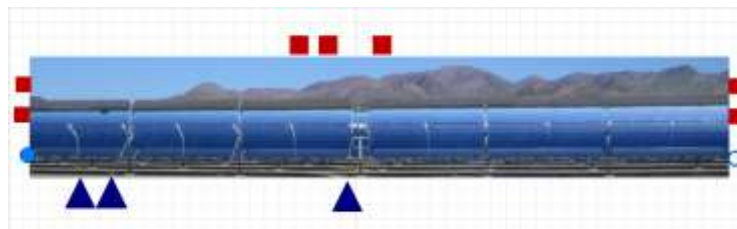


Figure 34. Representation of the SemiCollector in Dymola

The different ports that appear in the collector submodel are, the heat ports through which the heat losses will flow. The entrance and exit of the HTF. And the entrances of the radiation, the wind speed and the incidence angle.

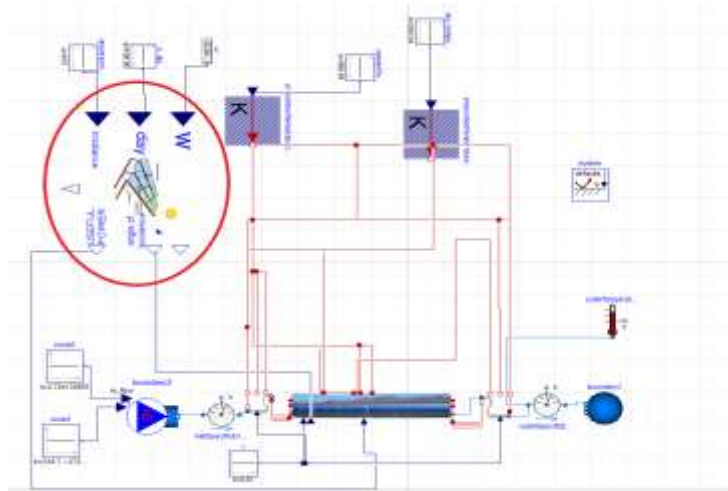


Figure 35. Complete model with the SolarPower4Loop submodel rounded.

This submodel (located in the *CCPLibrary*) calculates the values of the useful solar power, the angle of incidence and the wind speed, from the direct solar irradiance, the day of the year and the hour angle.



Figure 36. Representation of the SolarPower4Loop in Dymola.

EndIn and EndOut

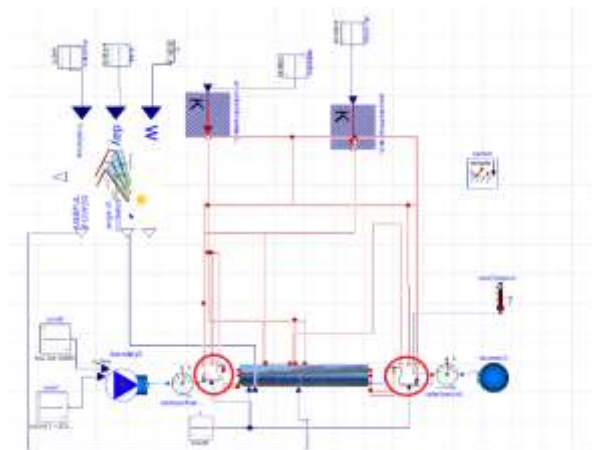


Figure 37. Complete model with the EndIn and EndOut submodels rounded.

This two models (also located in the *CCPLibrary*) represent the joint of the collector at its beginning and end. Both are equally composed, but their shape is antisymmetrical to each other.

They are formed by two *bends* from the *Modelica* standar library, in order to represent the real bends that can produce load losses. There are also a *Hose* and a *sharedPipe* (both located in the *CCPLibrary*) component trough which the HTF flows. This last two componets have some ports through which the heat losses flow. This heat losses can be due to radiation with the ambient or the mirror, and due to convection with the ambient.

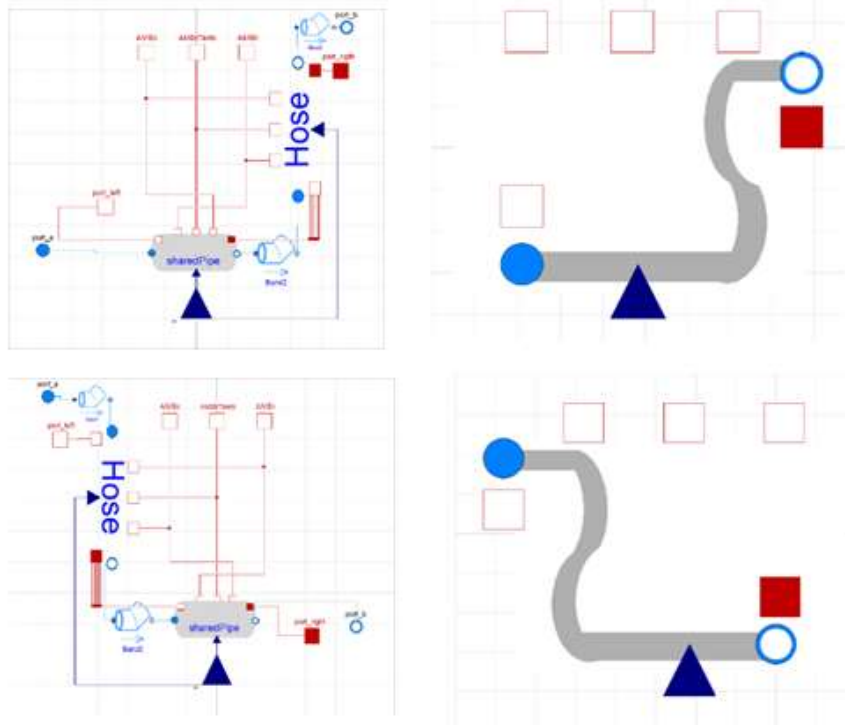


Figure 38. *EndIn* (top) and *EndOut* (down) in *Dymola* and their representation in the simulator.

The *Hose* component is build with two *SimpleCylinder* and a *MultipleCylinder*, to represent the different layers of the hose; there is also *DynamicFlexible* component from the *FluidTEK* library, this is used to represent the thermal behaviour of the HTF. There are also four *bends* from the *Modelica* standar library, as it has been said this are used to represent the bends of the real hose so the load losses are also represented. There are three heat transfer components too, one which represents the radiation with the ambient (*bodyRadiation*), another one the radiation with the mirror (*radiationHorizontalCylinderParalelPlate*), and the last one displays the convection with the ambient (*forcedConvectionCylinderPerpendicularExternalAir*), all from the *CCPLibrary*. Finally there are Five thermal ports and two fluid ports.

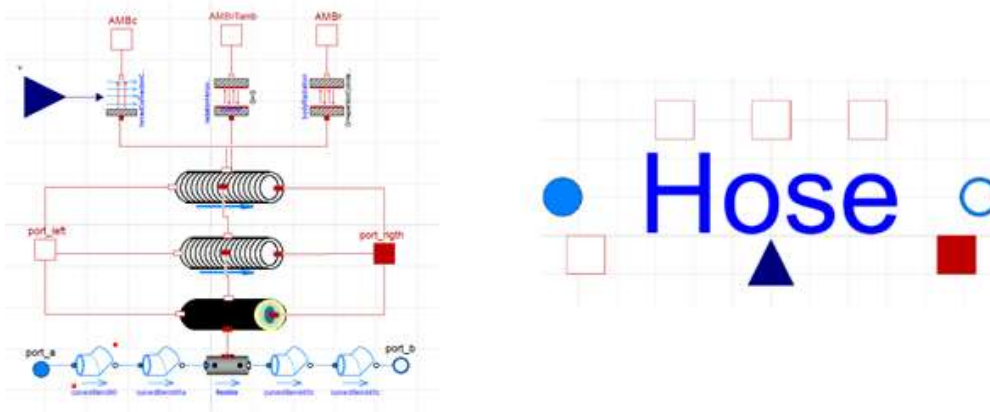


Figure 39. Hose in Dymola (right) and its representation in the simulator (left).

The component *sharedPipe* is composed of a *MultipleCylinder* to represent the different layers of the pipe. There also are, as in the case of the *Hose*, three heat transfer components too, one which represents the radiation with the ambient (*bodyRadiation*), another one the radiation with the mirror (*radiationHorizontalCylinderParalelPlate*), and the last one displays the convection with the ambient (*forcedConvectionCylinderPerpendicularExternalAir*), all from the *CCPLibrary*. Finally there are Five thermal ports and two fluid ports.

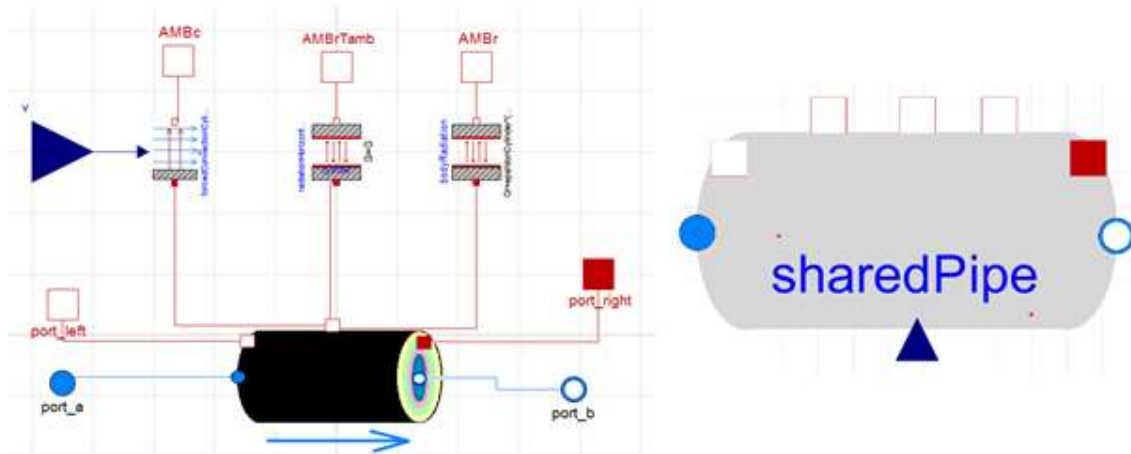


Figure 40. SharedPipe in Dymola (right) and its representation in the simulator (left).

As it has been previously said, the rest of the components that conform the principal model have been taken from the *Modelica* standard library. Some of this components are used to represent the parameters that are needed as data to display the behaviour of the model (*constant sources*, in order to quantify the direct solar irradiance, the day of the year, the ambient temperature and the sky temperature (both with a conversor that transforms the constant value on a temperature value), the HTF's inlet temperature and the HTF's mass flow; also a *RealExpression* component to quantify the value of the hour angle). The others are used as measurement tools (*inletSpecificEnthalpy*, *outletSpecificEnthalpy* and *outletTemperature*).

There are also two *boundary* components to set the conditons of the HTF before and after the entrence in the system.

Finally a *System* component is needed in each fluid model to provide system-wide settings, such as ambient conditions and overall modelling assumptions. The system settings are propagated to the fluid models using the inner/outer mechanism.

The different components from the Modelica standard library are more extensively explained in the next paragraphs.

Constant:

This component establishes a value constant in time, which has a k value. It is used to set the values of:

- Direct Normal Irradiance.
- Number of day.
- Hour angle.
- Mass flow.
- HTF's inlet temperature.
- Wind speed.
- Ambient temperature.
- Sky temperature.

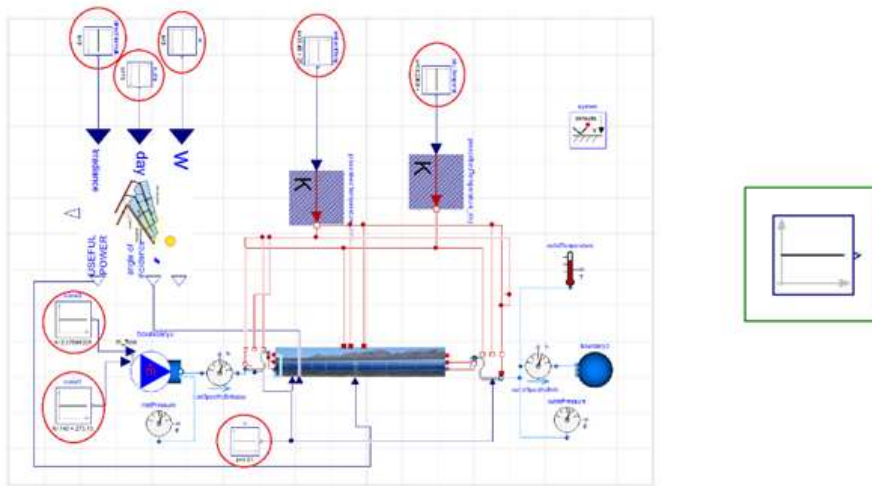


Figure 41. Location of different Constant components (left) and shape of the component (right).

PrescribedTemperature:

Transforms an input signal, such as a constant value, into a temperature signal in Kelvin. It is used to transform the constant signals of ambient temperature and sky temperature into temperature signals.

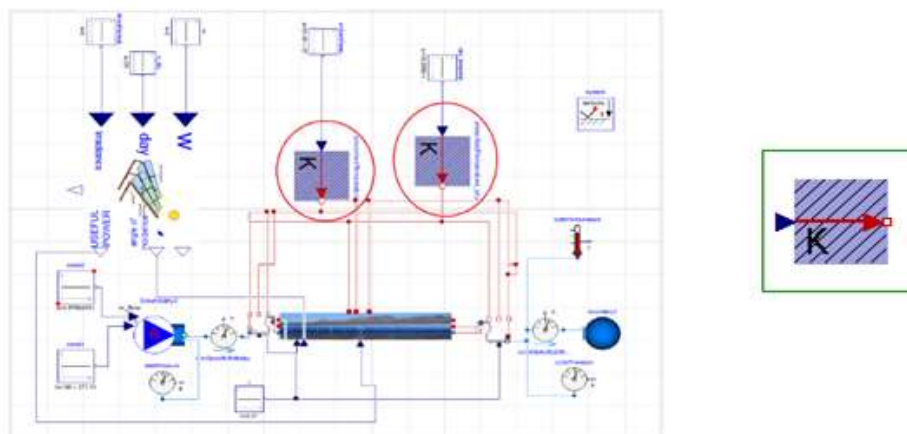


Figure 42. Location of different PrescribeTemperature components (left) and shape of the component (right).

Sensors:

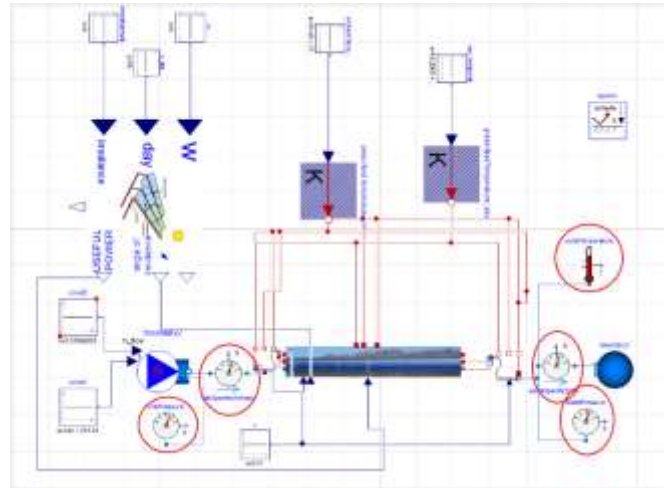


Figure 43. Location of different Pressure, Enthalpy and Temperature sensors components

- **Pressure sensor:** measures the values of pressure before (*inletPressure*) and after (*outletPressure*) the collector.

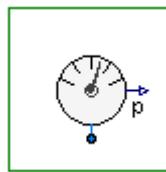


Figure 44. Pressure sensor.

- **Enthalpy sensor:** measures the values of enthalpy before (*inletSpecificEnthalpy*) and after (*outletSpecificEnthalpy*) the collector.

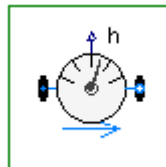


Figure 45. Enthalpy sensor.

- **Temperature sensor:** measures the temperature of the HTF at the exit of the collector (*outletTemperature*).

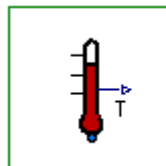


Figure 46. Temperature sensor.

MassFlowSource_T:

Ideal flow source that produces a prescribed mass flow with prescribed temperature, mass fraction and trace substances. In this case it is just established the mass flow and the inlet temperature, as well as the kind of fluid (Syltherm® 800).

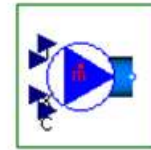
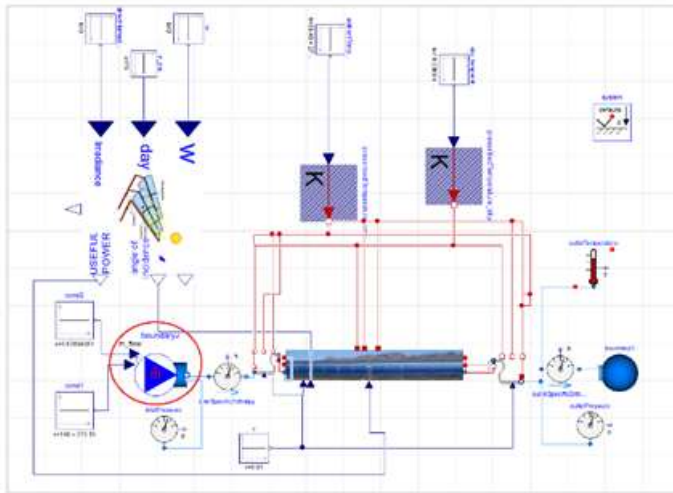


Figure 47. Location of the MassFlowSource_T component (left) and shape of the component (right).

FixedBoundary:

This model is used when using a fluid. Needs to have defined some constant values of boundary conditions:

- Boundary pressure or boundary density.
- Boundary temperature or boundary specific enthalpy.
- Boundary composition (only for multi-substance or trace-substance flows).

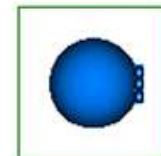
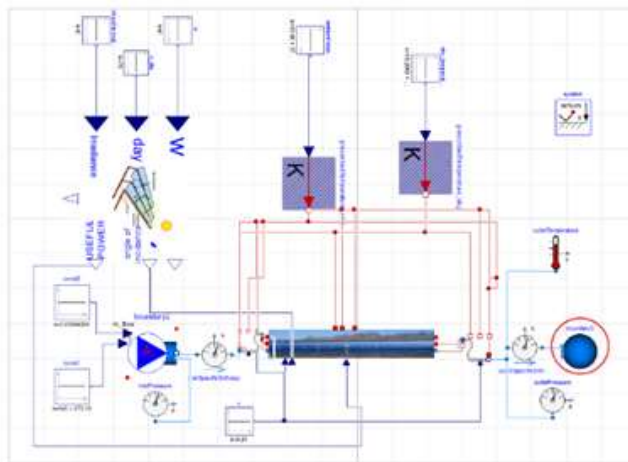


Figure 48. Location of the FixedBoundary component (left) and shape of the component (right).

System:

It is necessary in each fluid model to provide system-wide settings, such as ambient conditions and overall assumptions. The system settings are propagated to the fluid models using the inner/outer mechanism.

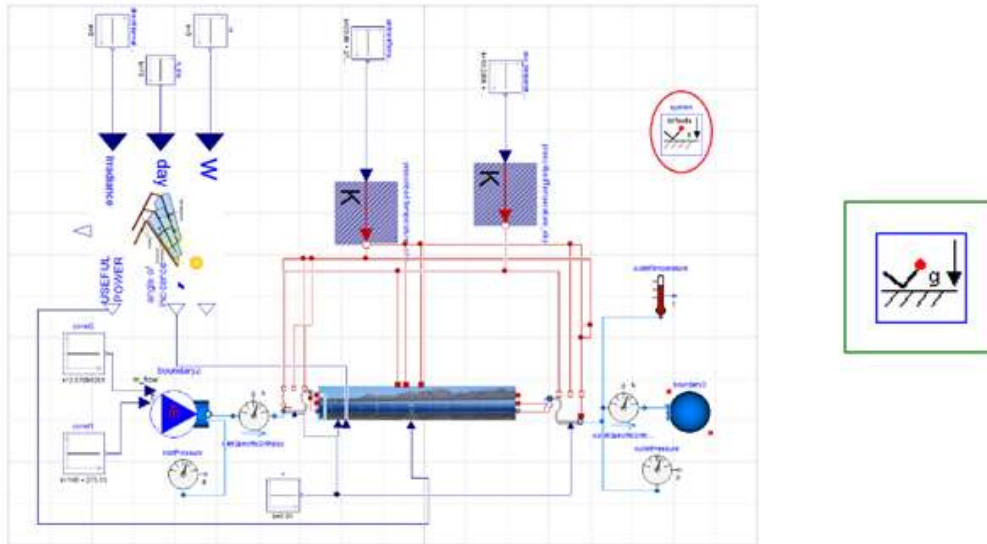


Figure 49. Location of the System component (left) and shape of the component (right).

Finally it is also possible to introduce data that depends on the month of the year. This has been obtained from the data collected by the PSA for each month. This data is tabulated and with the help of a *CombiTimeTable* it is transformed into the parameters that the simulator needs.

In order this works, there are also necessary some new components.

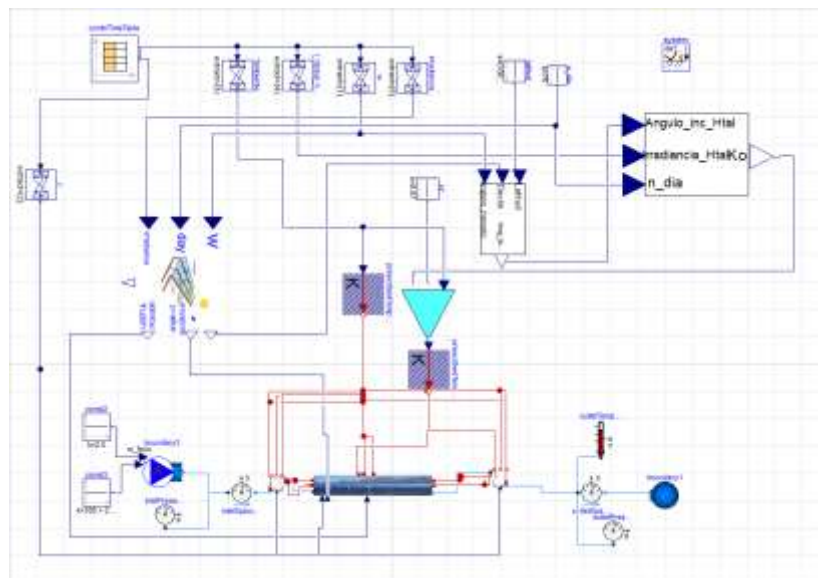


Figure 50. Model CollectorPSAwithMeteoDataTest.

- *ang_inc_Htal*: obtains the horizontal incidence angle from the latitude and declination of the plant, and the hour angle.
- *Indice_nubosidad*: from the horizontal irradiance angle, the number of day and the horizontal irradiance, obtains the sky clearness index which will be needed in the component *skyTemperatureDay* to know the sky temperature.
- *SkyTemperatureDay*: obtains the sky temperature from the sky clearness index and the relative humidity of the ambient, depending whether the sky is clear or not.

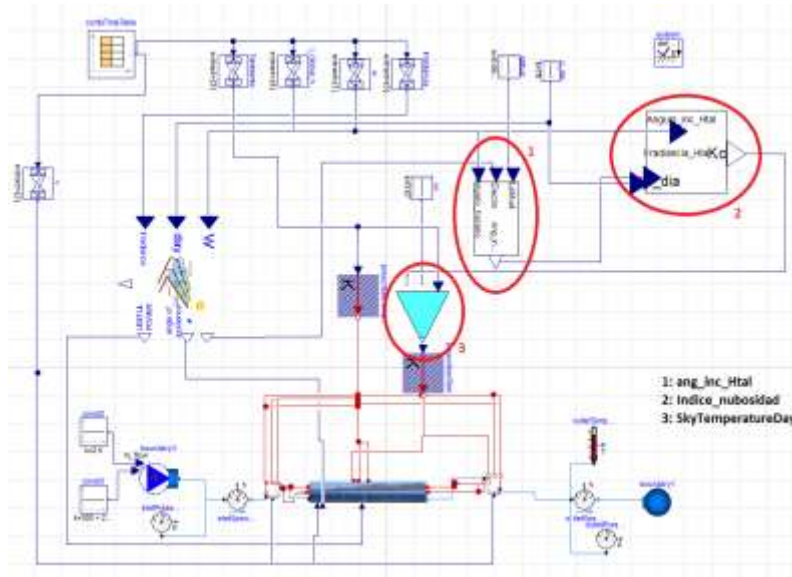


Figure 51. Model CollectorPSAwithMeteoDataTest with the new components marked.

Finally it has to be specified in each component where the Heat Thermal Fluid appears, the medium it is going to be used. In this case that medium is called Syltherm® 800 and is located in the MediaTEK library. This model with the help of the package from Modelica standard library establishes some state conditions of the HTF from its temperature and pressure. These state conditions are its density, heat capacity, conductivity, viscosity and vapour pressure.

2.4. Risk analysis

The implantation of a solar collection plant has nowadays some risks that should be marked.

For example, still nowadays the solar technology needs a benign regulation that allows it to obtain benefits from its exploitation. The main disadvantage of the thermal solar plants, is that they can only operate when there is sun (direct solar irradiance), so it is necessary a system to save the excess energy produced during day to use it at night or when there is not enough solar irradiation. Although in this respect many developments have been made, such as the use of thermal salts which have a huge thermal inertia, or the use of better electric batteries every day, there is still a long way to go.

Regarding what attains to this specific project, the main risks that have to be taken into account is when using the modelling program, because as it has been seen, many simplifications have been made. These simplifications, if not taken into account every time the model is simulated, can lead to obtaining results with huge errors.

Also, as it has been said, the used model has required a validation in order to ensure that the results it gives are close enough to the real results. During this validation it has been accepted an error percentage which has been considered low enough for the experiments which would after been carried out. But when using this same model for another use, it has to be taken into consideration that the model has been validated to use it to some purposes; when the aim of this model is distinct to the one during this project, it has to be used with caution so the error doesn't get bigger to unacceptable values.

3. METHODOLOGY

In the next paragraphs it is explained how the model has been validated, in order to have its results as close to the real ones as possible. First it has been analysed the influence of different parameters in the behaviour of the model. This has been carried out to choose the parameter which would be used for the validation.

3.1. Initial problems with the model.

The simulation model when the attaining project begun, was not totally “correct”, the heat losses that the model gave were less than what they should be in the reality. The main reason for this was that it is very complex to build a model which represents the reality exactly as it is, it is necessary to make some simplifications. Also, as the model was previously validated for another collector during another project, it was possible that some considerations made during that project were not the same as the ones necessary for this one. This could lead to an “error” in the model.

In the first instance, to know if the model had an error, and if it did, which it was, it was made a detailed study and found the nonexistence of any error in the formulation of the various correlations and equations that appear in it.

After checking the nonexistence of any error, it was studied different possibilities that could make the resulting heat losses of the model been less than the real losses.

First it was made a new model which considered there was no fluid flowing through the collector. This way, if the heat losses obtained correspond with the real ones, then the error would be in the heat transference from the fluid to the absorber’s inner part.

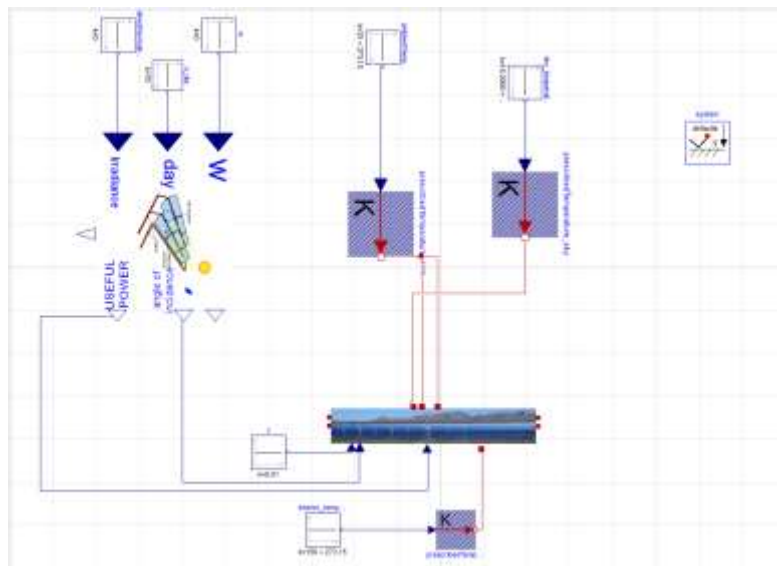


Figure 52. Model of the semicollector without HTF flowing through it.

In the picture above it is shown the model of the collector without fluid flowing through it. The temperature of the inner part of the absorber is set by a *HeatPort_a* from the *Modelica Standard Library*. This port allows the heat transference through it; and, as it has been said, establishes the temperature of the inner part of the absorber.

It has also been necessary the construction of some submodels, such as, the *SemiCollectorNoFluid* and the *ModulePSATestNoFluid*, which are the same as the *SemiCollector* and the *ModulePSATest* respectively, but without the fluid.

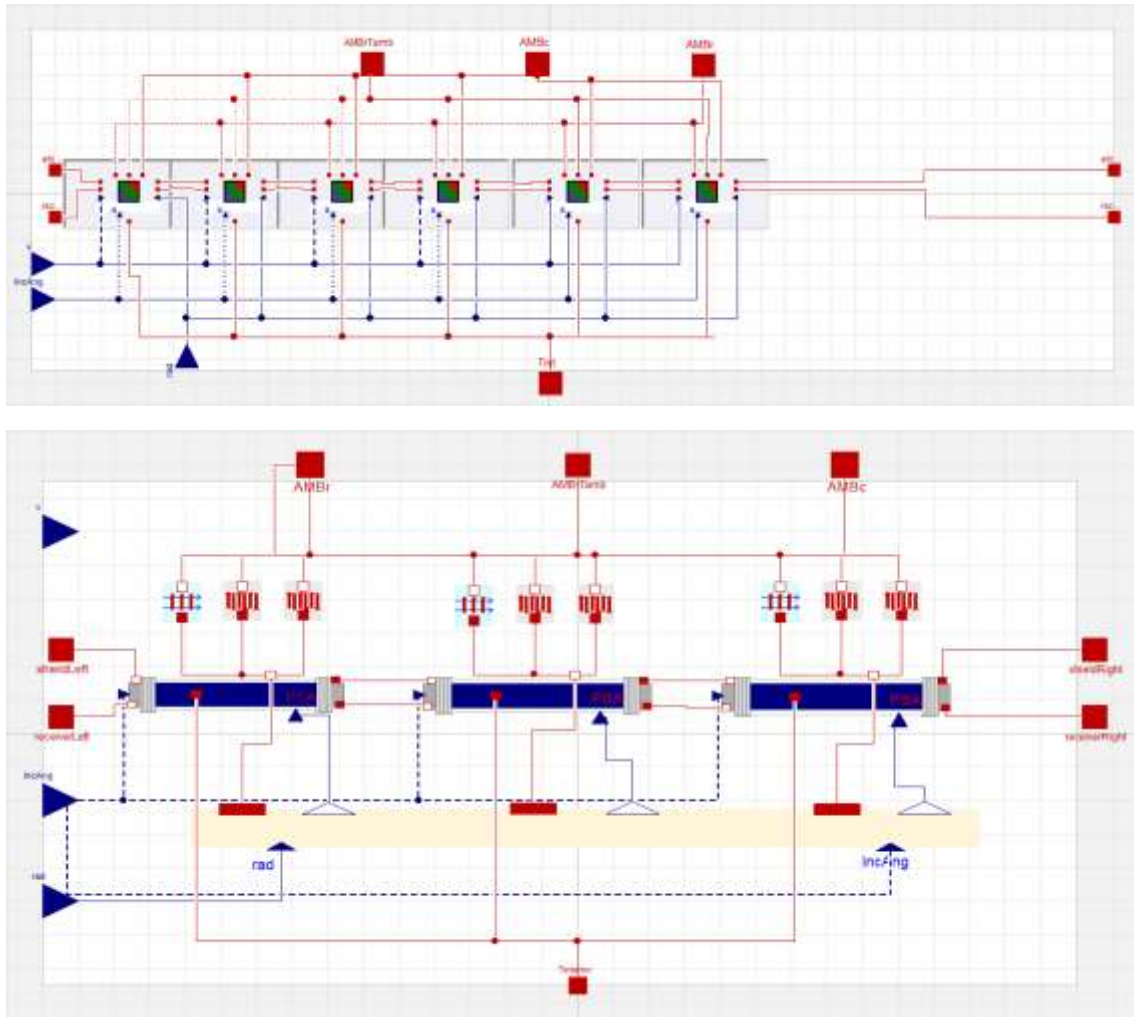


Figure 53. Submodels of *SemiCollectorNoFluid* (above) and the *ModulePSATestNoFluid* (below).

The model has been simulated and compared to the normal case where there is fluid (in this normal case the *endIn* and the *endOut* components have been taken out so the comparison is more reliable). The data used for both simulations (and also for the ones explained later) is:

- Direct Normal Irradiance=0 W/m².
- Ambient Temperature= 25 °C.
- Inlet HTF Temperature= 40-90-140 °C.
- Sky temperature= 18 °C.
- Mass flow=3,57694351 kg/s.
- Number of day=76.
- Hour angle=0.

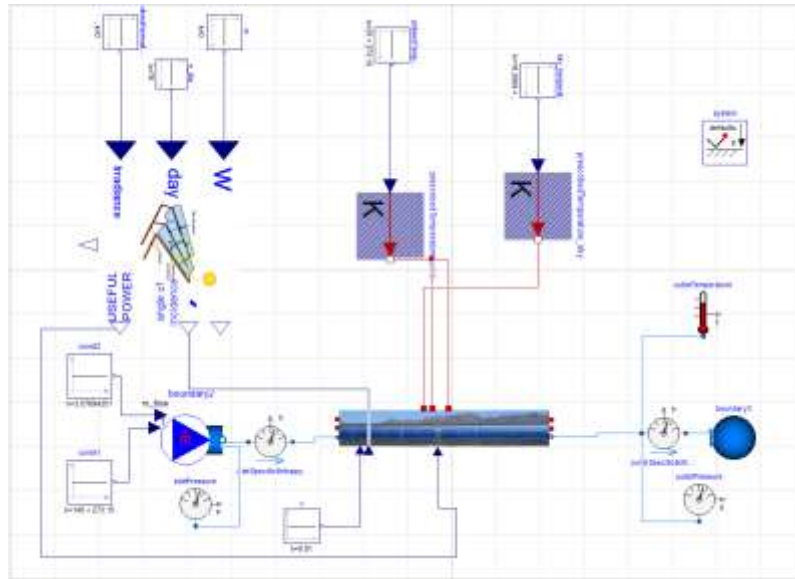


Figure 54. Model of the semicollector without endIn and endOut.

The results obtained are:

Table 2. Results of the simulation of the model without HTF.

DNI	n	w	T _{amb}	T _{sky}	Inlet T	Losses				Real heat losses
						Ambr	Ambc	Ambr Tamb	Total Losses	
0	76	0	25	18	40	-475,224	296,392	49,0142	129,8178	532,5
0	76	0	25	18	40	-473,17	299,713	45,883	127,574	532,5
0	76	0	25	18	90	-762,888	114,06	25,6875	623,1405	2307,5
0	76	0	25	18	90	-761,804	126,568	23,9961	611,2399	2307,5
0	76	0	25	18	140	-1292,06	-108,115	-18,4807	1418,656	4082,5
0	76	0	25	18	140	-1294,4	-85,5187	-17,5523	1397,471	4082,5

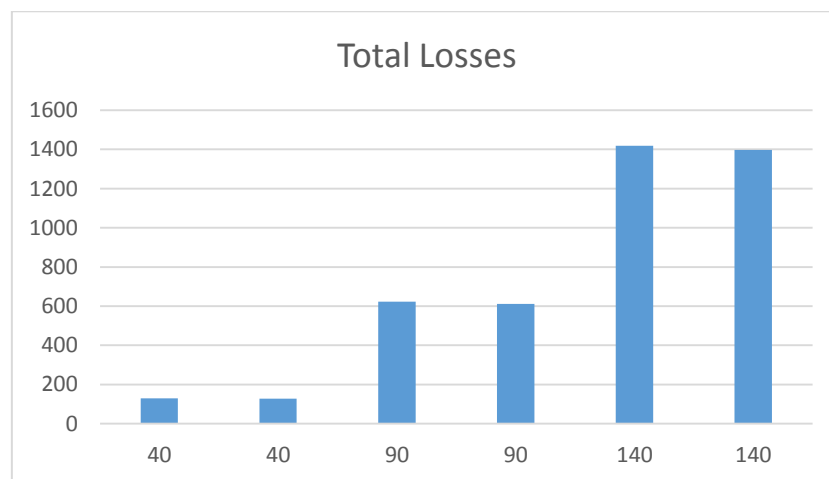


Figure 55. Results of the simulation of the model without HTF.

As it is shown in the tables above, the changes made don't affect considerably to the heat losses, so this possible error was discarded.

Afterwards, it was proceeded to analyse whether the simplifications during the calculation of the form factors could be the reason for the error. In the initial model, the form factors were calculated with the simplification of supposing that the parabolic mirror had half-cylinder shape. To check if this was the source of the error, the form factors were recalculated considering the mirror for what it is, a parabola.

As well as in the previous case, during the new calculation of the form factors, it has also used the Forristal and the *Cross String Theorem*.

In this case the form factors have been calculated considering the collector infinite and with a parabolic shape.

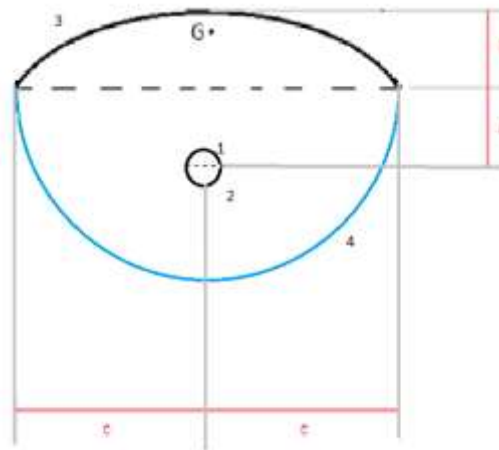


Figure 56. Real Shape of the collector, with the considered parts numbered.

Where:

$$b = \frac{c^2}{4 \cdot f}$$

$$a = b - f$$

$$c = \frac{A}{2}$$

- F: focal distance.
- A: Collector aperture.
- r1=r2: receptor's radius
- r4=c: imaginary surface's radius

$$A_1 = \pi \cdot r_1$$

$$A_2 = \pi \cdot r_2$$

$$A_3 = \left\{ \frac{2 \cdot f}{2} \cdot \ln \left[\frac{c}{2 \cdot f} + \sqrt{1 + \left(\frac{c}{2 \cdot f} \right)^2} \right] + \frac{c}{2} \cdot \sqrt{1 + \left(\frac{c}{2 \cdot f} \right)^2} \right\} - \left\{ \frac{2 \cdot f}{2} \cdot \ln \left[\frac{-c}{2 \cdot f} + \sqrt{1 + \left(\frac{-c}{2 \cdot f} \right)^2} \right] + \frac{-c}{2} \cdot \sqrt{1 + \left(\frac{-c}{2 \cdot f} \right)^2} \right\}$$

$$A_4 = 2 \cdot \pi \cdot r_4$$

- Due to convexity and flatness:

$$F_{11} = 0$$

$$F_{22} = 0$$

$$F_{12} = 0$$

$$F_{21} = 0$$

- Applying the cross strings theorem:

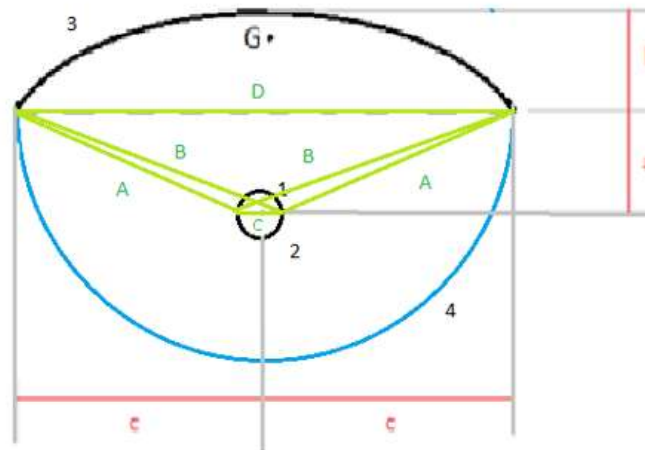


Figure 57. Scheme of the Cross String Method.

$$A = \sqrt{(c - r_1)^2 + a^2}$$

$$B = \sqrt{(c + r_1)^2 + a^2}$$

$$C = 2 \cdot r_1$$

$$D = 2 \cdot c$$

The Cross Strings Theorem establishes that the form factor F_{ij} is equal to the sum of the lengths of the strings crossing each other, extending from the ends of the two surfaces, minus the sum of the lengths of the strings uncrossed, divided by twice the length A_i .

F_{13}, F_{31}

$$F_{13} = \frac{2 \cdot B - 2 \cdot A}{2 \cdot A_1}$$

$$F_{31} = \frac{A_1}{A_3} * F_{13}$$

F_{14}, F_{41}

$$F_{11} + F_{12} + F_{13} + F_{14} = 1 \rightarrow F_{14} = 1 - F_{11} - F_{12} - F_{13}$$

$$F_{41} = \frac{A_1}{A_4} * F_{14}$$

F_{24}, F_{42}

$$F_{24} = \frac{2 \cdot B - 2 \cdot A}{2 \cdot A_2}$$

$$F_{42} = \frac{A_2}{A_4} * F_{24}$$

F_{23}, F_{32}

$$F_{21} + F_{22} + F_{23} + F_{24} = 1 \rightarrow F_{24} = 1 - F_{21} - F_{22} - F_{23}$$

$$F_{32} = \frac{A_2}{A_3} * F_{23}$$

F_{34}, F_{43}

$$F_{34} = \frac{2 \cdot D}{2 \cdot A_2}$$

$$F_{43} = \frac{A_3}{A_4} * F_{34}$$

F_{33}, F_{44}

$$F_{31} + F_{32} + F_{33} + F_{34} = 1 \rightarrow F_{33} = 1 - F_{31} - F_{32} - F_{34}$$

$$F_{41} + F_{42} + F_{43} + F_{44} = 1 \rightarrow F_{44} = 1 - F_{41} - F_{42} - F_{43}$$

$F_{(1+2)3}, F_{3(1+2)}$

$$F_{13} + F_{23} = F_{(1+2)3}$$

$$F_{31} + F_{32} = F_{3(1+2)}$$

Calling the set forming the tube (1 + 2), 1 for simplicity, and as $T_2 = T_3 = T_4 = T_5 = 0$. The resulting system of equation is which follows:

$$(A_1 \varepsilon_1 F_{11} + A_1 1R_1 F_{11} + A_3 1R_3 F_{31} + A_4 1R_4 F_{41})(1 - \varepsilon_1) = A_1 1R_1$$

$$(A_1 \varepsilon_1 F_{13} + A_1 1R_1 F_{13} + A_3 1R_3 F_{33} + A_4 1R_4 F_{43})(1 - \varepsilon_3) = A_3 1R_3$$

$$(A_1 \varepsilon_1 F_{14} + A_1 1R_1 F_{14} + A_3 1R_3 F_{34} + A_4 1R_4 F_{44})(1 - \varepsilon_4) = A_4 1R_4$$

Considering that the imaginary surfaces (2 and 4) as black surfaces.

$$\varepsilon_4 = 1$$

$$1R_4 = 0$$

So:

$$(A_1 \varepsilon_1 F_{11} + A_1 1R_1 F_{11} + A_3 1R_3 F_{31})(1 - \varepsilon_1) = A_1 1R_1$$

$$(A_1 \varepsilon_1 F_{13} + A_1 1R_1 F_{13} + A_3 1R_3 F_{33})(1 - \varepsilon_3) = A_3 1R_3$$

As ε_1 and ε_3 are known, from the system of equations it can be deduced $1R_1$ and $1R_3$ and with them \mathfrak{S}_{11} and \mathfrak{S}_{13} .

It also known that $\mathfrak{S}_{11} + \mathfrak{S}_{13} + \mathfrak{S}_{14} = 1$. As in the model when representing the energy exchange between the tube and the imaginary surface, it is really representing radiation between the tube and the sky, we can consider that: $\mathfrak{S} = \mathfrak{S}_{14}$, term obtained from the last equation.

After applying this calculations to the model, the values obtained for the form factor of the glass cover and the shield for the radiation with the sky and with the mirror are:

- $F_v = 0,918191769$ (Glass cover radiation with the sky).
- $F_s = 0,997369845$ (Shield radiation with the sky).
- $F_{v1} = 0,073715228$ (Glass cover radiation with the mirror).
- $F_{s1} = 0,002618386$ (Shield radiation with the sky).

The results obtained for the simulation with the new form factors has been:

Table 3. Results of the simulation of the model with the new Form Factors.

DNI	n	w	T amb	T sky	Inlet T	Outlet T	Losses				Real heat losses
							Ambr	Ambc	Ambr Tamb	Total Losses	
0	76	0	25	18	40	39,978	-475,224	296,392	49,0142	129,8178	532,5
0	76	0	25	18	40	39,9779	-474,717	299,659	45,0556	130,0024	532,5
0	76	0	25	18	90	89,8992	-762,888	114,06	25,6875	623,1405	2307,5
0	76	0	25	18	90	89,8991	-764,312	117,091	23,8563	623,3647	2307,5
0	76	0	25	18	140	139,781	-1292,06	-108,115	-18,4807	1418,6557	4082,5
0	76	0	25	18	140	139,781	-1297,54	-105,067	-16,3181	1418,9251	4082,5

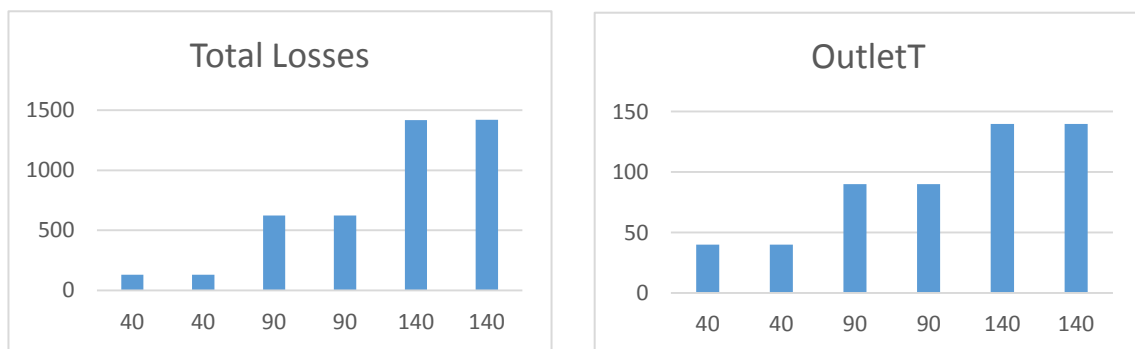


Figure 58. Results of the simulation of the model with new form factors. Total losses (left) and HTF's outlet temperature (right).

As well as in the previous case, the form factors, don't affect to the heat losses in an important way. So this failure is also discarded.

Once discarded the error in form factors, it is now examined the next possible source of error. The results presented in the article for the heat losses are provided by the manufacturer, obtained in a laboratory test (without mirrors and without HTF); and the predominant form of heat loss it is due to heat transfer by radiation the atmosphere. Therefore it is possible that the model error is due to considering both radiations with the environment and with the mirror, rather than just with the ambient. This section discusses the influence on the heat losses considering just the heat transfer through radiation with the ambient.

In order to see the influence of not having the mirror, it is necessary to build a new model where there are just heat losses through radiation with the ambient, this model is the same as the one used as data base, but without the model of radiation to the mirror. The new model does not have the *HeatPort_a* called *AMBrTamb* as it is not necessary. Finally the radiation model instead of using the form factors uses directly the values of the emittance of the glass cover and the sky.

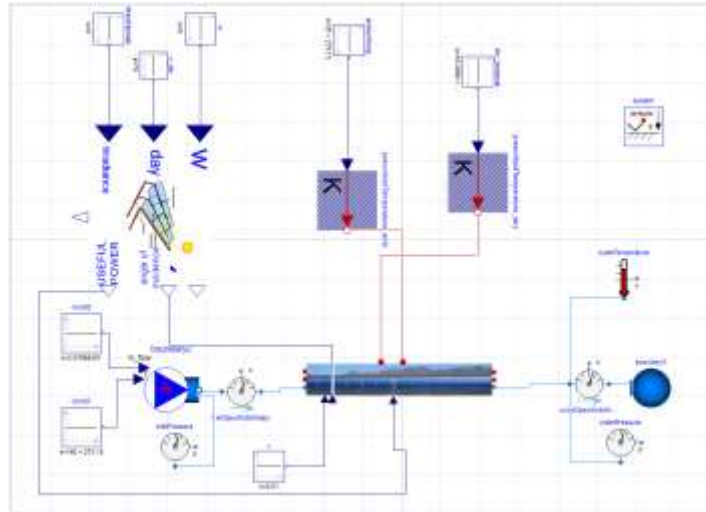


Figure 59. Model of the semicollector without heat transfer through radiation to the mirror.

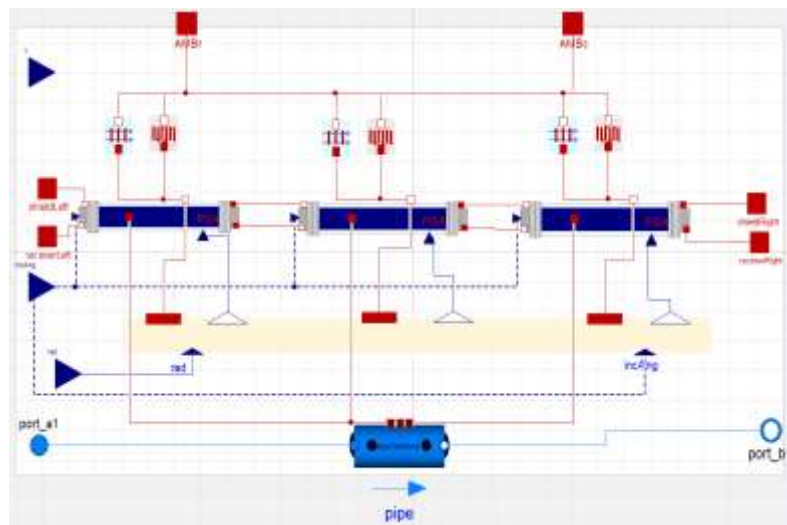


Figure 60. Submodel ModulePSATestNoMirror.

The results obtained for these simulations are presented in the next tables:

Table 4. Results of the simulation of the model without considering the radiation with the mirror.

DNI	n	w	T amb	T sky	Inlet T	Outlet T	Losses				Real heat losses
							Ambr	Ambc	Ambr Tamb	Total Losses	
0	76	0	25	18	40	39,978	-475,224	296,392	49,0142	129,8178	532,5
0	76	0	25	18	40	39,9786	-405,445	279,09	-	126,355	532,5
0	76	0	25	18	90	89,8992	-762,888	114,06	25,6875	623,1405	2307,5
0	76	0	25	18	90	89,9003	-676,179	59,7355	-	616,4435	2307,5
0	76	0	25	18	140	139,781	-1292,06	-108,115	-18,4807	1418,6557	4082,5
0	76	0	25	18	140	139,783	-1190,62	-217,485	-	1408,105	4082,5

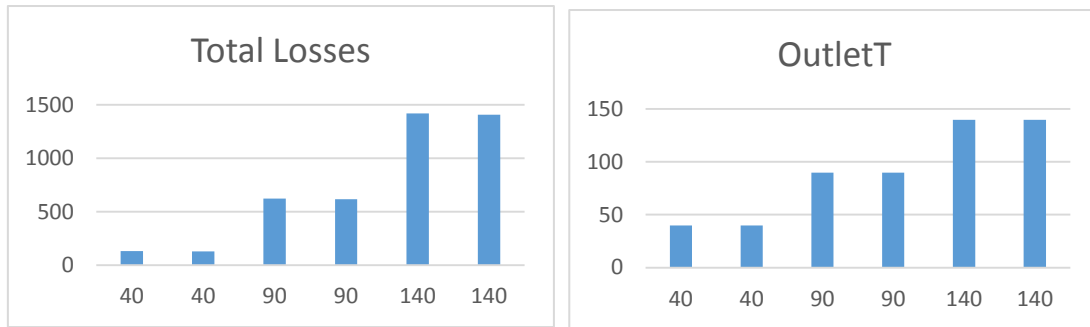


Figure 61. Results of the simulation of the model without considering the radiation with the mirror. Total Losses (left) and HTF's outlet temperature (right).

The tables above show how the heat transfer through radiation with the mirror has not enough influence in the heat losses

Finally it has been analysed if the combination of the two “errors”, considering the radiation just with the ambient, and considering that there is no HTF flowing through the collector, has the enough influence to reach the values of the real losses.

It has been necessary to build a new model, which is the combination of the mentioned two.

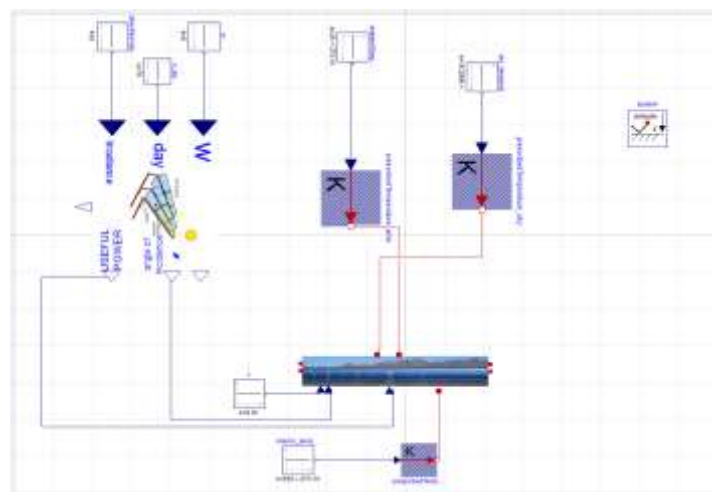


Figure 62. Model of the semicollector without neither HTF flowing through it, nor heat transfer through radiation to the mirror.

The results of assuming this possibility are presented in the table below:

Table 5. Results of the simulation of the model without considering neither the fluid, nor the radiation with the mirror.

DNI	n	w	T amb	T sky	Inlet T	Losses			Total Losses	Real heat losses
						Ambr	Ambc	Ambr Tamb		
0	76	0	25	18	40	-475,22	296,39	49,01	129,82	532,5
0	76	0	25	18	40	-404,98	281,41	-	123,56	532,5
0	76	0	25	18	90	-762,89	114,06	25,69	623,14	2307,5
0	76	0	25	18	90	-675,76	71,75	-	604,01	2307,5
0	76	0	25	18	140	-1292,06	-108,12	-18,48	1418,66	4082,5
0	76	0	25	18	140	-1191,76	-194,72	-	1386,48	4082,5

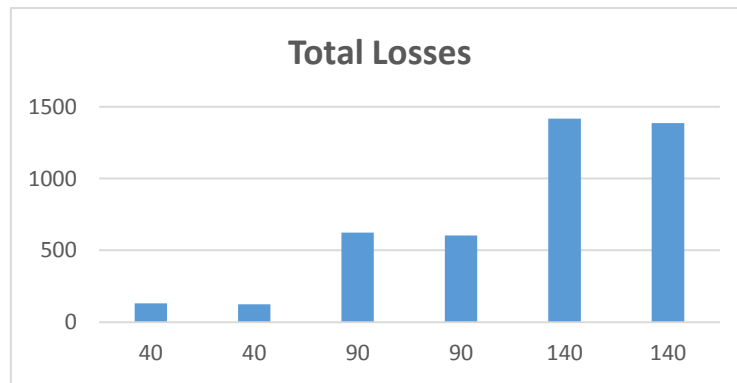


Figure 63. Results of the simulation of the model without considering neither the fluid, nor the radiation with the mirror.

As it is shown in the results, this consideration has very low effect in the heat losses, so it can be said that none of the possibilities analysed previously seem to be the reason for the difference with the real heat losses.

3.2. Sensitivity analysis

Once reached this point, it can be concluded that the model is “correct” in a theoretical way, but that there are some real factors which due to complexity or impossibility, can’t be included into the model, and that is the reason why the results are not equal. In order to validate the model, so it can be used to the analysis of the performance of the collector, it has been selected a parameter which has a great influence in the heat losses. To select this parameter a sensitivity analysis has been carried out. This analysis consists in comparing the influence in the heat losses (the test has been done to only one absorber) of some different parameters, such as:

- The emittance of the glass cover.
- The emittance of the absorber.
- The emittance of the shield.

As the evaluated test is the heat losses test, where there is no incidence radiation, there are some parameters that don’t affect the amount of losses, and so, it has no sense to analyse their influence.

On the next tables and graphics there are presented the results obtained from analysing the mentioned parameters.

3.2.1. The emittance of the glass cover.

Table 6. Results of simulating the heat losses test for different values of the glass cover’s emittance.

Tube Emissivity	Absorber losses			
	AmbrA	AmbrC	MirrA	TotalA
0,1	-113,404	-70,4669	-1,04647	-184,91737
0,2	-129,002	-83,1826	-2,39662	-214,58122
0,3	-134,581	-88,5257	-3,78673	-226,89343
0,4	-136,96	-91,4976	-5,17778	-233,63538
0,5	-137,892	-93,4161	-6,57663	-237,88473
0,6	-138,051	-94,7753	-7,98107	-240,80737
0,7	-137,737	-95,8121	-9,39103	-242,94013
0,8	-137,128	-96,644	-10,7921	-244,5641
0,9	-136,294	-97,3476	-12,1992	-245,8408
1	-135,455	-97,9351	-13,4803	-246,8704

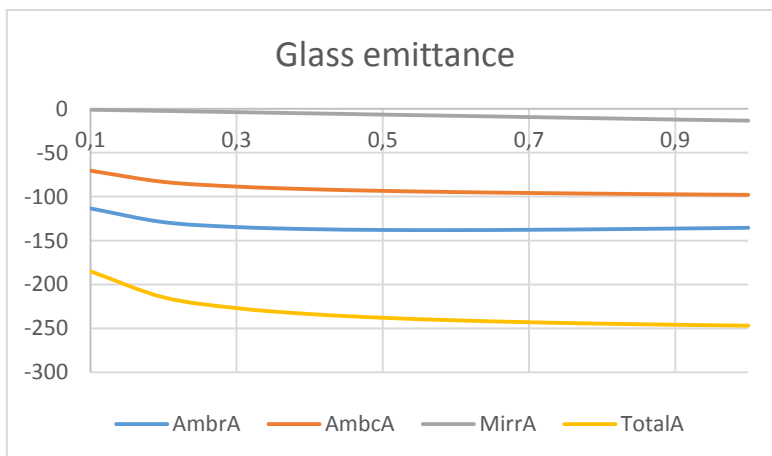


Figure 64. Results of simulating the heat losses test for different values of the glass cover's emittance.

3.2.2. The emittance of the absorber.

Table 7. Results of simulating the heat losses test for different values of the absorber's emittance.

Tube Emissivity	Absorber losses			
	AmbrB	AmbcB	MirrB	TotalB
0,1	-185,625	-340,28	-15,8453	-541,7503
0,2	-339,28	-640,274	-29,5173	-1009,0713
0,3	-482,872	-916,151	-42,294	-1441,317
0,4	-618,088	-1169,99	-54,3258	-1842,4038
0,5	-745,511	-1403,8	-65,664	-2214,975
0,6	-865,492	-1619,39	-76,3403	-2561,2223
0,7	-978,409	-1818,52	-86,3878	-2883,3168
0,8	-1084,62	-2002,75	-95,8386	-3183,2086
0,9	-1184,54	-2173,55	-104,73	-3462,82
1	-1278,56	-2332,16	-113,096	-3723,816

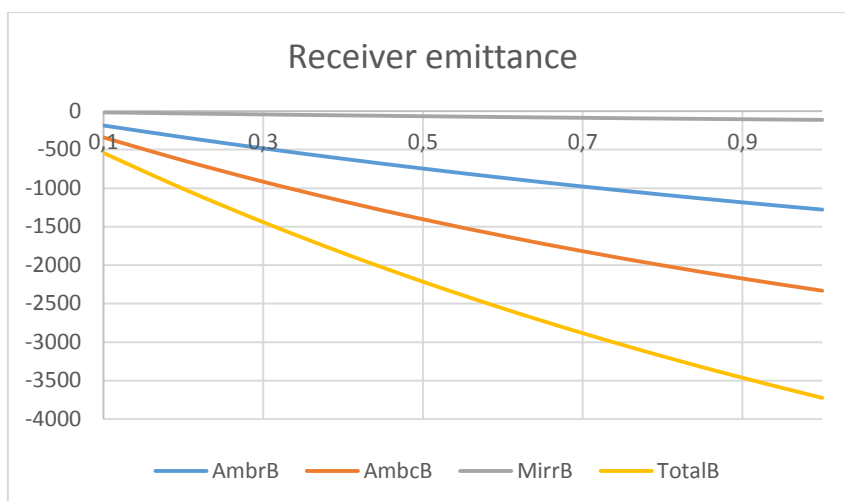


Figure 65. Results of simulating the heat losses test for different values of the absorber's emittance.

3.2.3. The emittance of the shield.

Table 8. Results of simulating the heat losses test for different values of the shield's emittance.

Tube Emissivity	Absorber losses			
	AmbrC	AmbrC	MirrC	TotalC
0,1	-136,68	-97,011	-11,5475	-245,2385
0,2	-136,603	-97,0122	-11,6228	-245,238
0,3	-136,526	-97,0142	-11,6982	-245,2384
0,4	-136,448	-97,0173	-11,7728	-245,2381
0,5	-136,368	-97,0214	-11,8477	-245,2371
0,6	-136,288	-97,0262	-11,9227	-245,2369
0,7	-136,207	-97,0319	-11,9979	-245,2368
0,8	-136,125	-97,0383	-12,0725	-245,2358
0,9	-136,042	-97,0459	-12,1475	-245,2354
1	-135,966	-97,053	-12,2154	-245,2344

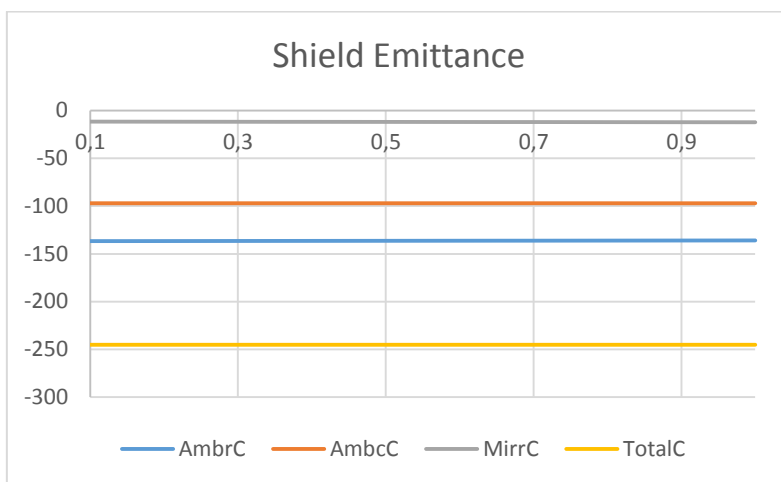


Figure 66. Results of simulating the heat losses test for different values of the shield's emittance.

3.2.4. All cases together

Table 9. Summary of the results of the 3 cases.

Absorber Emissivity	Absorber losses		
	TotalA	TotalB	TotalC
0,1	-184,91737	-541,7503	-245,2385
0,2	-214,58122	-1009,0713	-245,238
0,3	-226,89343	-1441,317	-245,2384
0,4	-233,63538	-1842,4038	-245,2381
0,5	-237,88473	-2214,975	-245,2371
0,6	-240,80737	-2561,2223	-245,2369
0,7	-242,94013	-2883,3168	-245,2368
0,8	-244,5641	-3183,2086	-245,2358
0,9	-245,8408	-3462,82	-245,2354
1	-246,8704	-3723,816	-245,2344



Figure 67. Summary of the results of the 3 cases.

The tables above show that the emittance of the absorber is the parameter that has the highest effect in the heat losses. So the next step is to validate the model using this parameter. The followed procedure for the validation is the one presented in the next pages.

3.3. Validation of the model.

The main problem with a simulation model is that it is really laborious to show all the affecting aspects of the reality, and sometimes some simplifications are necessary. In the case that attains this project, it has been impossible to reflect all the losses that appear in a PTC, so in order to liken the model to the reality as much as possible the emittance of the absorber tube has been selected so the result obtained from the model are the same as the results obtained in the tests carried out in the PSA that (L. Valenzuela, R. Lopéz-Martín, & E. Zarza, 2014) published in the article *“Optical and thermal performance of large-size parabolic-trough solar collectors from outdoor experiments: A test method and a case study.*

In this article there are presented some testing methods and the results obtained from those methods. The procedure it has been followed to obtain the equation that rules the behaviour of the emittance of the absorber tube is which follows.

First from the equation provided by the article for the heat losses, it has been obtained the value of these heat losses for different temperature levels.

$$\frac{\dot{Q}_1}{L} = 0.342 \cdot \Delta T + 1,163 \cdot 10^{-8} \cdot \Delta T^4$$

Where:

- ΔT : is the temperature difference between the HTF's medium temperature and the ambient temperature.
- L : is the length of the collector. Its value also varies with the temperature difference:

$$L = L_0 + \alpha_L \cdot L_0 \cdot \Delta T$$

Where:

- $L_0 = 73.08 \text{ m}$
- $\alpha_L = 1,73 \cdot 10^{-5} \frac{1}{^\circ\text{C}}$

Table 10. Real heat losses

ΔT [°C]	L [m]	$\frac{\dot{Q}_1}{L}$ [W/m]	\dot{Q}_1 [W]
0	73,08	0	0
40	73,13057136	13,7097728	1002,60352
80	73,18114272	27,8363648	2037,09699
120	73,23171408	43,4515968	3182,03491
160	73,28228544	62,3418368	4568,55228
200	73,3328568	87,008	6380,5452
240	73,38342816	120,665549	8854,85163
280	73,43399952	167,244493	12281,432
320	73,48457088	231,389389	17003,5499
360	73,53514224	318,459341	23417,9529
400	73,5857136	434,528	31975,053

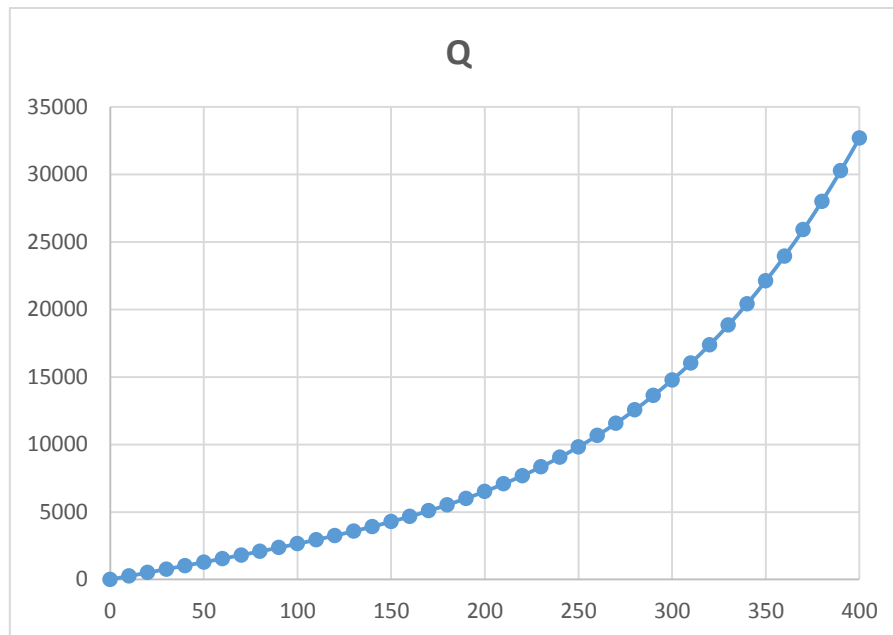


Figure 68. Real heat losses depending on the temperature difference between the HTF medium T and the ambient T .

The next step has been to simulate the model for different values of the emittance (from 0,1 to 0,3 W/m^2) and for different HTF temperatures (from 40 to 400 °C). The ambient temperature has been maintained constant at 20 °C. As the test that has to be represented is the heat losses test, the incident radiation is null, it has been considered a mass flow of 10 kg/s and the sky temperature has been established around 18°C.

Table 11. Summary of model heat losses depending on the emittance and the HTF medium T.

T_HTF [°C]	Tamb [°C]	ΔT [°C]	Absorber Emissivity[W/m ²]	h_Dif [kJ/kg]	mflow [kg/s]	Energy Losses [W]	Real Losses [W]
39,92	20	19,92	0,1	25,00	10	250,00	498,28
			0,2	42,60	10	426,00	
			0,3	58,60	10	586,00	
79,82	20	59,82	0,1	87,00	10	870,00	1507,51
			0,2	149,00	10	1490,00	
			0,3	207,00	10	2070,00	
119,79	20	99,79	0,1	171,00	10	1710,00	2582,74
			0,2	298,00	10	2980,00	
			0,3	415,00	10	4150,00	
159,70	20	139,70	0,1	281,00	10	2810,00	3824,36
			0,2	495,00	10	4950,00	
			0,3	692,00	10	6920,00	
199,59	20	179,59	0,1	424,00	10	4240,00	5389,22
			0,2	753,00	10	7530,00	
			0,3	1055,00	10	10550,00	
239,46	20	219,46	0,1	603,00	10	6030,00	7484,65
			0,2	1079,00	10	10790,00	
			0,3	1517,00	10	15170,00	
279,30	20	259,30	0,1	827,00	10	8270,00	10369,38
			0,2	1489,00	10	14890,00	
			0,3	2095,00	10	20950,00	
319,11	20	299,11	0,1	1102,00	10	11020,00	14353,14
			0,2	1993,00	10	19930,00	
			0,3	2806,00	10	28060,00	
358,89	20	338,89	0,1	1434,00	10	14340,00	19796,00
			0,2	2603,00	10	26030,00	
			0,3	3666,00	10	36660,00	
398,63	20	378,63	0,1	1832,00	10	18320,00	27107,52
			0,2	3336,00	10	33360,00	
			0,3	4697,00	10	46970,00	

As it is shown in the Table Above (the complete table is the Table A 1 from the annexes) the HTF's inlet temperature is not exactly the same as the one that has been set. That's because it suffers a low fall when it goes through the collector and the one that appears in the table is the medium temperature.

Table 12. Interpolated emittance values.

T_HTF [°C]	Emittance	T_HTF [°C]	Emittance
39,92	0,245173871	239,62	0,13055983
59,90	0,223885075	259,57	0,13049969
79,87	0,203018806	279,30	0,1317127
59,87	0,183966211	299,45	0,13405915
119,81	0,168719676	319,36	0,13740896
139,79	0,157130843	339,01	0,14162004
159,70	0,147399995	359,16	0,14667235
179,74	0,140098288	379,04	0,15226077
199,70	0,134930662	398,63	0,15842765
219,52	0,132051276		

The next step has been to find the fit-curve that best fits the real values of the emittance. This curve is a third order polynomial curve.

Table 13. Fit equation of the emittance and the error committed.

T_HTF [°C]	Emittance [W/m ²]	Emittance equation [W/m ²]	Difference [W/m ²]	Error [%]
39,92	0,2452	0,2464	0,0012	0,50%
59,90	0,2239	0,2226	0,0013	0,58%
79,87	0,2030	0,2019	0,0011	0,53%
59,87	0,1840	0,1843	0,0004	0,20%
119,81	0,1687	0,1696	0,0008	0,49%
139,79	0,1571	0,1574	0,0003	0,19%
159,70	0,1474	0,1478	0,0004	0,26%
179,74	0,1401	0,1404	0,0003	0,23%
199,70	0,1349	0,1352	0,0002	0,18%
219,52	0,1321	0,1319	0,0002	0,15%
239,62	0,1306	0,1303	0,0003	0,22%
259,57	0,1305	0,1302	0,0003	0,20%
279,30	0,1317	0,1316	0,0001	0,09%
299,45	0,1341	0,1341	0,0001	0,05%
319,36	0,1374	0,1377	0,0003	0,19%
339,01	0,1416	0,1420	0,0004	0,29%
359,16	0,1467	0,1470	0,0004	0,25%
379,04	0,1523	0,1525	0,0002	0,16%
398,63	0,1584	0,1583	0,0002	0,11%

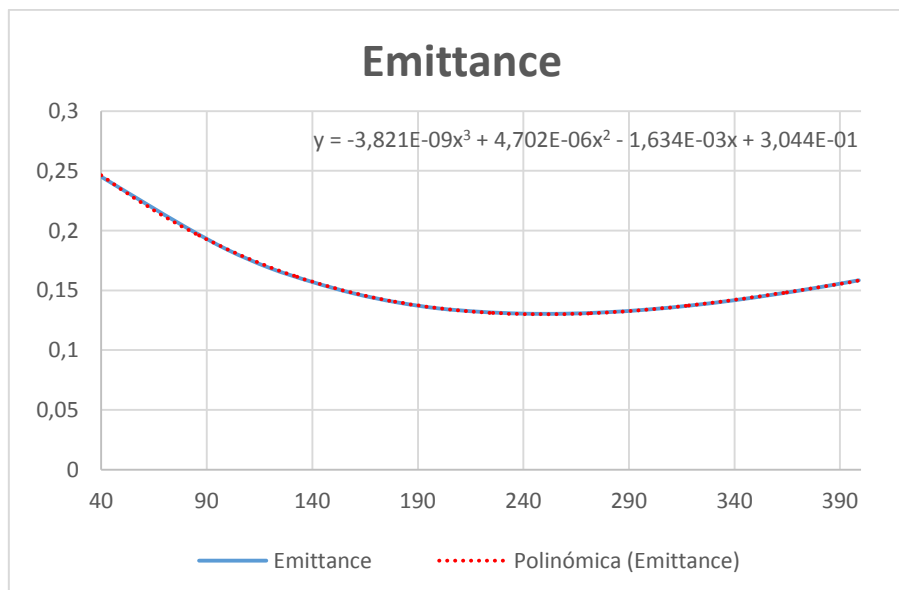


Figure 69. Real emittance and its fitting curve

So the equation that governs the behaviour of the emittance related to the HTF medium temperature is:

$$emittance = -3,821 \cdot 10^{-9} \cdot T^3 + 4,702 \cdot 10^{-6} \cdot T^2 - 1,634 \cdot 10^{-3} \cdot T + 0,3044$$

Once the emittance is known and introduced into the model, it has to be verified its legacy. The procedure followed to obtain this is to repeat the test from the article with the simulator and see if the error that is committed is acceptable or not.

3.3.1. Heat losses test validation

First it has been compared the new heat losses obtained from the simulator to the ones from the article. This are the results obtained:

Table 14. Heat losses test results.

Tamb [°C]	T_HTF [°C]	ΔT [°C]	Real Losses [W]	Total Losses [W]	Losses difference [W]	Error losses [%]	energy Losses [W]	Enthalpy difference [W]	Error energy [%]
20	39,92	19,93	498,50	502,59	4,08	0,82%	502	3,50	0,70%
20	79,87	59,87	1508,72	1492,83	15,88	1,05%	1510	1,28	0,09%
20	119,81	99,81	2583,48	2569,42	14,06	0,54%	2610	26,52	1,03%
20	159,70	139,76	3826,67	3807,85	18,81	0,49%	3860	33,33	0,87%
20	199,70	179,70	5394,44	5355,45	38,99	0,72%	5430	35,56	0,66%
20	239,62	219,62	7494,87	7433,37	61,50	0,82%	7520	25,13	0,34%
20	279,30	259,51	10387,35	10322,24	65,11	0,63%	10420	32,65	0,31%
20	319,36	299,36	14381,79	14347,05	34,74	0,24%	14470	88,21	0,61%
20	359,16	339,15	19837,59	19841,75	4,16	0,02%	19980	142,41	0,72%
20	398,63	378,89	27162,36	27103,69	58,67	0,22%	27260	97,64	0,36%

As it is shown in the Table Above the errors committed are really low, so the equation for the emittance for this test is acceptable.

3.3.2. Peak optical efficiency test validation

For the realisation of this test the data given by the article has been introduced in the model:

Table 15. Peak optical efficiency test data.

Test	Direct Normal Irradiance [W/m ²]	HTF flow rate [kg/s]	Inlet HTF Temperature [°C]	Ambient Temperature [°C]	Collecting area [m]	Incidence angle [°]
1	815,00	3,58	104,80	31,40	409,91	0
2	910,00	3,55	106,10	31,10	409,91	0
3	877,00	3,61	105,40	32,80	409,91	0
4	918,00	3,57	106,60	35,80	409,91	0
5	981,00	3,57	113,20	36,30	409,91	0

And the results obtained from the simulator and the error committed compared to the article:

Table 16. Peak optical efficiency test results.

Test	Inlet HTF T [°C]	article Outlet HTF T [°C]	model Outlet HTF T [°C]	Outlet T difference	Error Outlet T [%]	article Peak Optical Efficiency [-]	Model peak optical Efficiency [-]	Dif POE [-]	error POE [%]
1	104,8	143,1	148,22	5,12	1,22%	0,76	0,80	0,0413	5,43%
2	106,1	149,7	154,85	5,15	1,20%	0,78	0,80	0,0221	2,83%
3	105,4	147,6	151,78	4,18	0,98%	0,78	0,80	0,0221	2,83%
4	106,6	149,4	155,49	6,09	1,42%	0,76	0,80	0,0424	5,58%
5	113,2	159,8	165,15	5,35	1,22%	0,76	0,80	0,0421	5,53%

Although the errors committed during this test are higher than the ones committed in the previous ones, they are still acceptable.

3.3.3. Dynamic efficiency test validation

Finally it has been compared the dynamic test made in the PSA with the model when the same data is introduced. In this test the day of the year when the test was made comes into action, as it will affect to the hour angle, and so to the angle of incidence. The data introduced in the model is:

Table 17. Dynamic efficiency test data.

Date	Local time (start)	Local time (end)	Direct normal irradiance (W/m ²)	HTF flow rate (kg/s)	Inlet temperature (°C)	Ambient temperature (°C)
05/06/2012	12:44	12:54	894	2,962827141	250,6	28,9
11/06/2012	15:15	15:25	943	2,859176925	284,9	34,1
16/07/2012	12:15	12:25	798	2,856122825	286	25,6
05/07/2012	13:30	13:40	927	2,71966293	316,5	33,8
05/07/2012	15:20	15:30	911	2,721362068	316,9	35,1
17/07/2012	12:40	12:50	833	2,723286731	316,5	26,4
17/07/2012	15:20	15:30	875	2,724135855	316,7	27,7
12/06/2012	11:50	12:00	904	2,663385215	334,8	24,6
12/06/2012	12:40	12:50	918	2,651119625	334,8	25,2
19/07/2012	13:20	13:30	919	2,699964584	334,5	32,9

From this data has first calculated the data that can be introduced into the model: the day of the year, the hour angle and the duration of the test.

Table 18. Dynamic efficiency data for introducing in the model.

Date	n	w start [rad]	Duration [s]
05/06/2012	156,00	-0,3645	600,00
11/06/2012	162,00	0,2895	600,00
16/07/2012	197,00	-0,5252	600,00
05/07/2012	186,00	-0,1907	600,00
05/07/2012	186,00	0,2893	600,00
17/07/2012	198,00	-0,4166	600,00
17/07/2012	198,00	0,2816	600,00
12/06/2012	163,00	-0,6059	600,00
12/06/2012	163,00	-0,3877	600,00
19/07/2012	170,00	-0,2197	600,00

It has to be taken into account that the hour angle varies as the time advances (15° each hour, so 0,261799388 rad) so the equation that rules the behaviour of the hour angle is:

$$w[\text{rad}] = w_0 + \left(\frac{\text{time}}{3600}\right) * 0,261799388$$

The results obtained from the model, and the errors committed are presented in the next tables:

Table 19. Dynamic efficiency test results.

Date	DNI [W/m ²]	Inlet T [°C]	Outlet T [°C]	Model Outlet T [°C]	T difference [°C]	Relative error T [%]	Relative error T [°C] [%]	Delta T difference [°C]	Error delta T [%]
05/06/2012	894	250,6	292,5	299,04	6,54	1,16%	2,24%	6,543	15,6%
11/06/2012	943	284,9	330	331,84	1,84	0,31%	0,56%	1,845	4,09%
16/07/2012	798	286	320	322,70	2,70	0,45%	0,84%	2,698	7,93%
05/07/2012	927	316,5	362,5	360,89	1,61	0,25%	0,44%	1,608	3,50%
05/07/2012	911	316,9	360,9	358,87	2,03	0,32%	0,56%	2,027	4,61%
17/07/2012	833	316,5	354,4	353,30	1,10	0,18%	0,31%	1,099	2,90%
17/07/2012	875	316,7	358,5	356,91	1,59	0,25%	0,44%	1,589	3,80%
12/06/2012	904	334,8	372	369,15	2,85	0,44%	0,77%	2,853	7,67%
12/06/2012	918	334,8	378,1	374,29	3,81	0,58%	1,01%	3,809	8,80%
19/07/2012	919	334,5	379,1	375,85	3,25	0,50%	0,86%	3,249	7,28%

Date	Total Losses [W]	Enthalpy difference [kJ/kg]	Mass flow	Energy [W]	collecting area [m]	Useful Solar Radiant Power [W]
05/06/2012	14.867,10	97.760,53	2,96	290.226,85	409,908	348.275,72
11/06/2012	16.496,78	97.265,31	2,86	278.654,91	409,908	370.807,41
16/07/2012	15.882,13	75.510,34	2,86	216.098,13	409,908	292.179,73
05/07/2012	18.692,36	94.239,78	2,72	256.813,03	409,908	375.384,26
05/07/2012	18.267,05	88.971,34	2,72	242.607,46	409,908	358.205,47
17/07/2012	18.206,58	77.656,88	2,72	211.904,92	409,908	318.707,73
17/07/2012	18.650,23	85.104,11	2,72	232.298,83	409,908	344.448,10
12/06/2012	19.960,67	73.455,39	2,66	196.031,27	409,908	319.165,66
12/06/2012	20.635,35	84.831,28	2,65	225.347,67	409,908	355.255,22
19/07/2012	20.121,72	88.283,72	2,70	238.839,63	409,908	370.502,34

Date	Model efficiency [-]	Measured efficiency [-]	Calculated efficiency [-]	Error measured [%]	Error calculated [%]
05/06/2012	0,833	0,727	0,721	14,63%	15,58%
11/06/2012	0,751	0,727	0,72	3,37%	4,37%
16/07/2012	0,740	0,698	0,688	5,96%	7,50%
05/07/2012	0,684	0,718	0,72	4,72%	4,98%
05/07/2012	0,677	0,718	0,709	5,67%	4,47%
17/07/2012	0,665	0,696	0,693	4,47%	4,06%
17/07/2012	0,674	0,709	0,706	4,88%	4,47%
12/06/2012	0,614	0,679	0,661	9,54%	7,08%
12/06/2012	0,634	0,706	0,693	10,15%	8,47%
19/07/2012	0,645	0,711	0,709	9,33%	9,08%

In this last test the committed errors are higher than in the previous ones, but still this error are acceptable, because this are usual errors committed during the real testing.

So in conclusion the fit equation found for the emittance of the absorber tube is acceptable And is the one that it's going to be used during the rest of the project. For the sensible analysis of the collector, it is going to be used the data from the second case of the Dynamic efficiency test (the one from the 11/06/2012), as it is the one which makes the least error.

4. CALCULATIONS

In this section it is explained the sensitivity analysis carried out. In it, it is studied how the variation of different parameters of the collector affect to its behaviour.

4.1. Sensitivity analysis

Once the model has been validated, there have been analysed different parameters, to see how they affect to the behaviour of the collector. First it has been studied how they affect to the efficiency test, comparing the results which have been obtained, with the ones obtained in the efficiency test done during the validation of the model.

The initial data selected is the same as the one which had the lowest errors during the validation efficiency test.

After studying the influence of these parameters in the efficiency test, it has been done the same for the heat losses test. This way it has also seen how some of the parameters analysed previously, affect to the heat losses.

The parameters evaluated in the first part have been:

- Reflectivity of the mirror.
- Transmittance of the glass cover.
- Hydrogen infiltration in the gap between the glass cover and the absorber.
- Degradation of the HTF.
- Air infiltration in the gap between the glass cover and the absorber.
- Absorptance of the absorber.
- Emittance of the absorber.
- Emittance of the glass cover.
- Emittance of the shield.
- Interception factor of the collector.

As it has no sense to analyse some of this parameters for the second part, because they have no influence in the heat losses, just a few of them have been studied:

- Hydrogen infiltration in the gap between the glass cover and the absorber.
- Degradation of the HTF.
- Air infiltration in the gap between the glass cover and the absorber.
- Emittance of the absorber.
- Emittance of the glass cover.
- Emittance of the shield.

In the next tables appear the data used for the tests, the dynamic efficiency test and the heat losses test

Table 20. Data for the dynamic efficiency test.

Date	n (-)	w (rad)	Duration (s)	Direct normal irradiance (W/m ²)	HTF flow rate (kg/s)	Inlet T (°C)	Ambient T (°C)	Absorber's Start T (°C)	Collecting area (m ²)
11/06/2012	162,00	0,2895	600,00	943	2,859177	284,9	34,1	285	409,908

Table 21. Data for the Heat losses test.

Direct normal Irradiance (W/m ²)	n (-)	w (rad)	Ambient T (°C)	Sky T (°C)	Inlet T (°C)	Mass flow (kg/s)
0	76	0	25	18	40	3,57694351
0	76	0	25	18	90	3,57694351
0	76	0	25	18	140	3,57694351

The tables and graphs of most of the test are presented at the end of this text, in the annexes. In the next paragraphs it is explained how the different parameters mentioned affect to the collector's behaviour.

4.1.1. Reflectivity of the mirror

When it has been studied the reflectivity of the collector's mirror, it has just been carried out the dynamic efficiency test, because during the heat losses test the irradiance is null, so the effect of the variation of the reflectivity is none. This parameter measures the amount of solar radiation that the mirror reflects, out of the total radiation that reaches its surface. Its value can be reduced with the degradation of the mirrors or, which is more normal, due to dust and dirt on the mirror surface.

To analyse the influence of this parameter it has been simulated the model varying its value first from 0,1 to 1 [results presented in Table-A 4 and in Figure-A 1]. Although considering values of reflectivity below 0,8 has not much sense (its value will never reach this point during the collector's live), it has done the test assigning to the parameter extreme values to confirm if the influence was enough to consider this parameter during the rest of the project.

In the table there appear different columns. The *Energy* has been calculated as the product of the mas flow and the enthalpy increase. The *Total Losses* are the sum of the total losses due to convection and radiation of the collector, the endIn and the endOut. Finally the *Useful solar Radiant Power* is the product of the direct normal irradiance, the collecting area and the cosine of the incidence angle. These operations are the ones used during the rest of the tests.

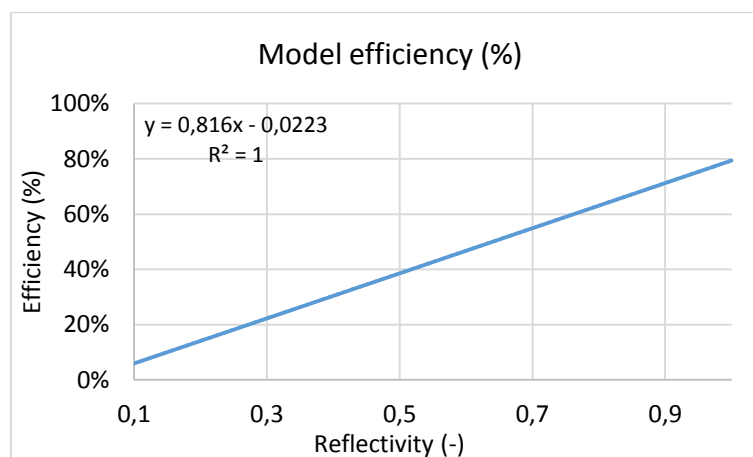


Figure 70. Results for the efficiency when the reflectivity varies from 0,1 to 1.

The results show that the reflectivity of the collector has great influence in its behaviour. As expected, when the value of this parameter decreases it does so the efficiency, the energy absorbed by the HTF and its outlet temperature. This is obvious, because if the reflectivity

decreases, the incident irradiation on the tube also decreases. Although the heat losses decrease when the reflectivity does so, they are not related; the heat losses decrease because less solar energy reaches the collector.

There are also exposed the results of how this variation affects but expressed in percentages the variation from the nominal case [presented in Table-A 5 and in Figure-A 2].

After seen that the reflectivity has a big influence, it has been made an analysis for more realistic values, where the value of this parameter decreases a maximum of a 10% of its initial values. [The results of this test are in Table-A 6 and in Figure-A 3].

There have also been represented the previous result, but in percentage over its nominal value [results in Table-A 7 and in Figure-A 4].

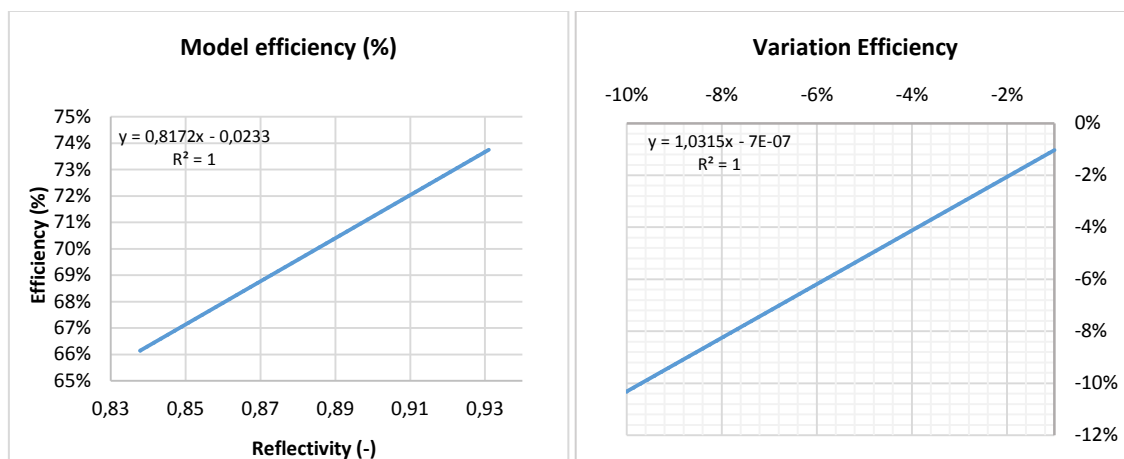


Figure 71. Results of the efficiency (real value and percentage) when the reflectivity varies from 0,83 to 0,93.

The results show how the variation is lineal; a variation of 10% in the reflectivity makes the same variation in the absorbed energy and the collector's efficiency.

4.1.2. Transmittance of the glass cover

As well as happened to the mirror reflectivity, when studying the effect of the transmittance of the glass cover, it just has sense to analyse its effect in the dynamic efficiency test, cause it affects the entering irradiance, but not the heat losses.

Like in the previous case, first it has been seen the effect when varying the parameter from 0,1 to 1, in order to see if its influence is important enough [results presented in Table-A 8 and in Figure-A 5]. There are also exposed the results of how this variation affects but expressed in percentages [presented in Table-A 9 and in Figure-A 6].

After seen that the transmittance has a big influence, it has made an analysis for more realistic values, where the value of this parameter decreases a maximum of around 15% of its initial values [The results of this test are the ones in Table-A 10 and in Figure-A 7]. As in the previous cases, it has also been presented the results in percentages [Table-A 11 and in Figure-A 8].

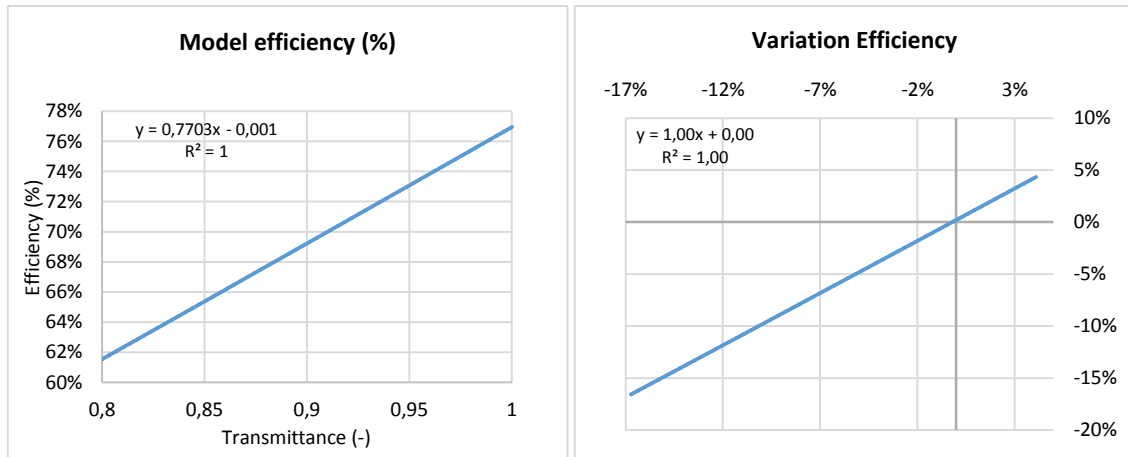


Figure 72. Results of the efficiency when the transmittance of the collector varies from 0,8 to 1.

As we can see in the figures above, there is a direct linear response in the efficiency of the collector when its transmittance varies. When its value decreases a 10%, so it does the efficiency.

On another hand, as we can see in the Table-A 11 (also in the previous ones) the heat losses increase a lot when the transmittance of the glass cover decreases, in comparison with the case of the variation of the reflectivity of the glass cover. The reason for this is that when the transmittance of the glass cover is reduced, less amount of energy cross the glass, but as the same amount of it reach its surface, this energy exceed is traduced in a higher glass cover temperature, and as a result in higher amount of heat losses to the ambient.

4.1.3. Infiltration of hydrogen

As time passes, and the absorber tube is slowly degrading, it frees some hydrogen that stays in the space between the tube and the glass cover. The use of getters is for this reason, to absorb those particles that infiltrate in the vacuum space; but when the getters are saturated, and they are no able to absorb more particles, those particles stay in the gap and contribute to the increase of the heat losses through convection.

To simulate this situation, it is necessary to build a new component model that substitutes the ConvConcentricCylindVacuum. In the next paragraphs, it is going to be analysed the influence of the infiltration of hydrogen. To simulate the model, it has been necessary to build a new convection component. This new component is explained below.

ConvConcentricCylindHydrogen

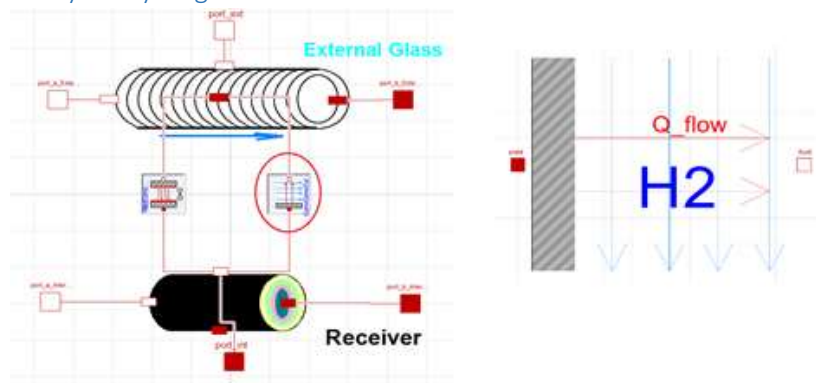


Figure 73. Component of the convection in the interior of the collector when there is hydrogen.

As is been said, this model is used to quantify the heat transference through convection when there is hydrogen in the gap between the absorber and the glass cover.

It follows the same principles as the component ConvConcentricCylindVacuum but with different equation and correlation to explain the behaviour in an ambient with hydrogen. These correlations have been proposed by (T. Beikircher and W. Spirki, 1996).

To explain the behaviour of heat transfer by convection in a rarefied gas ambient (like in this case), first it has to be differentiated three possible regimes, free molecular, transition, and continuum. To differentiate when each case is applied, it is used the concept of the Knudsen number:

$$Kn = \frac{\lambda}{L}$$

Where:

- *Kn: Knudsen number.*
- *L: Characteristic Length of the space containing the gas.*
- *λ: the mean free path of gas molecules between intermolecular collisions.*

$$\lambda = \frac{R \cdot T_{avg}}{\sqrt{2} \cdot \pi \cdot d^2 \cdot N_A \cdot P}$$

Where:

- *R: Constant of the ideal gases.*
- *T_{avg}: Mid temperature.*

$$T_{avg} = \frac{T_1 + T_2}{2}; T_1 \text{ and } T_2, \text{ temperatures of the interior and exterior cilinder respectively}$$

- *d: Diameter of a gas molecule.*
- *N_A: Avogadro number. N_A = 6,0221367 · 10²³.*
- *P: Gas pressure.*

Each regime is determined by the value of the Knudsen number.

	Kn < 0,01	Continuum
0,01 < Kn < 10		Transition
10 < Kn		Free molecular

In the free molecular regime, the heat transference depends on the gas pressure. It quantified by the next equation:

$$q_{FM} = \frac{1}{\frac{1}{\alpha_1} + \left(\frac{R_1}{R_2}\right)\left(\frac{1}{\alpha_2} - 1\right)} \cdot \frac{P \cdot \left(C_v + \frac{R}{2}\right)}{(2 \cdot \pi \cdot M \cdot R \cdot T_{avg})^{1/2}} \cdot (T_1 - T_2) \cdot 2 \cdot \pi \cdot R_1$$

Where:

- *q_{FM}: Free molecular heat transfer from inner cylinder [$\frac{W}{m}$].*
- *P: Pressure of a Maxwelliam gas al the same density as the gas between the plates at temperature T_{avg}*
- *R₁, R₂: Inner and outer radii, respectively.*
- *R: Is the gas constant.*

- C_v : Heat capacity of the gas constant volume.
- T_1, T_2 : Inner and outer cylinders' temperatures.
- T_{avg} : Mid temperature.
- α_1, α_2 : Accommodation coefficients of the gas on the inner and outer cylinders.

The accommodation coefficients are “the fractional extent to which those molecules that fall on the surface and are reflected or re-emitted from it, have their mean energy adjusted or ‘accommodated’ toward what it would be if the returning molecules were issuing as a stream of as at the temperature of the wall”, according to the interpretation of (E.H. Kennard, 1938) to the Knudsen’s definition.

Their values are between 0 and 1. An accommodation coefficient of 1 means that a molecule’s velocity after collision with a surface is determined entirely by the surface temperature and it also signifies that energy was fully exchanged between the molecule and the surface. An accommodation coefficient of 0 means that the molecule’s velocity after the collision is the same as its velocity before the impact, so not energy has been exchanged during the collision. In this case:

- $\alpha_1 = 0,34$
- $\alpha_2 = 0,25$

The heat transfer in continuum regime is not function of the pressure, the equation that quantifies it is:

$$q_{continuum} = \frac{2 \cdot \pi \cdot k_{gas} \cdot (T_1 - T_2)}{\ln\left(\frac{R_2}{R_1}\right)}$$

Where:

- $q_{continuum}$: Continuum heat transfer from inner cylinder [$\frac{W}{m}$].
- k_{gas} : Thermal conductivity of the gas
- R_1, R_2, T_1, T_2 : Defined previously.

Finally the expression that quantifies the heat transfer in transition regime proposed by Sherman, is which follows:

$$\frac{1}{q_{transition}} = \frac{1}{q_{FM}} + \frac{1}{q_{continuum}}$$

Once acquainted with the new model, as it was done with the previous tests, the model has been simulated for different hydrogen pressures inside the space between the absorber and the glass cover. First it has seen the influence in the dynamic efficiency test, and later in the heat losses test.

In the dynamic efficiency test the value of the hydrogen pressure has first been varied from 0 to 5065 Pa to see how a huge modification affects [results in Table-A 12 and in Figure-A 11].

We can see in the results above, that once reached a pressure of the hydrogen, the results get stable, but first there are huge changes (decrease of the efficiency, the energy absorbed by the HTF and in its temperature; and increase of the heat losses). The reason for this is because the heat transferred by convection is bigger in an atmosphere with hydrogen than when it is in a vacuum one.

The stabilisation of the results happen because it is reached the continuum regime. As it has previously said, when the value of the Knudsen number (which decreases when the pressure increases) is low enough, the heat transfer happens in a continuum regime, and it doesn't depend on the value of the gas pressure.

As it has been done with the previous tests, there are also exposed the results of how this variation affects but expressed in percentages [presented in Table-A 13 and in Figure-A 12].

The next step has been to study the behaviour of the collector at lower pressures (between 0,0001 and 8 Pa), in order to appreciate how it really affects [results in Table-A 14 and in Figure-A 13].

We can see that in the case the variation is less abrupt. Below the previous results in the annexes it is presented how the variation affects but expressed in percentages [Table-A 15 and in Figure-A 14].

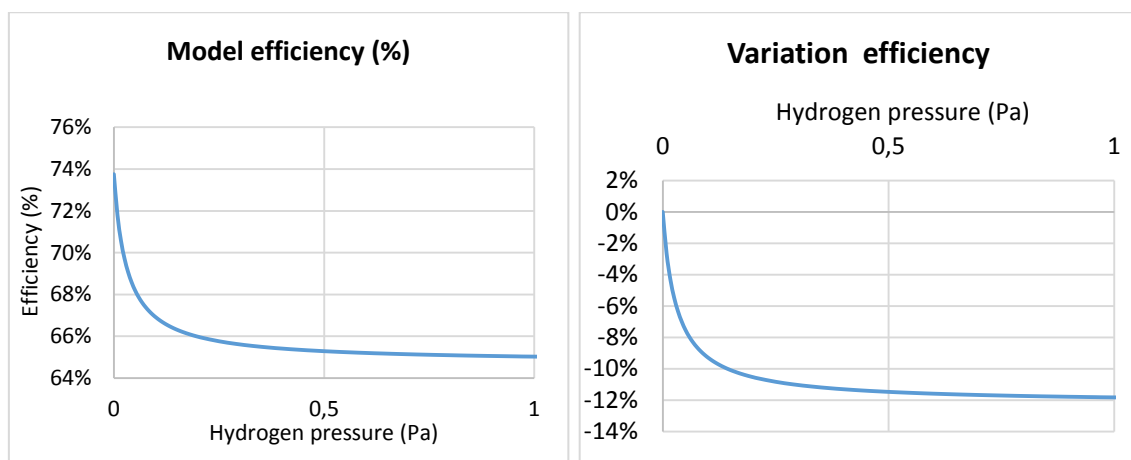


Figure 74. Results of the efficiency when there is hydrogen infiltration.

The results from the dynamic efficiency test show how as more hydrogen infiltrates the space between the glass cover and the metallic tube (the pressure of hydrogen increases) the results obtained from the collector are worse. This happens until the pressure of the hydrogen is around 1 Pa, when the results get stable. In the stable situation, the efficiency of the collector and the energy absorber by the collector are around 12% lower than in the nominal case; and the heat losses in that situation are more than twice higher.

On the other hand it has also been analysed the influence of the infiltration of hydrogen in the heat losses test. This test has been studied for three different HTF's inlet temperatures (40, 90 and 140 °C). The obtained results are presented in the annexes.

- When the HTF's inlet temperature is 40°C [Table-A 16 and in Figure-A 15].
- When the HTF's inlet temperature is 90°C [Table-A 17 and in Figure-A 16].
- When the HTF's inlet temperature is 140°C [Table-A 18 and in Figure-A 17].
- Comparing the three cases [Figure-A 18].

The next tables and graphs present how the variation affects but expressed in percentages.

- When the HTF's inlet temperature is 40°C [Table-A 19 and in Figure-A 19].
- When the HTF's inlet temperature is 90°C [Table-A 20 and in Figure-A 20].
- When the HTF's inlet temperature is 140°C [Table-A 21 and in Figure-A 21].

- Comparing the three cases [Figure-A 22].

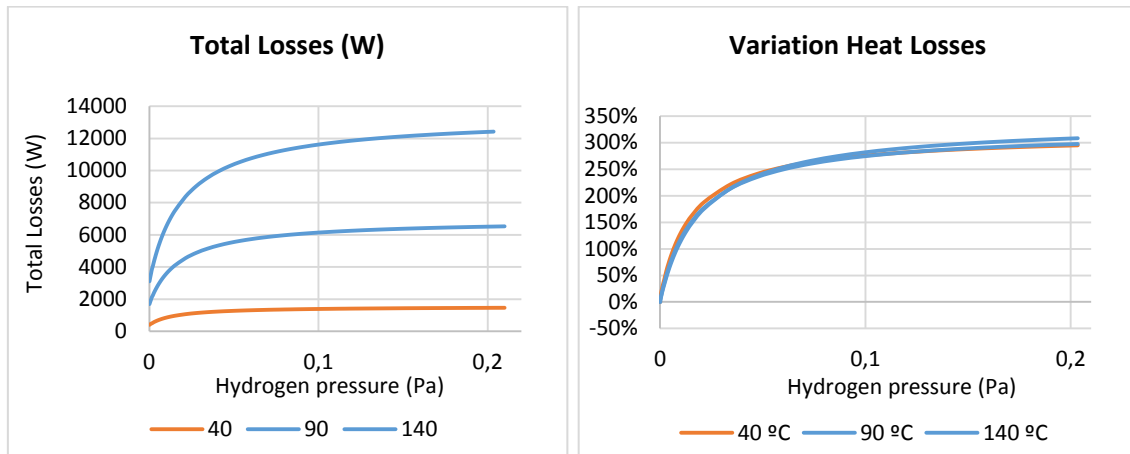


Figure 75. Results of the heat losses when there is hydrogen infiltration.

We can see, how as it was expected, when the hydrogen infiltrates the heat losses increase in a huge way. This can be taken into account when analysing the reasons for the worsening of the results in a collector operating in a real plant.

4.1.4. Infiltration of air

In this case, it is going to be analysed the effect of the entrance of air, in the gap between the absorber and the glass cover. The difference with the previous case is that the entrance of air is in most of the cases because of a fissure of the glass cover, this makes the pressure of the interior, equal the ambient pressure. So in this case it is also necessary to build a new convection model. This new model is which follows.

ConvConcentricCylindP

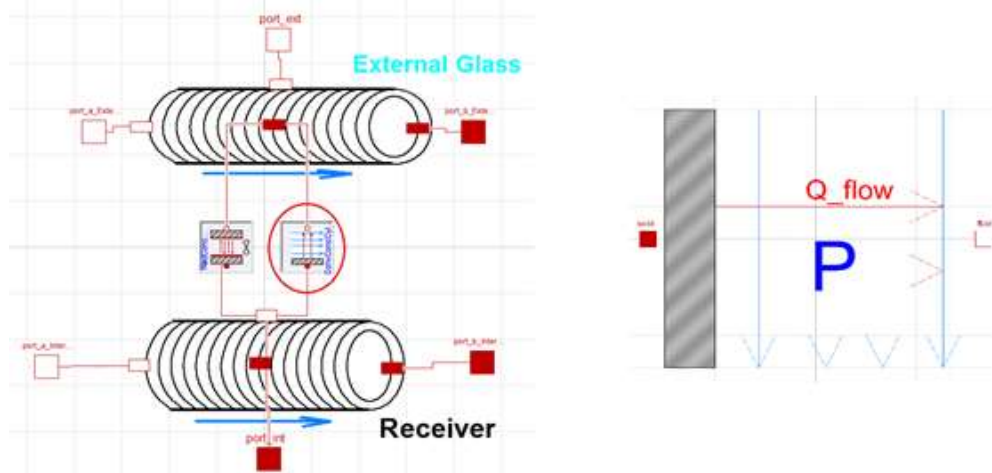


Figure 76. Component of the convection in the interior of the collector when there is air inside.

Like happened with the ConvConcentricCylindHydrogen, this new component is the same as the model for the heat transfer in a vacuum atmosphere, but instead of vacuum, it is used to study the case when air enters the gap between the glass cover and the absorber. The model has to consider the equation for the heat transfer through convection between concentric cylinders when there is air at ambient pressure.

As the air inside is between two cylinders and at ambient pressure. According with (P. Incropera, & D. De Witt, (2008) in the chapter *Convección Libre* of the book *Fundamentos de Transferencia de Calor* the equation and correlations used are the next ones.

$$Q = Gc \cdot \Delta T$$

Where:

- $\Delta T = (T_{solid} - T_{fluid})$.
- $Gc = \frac{2 \cdot \pi \cdot k_{ef}}{\ln\left(\frac{D_o}{D_i}\right)}$
- k_{ef} : effective thermal conductivity. its value depends on the value of Ra_c^* .

$$\text{for } 100 < Ra_c^* < 10^7$$

$$k_{ef} = k \cdot 0,386 \cdot \left(\frac{Pr}{0,861 + Pr}\right)^{1/4} \cdot (Ra_c^*)^{1/4}$$

Where:

- Pr : Prandtl number.

$$Pr = 1,60751 \cdot 10^{-17} \cdot T_{air}^6 - 5,60308 \cdot 10^{-14} \cdot T_{air}^5 + 7,92931 \cdot 10^{-11} \cdot T_{air}^4 - 5,86171 \cdot 10^{-8} \cdot T_{air}^3 + 2,41773 \cdot 10^{-5} \cdot T_{air}^2 - 5,38155 \cdot 10^{-3} \cdot T_{air} + 1,216$$

- k : Thermal conductivity.

$$k = -1,6864 \cdot 10^{-8} \cdot T_{air}^2 + 8,04930 \cdot 10^{-5} \cdot T_{air} - 3,40488 \cdot 10^{-3}$$

- Ra_c^* : Rayleigh number.

$$Ra_c^* = \frac{\left[\ln\left(\frac{D_o}{D_i}\right)\right]^{1/4}}{L^3 \cdot \left(D_i^{-3/5} + D_o^{-3/5}\right)^5} \cdot Ra_L$$

- L : Length of the section of the tube in which the convection happens.
- Ra_L : Rayleigh number.

$$Ra_L = Pr \cdot Gr_L$$

- Gr_L : Grashof number.

$$Gr_L = \frac{9,81 \cdot \beta \cdot (T_{solid} - T_{fluid}) \cdot L^3}{\mu^2}$$

- β : Cubic expansion coefficient.

$$\beta = \frac{1}{T_{air}}$$

- T_{air} : Average temperature.

$$T_{air} = \frac{(T_{solid} + T_{fluid})}{2}$$

- μ : cinematic viscosity of the fluid.

$$\mu = 7,36821 \cdot 10^{-11} \cdot T_{air}^2 + 5,26183 \cdot 10^{-8} \cdot T_{air} - 6,64534 \cdot 10^{-6}$$

Once known how the new component is built and which its function is, it is going to proceed to explain the results obtained in the two tests (dynamic efficiency test and the heat losses test).

The results of the dynamic efficiency test are exposed in the annexes [results in Table-A 21 and in Figure-A 21].

Those results reveal that when air enters to the gap, the collector responds with worse results than in the nominal situation (lower efficiency, HTF's outlet temperature and absorbed energy by the collector; and higher energy losses). This is what was expected, because the heat transference by convection in a vacuum atmosphere is lower than when that atmosphere is full of air at ambient pressure.

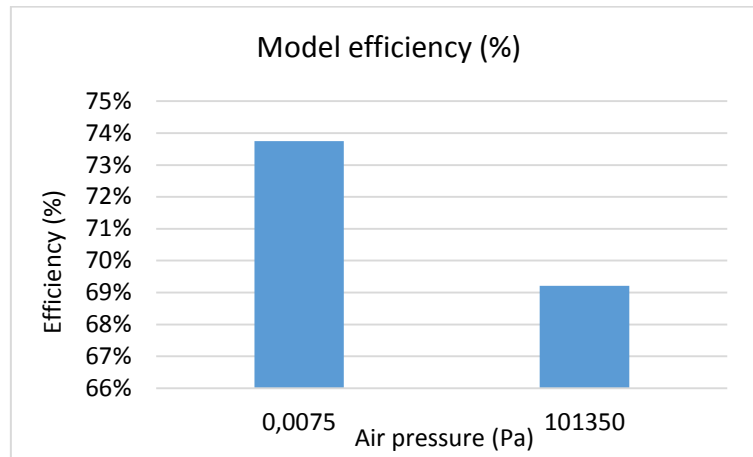


Figure 77. Results for the efficiency when there is air infiltration.

In order to know how this parameter really affects to the collector behaviour, they have been expressed the results in percentage [Table-A 23]. This table confirms what has been said in the paragraphs before.

After this test, it has also been carried out the heat losses efficiency tests for the different HTF's inlet temperatures, so more results are obtained in addition. Results exposed in the anexes [Table-A 24 and in Figure-A 22; and in percentages in Table-A 25].

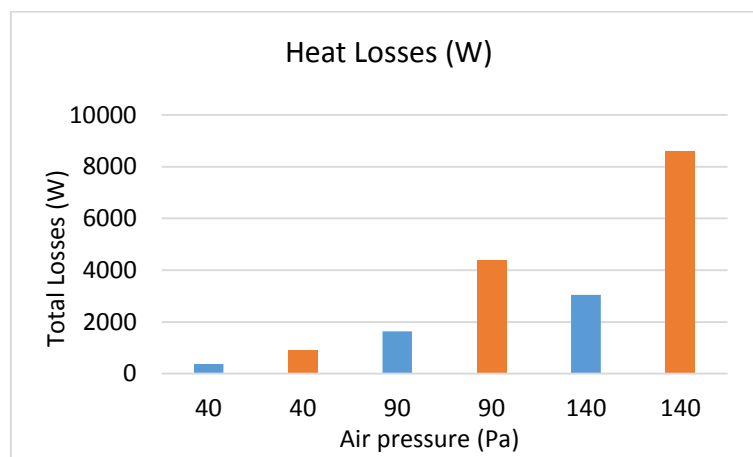



Figure 78. Results of the heat losses when there is air infiltration.

We can see that these results also reveal that the heat losses increase when there is air infiltration in the space between the absorber and the glass cover. The **¡Error! No se encuentra el origen de la referencia.** also shows that the effect of the air infiltration increases when it does the HTF's inlet temperature. Meanwhile the outlet temperature is not affected at all.

4.1.5. Degradation of the HTF.

During this test it has been tried the effect of the degradation of the Syltherm® 800. Some test carried out by the TEKNIKER enterprise show that the only parameter of the HTF which is

affected by its degradation and could have some influence in the thermal behaviour of the collector is the cinematic viscosity. So during these tests, it will be seen how this parameter affects to the results. On the next image there are presented the result obtained for the degradation of the HTF.


Heat transfer fluids

HTF CHARACTERIZATION **USED FLUID CHARACTERIZATION**

With characterization of HTF user can optimize their consumption through knowledge of the actual state of degradation and predictive and proactive replacement, and not purely preventive, of the deteriorated liquids.

Test	Value	Significance
"Low Boilers" content (ASTM D 2887)	0%	Low boiler above 1% should be removed by the consumer in a safe and environmental acceptable way. These products may create excessive pressure pump cavitation and poor circulation
"High Boilers" content (ASTM D 2887)	0-10%	High boiler above 10% generally warrant the fluid replacement.
Residue	0-1%	Could cause mechanical problems within the heat transfer system, due to the erosion of metal surface
Insolubles (ASTM D 883)	0-0.5 g/l	High levels indicate thermal degradation of the fluid and sludge problems. Decrease the efficiency
Water (ASTM D 1744)	0-400 ppm	Similar in effect to low boilers
Acid Number (ASTM D 974)	001-0.2mg	Acid usually are formed in HTF from contamination from material outside the system.
Flas point V/C (ASTM D 93)	110-10	Low boilers created as a result of thermal degradation will lower of the flas point. Outside contaminants may have similar effect
Cinematic Viscosity at 40° C (ASTM D 445)	2.48-10	Viscosity can be used as indicator of thermal degradation since low boilers will trend to reduce viscosity while high boilers will increase it
Cinematic Viscosity at 100° C (ASTM D 445)	0.99-10	Viscosity changes also affect the overall heat transfer capabilities of the fluid
pH (extracción en agua)	5-8	May indicate systems contamination with oxygen or foreign material

Figure 79. Results of the tests carried out to analyze the degradation of the Heat Transfer Fluid.

For the realisation of both tests it has been necessary the construction a new media model. This kind of models quantifies some qualities of a fluid (in this case Syltherm® 800) depending on its condition such as pressure and temperature. The new built model allows increasing the value of the fluids cinematic viscosity a percentage selected by the user.

According to the mentioned test, the degradation of the HTF can make the cinematic viscosity change its value 10% up or down depending on the working temperatures, so that is the change that is going to be evaluated.

In the tables included in the annexes for this part, they are presented the results for both tests. First the results of the dynamic efficiency test [Table-A 26 and in Figure-A 23 and in percentages in Table-A 27 and in Figure-A 24], and after the ones obtained in the heat losses tests.

The results from the dynamic efficiency test show how the effect of the cinematic viscosity is almost imperceptible. This means that it will be nearly impossible to appreciate an efficiency decrease which is caused by the degradation of the HTF.

It has also analysed the effect of the variation of this parameter in the heat losses test, to see whether it has any effect on it. The results are which appear below.

- When the HTF's inlet temperature is 40°C [Table-A 28 and in Figure-A 25].
- When the HTF's inlet temperature is 90°C [Table-A 29 and in Figure-A 26].
- When the HTF's inlet temperature is 140°C [Table-A 30 and in Figure-A 27].
- Comparing the three cases [Figure-A 28].

The results of the heat losses test show, as the ones of the dynamic efficiency test did, that the HTF's degradation has not an appreciable effect. So this parameter is not going to be considered as guilty for a worse performance of the collector.

4.1.6. Absorptance of the absorber tube

During this tests it is going to be evaluated the effect of the decrease of the value of the absorber's absorptance. This parameter gets worse as the absorber degrades. As this parameter quantifies the amount of radiation that the absorber absorbs out of the radiation that reaches its surface, it has no sense to analyse the influence in the heat losses test as, during that test, there is no incident irradiation. So in this case it will just be carried out the dynamic efficiency test.

Like in previous, first the value of the absorptance has been varied from 0 to 1, in order to see whether its influence is significant [results in Table-A 31 and in Figure-A 29]. Afterwards, if it is, it is going to analyse its effect with more realistic values.

The results presented in the **¡Error! No se encuentra el origen de la referencia.** show that the absorptance of the absorber has a huge influence in the efficiency of the absorber. Now it will be studied its influence when the variation of its value is more realistic, such as values from 0,8 to 1 [results in Table-A 32 and in Figure-A 30, they are also exposed the same results in Table-A 33 and in Figure-A 31 expressed in percentages].

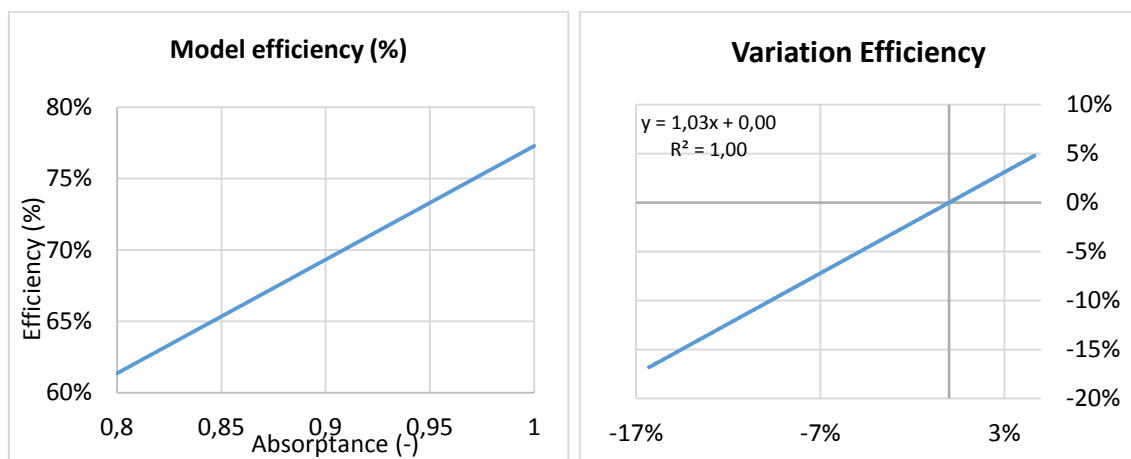


Figure 80. Results of the efficiency when the absorptance of the absorber varies from 0,8 to 1.

Those results show that the absorptance of the absorber has a strong influence in the efficiency of the collector. This is such, that a decrease of 10% in the value of the absorptance, decreases the efficiency 10% too.

4.1.7. Emittance of the absorber tube

This parameter, as well as the absorptance, gets worse (increases its value) with the degradation of the absorber. In the next paragraphs it is going to be studied how it affects to the collectors behaviour. In this case, as it does affect to the amount of heat losses, they are going to be analysed both tests, the dynamic efficiency test and the heat losses test.

As the model has been validated using the emittance of the absorber, during both tests, its value has been modified a percentage from its nominal value, and not its value itself. First during the dynamic efficiency test the value of the emittance has been varied from a 0% to a

100%, to see if its effect was remarkable. The results of this first test are exposed in the annexes [Table-A 34 and in Figure-A 32]

As we can see in the Table-A 36, the variation of the emittance does not affect much to the collector's efficiency. Its effect is just remarkable for the heat losses during this test. So it has no sense to study more the influence of this parameter for this test.

Although the influence in the efficiency is inappreciable, it has been carried out the heat losses test, to ensure whether the emittance affect them. Like in the previous cases it has tested the model for different values of the absorber's emittance, and for different HTF's inlet temperatures (40, 90 and 140°C).

- When the HTF's inlet temperature is 40°C [Table-A 35 and in Figure-A 33].
- When the HTF's inlet temperature is 90°C [Table-A 36 and in Figure-A 34].
- When the HTF's inlet temperature is 140°C [Table-A 37 and in Figure-A 35].
- Comparing the three cases [Figure-A 36].

In those results we can see that this parameter affects to the heat losses. To quantify its influence, after the previous results in the annexes, are presented the same results, but in percentage of the nominal result.

- When the HTF's inlet temperature is 40°C [Table-A 38 and in Figure-A 37].
- When the HTF's inlet temperature is 90°C [Table-A 39 and in Figure-A 38].
- When the HTF's inlet temperature is 140°C [Table-A 40 and in Figure-A 39].
- Comparing the three cases [Figure-A 40].

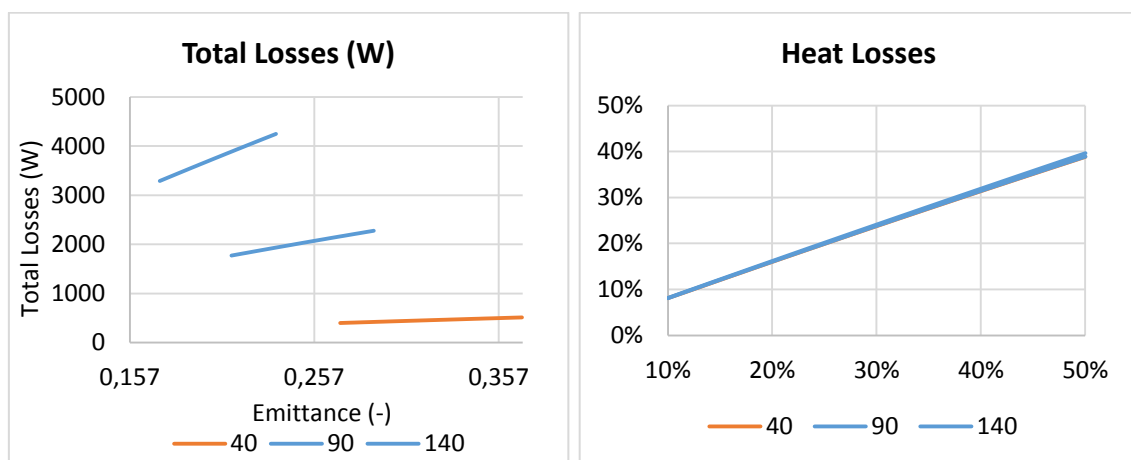


Figure 81. Results of the heat losses when the emittance of the receiver varies.

As it has been said the results show that when it comes to heat losses, the emittance of the metal tube has huge influence, to the point that heat losses can increase around a 50% when the emittance increases a 40%.

4.1.8. Emittance of the glass cover

In these paragraphs it has been analysed how the variation of the emittance of the glass cover affects in the different tests. As this parameter affects the heat losses, both test have been done.

First it has been realized the dynamic efficiency test, studying the results for values of the emittance from 0,1 to 1. It has to take into account take this parameter also affects to the form factors.

Table 22. Form factors of the glass cover for different values of its emittance.

Glass emittance[-]	Fv	Fv1
0,85	0,9091	0,0809
0,1	0,9902	0,0096
0,2	0,9802	0,0192
0,3	0,96997	0,0288
0,4	0,9595	0,0383
0,5	0,9487	0,0478
0,6	0,9377	0,0573
0,7	0,9264	0,0668
0,8	0,91497	0,0762
0,9	0,9032	0,0856
0,99	0,8925	0,0941

*Fv stands for the glass' form factor to the sky and Fv1 to the mirror.

In the results in Table-A 41 and in Figure-A 41 it can be seen that the emittance of the glass cover does not really affect to the efficiency of the collector, so it is not necessary to repeat the test for more realistic variation of the parameter.

Although there is not big effect on the efficiency test, it is has also done the heat losses test to ensure that it has not much influence.

- When the HTF's inlet temperature is 40°C [Table-A 42 and in Figure-A 42].
- When the HTF's inlet temperature is 90°C [Table-A 43 and in Figure-A 43].
- When the HTF's inlet temperature is 140°C [Table-A 44 and in Figure-A 44].
- Comparing the three cases [Figure-A 45].

The results show what was previously expected, the emittance of the glass cover has a very low influence in the behaviour of the collector when real variation of that parameter happen. This means that it is nearly impossible to blame this parameter for an efficiency or heat losses variation, because these variations are imperceptible.

4.1.9. Emittance of the shield

The next parameter to be analysed has been the emittance of the shield. As it was explained some pages before, the shields are the metallic ends of the collector, which are used to join the glass cover and the absorber, as well as compensate the differential dilatations that could appear.

In this case, the values of the emittance analysed go from 0,01 to 0,1.

The shield's emittance also affect to its form factors:

Table 23. Form factors of the shield for different values of its emittance.

Shield emittance[-]	Fs	Fs1
0,03	0,9091	0,0809
0,01	0,9902	0,0096
0,02	0,9802	0,0192
0,03	0,96997	0,0288
0,04	0,9595	0,0383

0,05	0,9487	0,0478
0,06	0,9377	0,0573
0,07	0,9264	0,0668
0,08	0,91497	0,0762
0,09	0,9032	0,0856
0,1	0,8925	0,0941

*Fs stand for the shield's form factor to the sky and Fs1 to the mirror.

The results presented in the Table-A 45 and in Figure-A 46 show that the emittance of the shield has no effect on the efficiency of the collector. Like in the previous case, it has also been studied the influence of this parameter on the heat losses.

- When the HTF's inlet temperature is 40°C [Table-A 46 and in Figure-A 47].
- When the HTF's inlet temperature is 90°C [Table-A 47 and in Figure-A 48].
- When the HTF's inlet temperature is 140°C [Table-A 48 and in Figure-A 49].
- Comparing the three cases [Figure-A 50].

As it is shown in the results above, the emittance of the shield has neither influence on the heat losses. So it can be concluded that when in the reality a change in the efficiency or in the heat losses happen, it is not due to the change in the shield's emittance.

4.1.10. Interception factor

This factor, as has previously explained, quantifies the amount of solar irradiation reaches the collector out of the energy reflected by the mirrors. It depends of different factors, such as the geometry of the parabola, the solar tracking, the position of the collector's axis etc. it is interesting to analyse its effect as the change in its value affects to the efficiency.

Like happened in the case where the reflexivity has been studied, it has no sense to see the effects on the heat losses test, as this parameter only affects to the incident radiation. So it has just carried out the dynamic efficiency test. First it has been studied its influence when its value varies from 0 to 1. These results are exposed in the annexes [in Table-A 49 and in Figure-A 51].

We can see how the effect of this parameter is lineal. This is because it acts directly in the solar radiation, reducing the amount of energy that reaches the glass cover when its value decreases. After analysing the case of huge changes in the interception factor, it has been studied what happens with more realistic changes, from 0,8 to 1 [results in Table-A 50 and in Figure-A 52; and in Table-A 51 and in Figure-A 53 expressed in percentage].

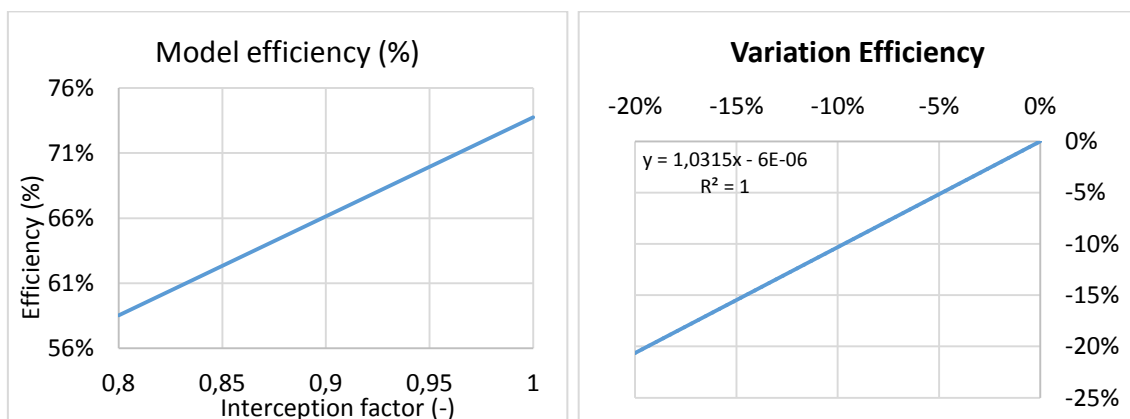


Figure 82. Results of the efficiency test when the interception factor varies.

The results of this test show what it was previously said, the behaviour of the collector varies linearly with the interception factor, a decrease of a 10% in this factor produces the same decrease in the energy absorbed by the collector and so in the efficiency.

5. FUTURE WORKS

When using a model for the simulation of real systems, it is important to have the model validated so the results given by it are as close as possible to the results from the reality. In this way during this project the validation carried out has been a static validation; this consists in approximating as much as possible the results of the simulation to the real ones when inlet information corresponds to one moment of time.

As it has been seen in this project, when it comes to the static validation of CCPs, they have been done the *Heat losses test*, the *peak optical efficiency test* and the *Dynamic efficiency test*. In the first two, the data, such as the solar irradiation, the inlet HTF's temperature and mass flow... are maintained constant and the results obtained, are collected once the system is stabilized. Then the same procedure is carried out in the model (introduce the same inlet data and collect the results); the results are compared with the real ones, error committed with the model is acceptable, the static validation is concluded, in other case, the model has to be modified to reduce the errors. The third test is also part of the static validation, but in contrast with the other two, in this case the results are collected during the all duration of the test, with the inlet data maintained constant.

The next step for a complete validation is to do the dynamic validation. This validation differs with the static one in the variability of the inlet data, which means that the data introduced in the model (solar irradiation, Temperature, mass flow...) have no longer constant values. The results obtained are also variable, and the information recollected has to be from a period of time long enough to appreciate the influence of the variation in the inlet data.

In the case of the dynamic validation of the CCPs the tests that could be carried out are which follow:

- Variation in the HTF's mass flow:
Take the system to a stable situation where all the inlet parameters are constant and with a determined value, and once reached that point increase the HTF's mass flow enough so that increase produces changes in the exit of the system, maintaining the rest of the parameters constant. Then wait until the system is stable again. It is also possible to decrease the mass flow instead of increasing it.
- Variation in the HTF's inlet temperature:
This test is the same as the previous one, but instead of changing the mass flow, in this case the inlet temperature is varied. The answer of the system to this variation is not as quick as the previous one, as it is not possible to vary the inlet temperature instantly.
- Combine variation of the HTF's mass flow and inlet temperature:
This one is a combination of the previous two tests.
- Variation of the solar irradiation:
This one is the same as the previous ones. First the system is taken to a stable situation, where the input data and the answer... of the system to this data are constant. Then the variation in the solar radiation is produced. This is easy when the system validated is small, as it can be covered and discovered from the solar radiation by put anything between the sun light and the collector. But when it comes to huge collectors, it is not so easy; in this cases the possibilities are, if there are clouds on the sky, wait until one crosses and covers the collector from the sun (this has to be done carefully, because it is necessary that the system gets the stable situation before and

after the cross of the cloud, and that is not easy if there are too many clouds crossing as the final stable situation is not reached). Another possibility is to defocus the collector for some minutes (in this case it is necessary to measure the real radiation the reaches the collector, which is not always possible, because the radiation meter is usually apart of the collector, and does not take into account whether the collector is focused or not, in measures the radiation that reaches the Earth ground).

One collected all the information from the real system; it is introduced into the model, and compared the results in both cases as it was done in the static validation. If the errors committed in these tests are acceptable, it can be concluded that the model represents the real system accurately. If not, the model has to be modified (trying to affect as less as possible to the results of the state case) until the error committed is acceptable.

The use of this kind of models could have a great influence during the planning of new solar plants, because, with their help, introducing the information of the plant, the model can give anticipate how the plant is going to work.

Finally it would be interesting to analyse how the degradation of the different components (and so the degradation of their properties) appear during the lifetime of a collector. A combination of this study with the done during this project, implemented in a model, would allow simulating all the useful lifetime of a collector, and see when it is really necessary to replace a component.

6. ECONOMICS

On the next paragraphs it is presented an economic analysis of this kind of investigation projects. The aim of this study is to see in an approximated way how which are the cost of an investigation project.

First of all, this project is part of the STAGE project, so the funds come from it. Finally it has to be taken into account that the values presented are approximated and in the reality may vary.

6.1. Internal hours

In this part they are included the hours worked by any worker involved in the project, and the cost per hour of each.

Table 24. Summary of the internal hours.

	Number of hours	Cost per hour [€/h]	Total Cost [€]
Project director	70 hours	100 €/h	7.000,00 €
Project Engineer	750 hours	50 €/h	37.500,00 €
Project Draftsman	35 hours	25 €/h	875,00 €
		Subtotal	45.375,00 €

6.2. Amortizations

This are the fixed assets of the company used for the project. In this case, it is only included the license of the informatics program Dymola®. As the duration of the project has been of 7 month, this has to be taken into account to see how much the license has really cost.

Table 25. Summary of the amortization.

	Annual Cost [€/year]	Total Cost [€]
Dymola license	6.000,00 €/year	3.500,00 €
	Subtotal	3.500,00 €

6.3. Costs

In this part they are included the cost of everything used during the Project, but why no use once this has concluded.

Table 26. Summary of the costs.

	Cost per month [€/month]	Total Cost [€]
Office amortization	800,00 €/month	5.600,00 €
General services (light, water, cleaning...)	400,00 €/month	2.800,00 €
Office supplies	110,00 €/month	770,00 €
Telephone, informatics (printer)	350,00 €/month	2.450,00 €
	Subtotal	8.470,00 €

6.4. Budget summary

Finally this part includes a summary of all the previous sections in one table.

Table 27. Budget summary.

	Coste Total[€]
INTERNAL HOURS:	45.375,00 €
AMORTIZATIONS:	3.500,00 €
COSTS:	8.470,00 €
TOTAL COSTS:	57.345,00 €

We can see in the results presented above that the main cause for the cost of this project corresponds to the internal hour. This is really common in investigation projects like this one, because there is no use of material at all, neither use of machinery.

7. CONCLUSIONS

During the sensitivity analysis carried out, it has been seen how different parameters affect to the collectors behaviour. Some of them have no influence at all, neither in the efficiency of the collector during a dynamic test, nor in the heat losses during the heat losses test. These parameters are the degradation of the Heat Transference Fluid, and the emittance of both the glass cover and the shield.

It has also seen that the emittance of the metal tube just affects to the heat losses in an appreciable way. When the value of the emittance increases around a 50% of its nominal value, the heat losses increase around a 40%. When it comes to operation in a solar plant the degradation of this parameter will not be appreciated during the normal operation of the plant, but its influence exists. That is why it is recommended to make periodically heat losses test so the degradation of the absorber tube is reflected.

Finally the other parameters that have been studied do have a huge influence in the efficiency of the collector. First, the infiltration of hydrogen or air in the gap between the glass cover and the metal tube affect both the efficiency and the heat losses. The first one has a bigger influence. When hydrogen enters the gap the efficiency decreases quickly until the pressure of the hydrogen is around 1 Pa, when the efficiency gets stable and around 12% lower than its nominal value. This same pressure increase, affects the heat losses during the heat losses test to be 300% higher. During the operation of a solar plant, as the infiltration of hydrogen occurs really slowly, its influence will not appear spontaneously, but if the efficiency is measured, it will be seen how its value change until it decreases around a 12% where it gets stable. When this happens, it could be carried out a heat losses test and see how much the heat losses have change; if this change is around a 300% the reason for the efficiency loss will be located.

The infiltration of air has less influence, but it also has a considerable influence. When air enters the gap it is because the glass cover has broken, or because there is a fissure in the glass. In both cases air enters and the pressure in the gap is equalised to the ambient temperature. When this happens the efficiency of the collector is reduced around a 6%; and the heat losses increase 150-180% depending on the temperature of the HTF during the heat losses test. This failure is easily recognised because when air gets in contact with the metal tube, its colour gets kind of yellow, so when a decrease in the efficiency of a 6% appears and the collector's tubes are yellow, it is because air has infiltrated.

Finally the other parameters that affect the efficiency are the reflectivity of the mirror, the transmittance of the glass cover, absorptance of the metal tube, and the interception factor. All of them affect the efficiency in the same way (a decrease of a 10% of their value makes a decrease of a 10% in the efficiency). This makes it difficult to differentiate the responsible of the efficiency decrease at first sight; it is required to make some tests.

When the responsible is the reflectivity of the mirrors, it is easily recognised because this parameter is usually measured before any test is carried out.

The other three parameters are harder to blame, because there is no direct way of measuring their value in plant. When a decrease in the efficiency happens and any of the parameters mentioned before is the responsible, it can be measured the temperature of the glass cover's surface, because when the transmittance decreases this temperature increases as less energy trespasses the glass cover.

The only way to differentiate the influence of the absorptance of the metal tube from the intercept factor is to measure the solar radiation that reaches the collector once reflected; if the reflectivity remains at its normal value, but the radiation that reaches the collector is less than what it should be, the responsible for that decrease is the interception factor. So finally it can blame the absorptance for the efficiency decrease when any of the other parameters is responsible of it.

As it has been said in the part of the future works, it would be interesting to study how the analysed parameters vary with the time, so once this variation is introduced into a model, it will be possible to know which is going to be the behaviour of a solar plant during its years of operation, and foresee when the different components of a solar collector should be replaced.

8. REFERENCES

- Beikircher, T., & Spirkel, W. (1996). Analysis of Gas Heat Conduction in Evacuated Tube Solar Collectors. *Journal of Solar Energy Engineering*. 118(3).
- CIEMAT (2014) Plataforma Solar de Almería. Annual Report 2014.
- Dynasim AB (2004). *Dymola. Dynamic modeling Laboratory. User's Manual*. Recovered 8 of November of 2015.
<https://www.inf.ethz.ch/personal/cellier/Lect/MMPS/Refs/Dymola5Manual.pdf>
- Forristal, R (2003). Heat Transfer Analysis and Modelling of a Parabolic Trough Absorber Implemented in Engineering Equation Solver. In R. Forristal, *Heat Transfer Analysis and Modeling of a Parabolic Trough Solar Receiver Implemented in Engineering Equation Solver*. (Pages 98-102).
- Greenpeace International, STELA, & SolarPACES (2016). *Solar Thermal Electricity*. Recovered 15 of March of 2016.
<http://www.greenpeace.org/international/Global/international/publications/climate/2016/Solar-Thermal-Electricity-Global-Outlook-2016.pdf>
- Incropera, F., & De Witt, D. (2008). Convección libre. In F. Incropera & D. De Witt *Fundamentos de Transferencia de Calor*. (4th edition, page 512). Prentice Hall.
- Information about the STAGE project. Recovered 15 of October of 2015.
<http://www.stage-ste.eu/>
- Kennard, E. H. (1938). *Kinetic Theory of Gases*. (Pages 311-327). New York: McGraw-Hill Book Co.
- Román, P. (2011). *Historia de la Energía Solar Térmica*. Recovered 20 of February of 2016.
<http://es.slideshare.net/geopaloma/historia-de-la-energa-solar-termica-i>
- Romero, J. A., Urquía, M. (2015). ParaTrough: Librería en Modelica para el modelado y simulación de plantas termo-solares de colectores cilindro-parabólicos.
- Sherman, F. S. (1963). *A Survey of Experimental Results and Methods for the Transition Regime of Rarefied Gas Dynamics*. New York: Academic Press.
- Smith, C. (1995). *History of Solar Energy*. Recovered 20 of February of 1016.
<http://solarenergy.com/info-history>
- Valenzuela, L., Lopez-Martin, R., & Zarza, E. (2014). Optical and Thermal performance of large-size parabolic-through solar collector from outdoor experiments: A test method and case study. *Elsevier*. 70. 456-464.
- Zarza, E., & M^a Téllez (2006). *Documentación del Curso: Sistemas Solares de concentración*. Course taught by CIEMAT, Unidad de Formación en Energía y Medioambiente.

9. ANNEX I: TABLES AND GRAPHS

Model Validation

Table A 1. Model heat losses depending on the emittance and the HTF medium T.

T _{HTF} [°C]	T _{amb} [°C]	ΔT [°C]	Absorber Emissivity[W/m ²]	h _{Dif} [kJ/kg]	mflow [kg/s]	Energy Losses [W]	Real Losses [W]
39,92	20	19,92	0,1	25,00	10	250,00	498,28
			0,2	42,60	10	426,00	
			0,3	58,60	10	586,00	
59,87	20	39,87	0,1	53,40	10	534,00	999,36
			0,2	91,60	10	916,00	
			0,3	126,50	10	1265,00	
79,82	20	59,82	0,1	87,00	10	870,00	1507,51
			0,2	149,00	10	1490,00	
			0,3	207,00	10	2070,00	
99,83	20	79,83	0,1	126,00	10	1260,00	2032,49
			0,2	218,00	10	2180,00	
			0,3	303,00	10	3030,00	
119,79	20	99,79	0,1	171,00	10	1710,00	2582,74
			0,2	298,00	10	2980,00	
			0,3	415,00	10	4150,00	
139,74	20	119,74	0,1	222,00	10	2220,00	3174,09
			0,2	389,00	10	3890,00	
			0,3	544,00	10	5440,00	
159,70	20	139,70	0,1	281,00	10	2810,00	3824,36
			0,2	495,00	10	4950,00	
			0,3	692,00	10	6920,00	
179,64	20	159,64	0,1	348,00	10	3480,00	4554,63
			0,2	616,00	10	6160,00	
			0,3	862,00	10	8620,00	
199,59	20	179,59	0,1	424,00	10	4240,00	5389,22
			0,2	753,00	10	7530,00	
			0,3	1055,00	10	10550,00	
219,52	20	199,52	0,1	508,00	10	5080,00	6355,64
			0,2	906,00	10	9060,00	
			0,3	1272,00	10	12720,00	
239,46	20	219,46	0,1	603,00	10	6030,00	7484,65
			0,2	1079,00	10	10790,00	
			0,3	1517,00	10	15170,00	
259,38	20	239,38	0,1	709,00	10	7090,00	8810,18
			0,2	1273,00	10	12730,00	
			0,3	1790,00	10	17900,00	
279,30	20	259,30	0,1	827,00	10	8270,00	10369,38
			0,2	1489,00	10	14890,00	
			0,3	2095,00	10	20950,00	
299,21	20	279,21	0,1	958,00	10	9580,00	12202,55
			0,2	1728,00	10	17280,00	
			0,3	2433,00	10	24330,00	
319,11	20	299,11	0,1	1102,00	10	11020,00	14353,14
			0,2	1993,00	10	19930,00	
			0,3	2806,00	10	28060,00	
339,01	20	319,01	0,1	1261,00	10	12610,00	16867,73
			0,2	2284,00	10	22840,00	
			0,3	3217,00	10	32170,00	
358,89	20	338,89	0,1	1434,00	10	14340,00	19796,00
			0,2	2603,00	10	26030,00	
			0,3	3666,00	10	36660,00	
378,77	20	358,77	0,1	1624,00	10	16240,00	23190,68
			0,2	2954,00	10	29540,00	
			0,3	4159,00	10	41590,00	
398,63	20	378,63	0,1	1832,00	10	18320,00	27107,52
			0,2	3336,00	10	33360,00	
			0,3	4697,00	10	46970,00	

Sensitivity analysis

Table A 2. Data for the dynamic efficiency test.

Date	n (-)	w (rad)	Duration (s)	Direct normal irradiance (W/m ²)	HTF flow rate (kg/s)	Inlet T (°C)	Ambient T (°C)	Absorber's Start T (°C)	Collecting area (m ²)
11/06/2012	162,00	0,2895	600,00	943	2,859177	284,9	34,1	285	409,908

Table A 3. Data for the Heat losses test.

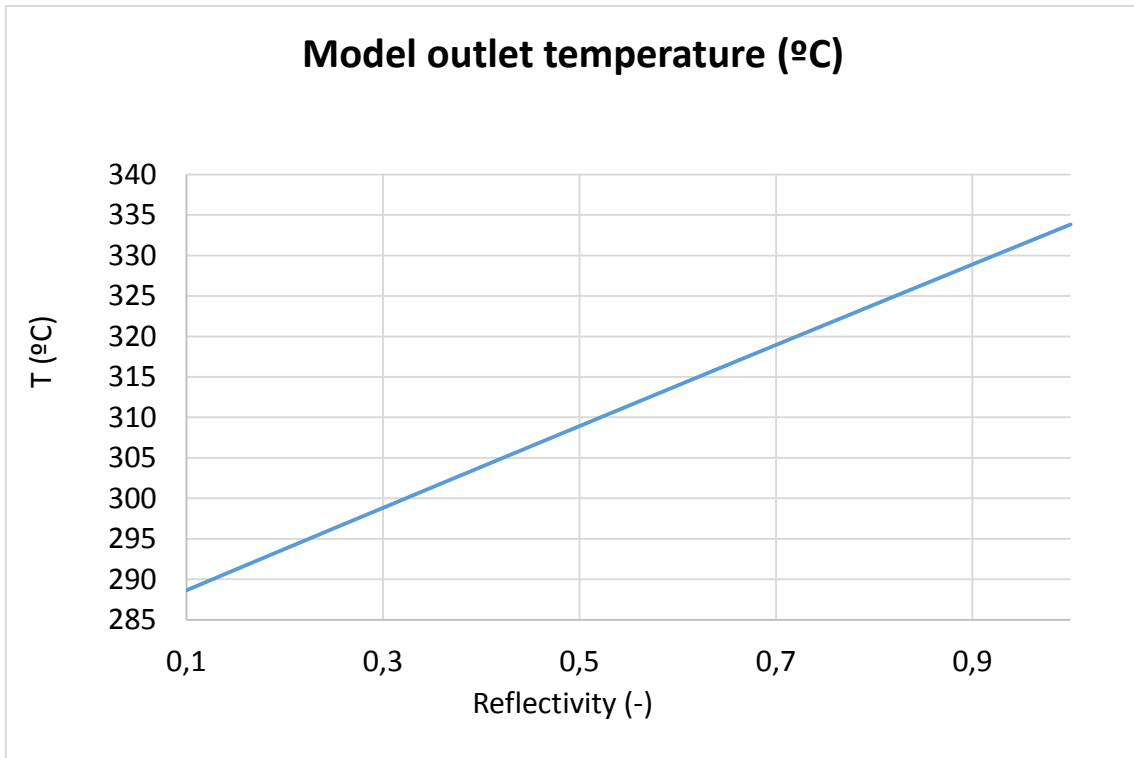
Direct normal Irradiance (W/m ²)	n (-)	w (rad)	Ambient T (°C)	Sky T (°C)	Inlet T (°C)	Mass flow (kg/s)
0	76	0	25	18	40	3,57694351
0	76	0	25	18	90	3,57694351
0	76	0	25	18	140	3,57694351

Reflectivity of the mirror

Table A 4. Results for the dynamic efficiency test when the reflectivity of the collector varies from 0,1 to 1.

Test	Incidence angle (°)	Mirror Reflectance (-)	Model Outlet temperature (°C)	Total Losses (W)	Energy (W)	Useful Solar Radiant Power (W)	Model efficiency (%)
1	16,372	0,931	330,42	16357,62	273524,09	370869,74	73,75%
2	16,372	0,1	288,64	9950,46	22079,84	370869,74	5,95%
3	16,372	0,2	293,75	10653,59	52318,38	370869,74	14,11%
4	16,372	0,3	298,82	11386,68	82498,66	370869,74	22,24%
5	16,372	0,4	303,88	12129,21	112752,60	370869,74	30,40%
6	16,372	0,5	308,92	12887,38	142983,33	370869,74	38,55%
7	16,372	0,6	313,94	13667,76	173261,11	370869,74	46,72%
8	16,372	0,7	318,94	14454,76	203539,34	370869,74	54,88%
9	16,372	0,8	323,92	15266,77	233824,04	370869,74	63,05%
10	16,372	0,9	328,89	16096,69	264130,47	370869,74	71,22%
11	16,372	1	333,83	16944,71	294442,50	370869,74	79,39%

The *Energy* has been calculated as the product of the mass flow and the enthalpy increase. The *Total Losses* are the sum of the total losses due to convection and radiation of the collector, the endIn and the endOut. Finally the *Useful solar Radiant Power* is the product of the direct normal irradiance, the collecting area and the cosine of the incidence angle. These operations are the ones used during the rest of the tests.



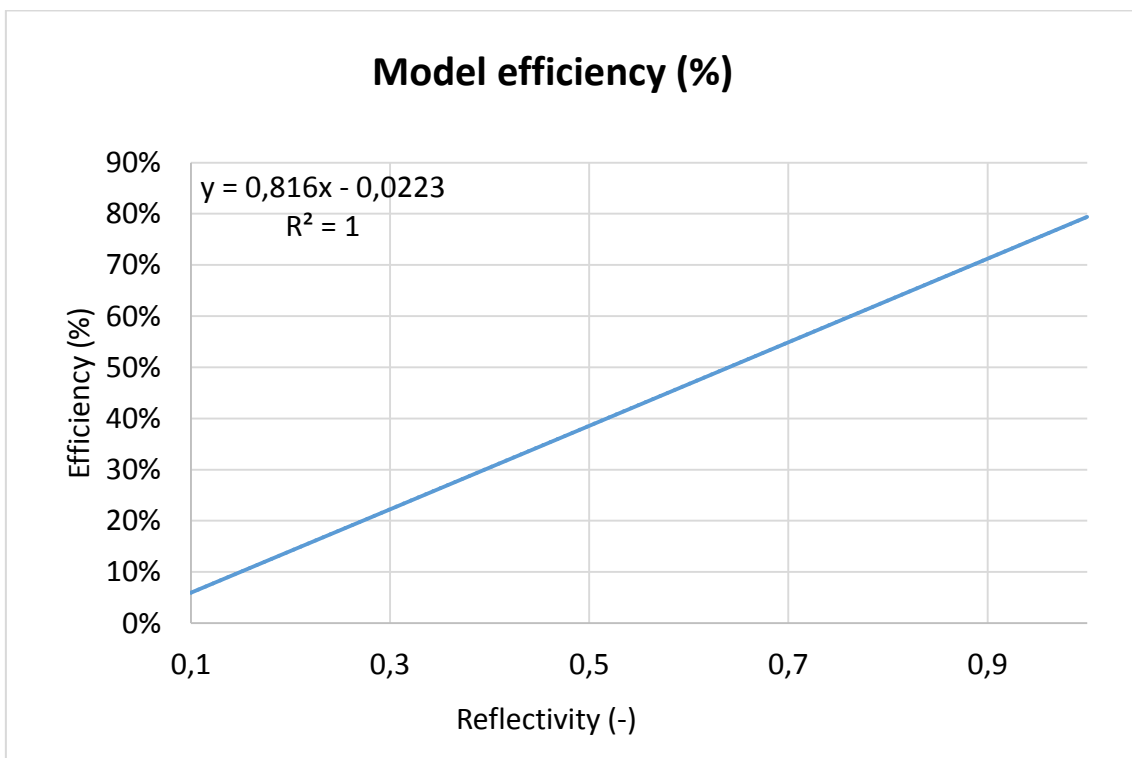
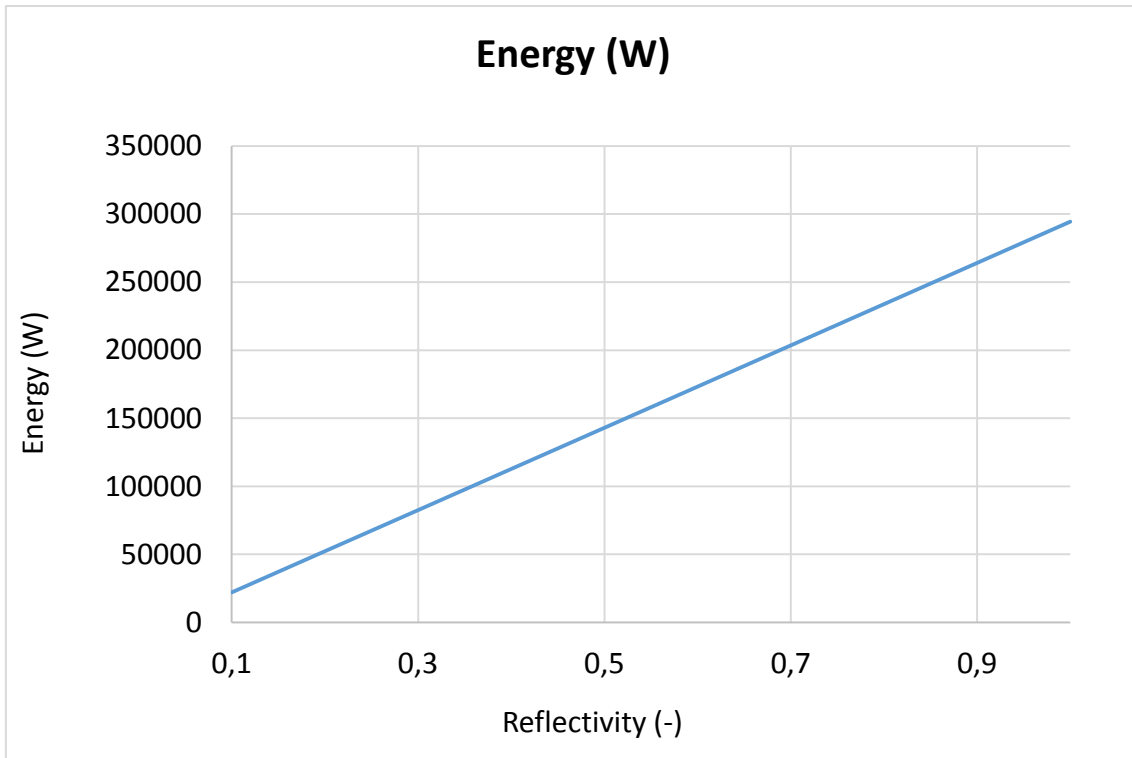
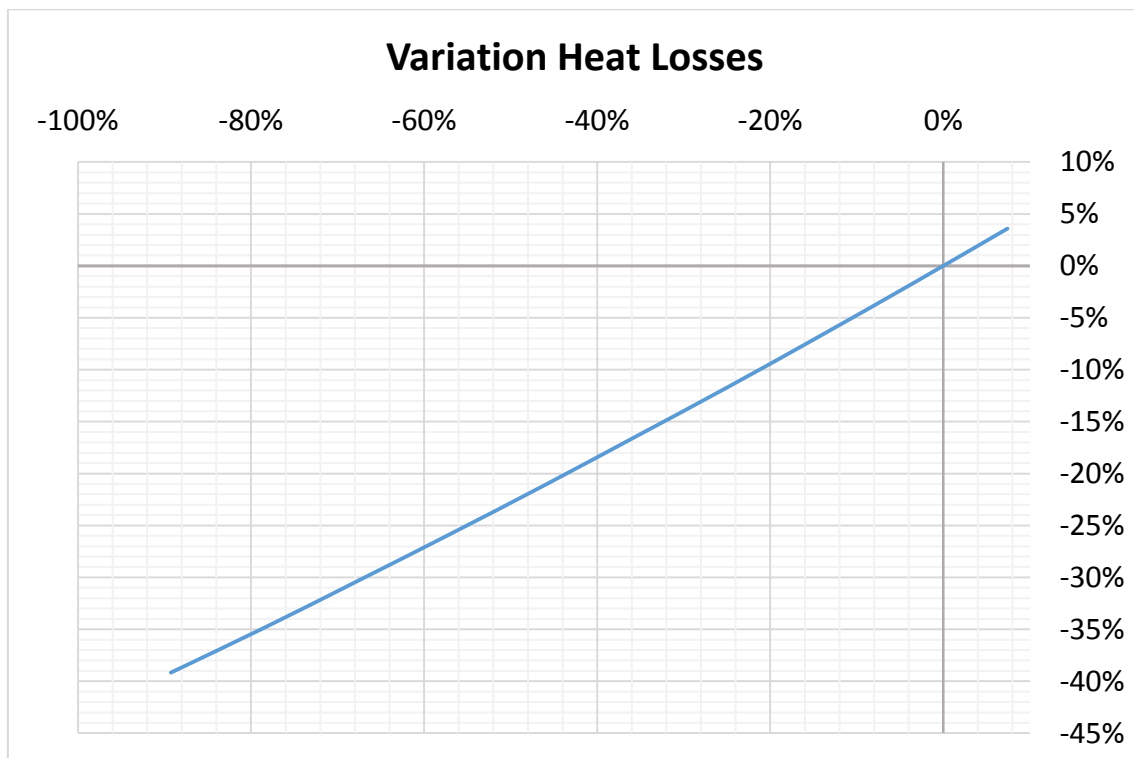


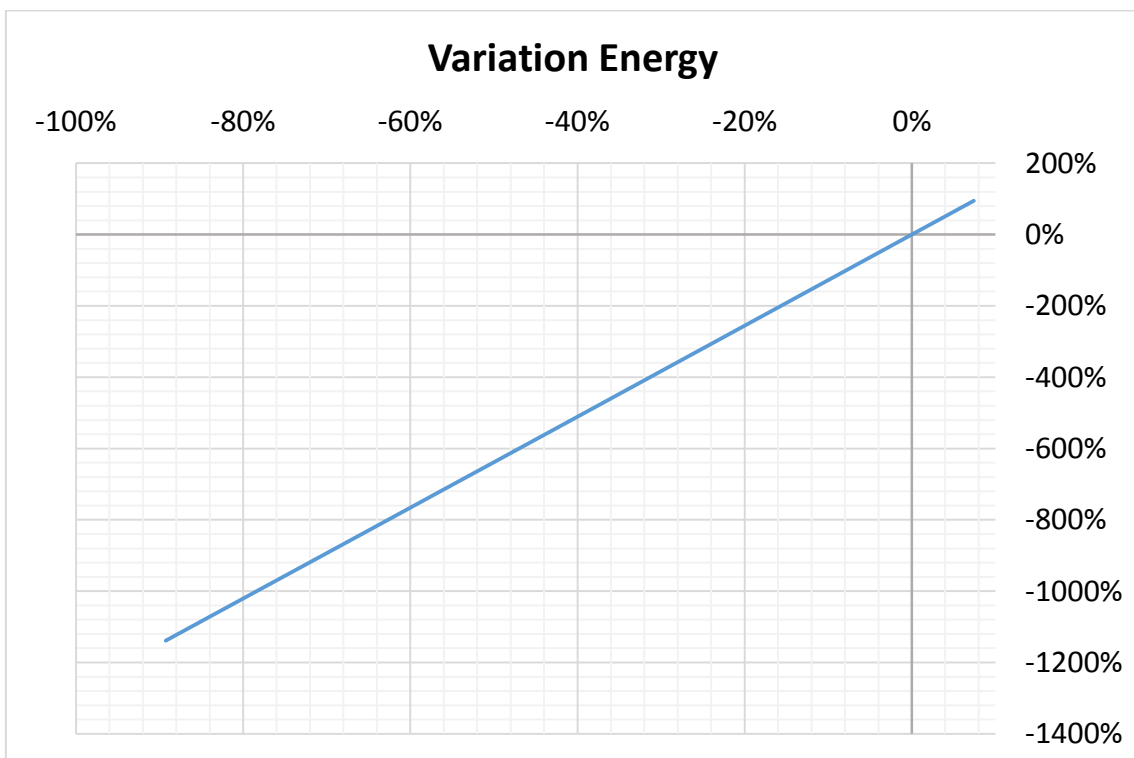
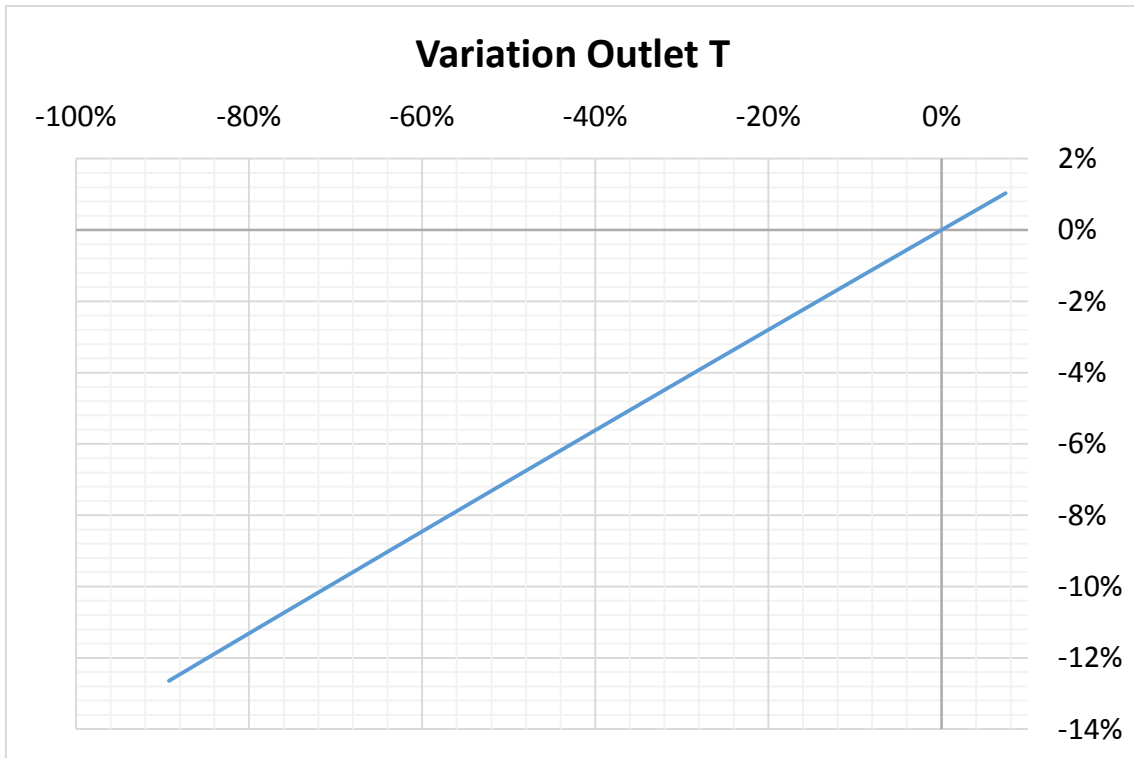
Figure-A 1. Graphs of the results for the dynamic efficiency test when the reflectivity of the collector varies from 0,1 to 1.

Below it is presented how the variation affects but expressed in percentages.

Table A 5. Results from the dynamic efficiency test expressed in percentages when the reflectivity of the collector varies from 0,1 to 1.

Variation Mirror reflectance	Variation Outlet T	Variation Heat Losses	Variation Energy	Variation Efficiency
0,00%	0,00%	0,00%	0,00%	0,00%
-89,26%	-12,64%	-39,17%	-1138,80%	-91,93%
-78,52%	-11,10%	-34,87%	-1001,84%	-80,87%
-67,78%	-9,56%	-30,39%	-865,16%	-69,84%
-57,04%	-8,03%	-25,85%	-728,14%	-58,78%
-46,29%	-6,51%	-21,21%	-591,22%	-47,73%
-35,55%	-4,99%	-16,44%	-454,09%	-36,66%
-24,81%	-3,47%	-11,63%	-316,96%	-25,59%
-14,07%	-1,97%	-6,67%	-179,80%	-14,51%
-3,33%	-0,46%	-1,60%	-42,54%	-3,43%
7,41%	1,03%	3,59%	94,74%	7,65%





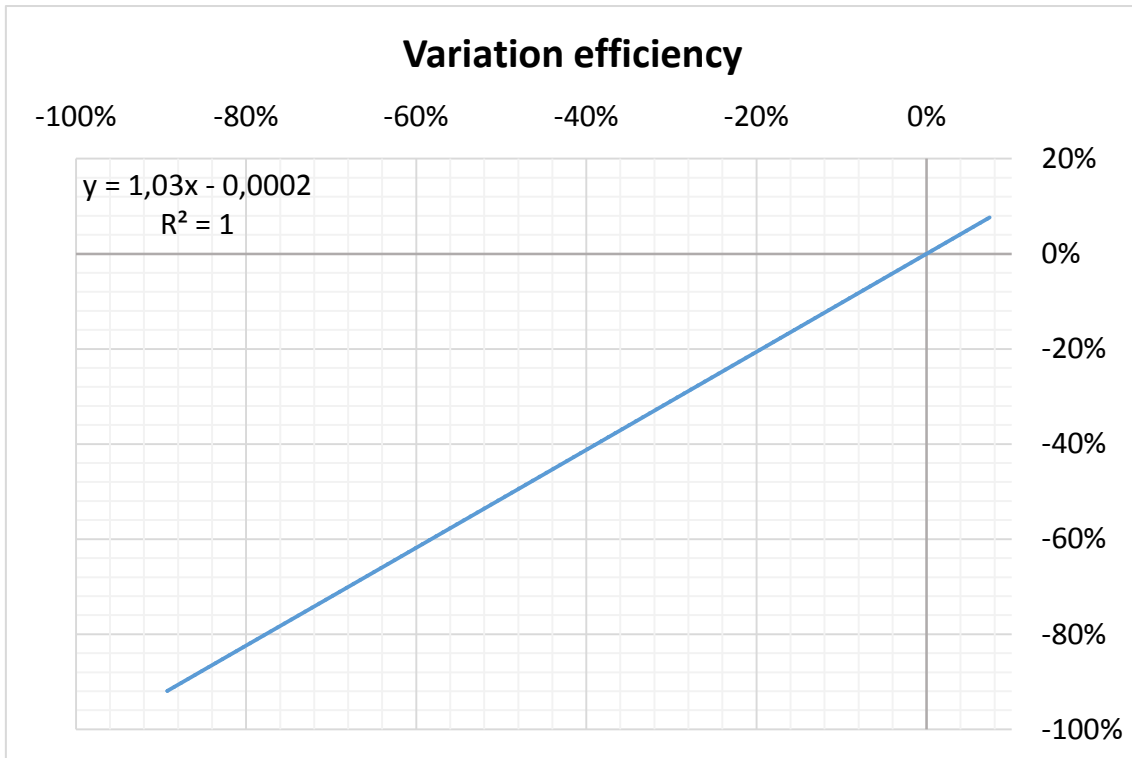
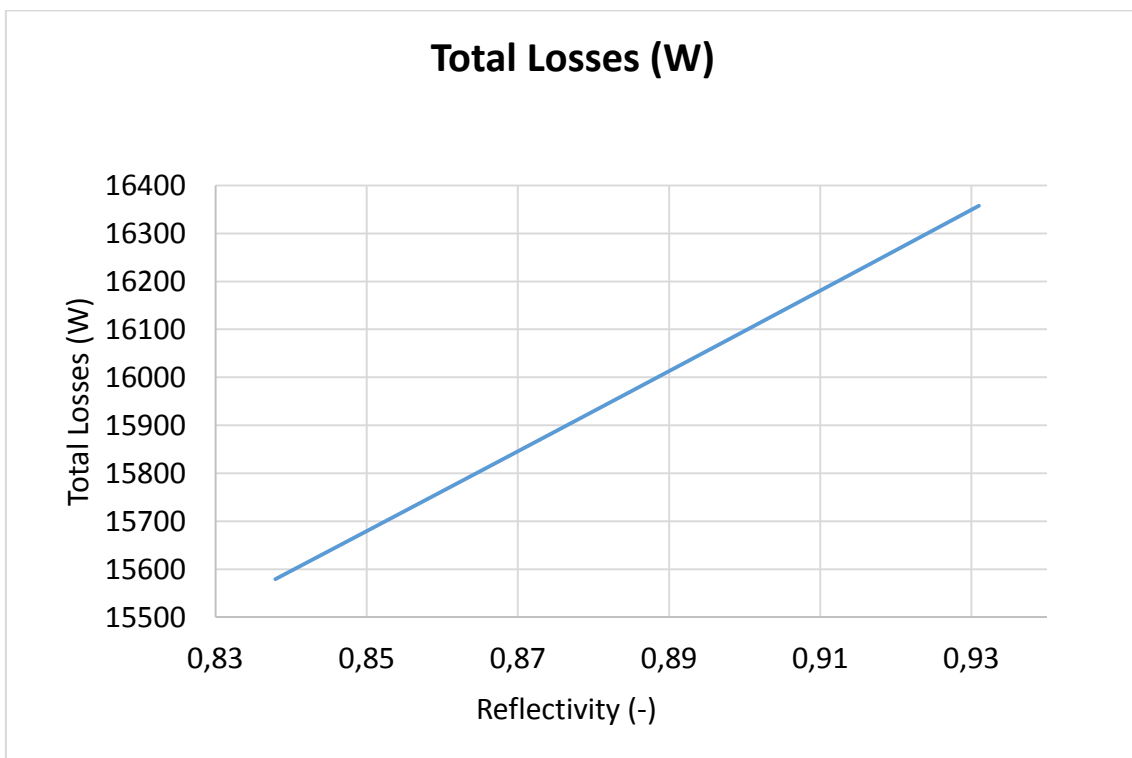
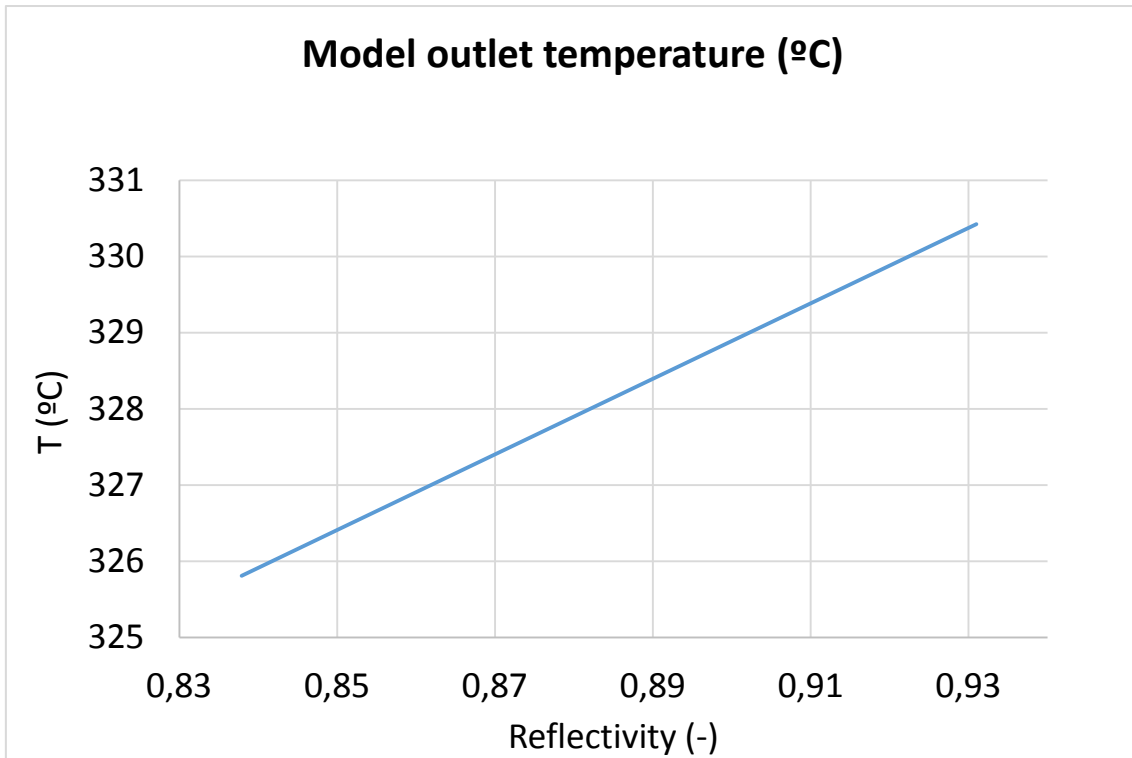


Figure-A 2. Graphs of the results from the dynamic efficiency test expressed in percentages when the reflectivity of the collector varies from 0,1 to 1.

Table A 6. Results for the dynamic efficiency test when the reflectivity of the collector varies from 0,84 to 0,93.

Test	Incidence angle (°)	Mirror Reflectance (-)	Mirror Reflectance (-)	Model Outlet temperature (°C)	Total Losses (W)	Energy (W)	Useful Solar Radiant Power (W)	Model efficiency (%)
1	16,37	0,931	0,931	330,42	16357,62	273524,09	370869,74	73,75%
2	16,37	0,8379	0,8379	325,81	15579,19	245308,64	370869,74	66,14%
3	16,37	0,84721	0,84721	326,27	15656,33	248130,12	370869,74	66,90%
4	16,37	0,85652	0,85652	326,73	15733,63	250951,73	370869,74	67,67%
5	16,37	0,86583	0,86583	327,19	15811,08	253773,42	370869,74	68,43%
6	16,37	0,87514	0,87514	327,66	15888,69	256595,26	370869,74	69,19%
7	16,37	0,88445	0,88445	328,12	15966,45	259416,93	370869,74	69,95%
8	16,37	0,89376	0,89376	328,58	16044,37	262238,95	370869,74	70,71%
9	16,37	0,90307	0,90307	329,04	16122,45	265061,06	370869,74	71,47%
10	16,37	0,91238	0,91238	329,50	16200,67	267879,24	370869,74	72,23%
11	16,37	0,92169	0,92169	329,96	16279,07	270701,63	370869,74	72,99%
12	16,37	0,931	0,931	330,42	16357,62	273524,09	370869,74	73,75%



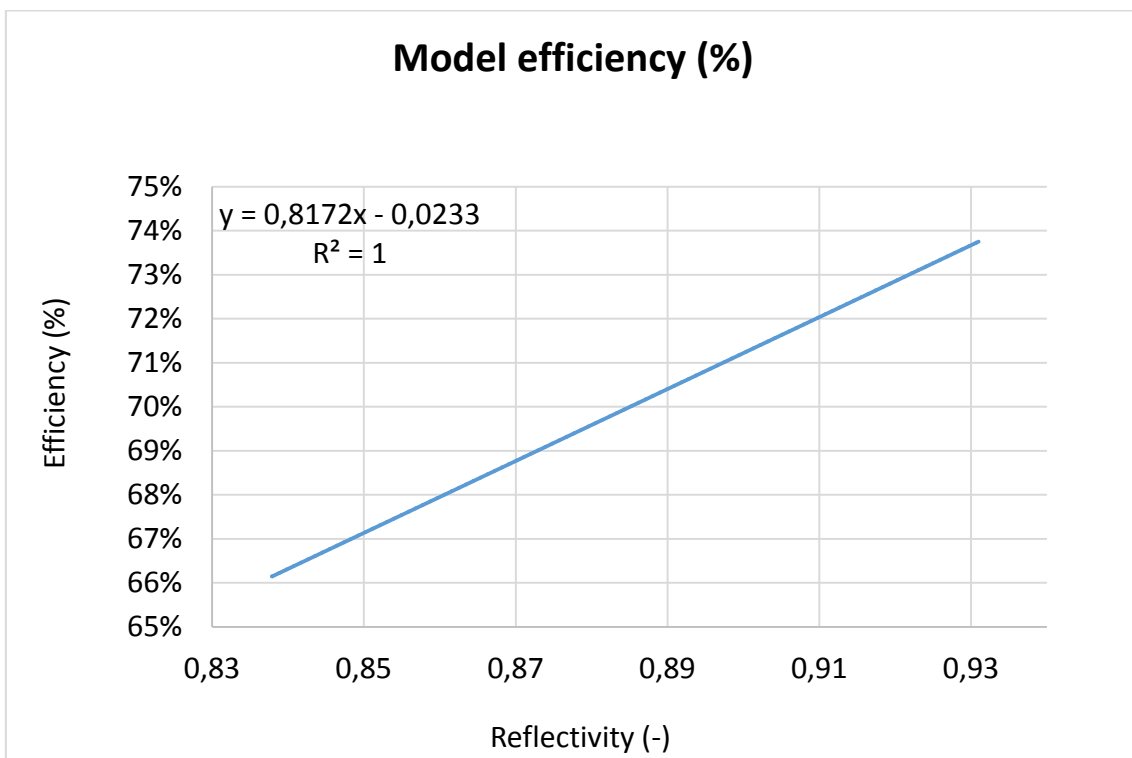
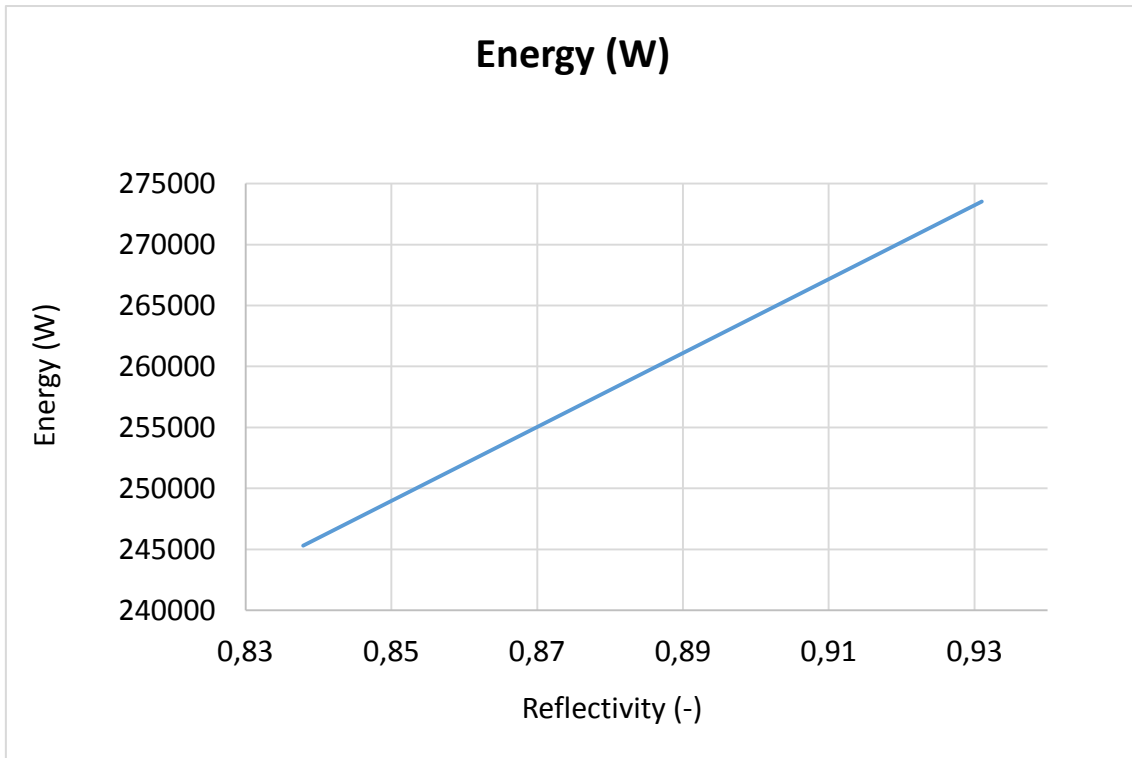
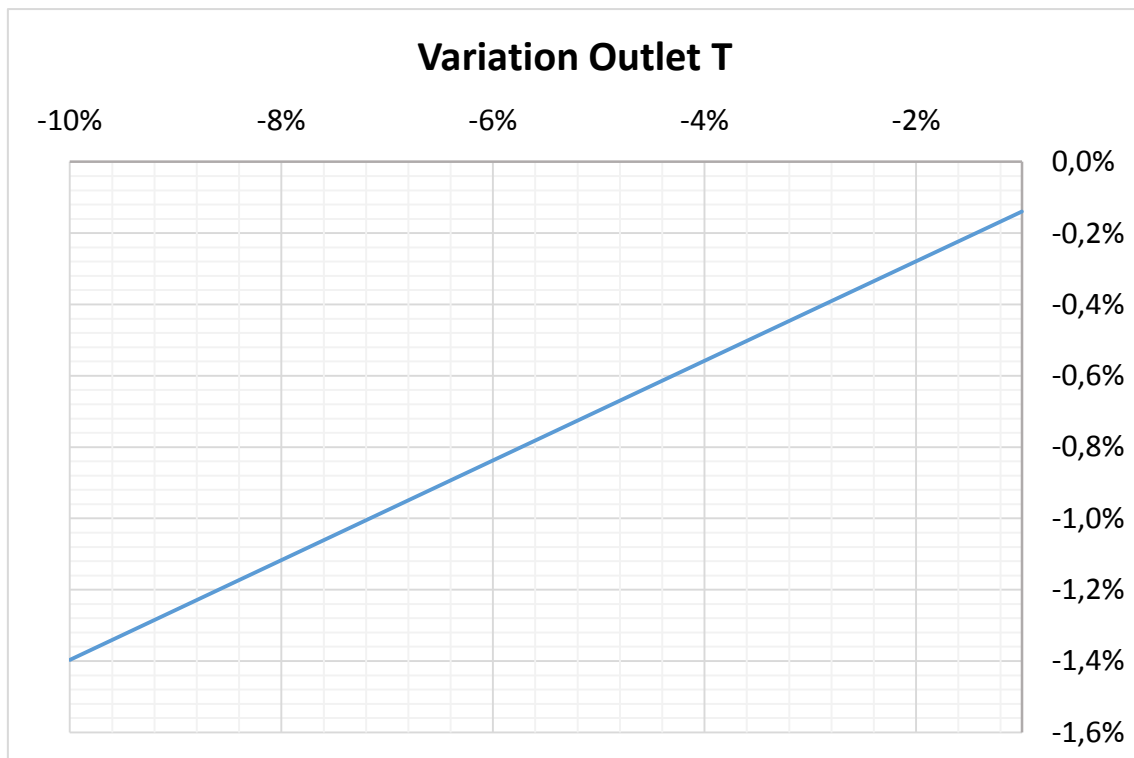


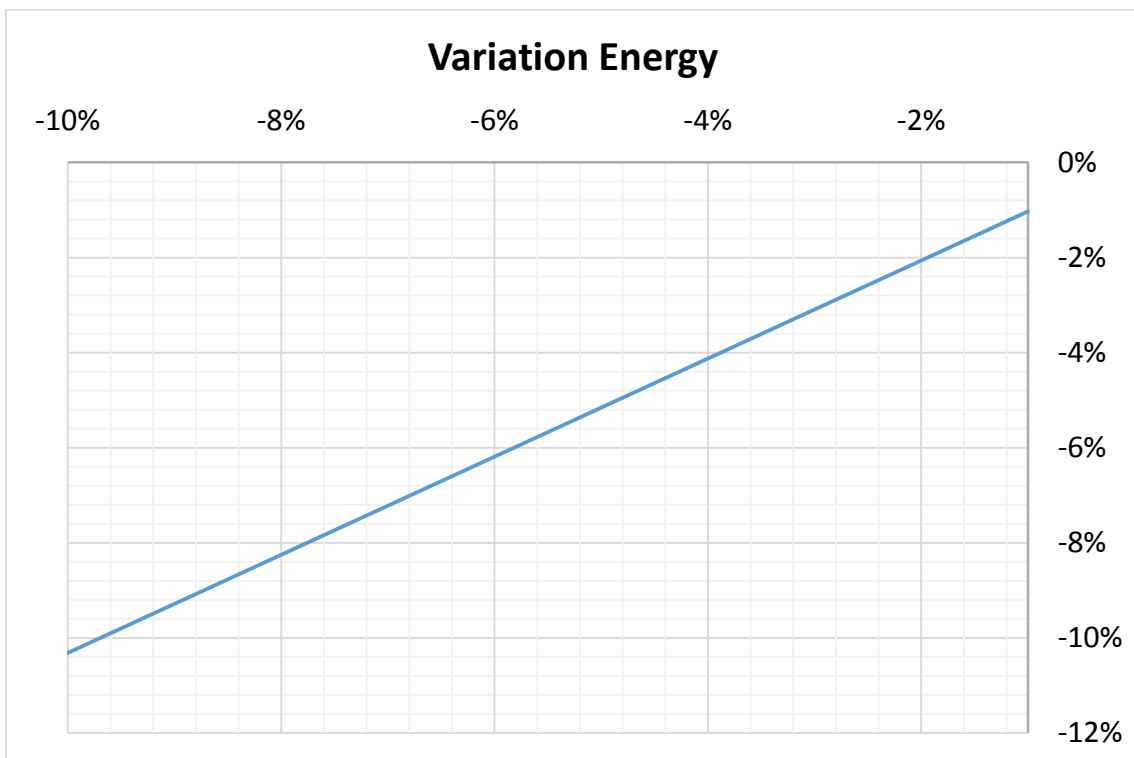
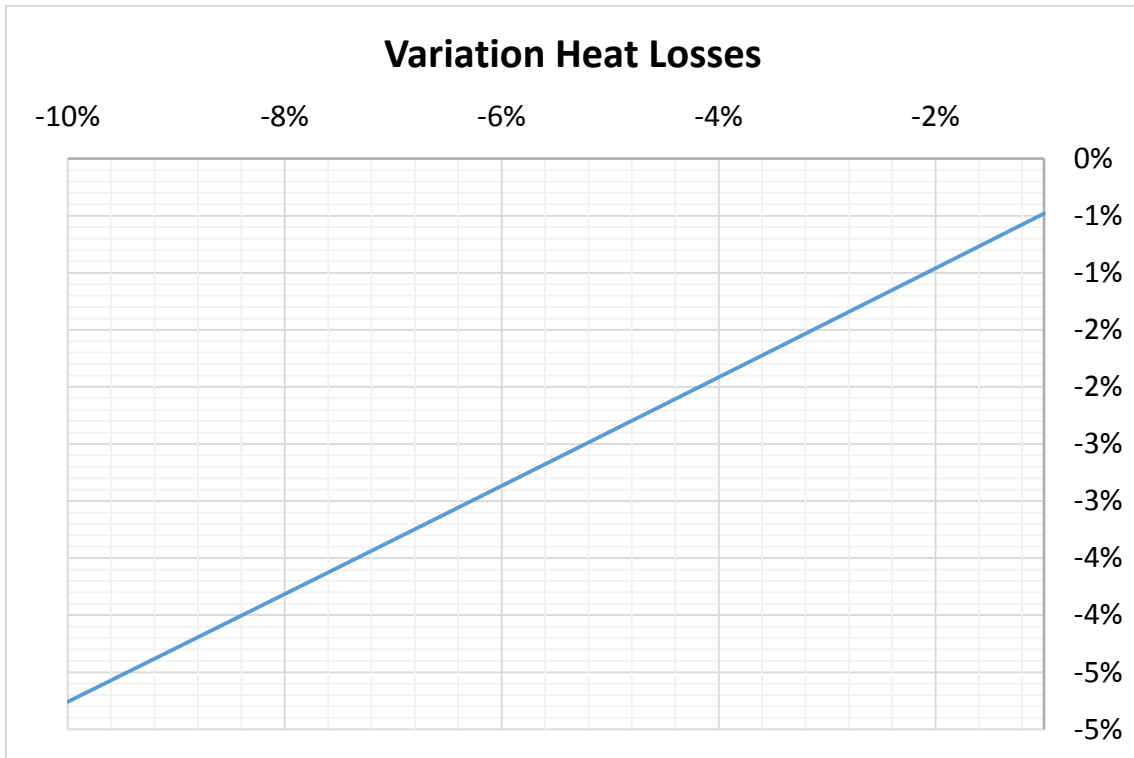
Figure-A 3. Graphs of the results for the dynamic efficiency test when the reflectivity of the collector varies from 0,84 to 0,93.

Below it has been represented the previous result, but in percentage over its nominal value.

Table A 7. Results from the dynamic efficiency test expressed in percentages for different values of the reflectivity.

Variation Mirror reflectivity	Variation Outlet T	Variation Heat Losses	Variation Energy	Variation Efficiency
0,00%	0,00%	0,00%	0,00%	0,00%
-10,00%	-1,40%	-4,76%	-10,32%	-10,32%
-9,00%	-1,26%	-4,29%	-9,28%	-9,28%
-8,00%	-1,12%	-3,81%	-8,25%	-8,25%
-7,00%	-0,98%	-3,34%	-7,22%	-7,22%
-6,00%	-0,84%	-2,87%	-6,19%	-6,19%
-5,00%	-0,70%	-2,39%	-5,16%	-5,16%
-4,00%	-0,56%	-1,91%	-4,13%	-4,13%
-3,00%	-0,42%	-1,44%	-3,09%	-3,09%
-2,00%	-0,28%	-0,96%	-2,06%	-2,06%
-1,00%	-0,14%	-0,48%	-1,03%	-1,03%





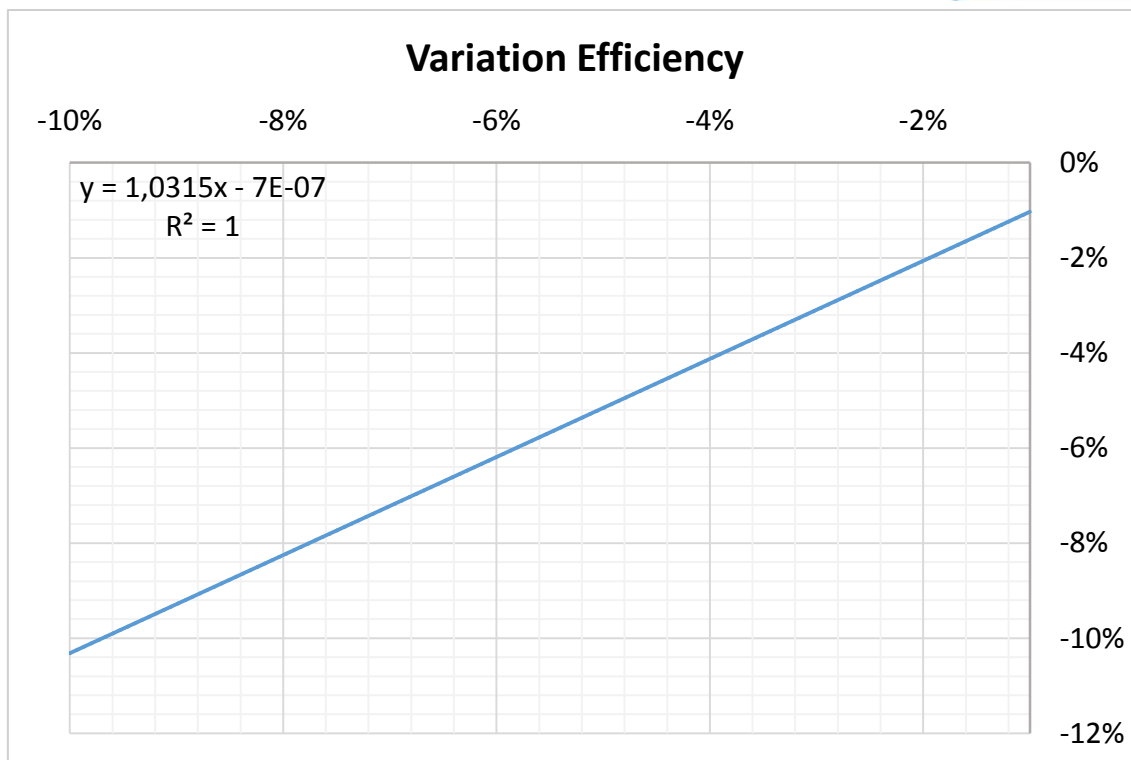
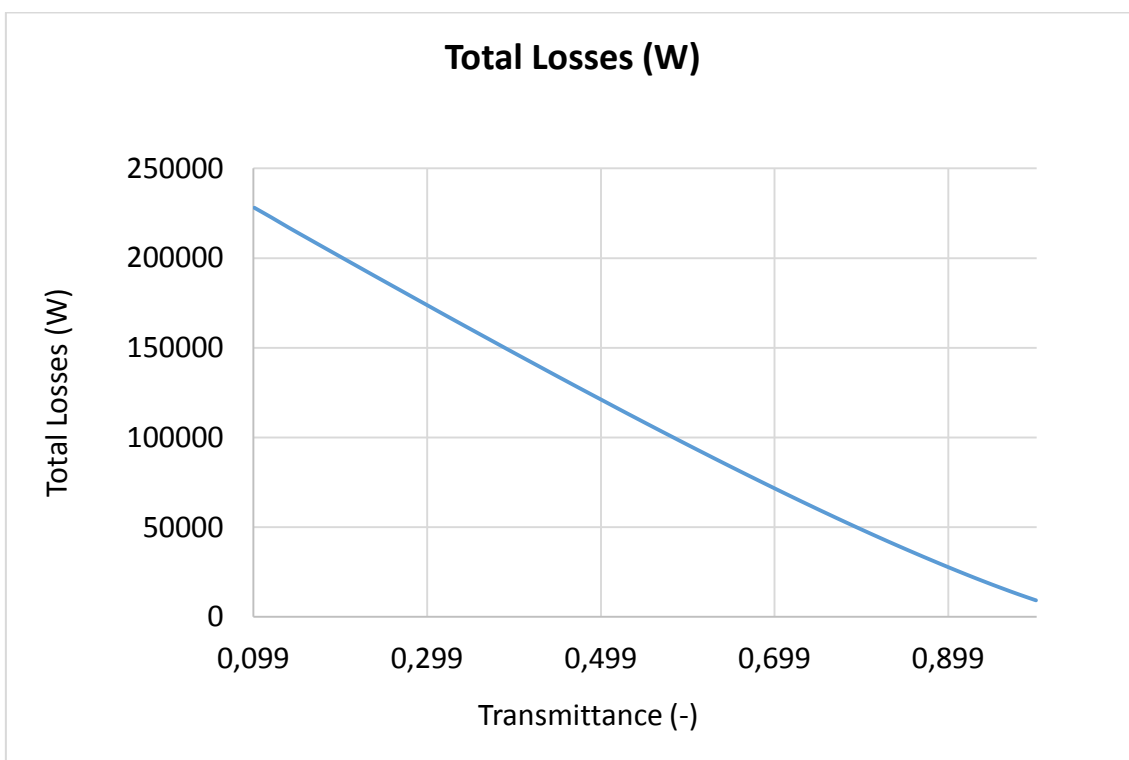
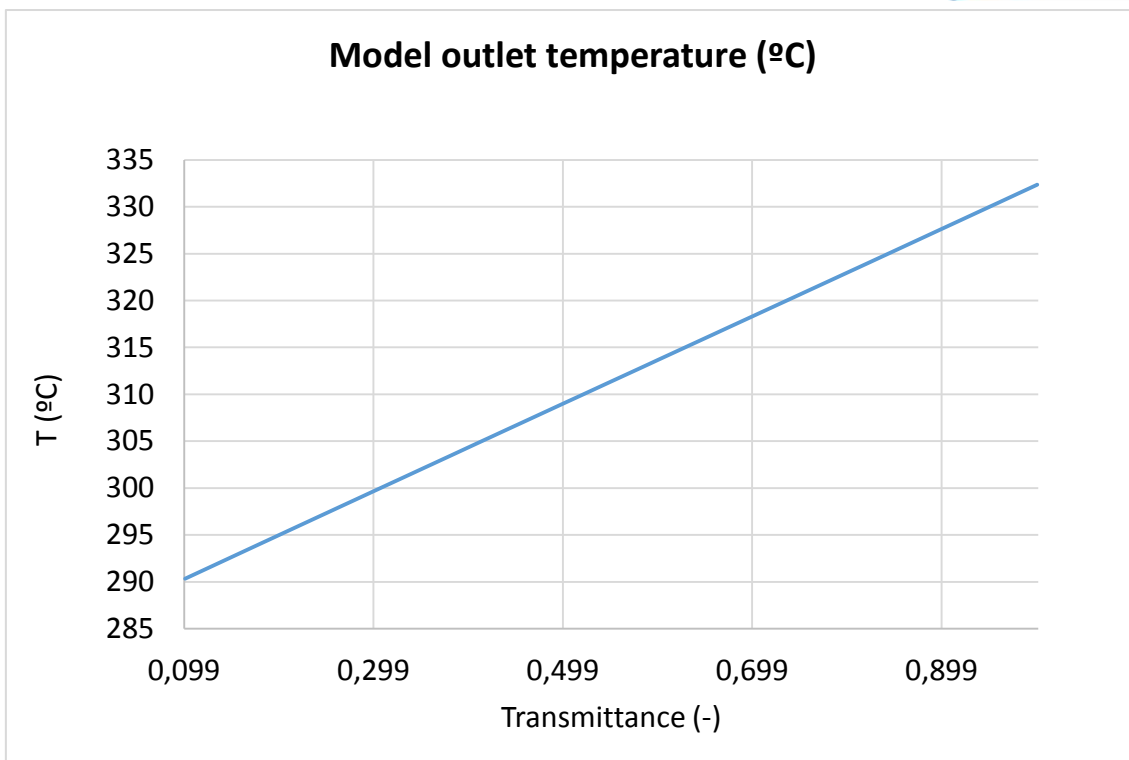


Figure-A 4. Graphs of the results for the dynamic efficiency test expressed in percentages for different values of the reflectivity from 0,84 to 0,93.

Transmittance of the glass cover

Table A 8. Results for the dynamic efficiency test when the transmittance of the glass cover varies from 0,1 to 1.

Test	Incidence angle (°)	Glass Transmittance (-)	Model Outlet temperature (°C)	Total Losses (W)	Energy (W)	Useful Solar Radiant Power (W)	Model efficiency (%)
1	16,37	0,96	330,42	16357,62	273524,09	370869,74	73,75%
2	16,37	0,10	290,33	228079,26	32079,06	370869,74	8,65%
3	16,37	0,20	295,02	200510,66	59915,11	370869,74	16,16%
4	16,37	0,30	299,70	173514,48	87775,02	370869,74	23,67%
5	16,37	0,40	304,38	146924,23	115721,50	370869,74	31,20%
6	16,37	0,50	309,04	120954,41	143716,01	370869,74	38,75%
7	16,37	0,60	313,70	95668,80	171777,03	370869,74	46,32%
8	16,37	0,70	318,35	71423,64	199953,29	370869,74	53,91%
9	16,37	0,80	323,01	48524,12	228250,53	370869,74	61,54%
10	16,37	0,90	327,68	27524,45	256744,86	370869,74	69,23%
11	16,37	1,00	332,36	9231,26	285396,41	370869,74	76,95%



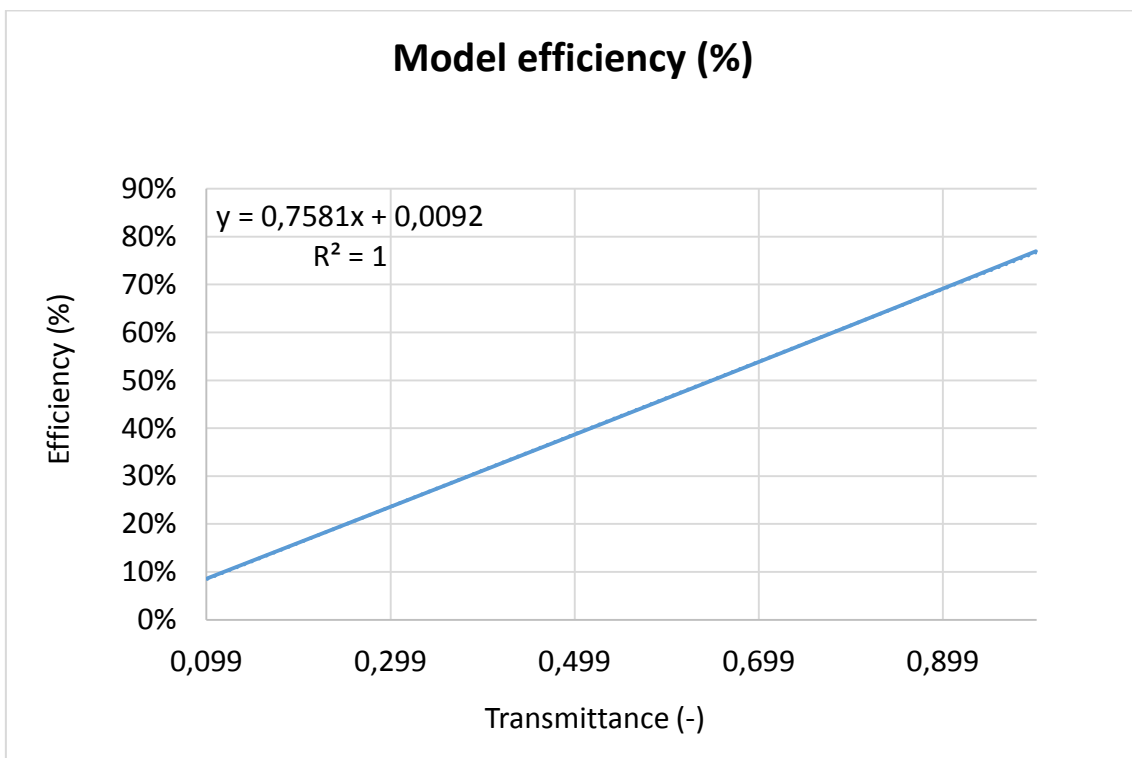
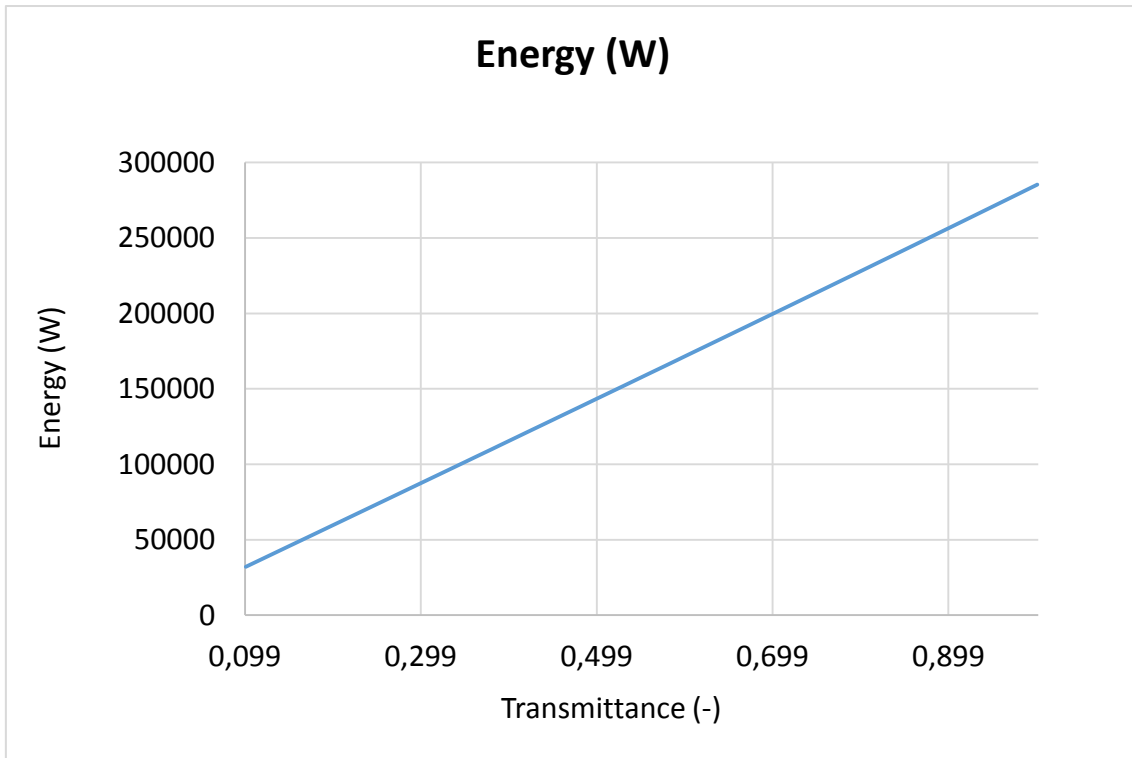
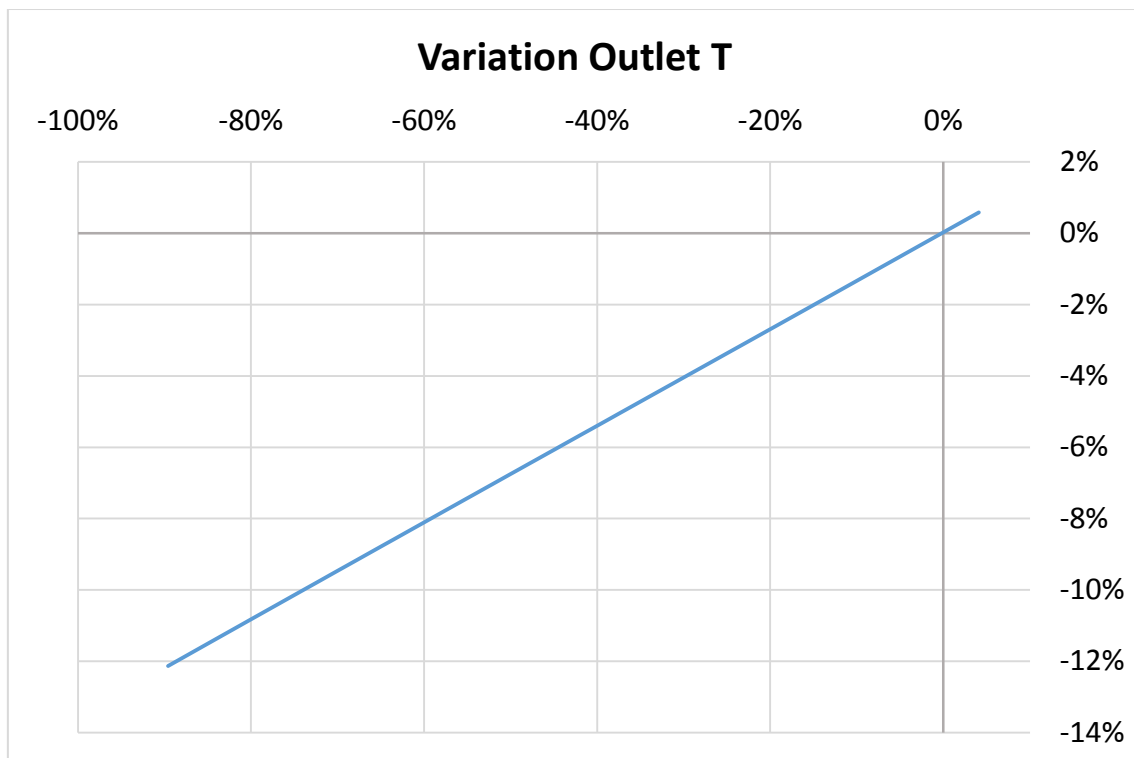


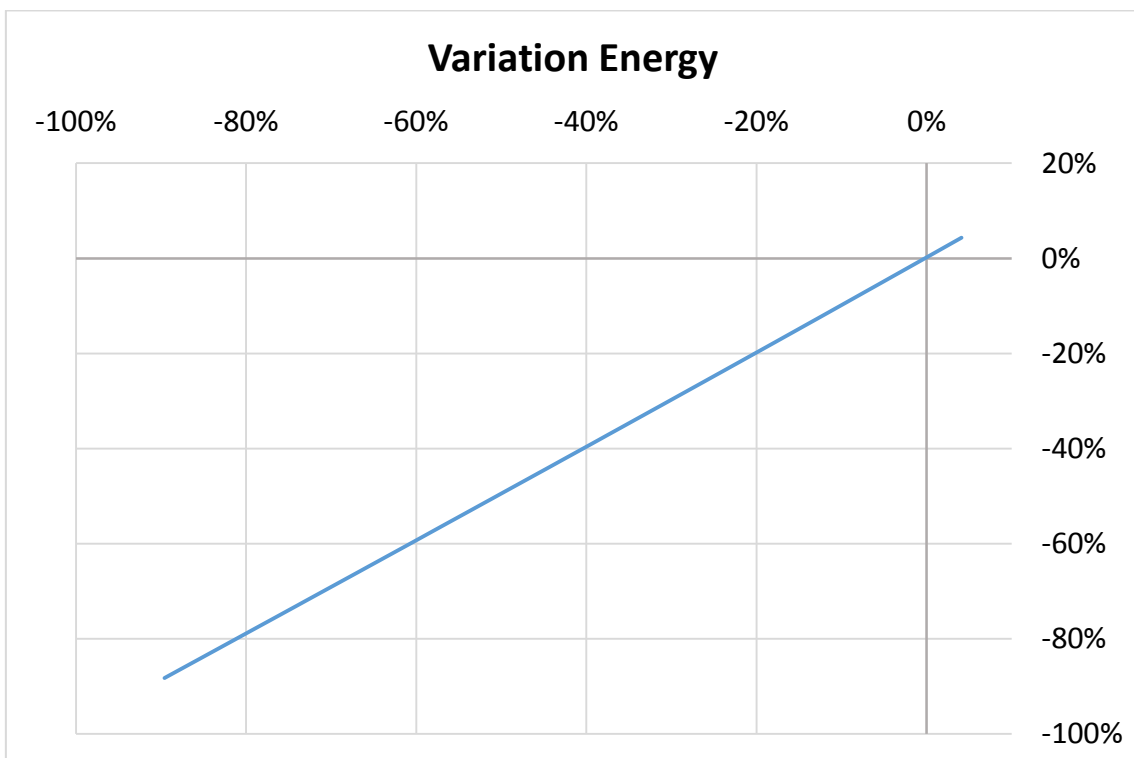
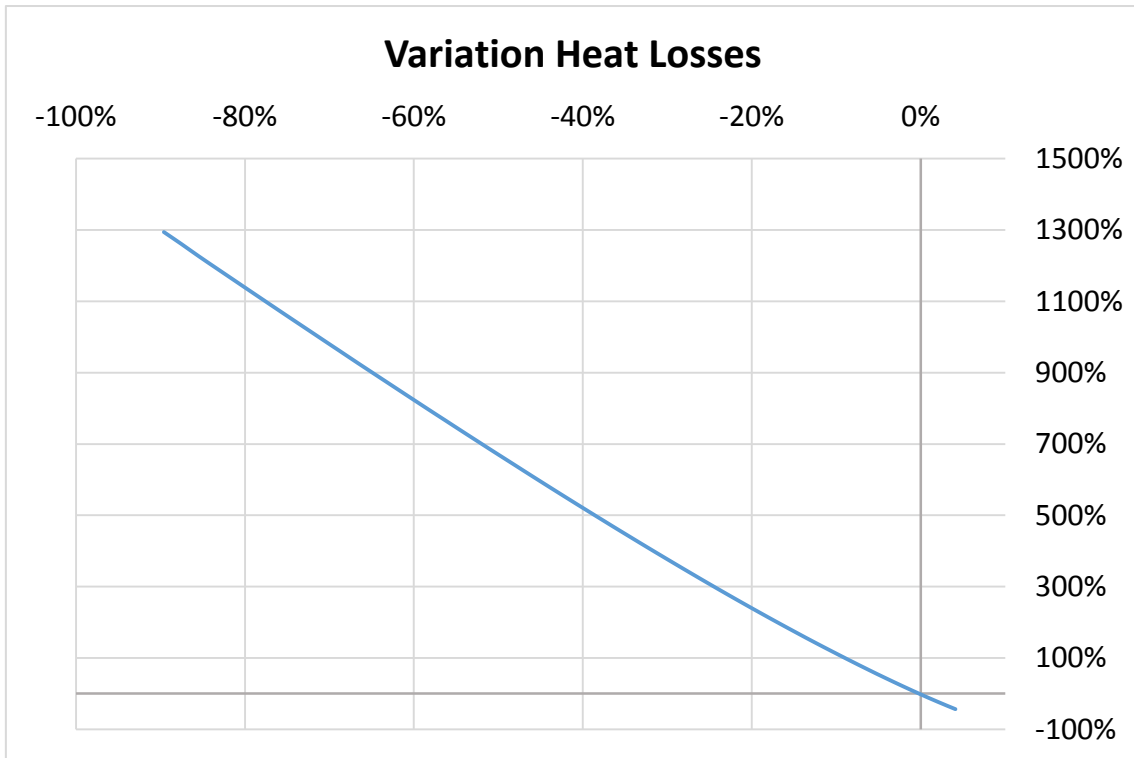
Figure-A 5. Graphs of the results for the dynamic efficiency test when the transmittance of the glass cover varies from 0,1 to 1.

Below it is presented how the variation affects but expressed in percentages.

Table A 9. Results from the dynamic efficiency test expressed in percentages for different values of the transmittance of the glass cover from 0,1 to 1.

Variation Glass transmittance	Variation Outlet T	Variation Heat Losses	Variation Energy	Variation Efficiency
0,00%	0,00%	0,00%	0,00%	0,00%
-89,59%	-12,13%	1294,33%	-88,27%	-88,27%
-79,18%	-10,71%	1125,79%	-78,10%	-78,10%
-68,77%	-9,30%	960,76%	-67,91%	-67,91%
-58,36%	-7,88%	798,20%	-57,69%	-57,69%
-47,95%	-6,47%	639,44%	-47,46%	-47,46%
-37,54%	-5,06%	484,86%	-37,20%	-37,20%
-27,13%	-3,65%	336,64%	-26,90%	-26,90%
-16,72%	-2,24%	196,65%	-16,55%	-16,55%
-6,31%	-0,83%	68,27%	-6,13%	-6,13%
4,11%	0,59%	-43,57%	4,34%	4,34%





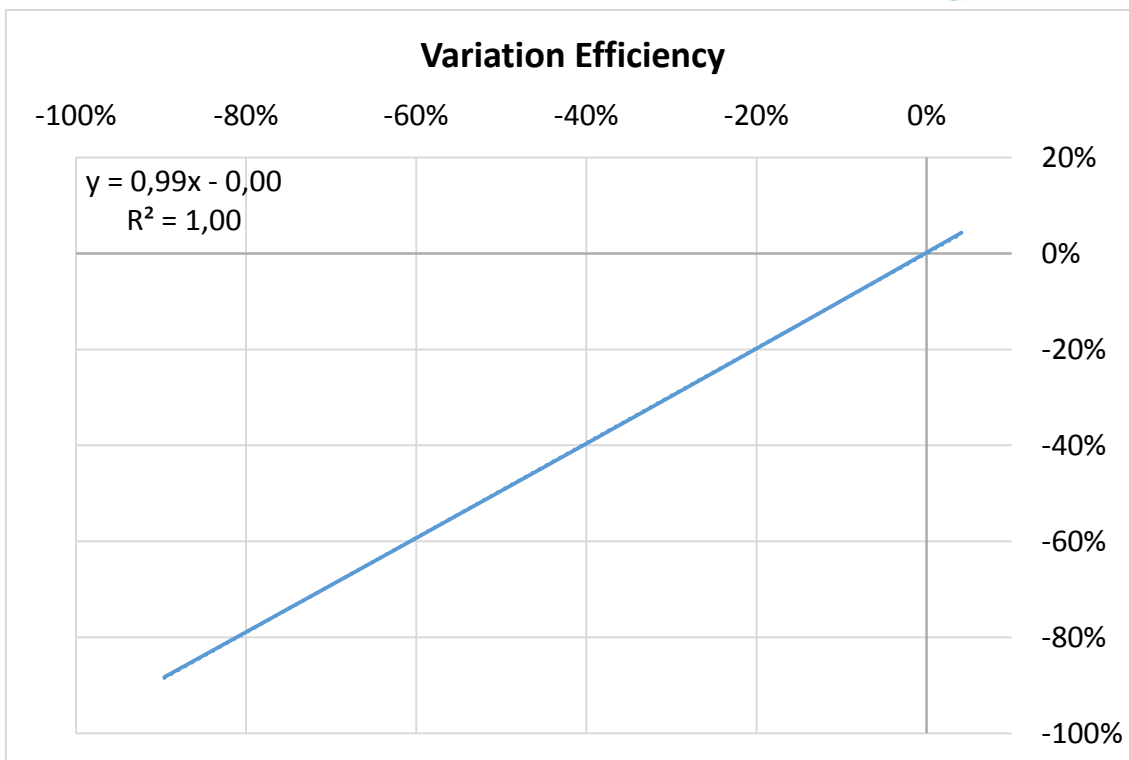
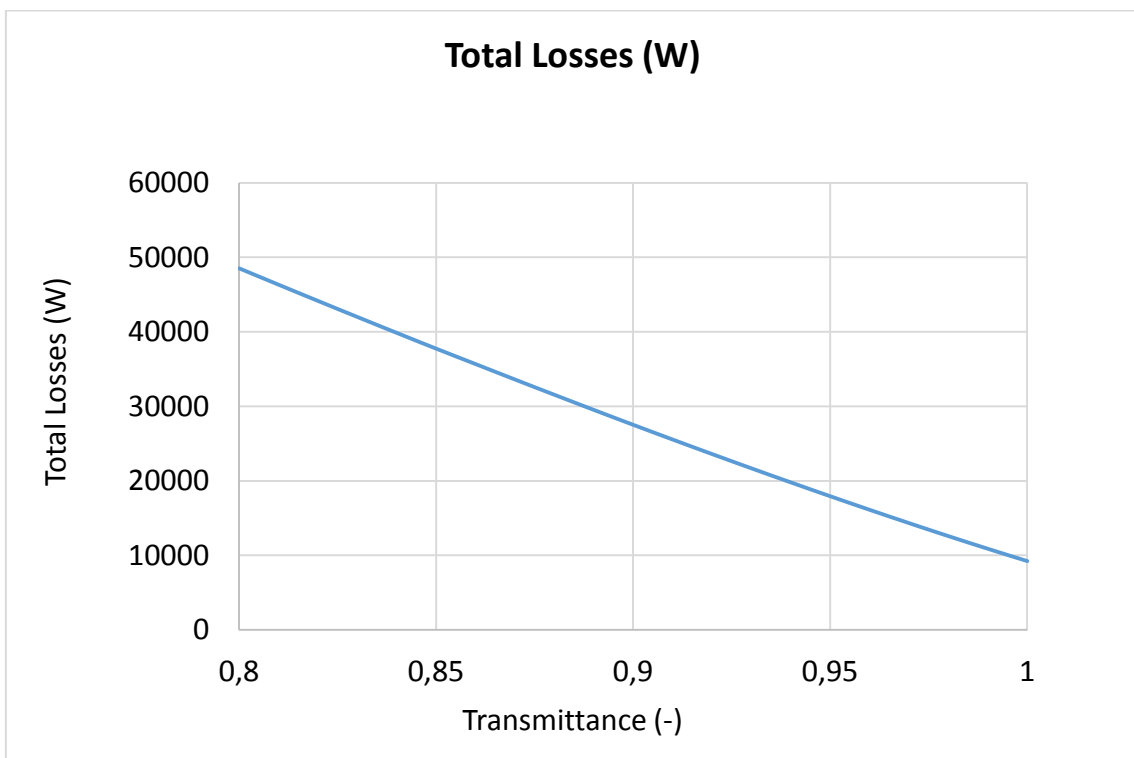
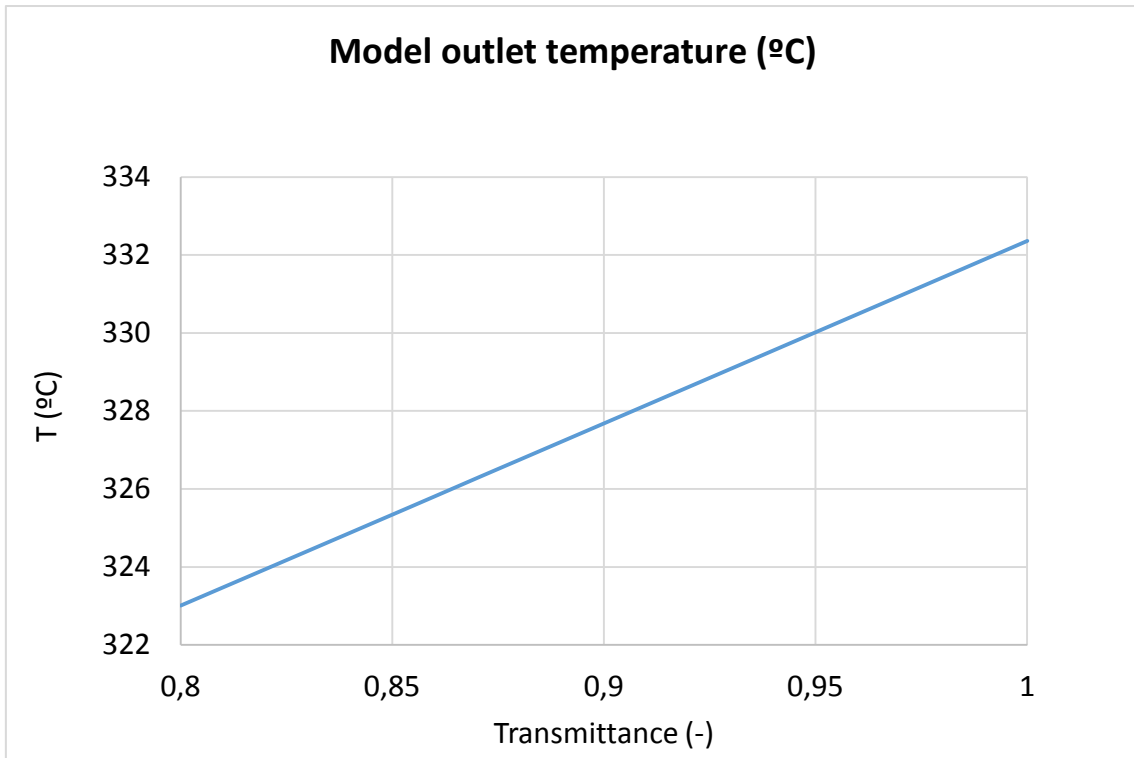


Figure-A 6. Graphs of the results for the dynamic efficiency test expressed in percentages for different values of the transmittance from 0,84 to 0,93.

Table A 10. Results for the dynamic efficiency test when the transmittance of the collector varies from 0,8 to 1.

Test	Incidence angle (°)	Glass Transmittance (-)	Model Outlet temperature (°C)	Total Losses (W)	Energy (W)	Useful Solar Radiant Power (W)	Model efficiency (%)
1	16,37	0,96	330,42	16357,62	273524,09	370869,74	73,75%
2	16,37	0,80	323,01	48524,12	228250,53	370869,74	61,54%
3	16,37	0,81	323,48	46329,11	231089,39	370869,74	62,31%
4	16,37	0,82	323,94	44152,97	233929,83	370869,74	63,08%
5	16,37	0,83	324,41	41996,33	236772,08	370869,74	63,84%
6	16,37	0,84	324,87	39859,84	239615,91	370869,74	64,61%
7	16,37	0,85	325,34	37744,21	242461,52	370869,74	65,38%
8	16,37	0,86	325,81	35676,05	245314,86	370869,74	66,15%
9	16,37	0,87	326,28	33604,40	248185,79	370869,74	66,92%
10	16,37	0,88	326,75	31553,15	251036,94	370869,74	67,69%
11	16,37	0,89	327,21	29526,18	253890,01	370869,74	68,46%
12	16,37	0,90	327,68	27524,45	256744,86	370869,74	69,23%
13	16,37	0,91	328,15	25549,03	259601,42	370869,74	70,00%
14	16,37	0,92	328,62	23601,11	262460,10	370869,74	70,77%
15	16,37	0,93	329,08	21682,01	265320,84	370869,74	71,54%
16	16,37	0,94	329,55	19793,22	268179,40	370869,74	72,31%
17	16,37	0,95	330,02	17936,55	271043,97	370869,74	73,08%
18	16,37	0,96	330,49	16114,10	273910,48	370869,74	73,86%
19	16,37	0,97	330,95	14328,44	276778,99	370869,74	74,63%
20	16,37	0,98	331,42	12582,86	279649,53	370869,74	75,40%
21	16,37	0,99	331,89	10881,73	282521,97	370869,74	76,18%
22	16,37	1,00	332,36	9231,26	285396,41	370869,74	76,95%



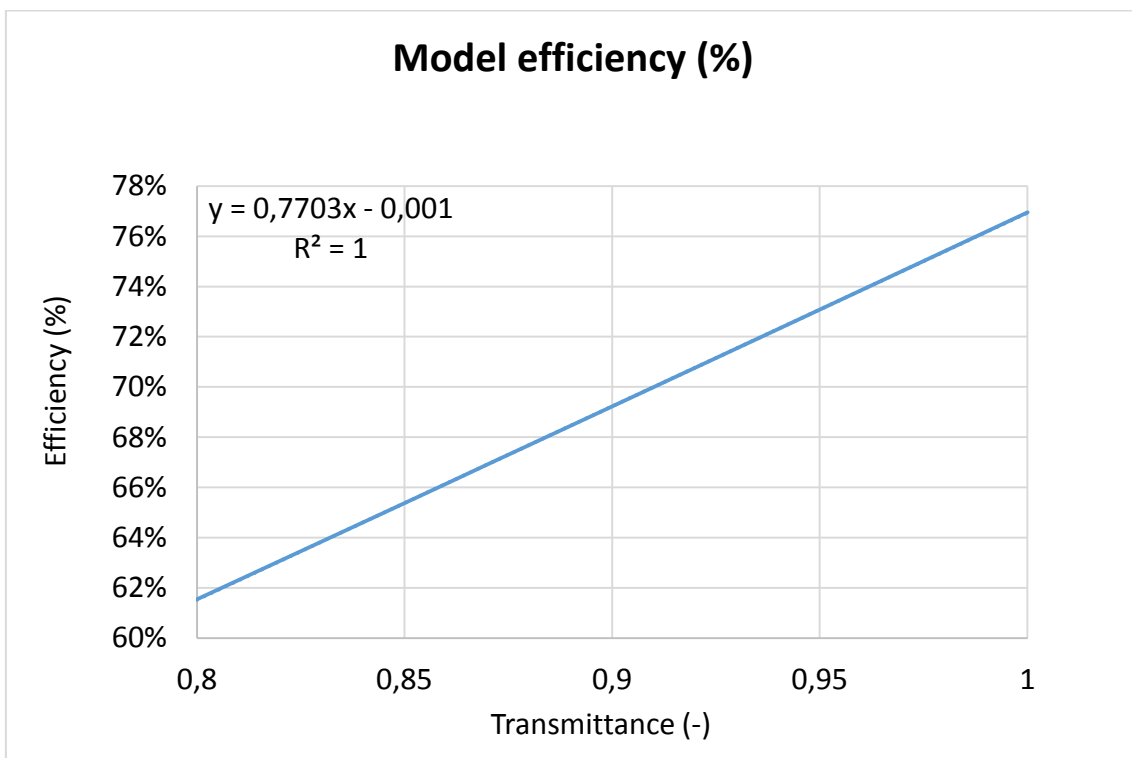
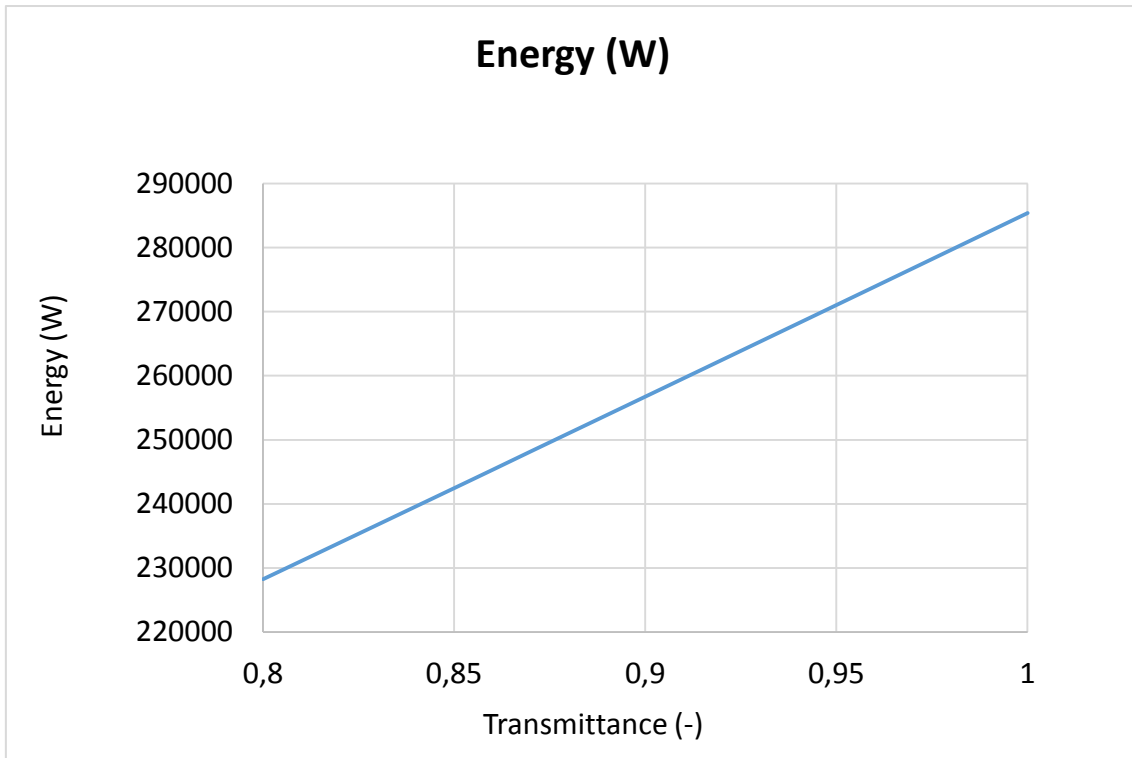
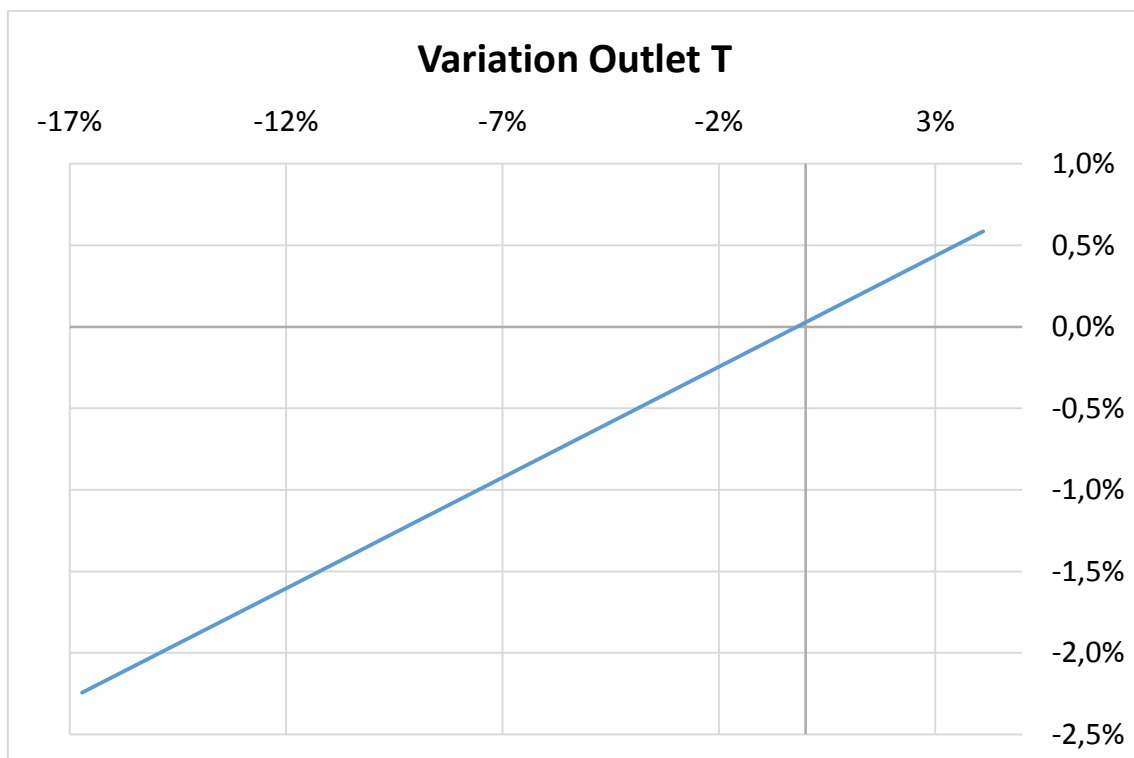


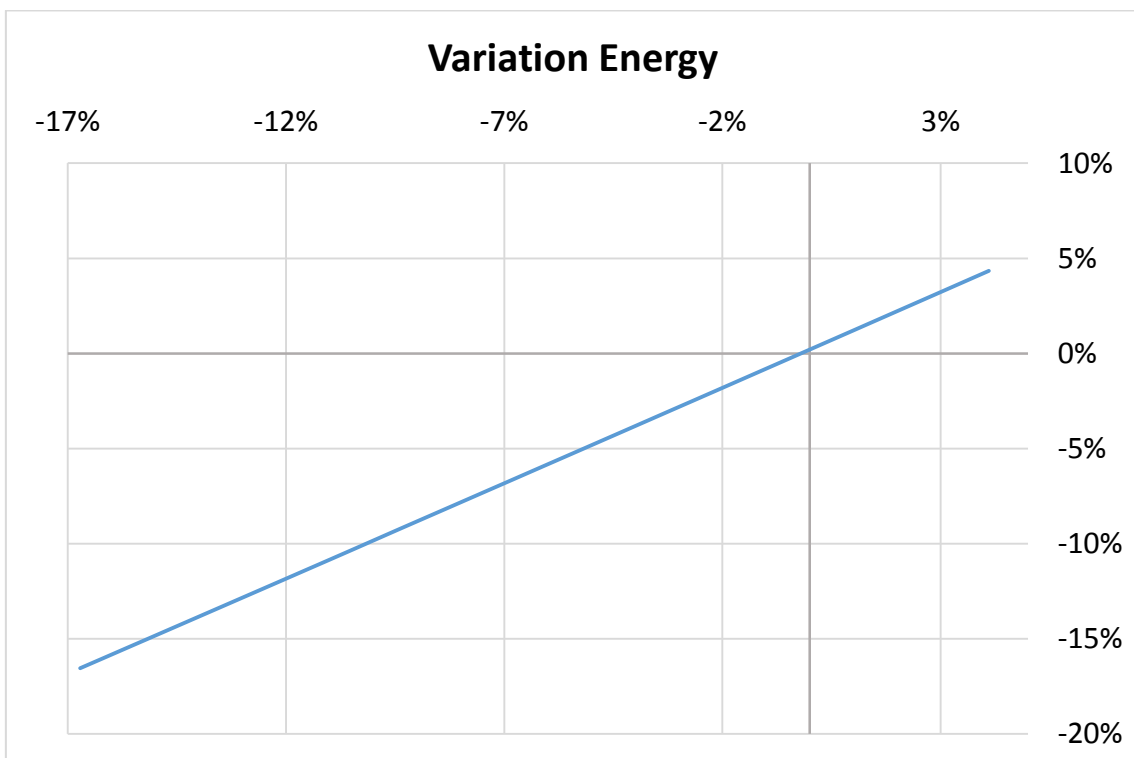
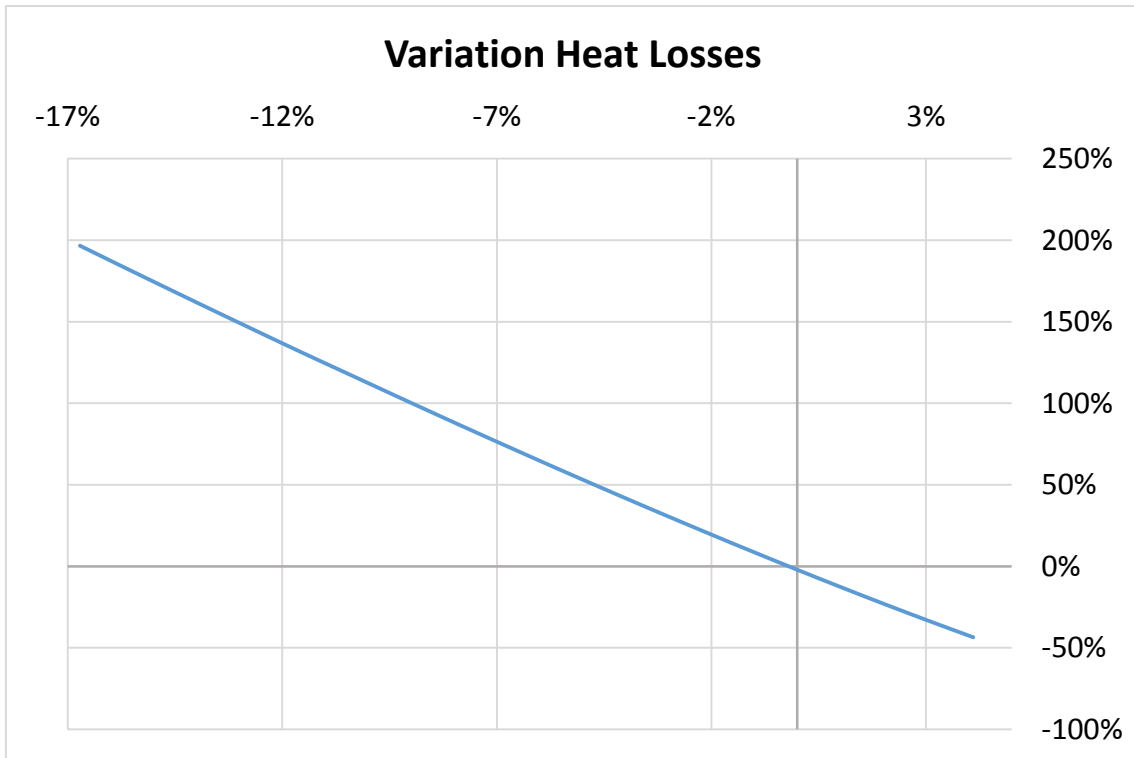
Figure-A 7. Graphs of the results for the dynamic efficiency test when the transmittance of the glass cover varies from 0,8 to 1.

Below it is presented how the variation affects but expressed in percentages.

Table A 11. Results from the dynamic efficiency test expressed in percentages for different values of the transmittance of the glass cover from 0,8 to 1.

Variation Glass transmittance	Variation Outlet T	Variation Heat Losses	Variation Energy	Variation Efficiency
0,00%	0,00%	0,00%	0,00%	0,00%
-16,72%	-2,24%	196,65%	-16,55%	-16,55%
-15,68%	-2,10%	183,23%	-15,51%	-15,51%
-14,64%	-1,96%	169,92%	-14,48%	-14,48%
-13,59%	-1,82%	156,74%	-13,44%	-13,44%
-12,55%	-1,68%	143,68%	-12,40%	-12,40%
-11,51%	-1,54%	130,74%	-11,36%	-11,36%
-10,47%	-1,40%	118,10%	-10,31%	-10,31%
-9,43%	-1,25%	105,44%	-9,26%	-9,26%
-8,39%	-1,11%	92,90%	-8,22%	-8,22%
-7,35%	-0,97%	80,50%	-7,18%	-7,18%
-6,31%	-0,83%	68,27%	-6,13%	-6,13%
-5,27%	-0,69%	56,19%	-5,09%	-5,09%
-4,22%	-0,55%	44,28%	-4,04%	-4,04%
-3,18%	-0,41%	32,55%	-3,00%	-3,00%
-2,14%	-0,26%	21,00%	-1,95%	-1,95%
-1,10%	-0,12%	9,65%	-0,91%	-0,91%
-0,06%	0,02%	-1,49%	0,14%	0,14%
0,98%	0,16%	-12,41%	1,19%	1,19%
2,02%	0,30%	-23,08%	2,24%	2,24%
3,06%	0,44%	-33,48%	3,29%	3,29%
4,11%	0,59%	-43,57%	4,34%	4,34%





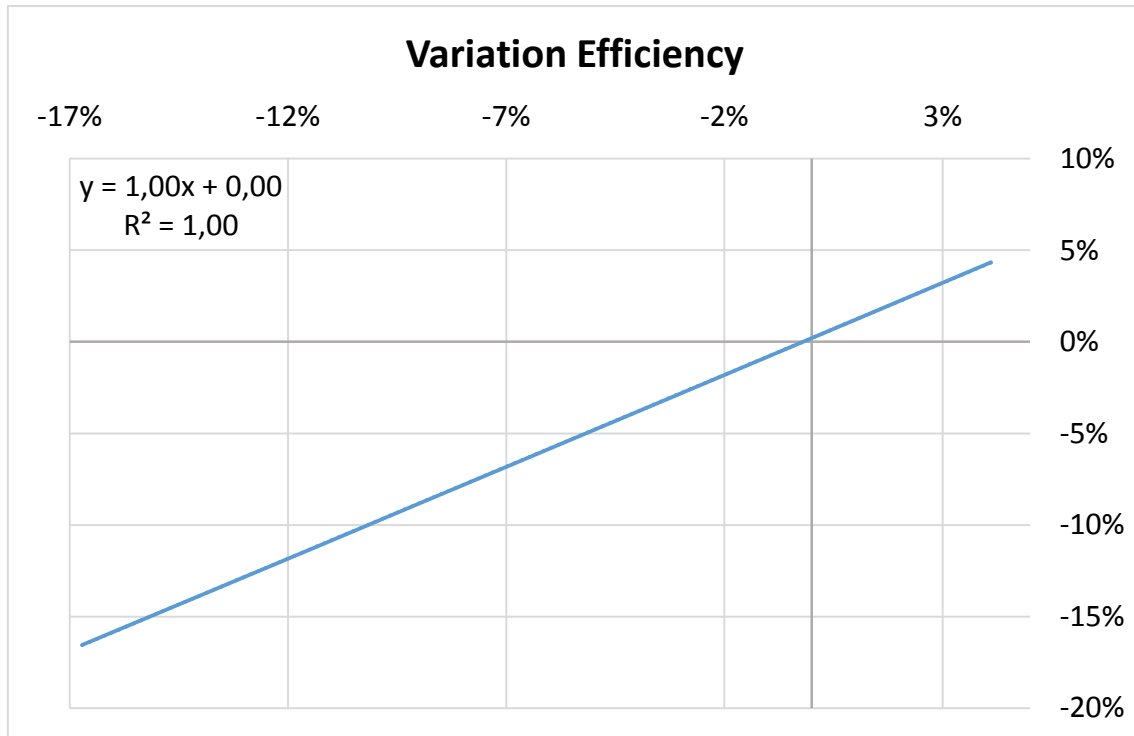
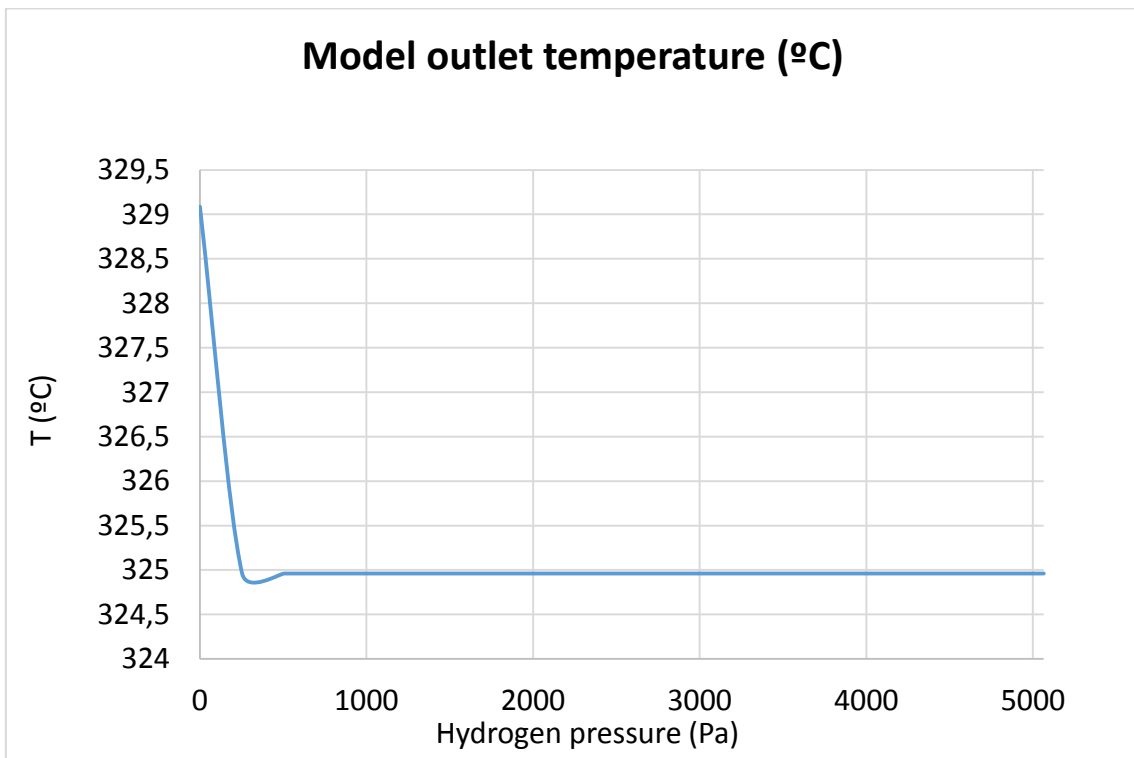
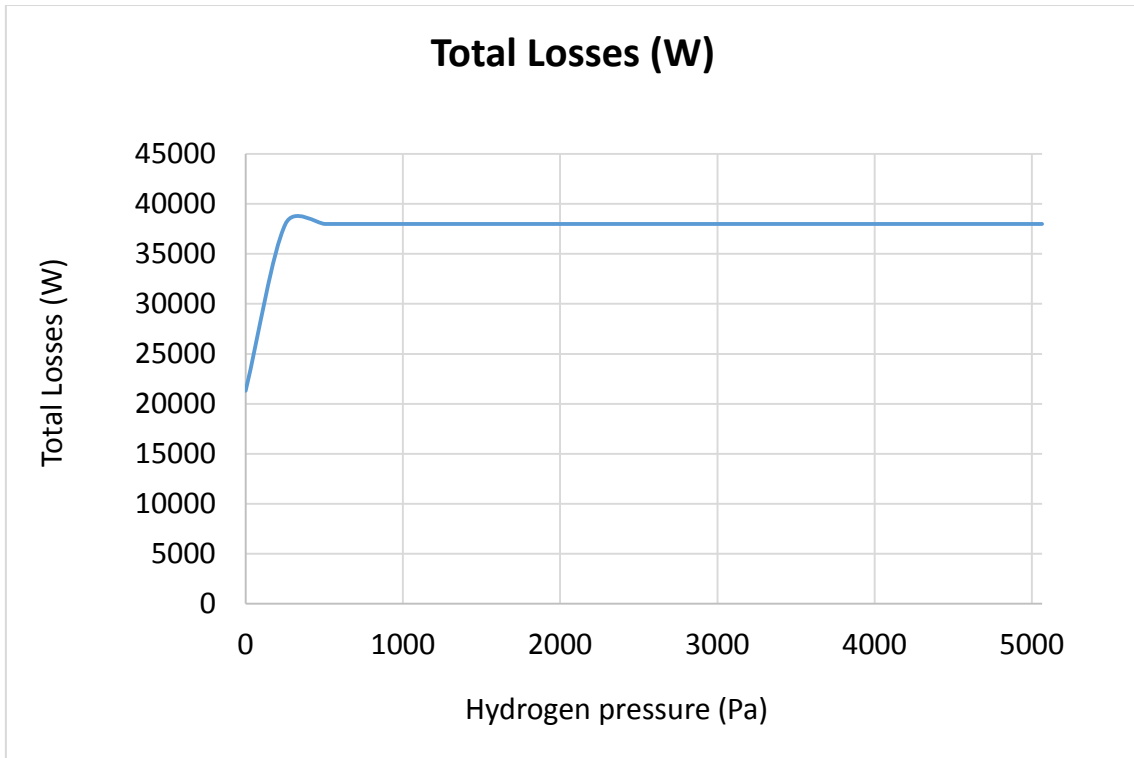


Figure-A 8. Graphs of the results for the dynamic efficiency test expressed in percentages for different values of the transmittance of the glass cover from 0,8 to 1.

Infiltration of hydrogen

Table A 12. Results for the dynamic efficiency test when there is infiltration of hydrogen, and its pressure varies from 0,01 Pa to 5065 Pa.

Test	Incidence angle (°)	Inlet Pressure (Pa)	Model Outlet T (°C)	Total Losses (W)	Energy (W)	Useful Solar Radiant Power (W)	Model efficiency (%)
1	16,37	0,00	330,42	16357,62	273524,09	370869,74	73,75%
2	16,37	0,01	329,09	21309,62	265342,05	370869,74	71,55%
3	16,37	253,26	324,96	37999,66	240143,37	370869,74	64,75%
4	16,37	506,51	324,96	37999,66	240143,37	370869,74	64,75%
5	16,37	759,76	324,96	37999,66	240143,37	370869,74	64,75%
6	16,37	1013,01	324,96	37999,66	240143,37	370869,74	64,75%
7	16,37	1266,26	324,96	37999,66	240143,37	370869,74	64,75%
8	16,37	1519,51	324,96	37999,66	240143,37	370869,74	64,75%
9	16,37	1772,76	324,96	37999,66	240143,37	370869,74	64,75%
10	16,37	2026,01	324,96	37999,66	240143,37	370869,74	64,75%
11	16,37	2279,26	324,96	37999,66	240143,37	370869,74	64,75%
12	16,37	2532,50	324,96	37999,66	240143,37	370869,74	64,75%
13	16,37	2785,75	324,96	37999,66	240143,37	370869,74	64,75%
14	16,37	3039,00	324,96	37999,66	240143,37	370869,74	64,75%
15	16,37	3292,25	324,96	37999,66	240143,37	370869,74	64,75%
16	16,37	3545,50	324,96	37999,66	240143,37	370869,74	64,75%
17	16,37	3798,75	324,96	37999,66	240143,37	370869,74	64,75%
18	16,37	4052,00	324,96	37999,66	240143,37	370869,74	64,75%
19	16,37	4305,25	324,96	37999,66	240143,37	370869,74	64,75%
20	16,37	4558,50	324,96	37999,66	240143,37	370869,74	64,75%
21	16,37	4811,75	324,96	37999,66	240143,37	370869,74	64,75%
22	16,37	5065,00	324,96	37999,66	240143,37	370869,74	64,75%



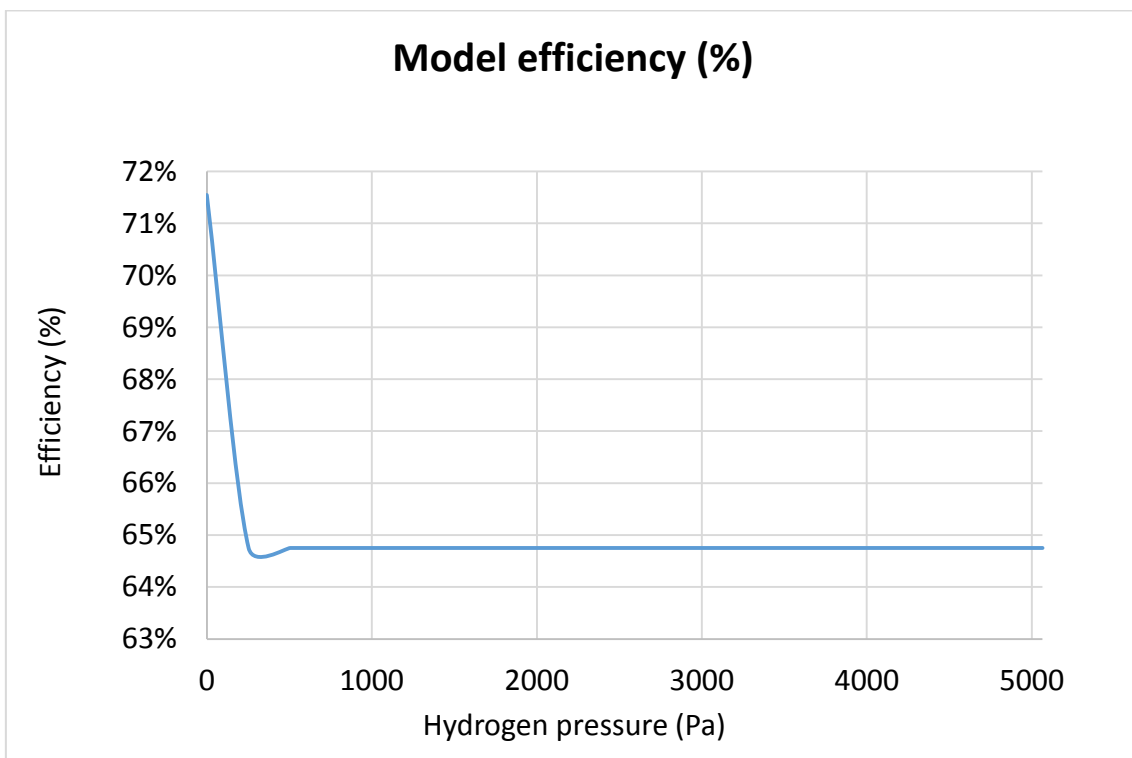
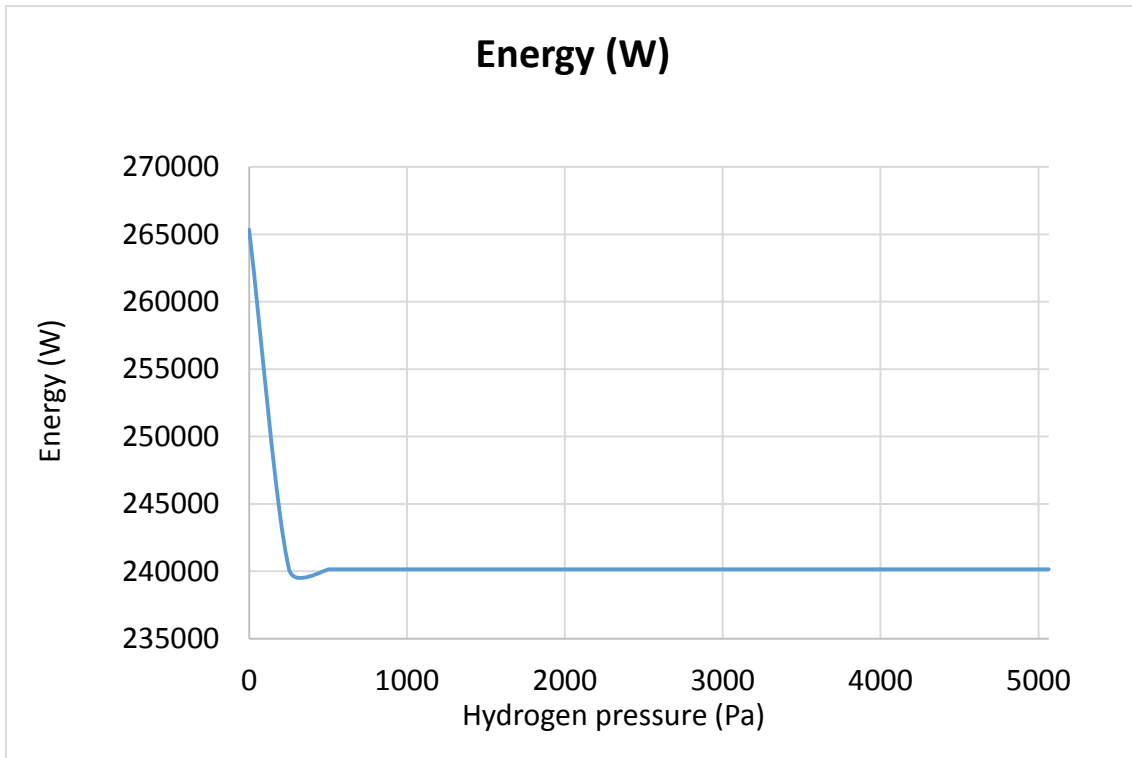
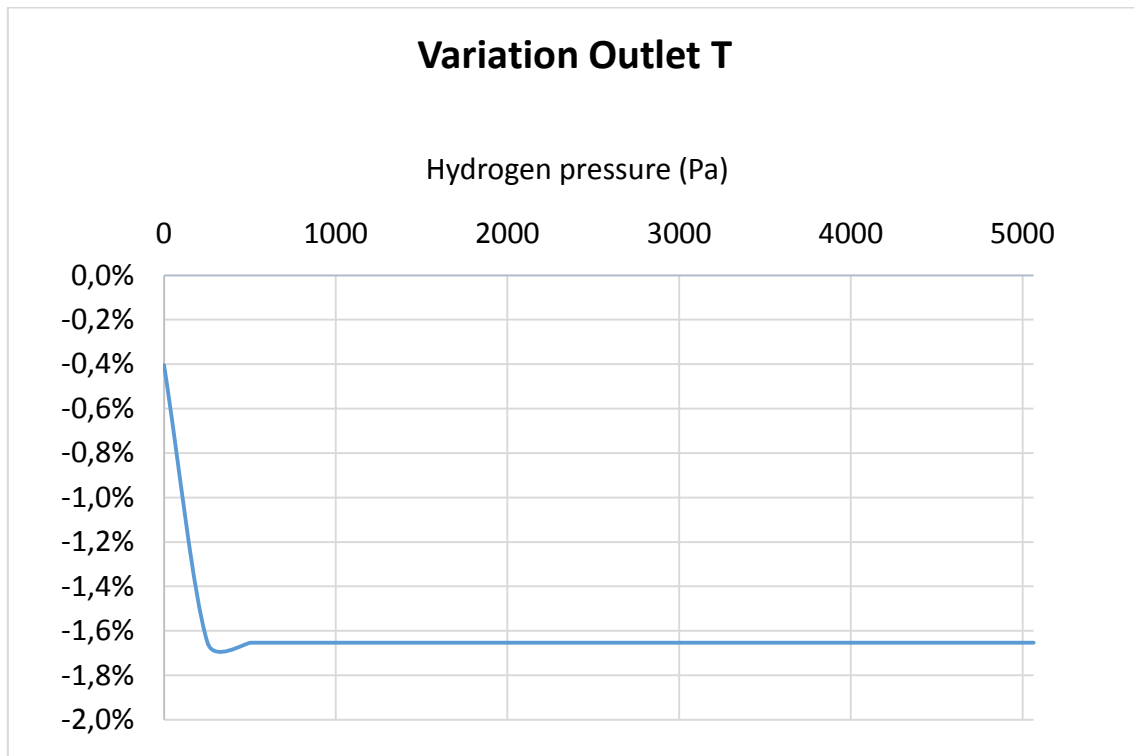


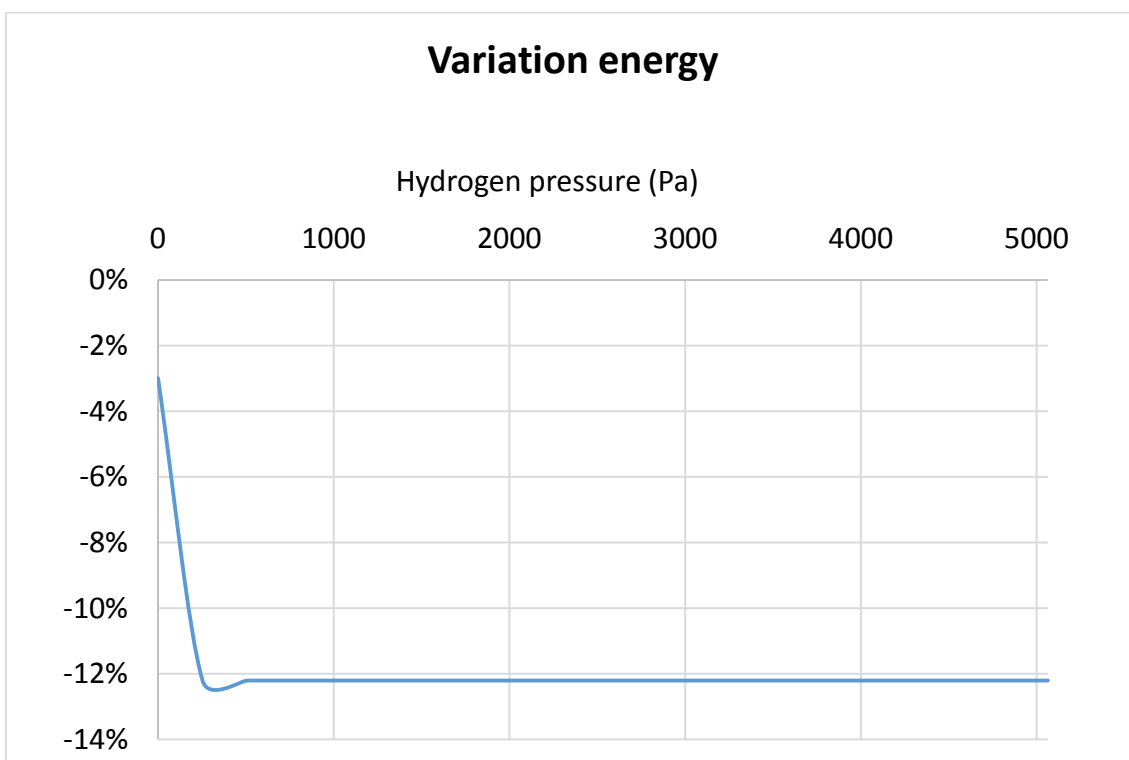
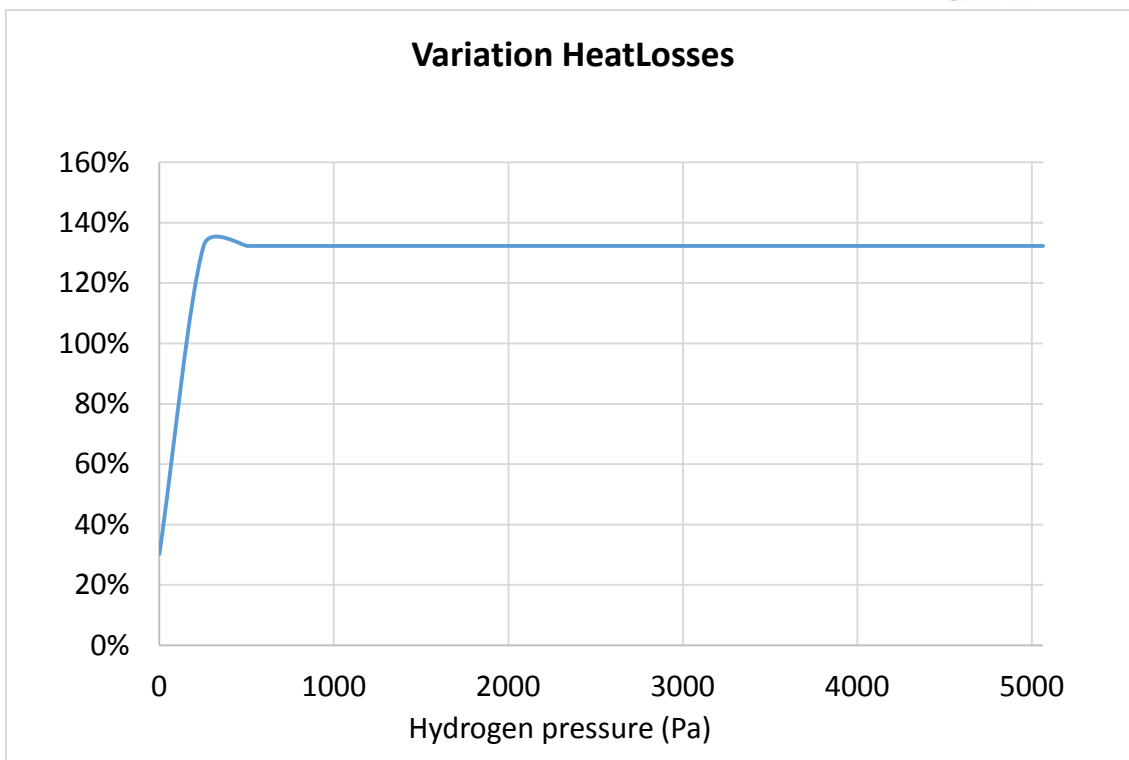
Figure-A 9. Graphs of the results for the dynamic efficiency test when there is infiltration of hydrogen, and its pressure varies from 0,01 Pa to 5065 Pa.

Below it is presented how the variation affects but expressed in percentages.

Table A 13. Results from the dynamic efficiency test expressed in percentages when there is infiltration of hydrogen, and its pressure varies from 0,01 Pa to 5065 Pa.

Inlet hydrogen pressure (Pa)	Variation Outlet T	Variation Heat Losses	Variation Energy	Variation Efficiency
0,00	0,00%	0,00%	0,00%	0,00%
0,01	-0,40%	30,27%	-2,99%	-2,99%
253,26	-1,65%	132,31%	-12,20%	-12,20%
506,509	-1,65%	132,31%	-12,20%	-12,20%
759,758	-1,65%	132,31%	-12,20%	-12,20%
1013,01	-1,65%	132,31%	-12,20%	-12,20%
1266,26	-1,65%	132,31%	-12,20%	-12,20%
1519,51	-1,65%	132,31%	-12,20%	-12,20%
1772,76	-1,65%	132,31%	-12,20%	-12,20%
2026,01	-1,65%	132,31%	-12,20%	-12,20%
2279,26	-1,65%	132,31%	-12,20%	-12,20%
2532,5	-1,65%	132,31%	-12,20%	-12,20%
2785,75	-1,65%	132,31%	-12,20%	-12,20%
3039	-1,65%	132,31%	-12,20%	-12,20%
3292,25	-1,65%	132,31%	-12,20%	-12,20%
3545,5	-1,65%	132,31%	-12,20%	-12,20%
3798,75	-1,65%	132,31%	-12,20%	-12,20%
4052	-1,65%	132,31%	-12,20%	-12,20%
4305,25	-1,65%	132,31%	-12,20%	-12,20%
4558,5	-1,65%	132,31%	-12,20%	-12,20%
4811,75	-1,65%	132,31%	-12,20%	-12,20%
5065	-1,65%	132,31%	-12,20%	-12,20%





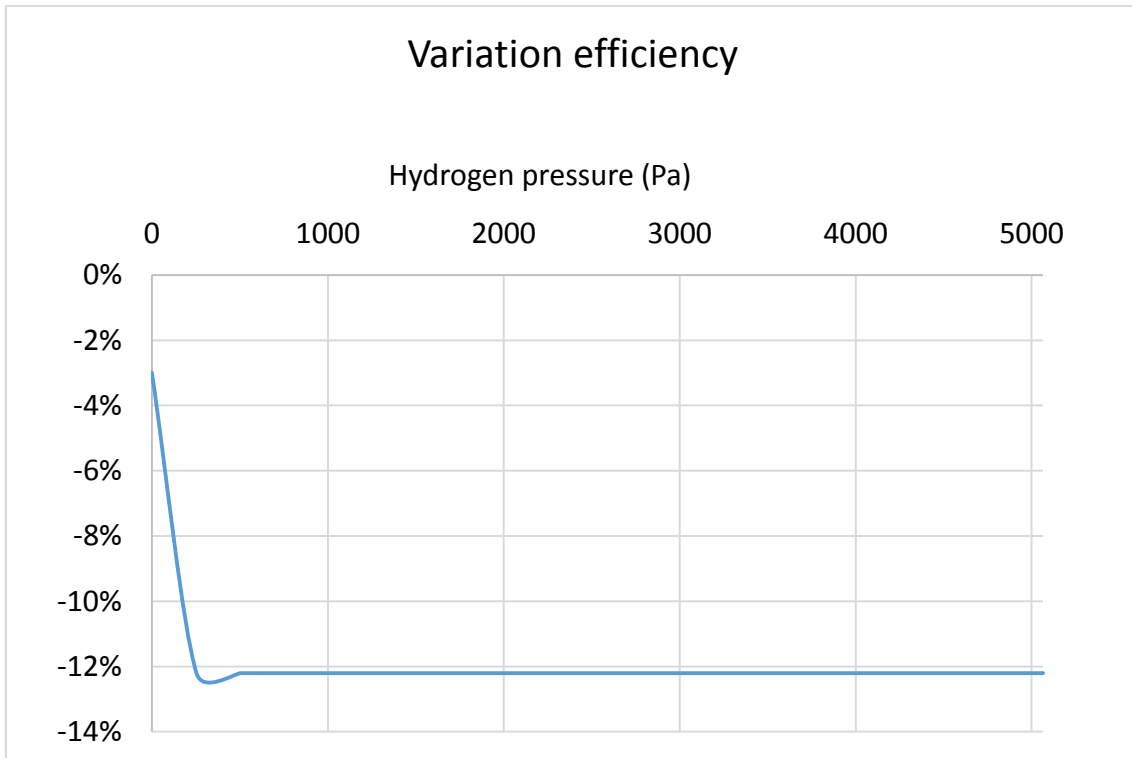
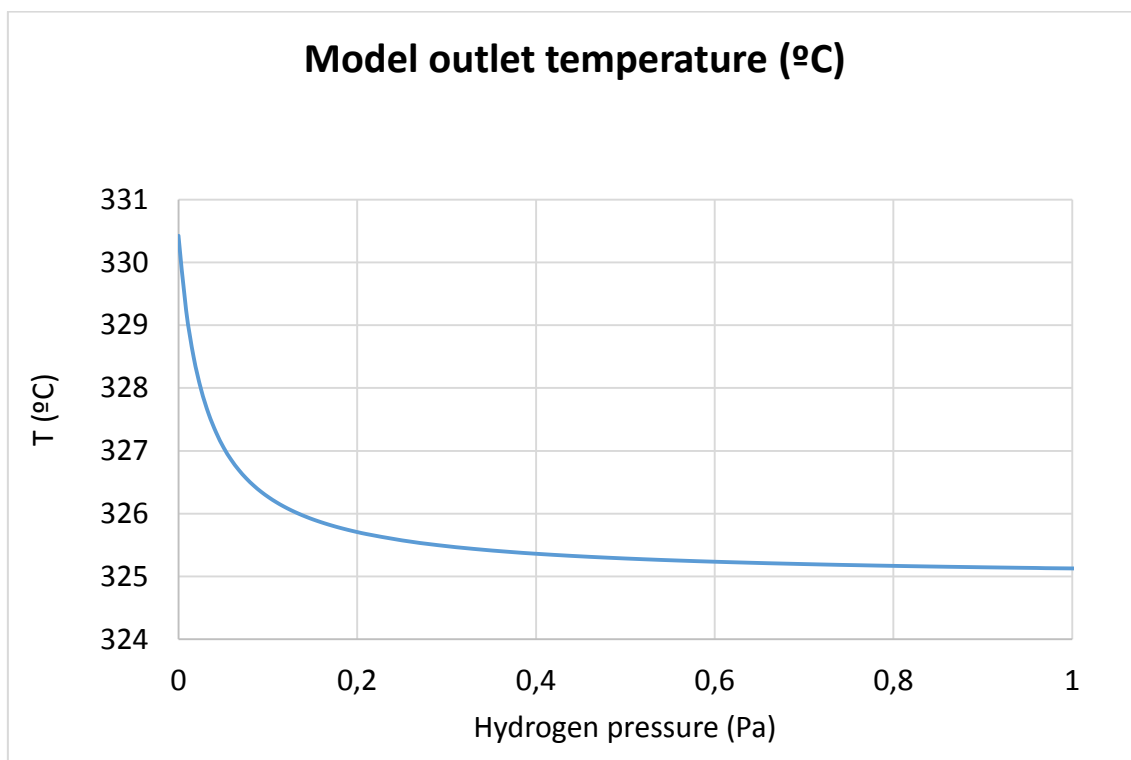


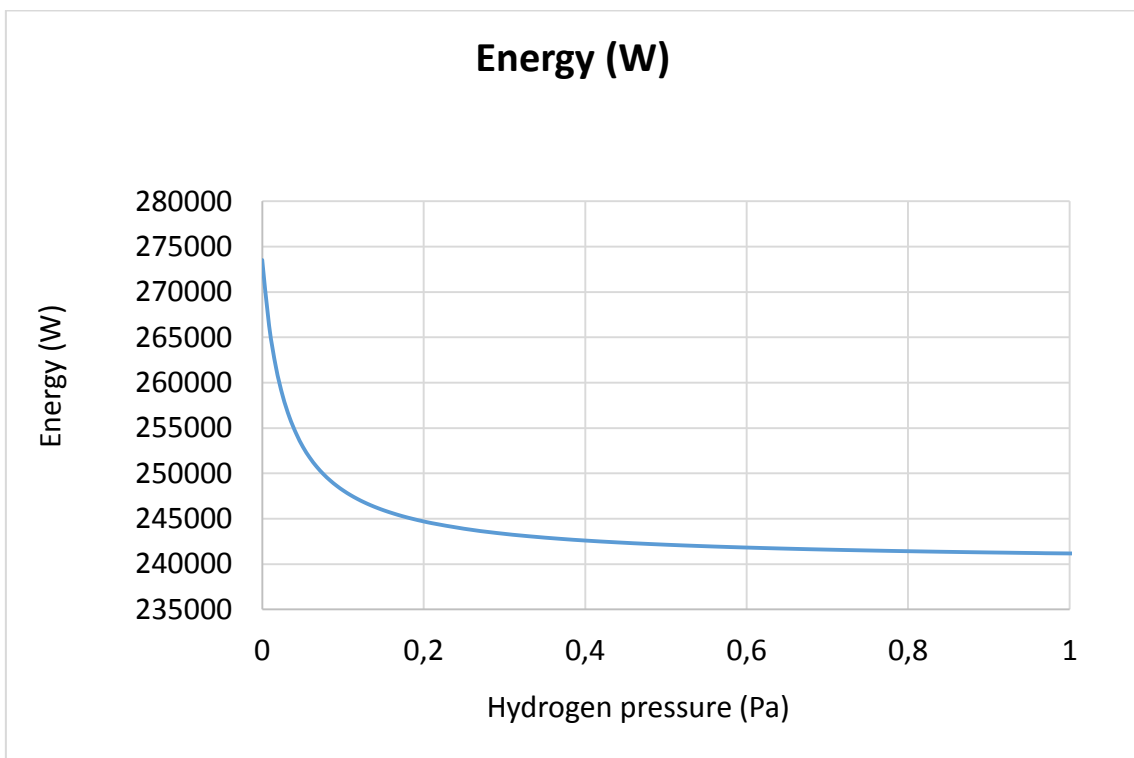
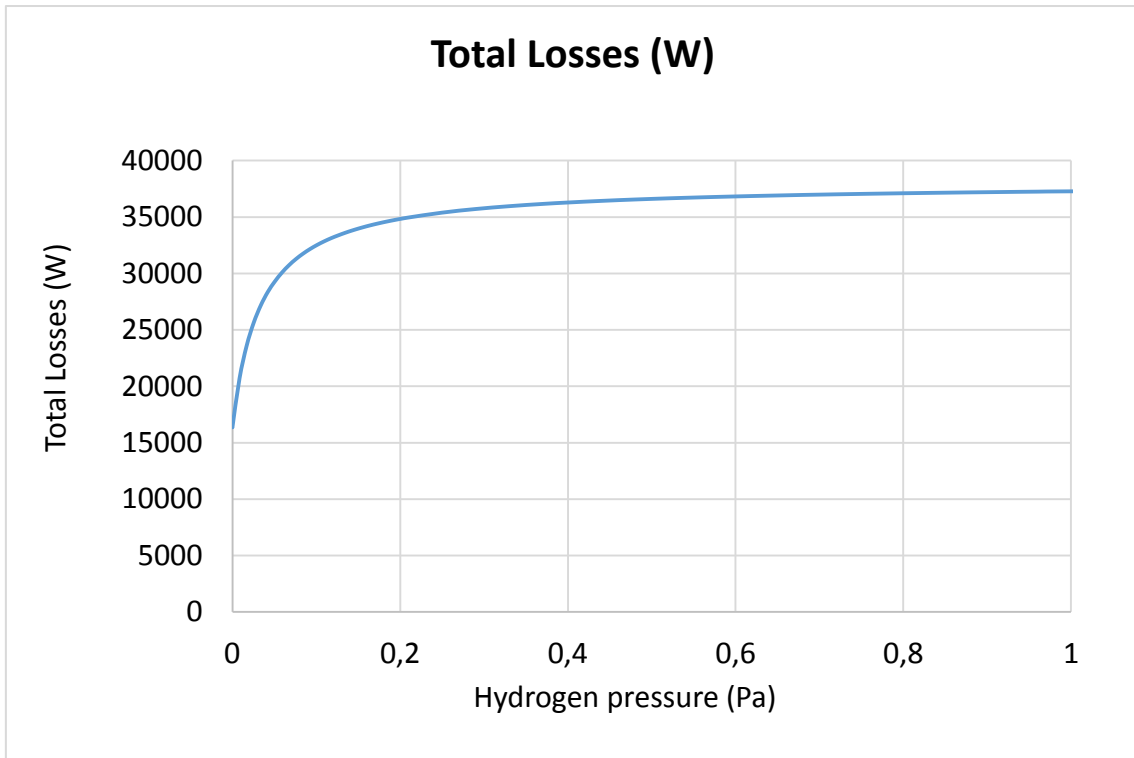
Figure-A 10. Graphs of the results for the dynamic efficiency test expressed in percentages when there is infiltration of hydrogen, and its pressure varies from 0,01 Pa to 5065 Pa.

Table A 14. Results for the dynamic efficiency test when there is infiltration of hydrogen, and its pressure varies from 0,00001 Pa to 8 Pa.

Test	Incidence angle (°)	Inlet Pressure (pa)	Model outlet temperature (°C)	Total Losses (W)	Energy (W)	Useful Solar Radiant Power (W)	Model efficiency (%)
1	16,37	0,00	330,42	16357,62	273524,09	370869,74	73,75%
2	16,37	0,0001	330,41	16420,24	273417,40	370869,74	73,72%
3	16,37	0,008496	329,24	20715,81	266299,10	370869,74	71,80%
4	16,37	0,016892	328,50	23575,56	261739,51	370869,74	70,57%
5	16,37	0,025288	327,98	25619,24	258554,48	370869,74	69,72%
6	16,37	0,033684	327,59	27154,04	256197,95	370869,74	69,08%
7	16,37	0,04208	327,29	28349,70	254381,54	370869,74	68,59%
8	16,37	0,050476	327,05	29281,30	252906,25	370869,74	68,19%
9	16,37	0,058872	326,86	30064,83	251729,78	370869,74	67,88%
10	16,37	0,067268	326,70	30718,71	250752,78	370869,74	67,61%
11	16,37	0,075664	326,56	31272,98	249928,26	370869,74	67,39%
12	16,37	0,084060	326,45	31748,43	249223,01	370869,74	67,20%
13	16,37	0,092456	326,35	32160,95	248612,85	370869,74	67,04%
14	16,37	0,100852	326,26	32522,27	248079,73	370869,74	66,89%
15	16,37	0,109248	326,18	32841,38	247609,78	370869,74	66,76%
16	16,37	0,117644	326,12	33125,28	247192,46	370869,74	66,65%
17	16,37	0,126040	326,06	33375,11	246819,49	370869,74	66,55%
18	16,37	0,134436	326,00	33604,04	246483,94	370869,74	66,46%
19	16,37	0,142832	325,95	33811,30	246180,63	370869,74	66,38%
20	16,37	0,151228	325,91	33999,84	245904,98	370869,74	66,30%

21	16,37	0,159624	325,86	34175,58	245656,08	370869,74	66,24%
22	16,37	0,168020	325,83	34333,60	245425,52	370869,74	66,18%
23	16,37	0,176416	325,79	34479,06	245213,57	370869,74	66,12%
24	16,37	0,184812	325,76	34613,38	245018,01	370869,74	66,07%
25	16,37	0,193208	325,73	34737,82	244837,04	370869,74	66,02%
26	16,37	0,201604	325,70	34853,42	244668,87	370869,74	65,97%
27	16,37	0,21	325,68	34961,09	244512,47	370869,74	65,93%
28	16,37	0,25	325,58	35391,56	243894,68	370869,74	65,76%
29	16,37	0,29	325,50	35712,52	243430,06	370869,74	65,64%
30	16,37	0,33	325,44	35963,11	243067,84	370869,74	65,54%
31	16,37	0,37	325,39	36164,19	242777,65	370869,74	65,46%
32	16,37	0,40	325,36	36290,72	242595,15	370869,74	65,41%
33	16,37	0,44	325,33	36434,57	242387,69	370869,74	65,36%
34	16,37	0,48	325,30	36556,08	242212,78	370869,74	65,31%
35	16,37	0,52	325,28	36660,06	242063,14	370869,74	65,27%
36	16,37	0,56	325,25	36750,07	241933,62	370869,74	65,23%
37	16,37	0,60	325,24	36828,74	241820,45	370869,74	65,20%
38	16,37	0,64	325,22	36898,08	241720,86	370869,74	65,18%
39	16,37	0,68	325,20	36960,27	241632,52	370869,74	65,15%
40	16,37	0,72	325,19	37015,34	241553,39	370869,74	65,13%
41	16,37	0,76	325,18	37064,85	241482,33	370869,74	65,11%
42	16,37	0,80	325,17	37109,63	241418,07	370869,74	65,10%
43	16,37	0,84	325,16	37150,32	241359,65	370869,74	65,08%
44	16,37	0,88	325,15	37187,44	241306,35	370869,74	65,06%
45	16,37	0,92	325,14	37221,46	241257,53	370869,74	65,05%
46	16,37	0,96	325,14	37252,74	241212,67	370869,74	65,04%
47	16,37	1,00	325,13	37281,60	241171,31	370869,74	65,03%





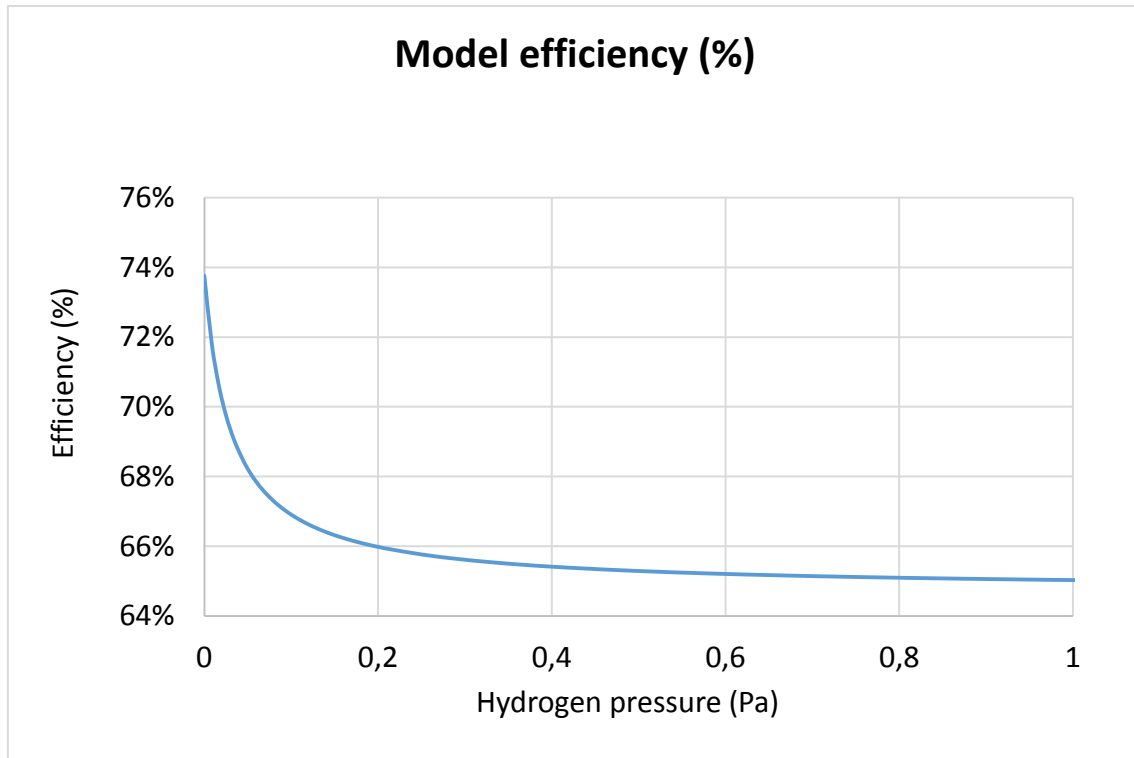


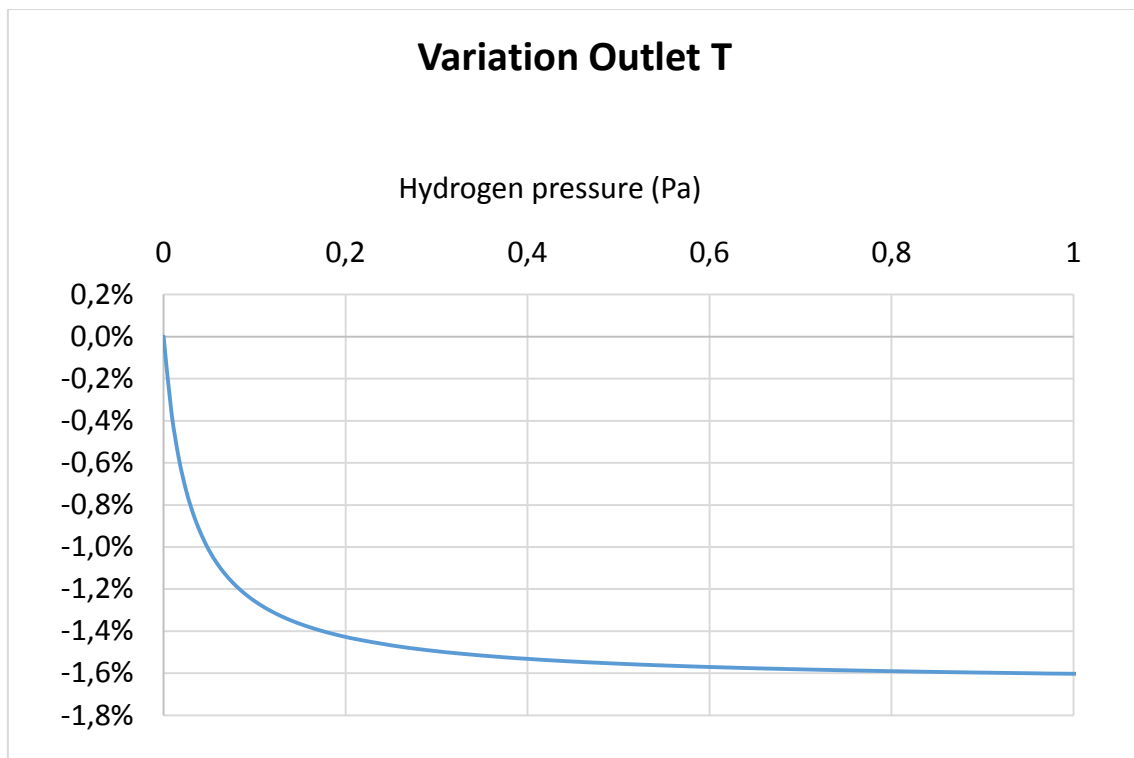
Figure-A 11. Graphs of the results for the dynamic efficiency test when there is infiltration of hydrogen, and its pressure varies from 0,0001 Pa to 8 Pa.

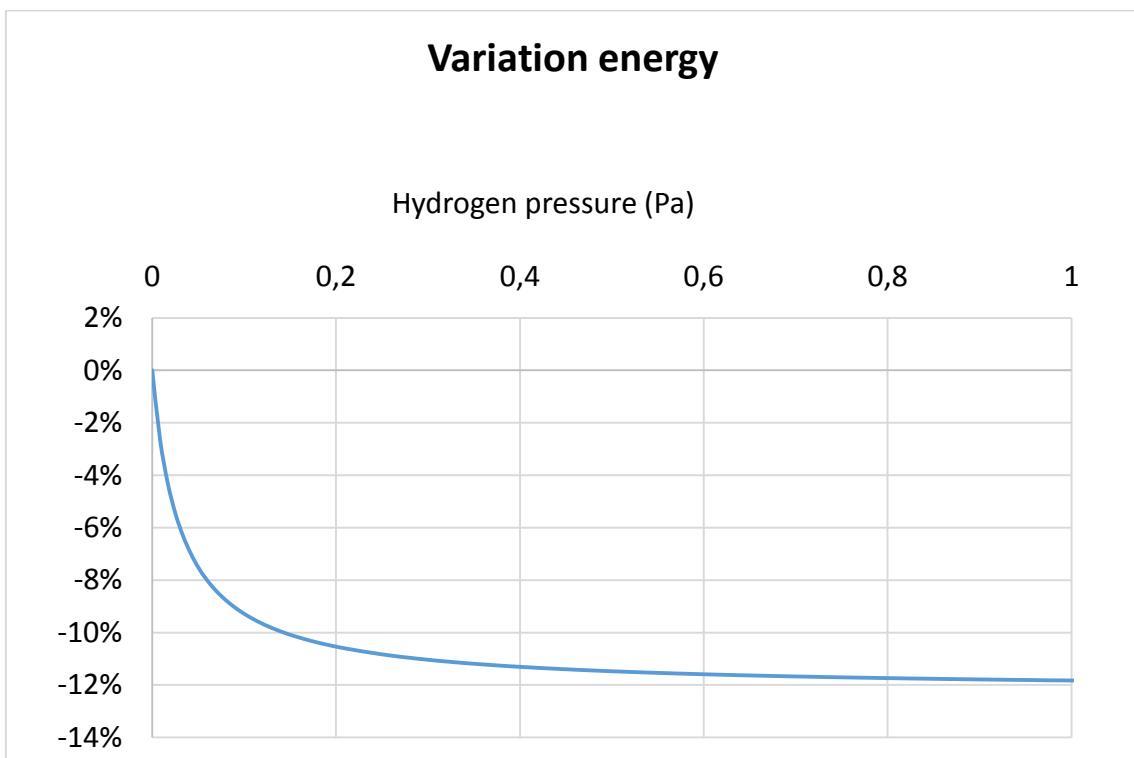
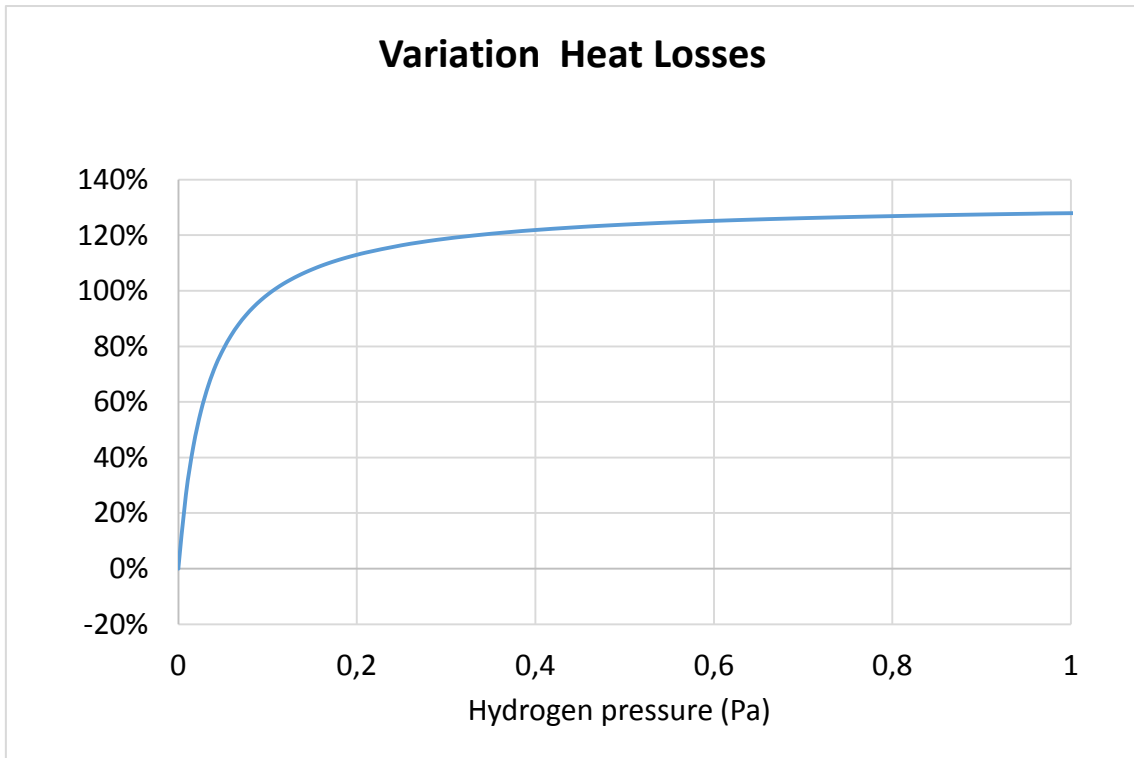
Below it is presented how the variation affects but expressed in percentages.

Table A 15. Results from the dynamic efficiency test expressed in percentages for different values of hydrogen's pressure from 0,0001 Pa to 8 Pa.

Inlet hydrogen pressure	Variation Outlet T	Variation Heat Losses	Variation energy	Variation efficiency
0,0001	0,00%	0,00%	0,00%	0,00%
0,0001	-0,01%	0,38%	-0,04%	-0,04%
0,008496	-0,36%	26,64%	-2,64%	-2,64%
0,016892	-0,58%	44,13%	-4,31%	-4,31%
0,025288	-0,74%	56,62%	-5,47%	-5,47%
0,033684	-0,86%	66,00%	-6,33%	-6,33%
0,04208	-0,95%	73,31%	-7,00%	-7,00%
0,050476	-1,02%	79,01%	-7,54%	-7,54%
0,058872	-1,08%	83,80%	-7,97%	-7,97%
0,067268	-1,13%	87,79%	-8,33%	-8,33%
0,075664	-1,17%	91,18%	-8,63%	-8,63%
0,08406	-1,20%	94,09%	-8,88%	-8,88%
0,092456	-1,23%	96,61%	-9,11%	-9,11%
0,100852	-1,26%	98,82%	-9,30%	-9,30%
0,109248	-1,28%	100,77%	-9,47%	-9,47%
0,117644	-1,30%	102,51%	-9,63%	-9,63%
0,12604	-1,32%	104,03%	-9,76%	-9,76%
0,134436	-1,34%	105,43%	-9,89%	-9,89%
0,142832	-1,35%	106,70%	-10,00%	-10,00%
0,151228	-1,37%	107,85%	-10,10%	-10,10%
0,159624	-1,38%	108,93%	-10,19%	-10,19%
0,16802	-1,39%	109,89%	-10,27%	-10,27%

0,176416	-1,40%	110,78%	-10,35%	-10,35%
0,184812	-1,41%	111,60%	-10,42%	-10,42%
0,193208	-1,42%	112,36%	-10,49%	-10,49%
0,201604	-1,43%	113,07%	-10,55%	-10,55%
0,21	-1,44%	113,73%	-10,61%	-10,61%
0,25	-1,47%	116,36%	-10,83%	-10,83%
0,29	-1,49%	118,32%	-11,00%	-11,00%
0,33	-1,51%	119,86%	-11,13%	-11,13%
0,37	-1,52%	121,08%	-11,24%	-11,24%
0,4	-1,53%	121,86%	-11,31%	-11,31%
0,44	-1,54%	122,74%	-11,38%	-11,38%
0,48	-1,55%	123,48%	-11,45%	-11,45%
0,52	-1,56%	124,12%	-11,50%	-11,50%
0,56	-1,56%	124,67%	-11,55%	-11,55%
0,6	-1,57%	125,15%	-11,59%	-11,59%
0,64	-1,58%	125,57%	-11,63%	-11,63%
0,68	-1,58%	125,95%	-11,66%	-11,66%
0,72	-1,58%	126,29%	-11,69%	-11,69%
0,76	-1,59%	126,59%	-11,71%	-11,71%
0,8	-1,59%	126,86%	-11,74%	-11,74%
0,84	-1,59%	127,11%	-11,76%	-11,76%
0,88	-1,60%	127,34%	-11,78%	-11,78%
0,92	-1,60%	127,55%	-11,80%	-11,80%
0,96	-1,60%	127,74%	-11,81%	-11,81%
1	-1,60%	127,92%	-11,83%	-11,83%





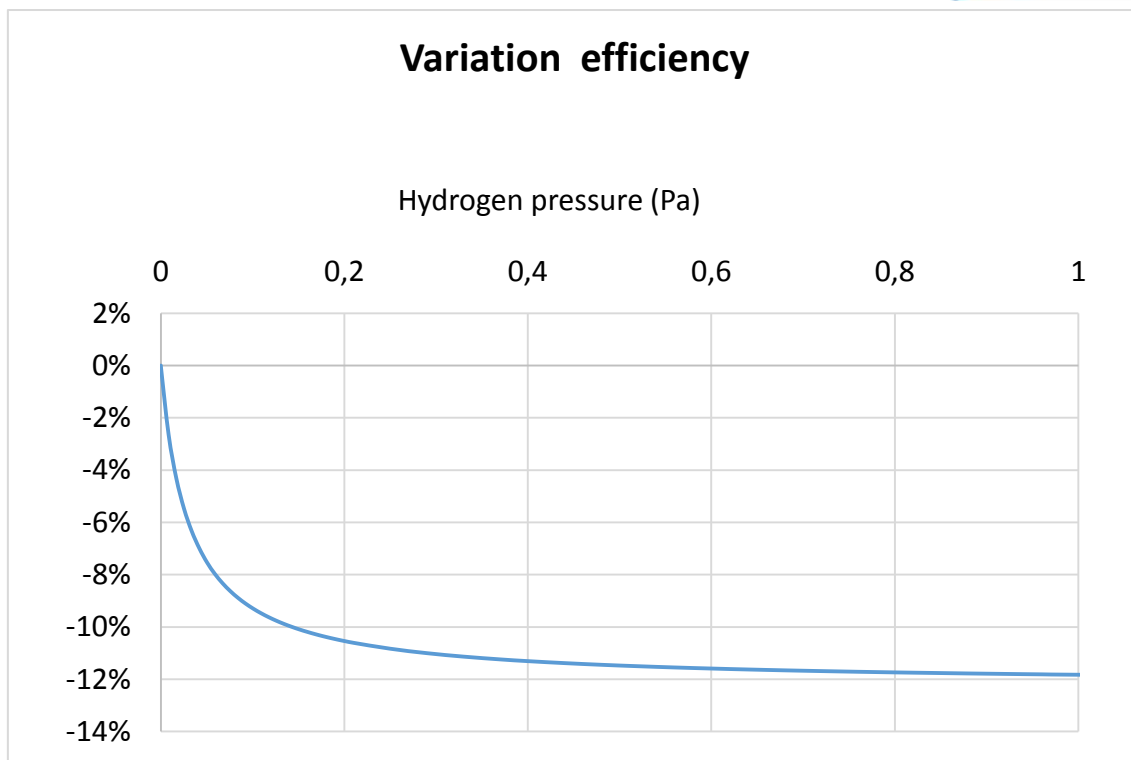


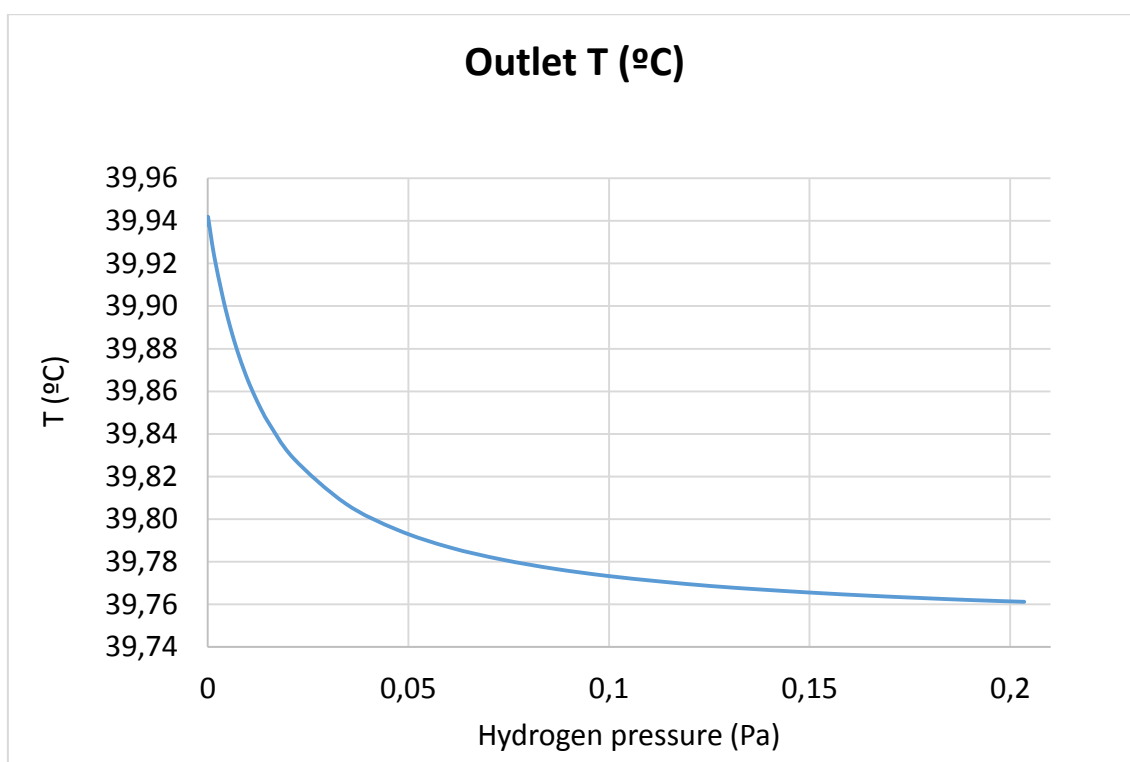
Figure-A 12. Graphs of the results for the dynamic efficiency test expressed in percentages for different values of the hydrogen's pressure.

- When the HTF's inlet temperature is 40°C:

Table A 16. Results from the heat losses test at 40°C for different values of hydrogen's pressure.

Test	Hydrogen partial pressure (Pa)	Outlet T (°C)	Total Losses (W)	Enthalpy difference (W)
1	0,0001	39,94	368,82	364,13
2	0,0001	39,94	398,81	343,39
3	0,00108333	39,93	471,19	416,00
4	0,00206667	39,92	524,52	475,73
5	0,00305	39,91	583,04	527,96
6	0,00403333	39,90	631,90	576,96
7	0,00501667	39,89	676,01	621,32
8	0,006	39,89	716,02	661,38
9	0,00698333	39,88	752,48	697,86
10	0,00796667	39,88	785,84	731,13
11	0,00895	39,87	816,48	761,89
12	0,00993333	39,87	844,73	790,15
13	0,0109167	39,86	870,84	816,26
14	0,0119	39,86	895,06	840,58
15	0,0128833	39,85	917,57	863,12
16	0,0138667	39,85	938,57	884,22
17	0,01485	39,85	958,18	903,89
18	0,021355	39,83	1061,32	1006,91
19	0,034365	39,81	1186,27	1132,10
20	0,047375	39,79	1259,20	1205,07
21	0,060385	39,79	1306,97	1253,00

22	0,073395	39,78	1340,69	1286,63
23	0,086405	39,78	1365,77	1311,67
24	0,099415	39,77	1385,14	1331,34
25	0,112425	39,77	1400,56	1346,72
26	0,125435	39,77	1413,12	1359,24
27	0,138445	39,77	1423,56	1369,61
28	0,151455	39,77	1432,36	1378,55
29	0,164465	39,76	1439,88	1386,07
30	0,177475	39,76	1446,40	1392,50
31	0,190485	39,76	1452,07	1398,23
32	0,203495	39,76	1457,08	1403,23



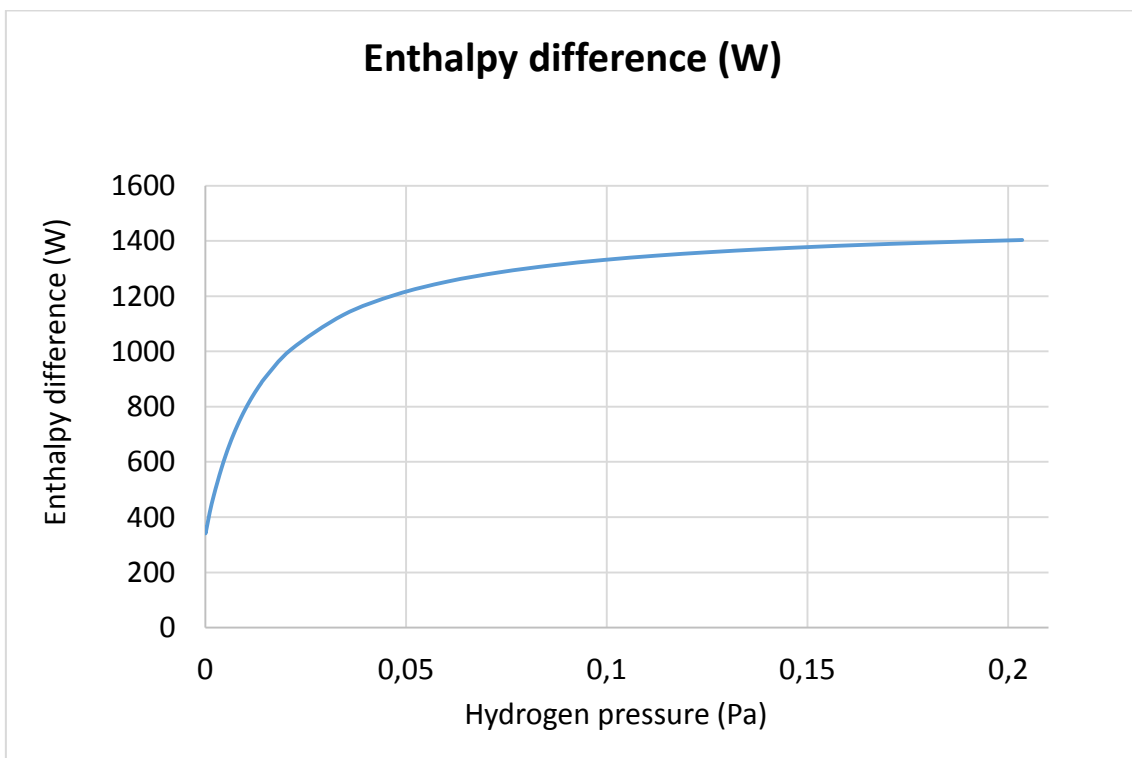
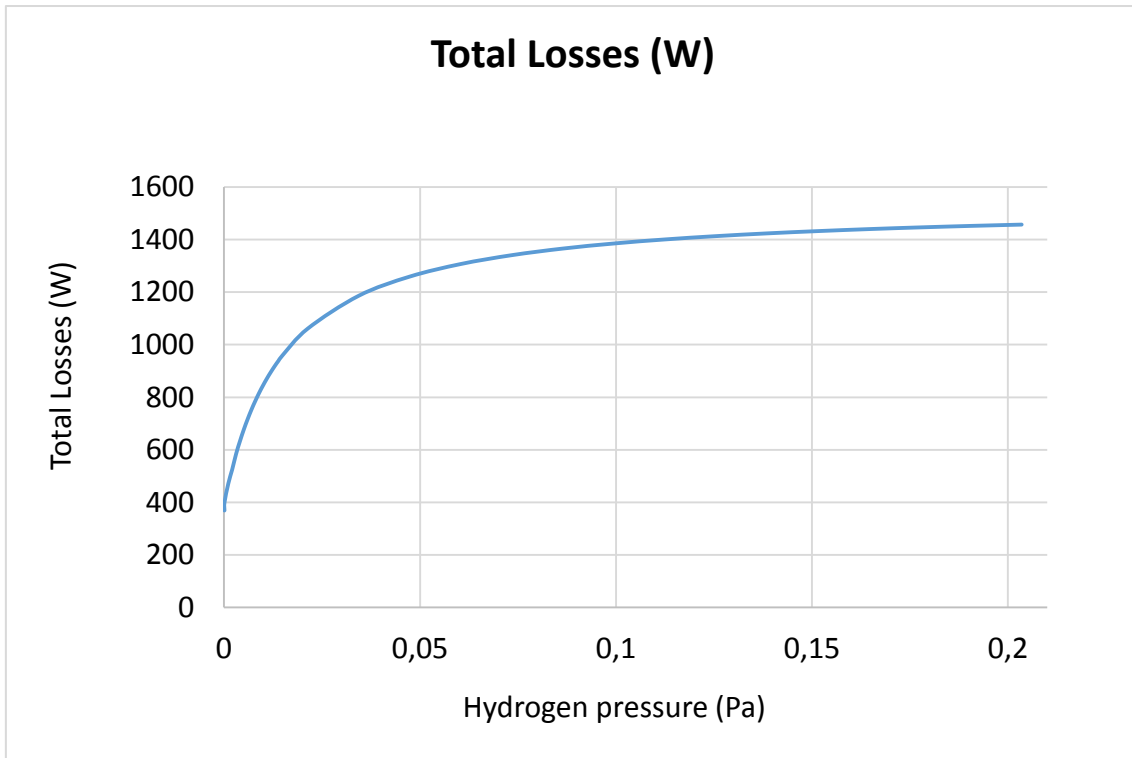
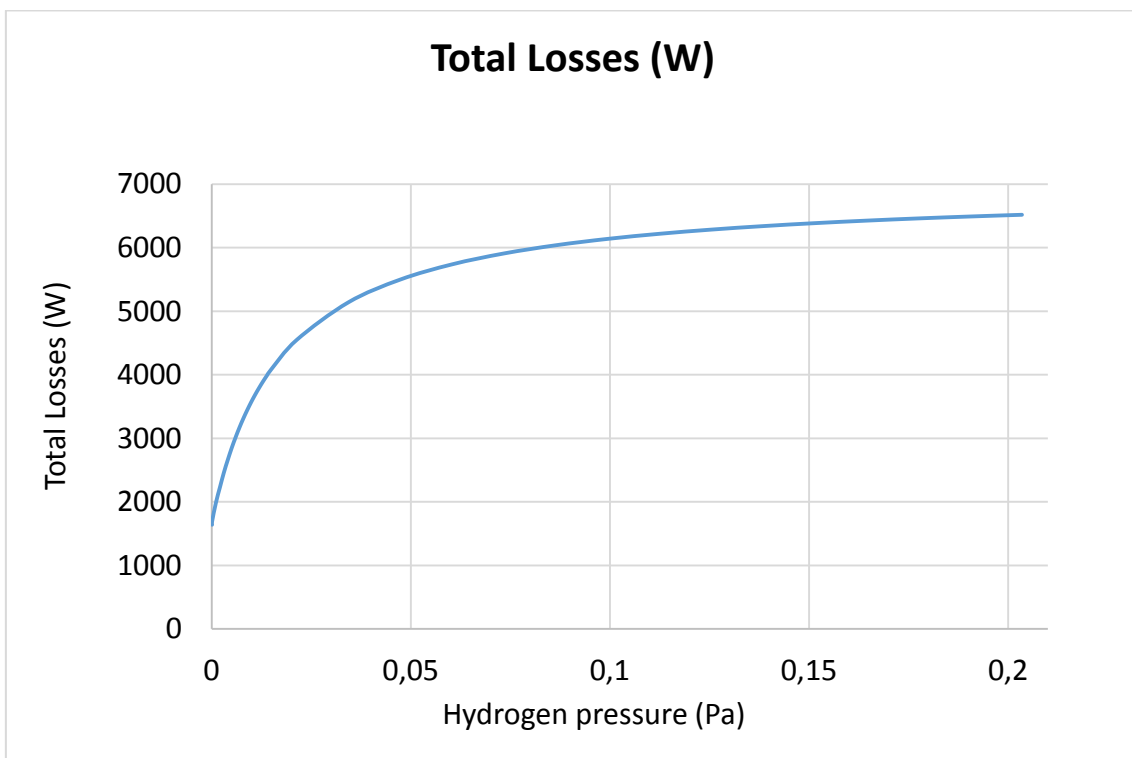
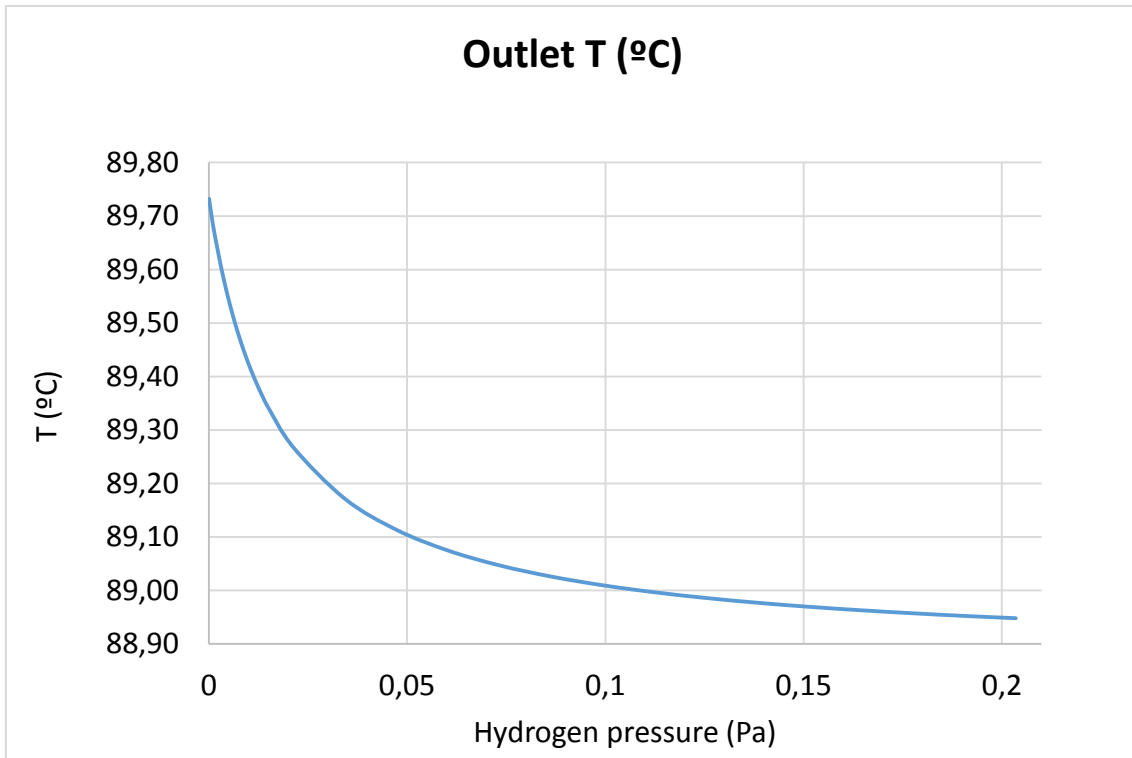


Figure-A 13. Graphs of the results for the heat losses test at 40°C for different values of hydrogen's pressure.

- When the HTF's inlet temperature is 90°C:

Table A 17. Results from the heat losses test at 90°C for different values of hydrogen's pressure.

Test	Hydrogen partial pressure (Pa)	Outlet T (°C)	Total Losses (W)	Enthalpy difference (W)
1	0,0001	89,73	1638,78	1656,12
2	0,0001	89,73	1686,84	1666,86
3	0,00108333	89,68	1987,89	1967,32
4	0,00206667	89,64	2224,91	2206,97
5	0,00305	89,61	2455,75	2435,90
6	0,00403333	89,57	2656,81	2636,21
7	0,00501667	89,54	2842,94	2822,21
8	0,006	89,52	3012,02	2993,90
9	0,00698333	89,49	3168,36	3147,71
10	0,00796667	89,47	3312,32	3294,36
11	0,00895	89,45	3445,54	3426,71
12	0,00993333	89,43	3569,22	3548,33
13	0,0109167	89,41	3684,27	3666,37
14	0,0119	89,39	3791,61	3773,68
15	0,0128833	89,37	3892,03	3873,83
16	0,0138667	89,36	3986,15	3966,83
17	0,01485	89,34	4074,58	4056,25
18	0,021355	89,27	4547,53	4528,41
19	0,034365	89,17	5140,32	5122,18
20	0,047375	89,11	5497,59	5479,88
21	0,060385	89,07	5736,70	5715,96
22	0,073395	89,05	5908,01	5887,65
23	0,086405	89,03	6036,82	6016,42
24	0,099415	89,01	6137,20	6116,57
25	0,112425	89,00	6217,63	6198,84
26	0,125435	88,99	6283,54	6263,23
27	0,138445	88,98	6338,52	6320,46
28	0,151455	88,97	6385,10	6366,96
29	0,164465	88,96	6425,05	6406,31
30	0,177475	88,96	6459,70	6442,08
31	0,190485	88,95	6490,05	6470,69
32	0,203495	88,95	6516,83	6499,31



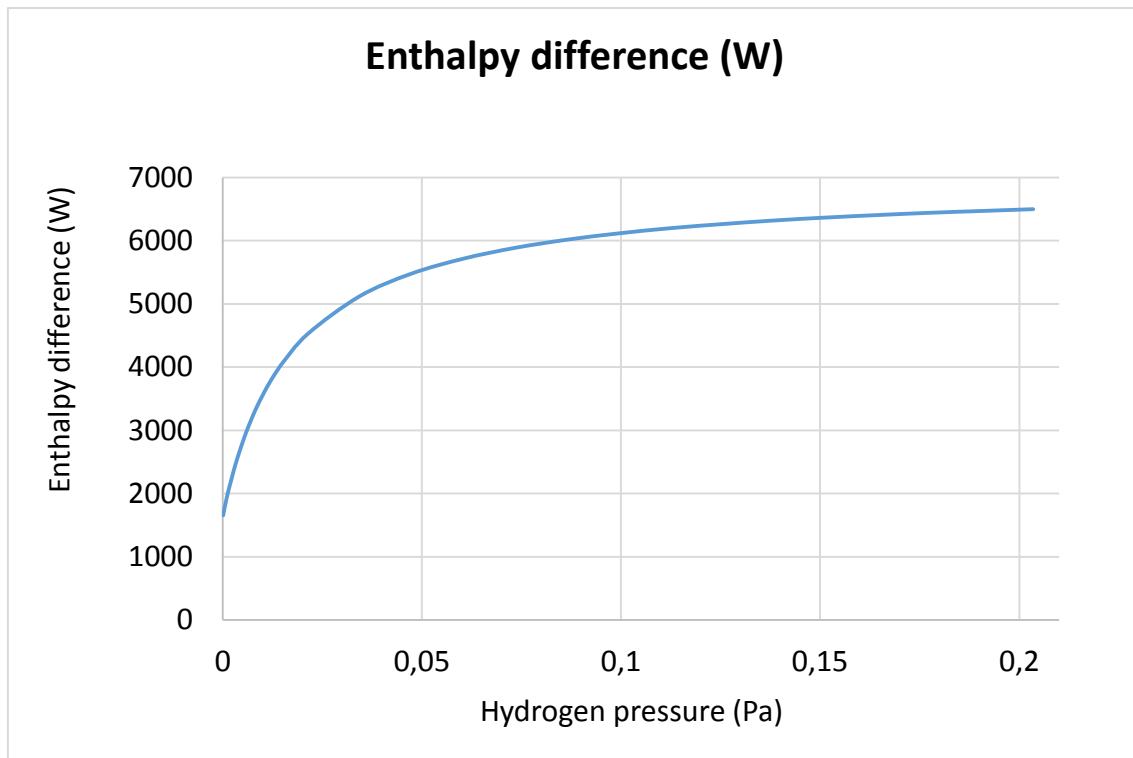


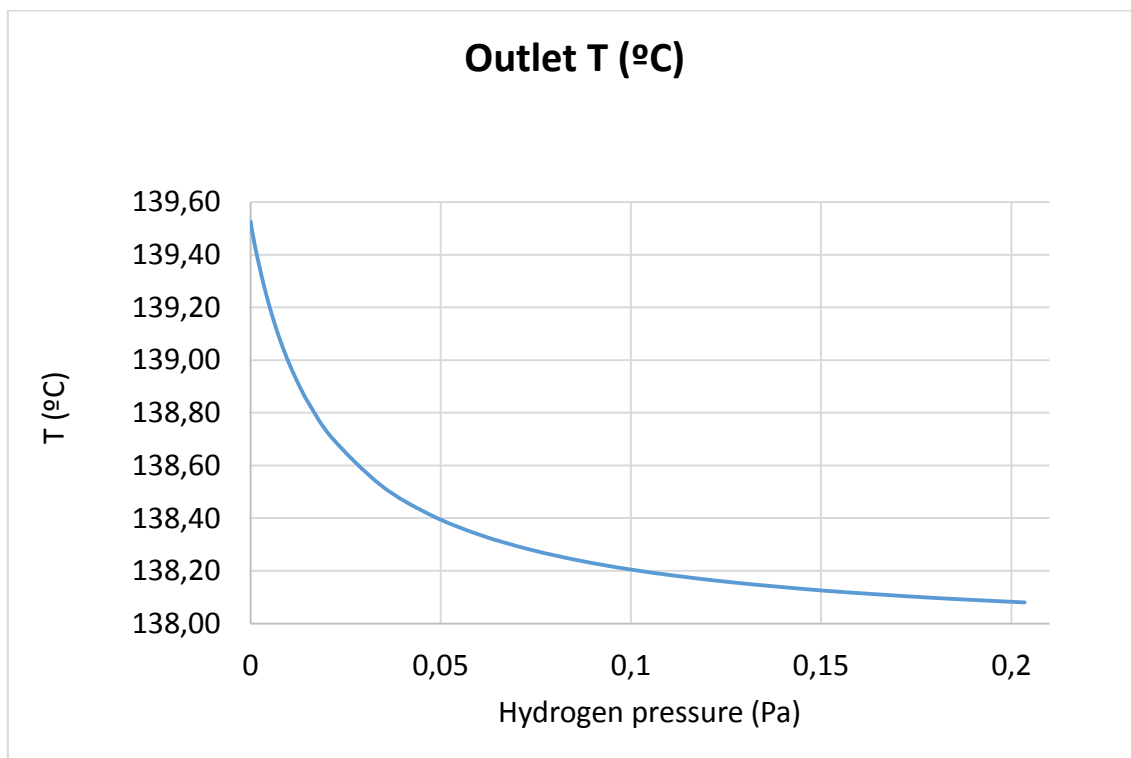
Figure-A 14. Graphs of the results for the heat losses test at 90°C for different values of hydrogen's pressure.

- When the HTF's inlet temperature is 140°C:

Table A 18. Results from the heat losses test at 140°C for different values of hydrogen's pressure.

Test	Hydrogen partial pressure (Pa)	Outlet T (°C)	Total Losses (W)	Enthalpy difference (W)
1	0,0001	139,53	3041,97	3079,75
2	0,0001	139,519	3104,927	3115,517797
3	0,00108333	139,44	3620,3973	3630,597663
4	0,00206667	139,374	4042,1596	4059,830884
5	0,00305	139,312	4448,255	4460,448557
6	0,00403333	139,255	4816,8626	4828,873739
7	0,00501667	139,203	5154,822	5168,683372
8	0,006	139,155	5465,9856	5479,877457
9	0,00698333	139,11	5753,5635	5766,032938
10	0,00796667	139,069	6020,2427	6034,303701
11	0,00895	139,031	6268,3104	6281,112804
12	0,00993333	138,995	6499,7006	6513,614132
13	0,0109167	138,962	6716,1074	6728,230742
14	0,0119	138,931	6918,9505	6932,116522
15	0,0128833	138,901	7109,5288	7121,694528
16	0,0138667	138,873	7288,9225	7300,541704
17	0,01485	138,847	7458,1219	7472,234992
18	0,021355	138,706	8374,3532	8387,932531
19	0,034365	138,524	9551,4142	9564,746946
20	0,047375	138,412	10277,4485	10290,86648
21	0,060385	138,336	10770,7818	10784,48468
22	0,073395	138,281	11128,0765	11142,17903
23	0,086405	138,239	11398,8936	11410,4498

24	0,099415	138,206	11611,2752	11625,06641
25	0,112425	138,18	11782,3208	11796,7597
26	0,125435	138,158	11923,0236	11936,26049
27	0,138445	138,14	12040,8245	12054,29963
28	0,151455	138,124	12140,8842	12154,45405
29	0,164465	138,111	12226,9352	12240,30069
30	0,177475	138,099	12301,7391	12315,4165
31	0,190485	138,089	12367,3464	12379,80149
32	0,203495	138,08	12425,3761	12437,03258



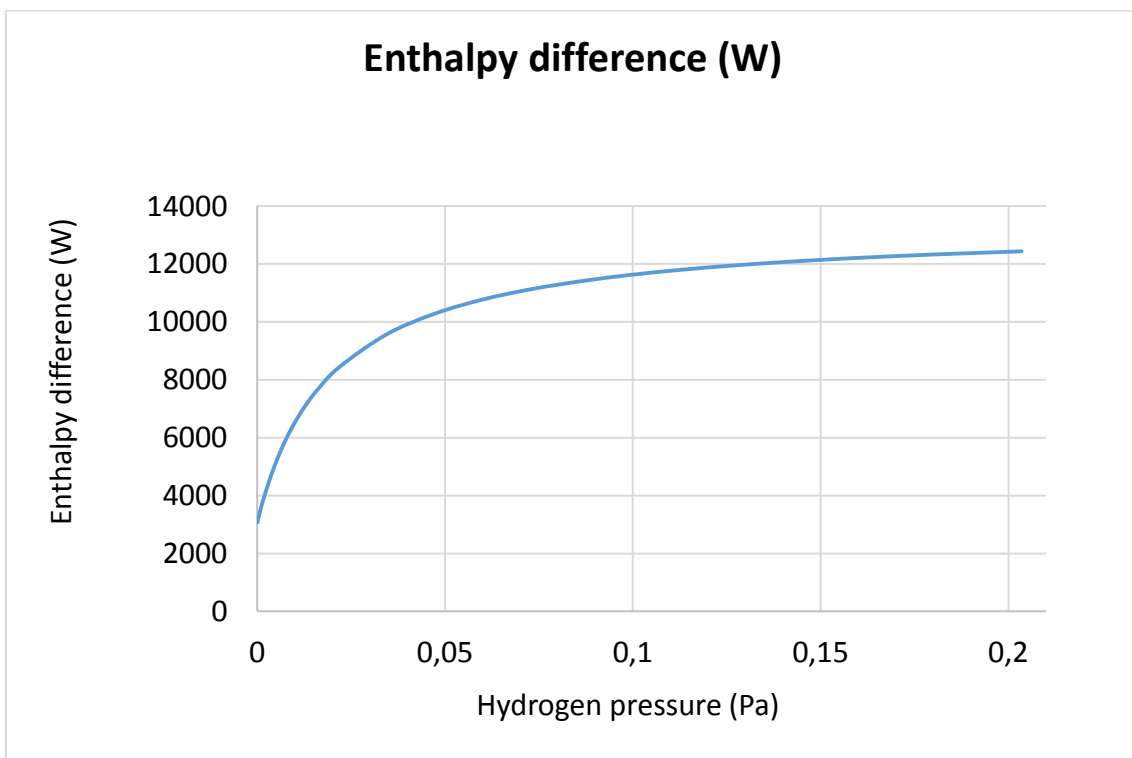
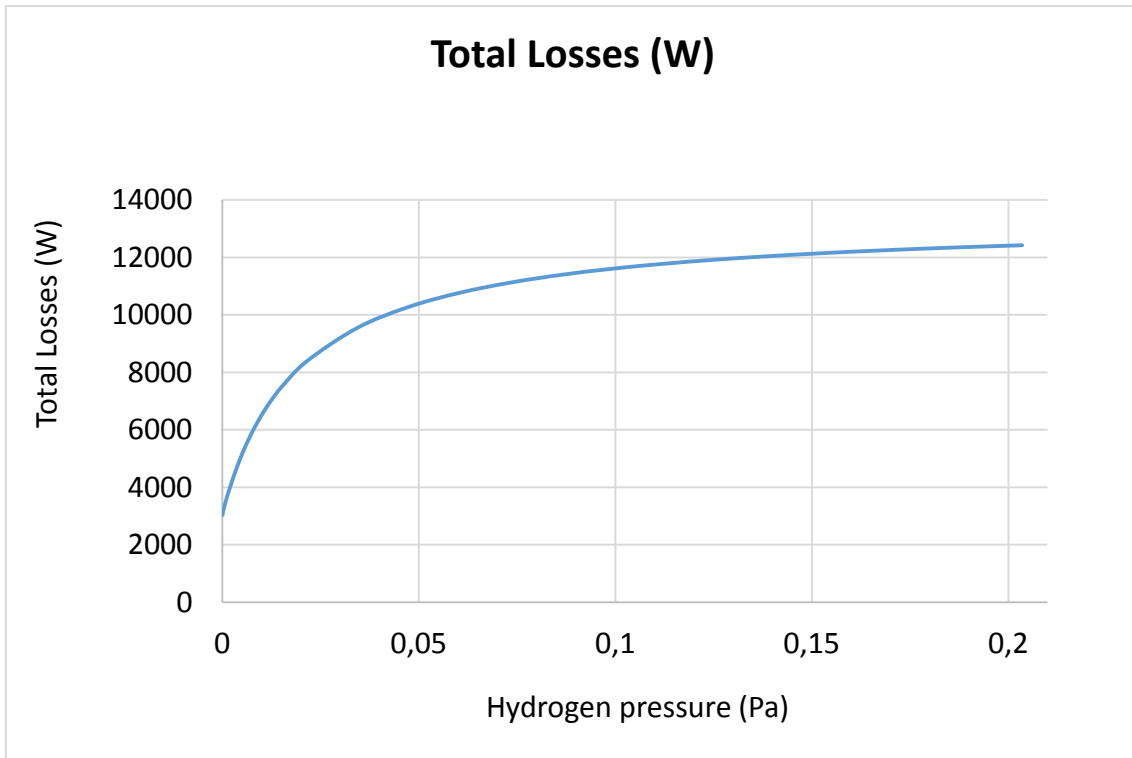
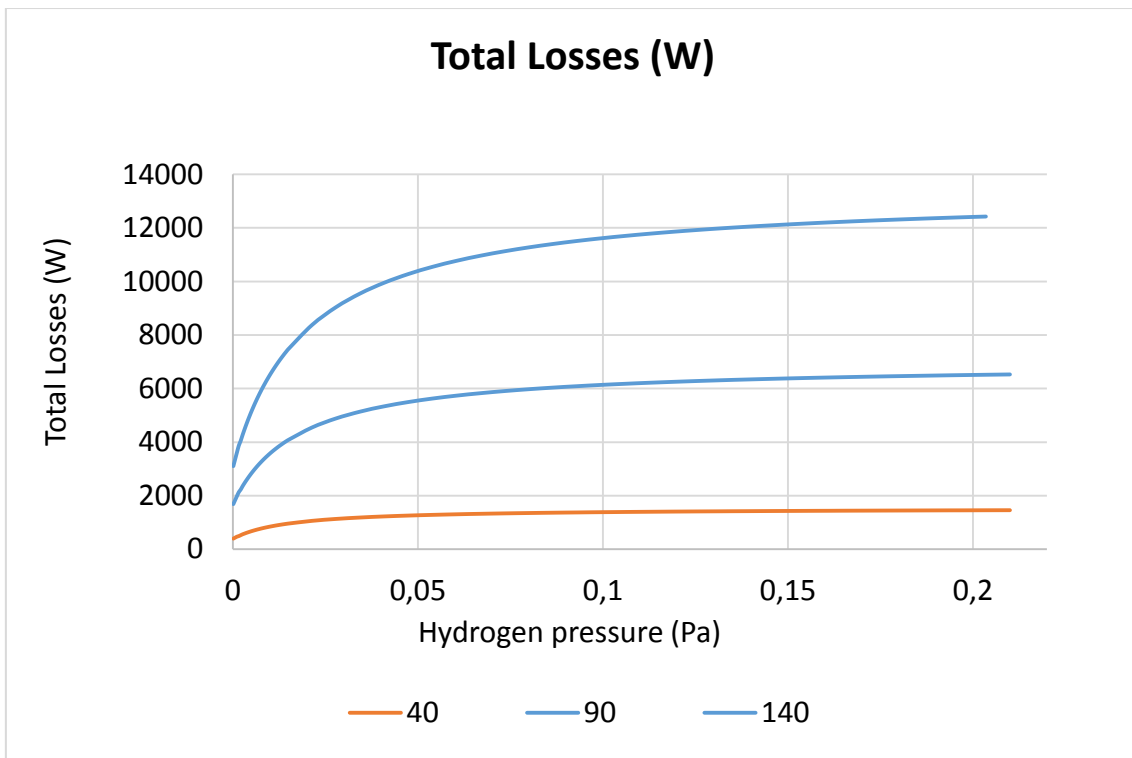
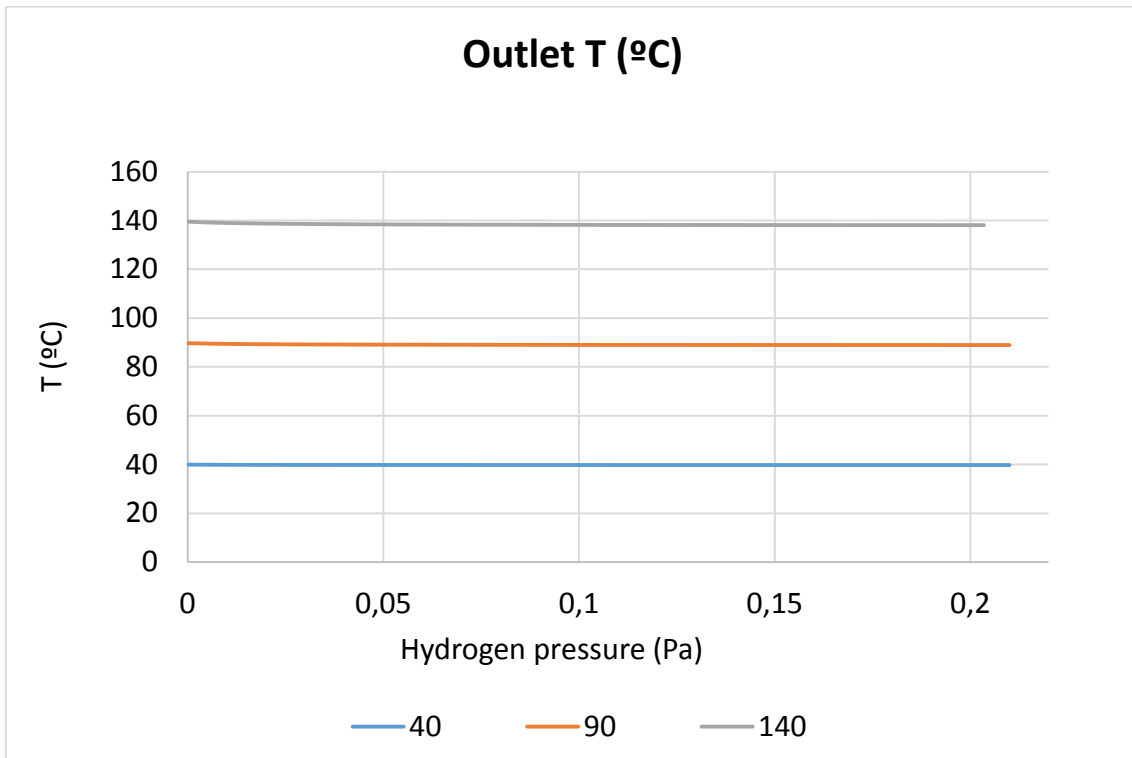


Figure-A 15. Graphs of the results for the heat losses test at 140°C for different values of hydrogen's pressure.

- Comparing the three cases:



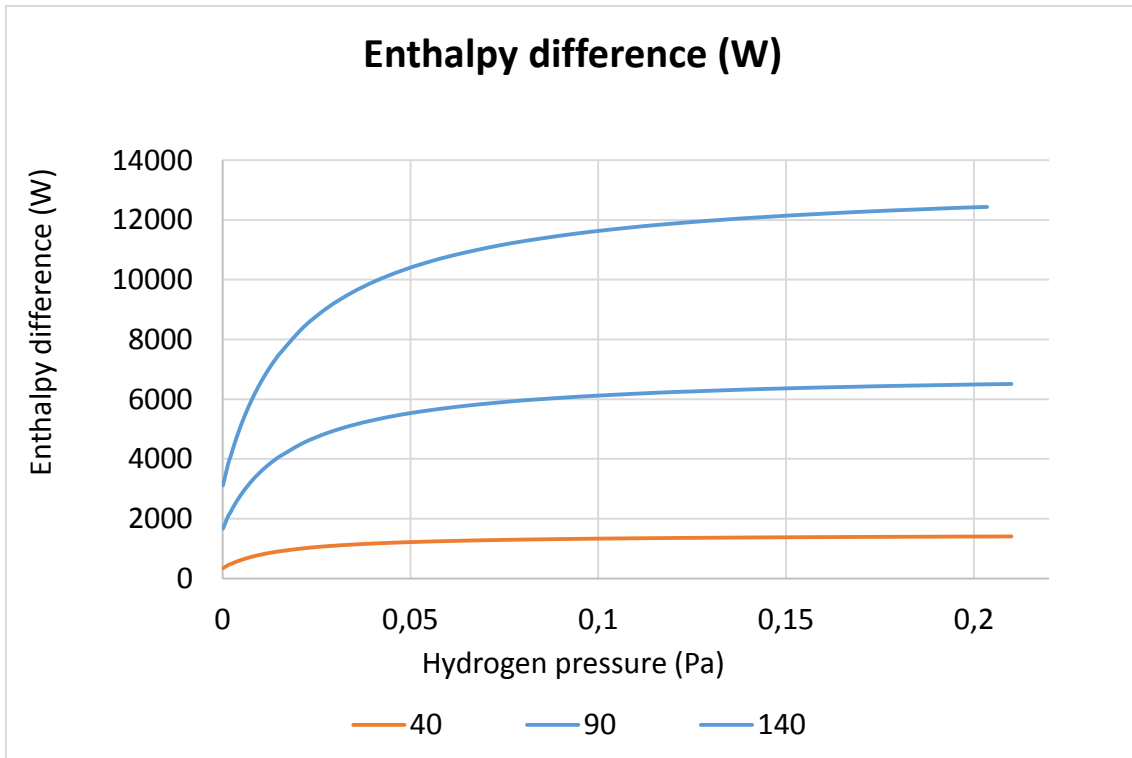


Figure-A 16. Graphs of the results for the heat losses test for the three cases for different values of hydrogen's pressure.

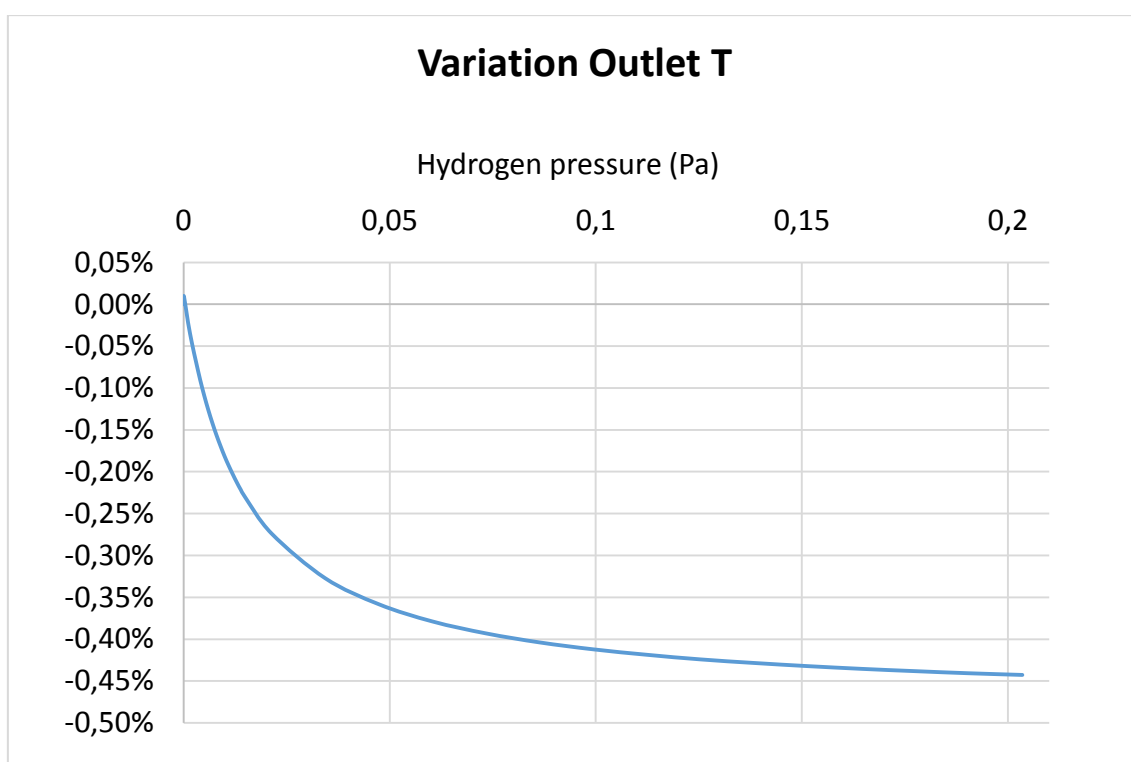
The next tables and graphs present how the variation affects but expressed in percentages.

- When the HTF's inlet temperature is 40°C:

Table A 19. Results from the heat losses test at 40°C expressed in percentages for different values of hydrogen's pressure.

Hydrogen partial pressure	Variation Outlet T	Variation Heat Losses	Variation Enthalpy difference
0	0,0001	0,00%	0,00%
0,0001	0,0001	0,01%	8,13%
0,00108333	0,00108333	-0,02%	27,76%
0,00206667	0,00206667	-0,05%	42,21%
0,00305	0,00305	-0,07%	58,08%
0,00403333	0,00403333	-0,09%	71,33%
0,00501667	0,00501667	-0,11%	83,29%
0,006	0,006	-0,13%	94,14%
0,00698333	0,00698333	-0,14%	104,02%
0,00796667	0,00796667	-0,16%	113,07%
0,00895	0,00895	-0,17%	121,38%
0,00993333	0,00993333	-0,18%	129,03%
0,0109167	0,0109167	-0,19%	136,11%
0,0119	0,0119	-0,20%	142,68%
0,0128833	0,0128833	-0,21%	148,79%
0,0138667	0,0138667	-0,22%	154,48%
0,01485	0,01485	-0,23%	159,80%
0,021355	2,14%	-0,27%	187,76%
0,034365	3,44%	-0,33%	221,64%
0,047375	4,74%	-0,36%	241,41%

0,060385	6,04%	-0,38%	254,36%
0,073395	7,34%	-0,39%	263,51%
0,086405	8,64%	-0,40%	270,31%
0,099415	9,94%	-0,41%	275,56%
0,112425	11,24%	-0,42%	279,74%
0,125435	12,54%	-0,42%	283,15%
0,138445	13,84%	-0,43%	285,97%
0,151455	15,15%	-0,43%	288,36%
0,164465	16,45%	-0,44%	290,40%
0,177475	17,75%	-0,44%	292,17%
0,190485	19,05%	-0,44%	293,71%
0,203495	20,35%	-0,44%	295,06%



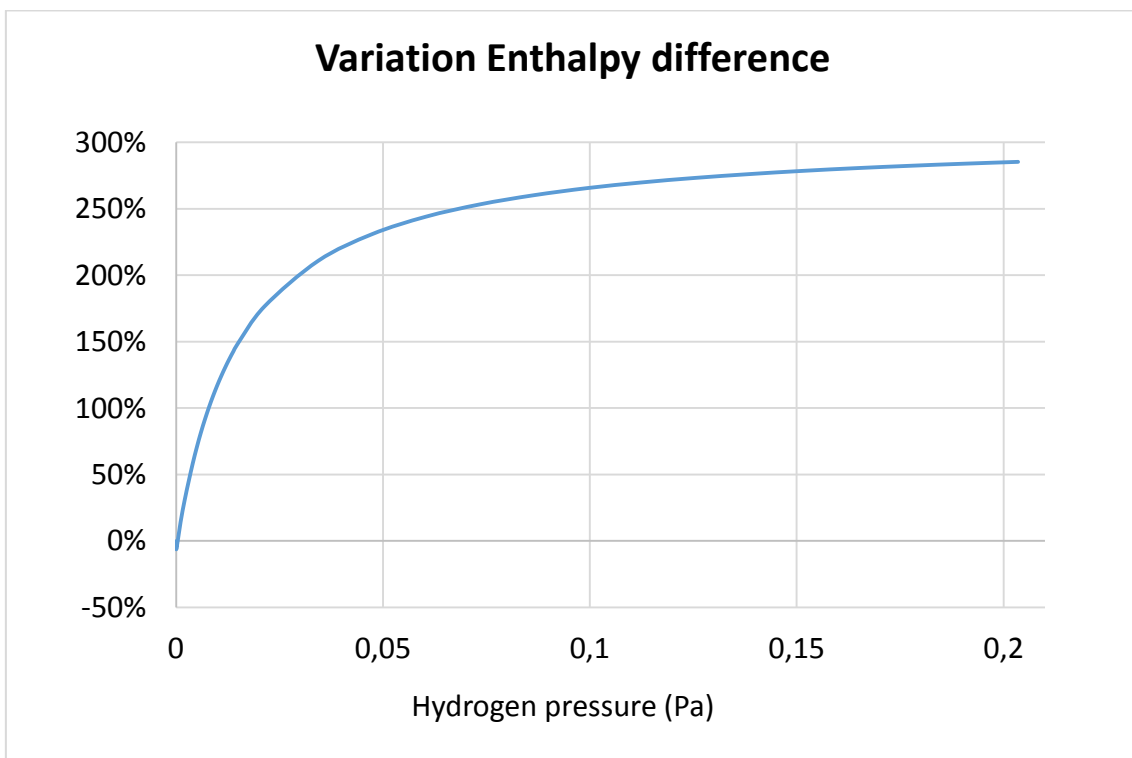
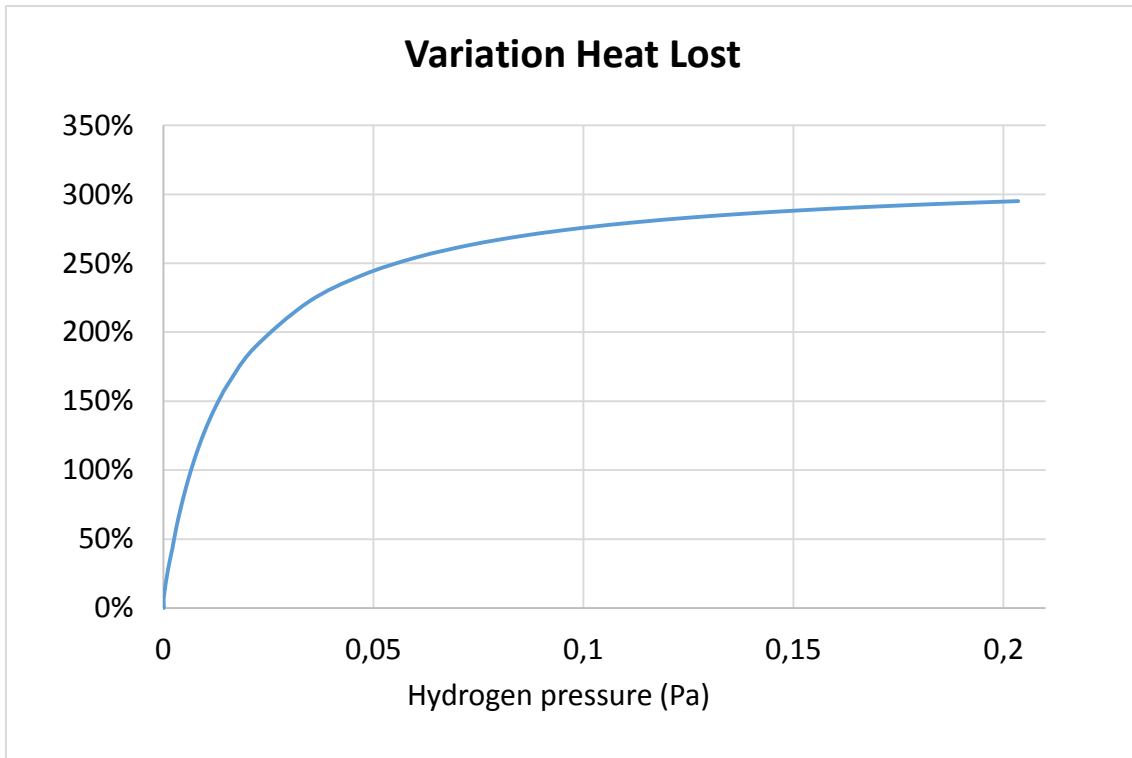
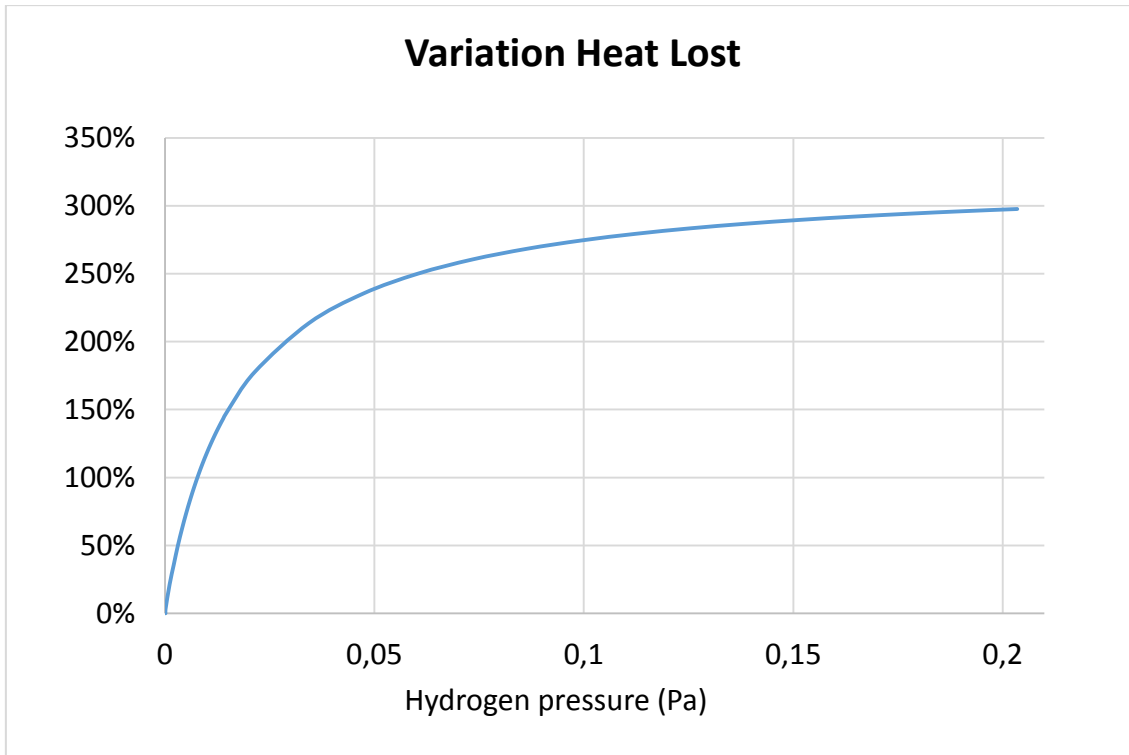
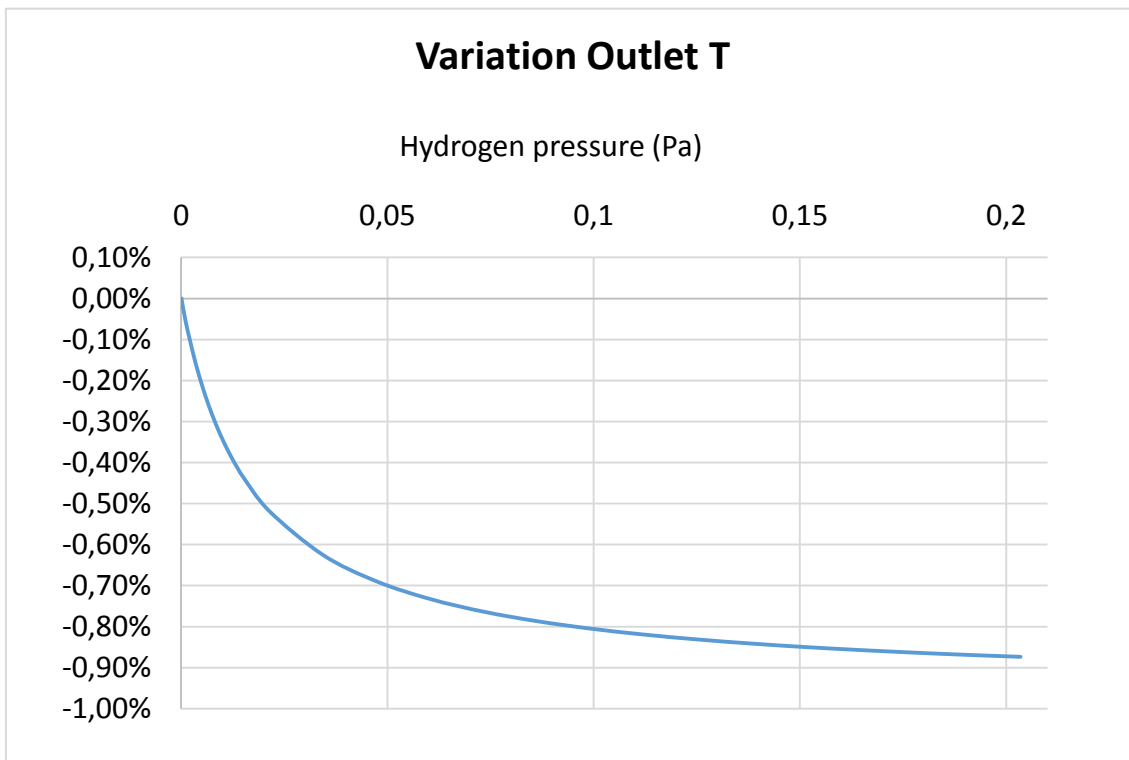


Figure-A 17. Graphs of the results for the heat losses test at 40°C expressed in percentages for different values of hydrogen's pressure.

- When the HTF's inlet temperature is 90°C:

Table A 20. Results from the heat losses test at 90°C expressed in percentages for different values of hydrogen's pressure.

Hydrogen partial pressure	Variation Outlet T	Variation Heat Losses	Variation Enthalpy difference
0,0001	0,00%	0,00%	0,00%
0,0001	0,00%	2,93%	0,65%
0,00108333	-0,06%	21,30%	18,79%
0,00206667	-0,10%	35,77%	33,26%
0,00305	-0,14%	49,85%	47,08%
0,00403333	-0,18%	62,12%	59,18%
0,00501667	-0,21%	73,48%	70,41%
0,006	-0,24%	83,80%	80,78%
0,00698333	-0,27%	93,34%	90,06%
0,00796667	-0,30%	102,12%	98,92%
0,00895	-0,32%	110,25%	106,91%
0,00993333	-0,34%	117,80%	114,25%
0,0109167	-0,36%	124,82%	121,38%
0,0119	-0,38%	131,37%	127,86%
0,0128833	-0,40%	137,50%	133,91%
0,0138667	-0,42%	143,24%	139,52%
0,01485	-0,43%	148,64%	144,92%
0,021355	-0,52%	177,49%	173,43%
0,034365	-0,63%	213,67%	209,29%
0,047375	-0,69%	235,47%	230,89%
0,060385	-0,73%	250,06%	245,14%
0,073395	-0,76%	260,51%	255,51%
0,086405	-0,79%	268,37%	263,28%
0,099415	-0,81%	274,50%	269,33%
0,112425	-0,82%	279,41%	274,30%
0,125435	-0,83%	283,43%	278,19%
0,138445	-0,84%	286,78%	281,64%
0,151455	-0,85%	289,63%	284,45%
0,164465	-0,86%	292,06%	286,83%
0,177475	-0,86%	294,18%	288,98%
0,190485	-0,87%	296,03%	290,71%
0,203495	-0,87%	297,66%	292,44%



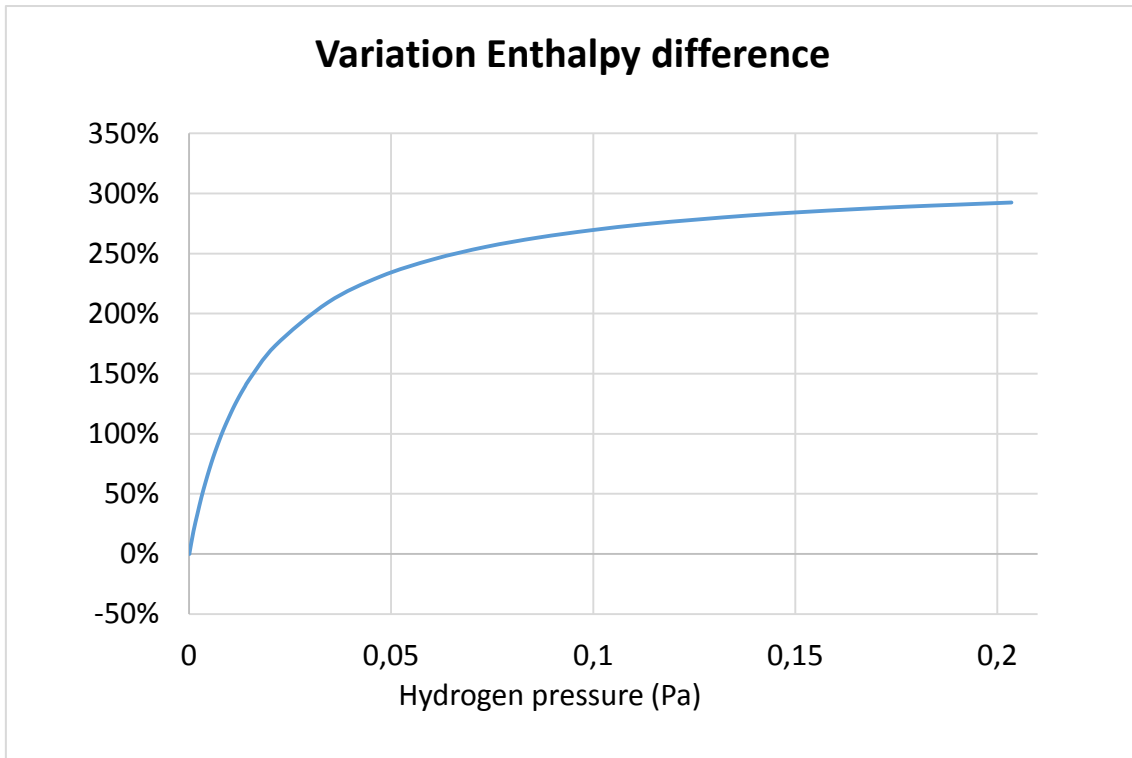


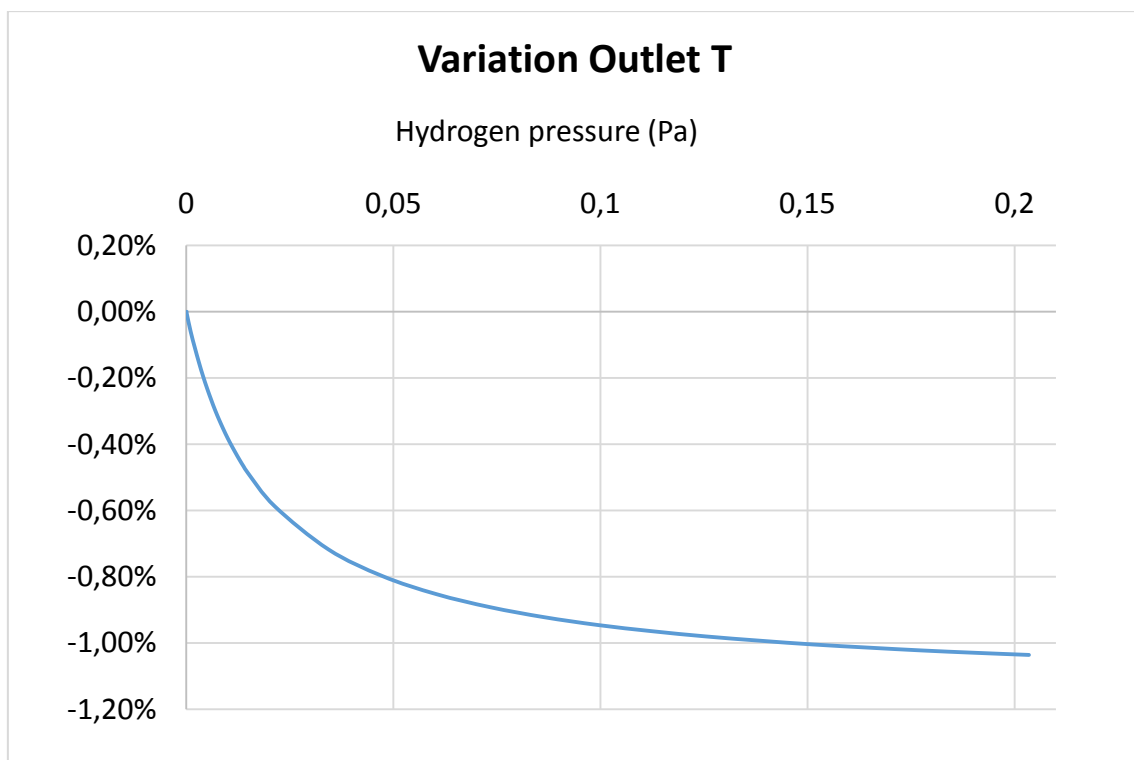
Figure-A 18. Graphs of the results for the heat losses test at 90°C expressed in percentages for different values of hydrogen's pressure.

- When the HTF's inlet temperature is 140°C:

Table A 21. Results from the heat losses test at 140°C expressed in percentages for different values of hydrogen's pressure.

Hydrogen partial pressure	Variation Outlet T	Variation Heat Losses	Variation Enthalpy difference
0,0001	0,00%	0,00%	0,00%
0,0001	0,00%	2,07%	1,16%
0,00108333	-0,06%	19,01%	17,89%
0,00206667	-0,11%	32,88%	31,82%
0,00305	-0,15%	46,23%	44,83%
0,00403333	-0,19%	58,35%	56,79%
0,00501667	-0,23%	69,46%	67,83%
0,006	-0,27%	79,69%	77,93%
0,00698333	-0,30%	89,14%	87,22%
0,00796667	-0,33%	97,91%	95,93%
0,00895	-0,35%	106,06%	103,95%
0,00993333	-0,38%	113,67%	111,50%
0,0109167	-0,40%	120,78%	118,47%
0,0119	-0,43%	127,45%	125,09%
0,0128833	-0,45%	133,71%	131,24%
0,0138667	-0,47%	139,61%	137,05%
0,01485	-0,49%	145,17%	142,62%
0,021355	-0,59%	175,29%	172,36%
0,034365	-0,72%	213,99%	210,57%
0,047375	-0,80%	237,85%	234,15%

0,060385	-0,85%	254,07%	250,17%
0,073395	-0,89%	265,82%	261,79%
0,086405	-0,92%	274,72%	270,50%
0,099415	-0,95%	281,70%	277,47%
0,112425	-0,96%	287,33%	283,04%
0,125435	-0,98%	291,95%	287,57%
0,138445	-0,99%	295,82%	291,41%
0,151455	-1,00%	299,11%	294,66%
0,164465	-1,01%	301,94%	297,44%
0,177475	-1,02%	304,40%	299,88%
0,190485	-1,03%	306,56%	301,97%
0,203495	-1,04%	308,46%	303,83%



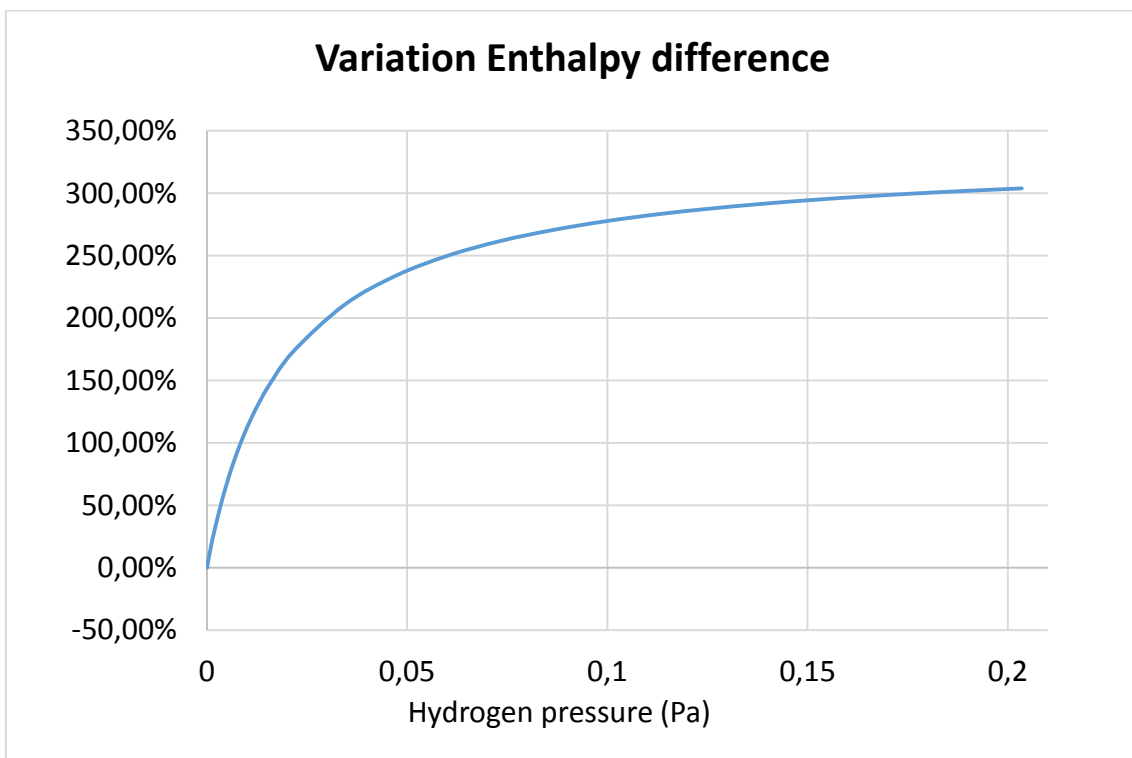
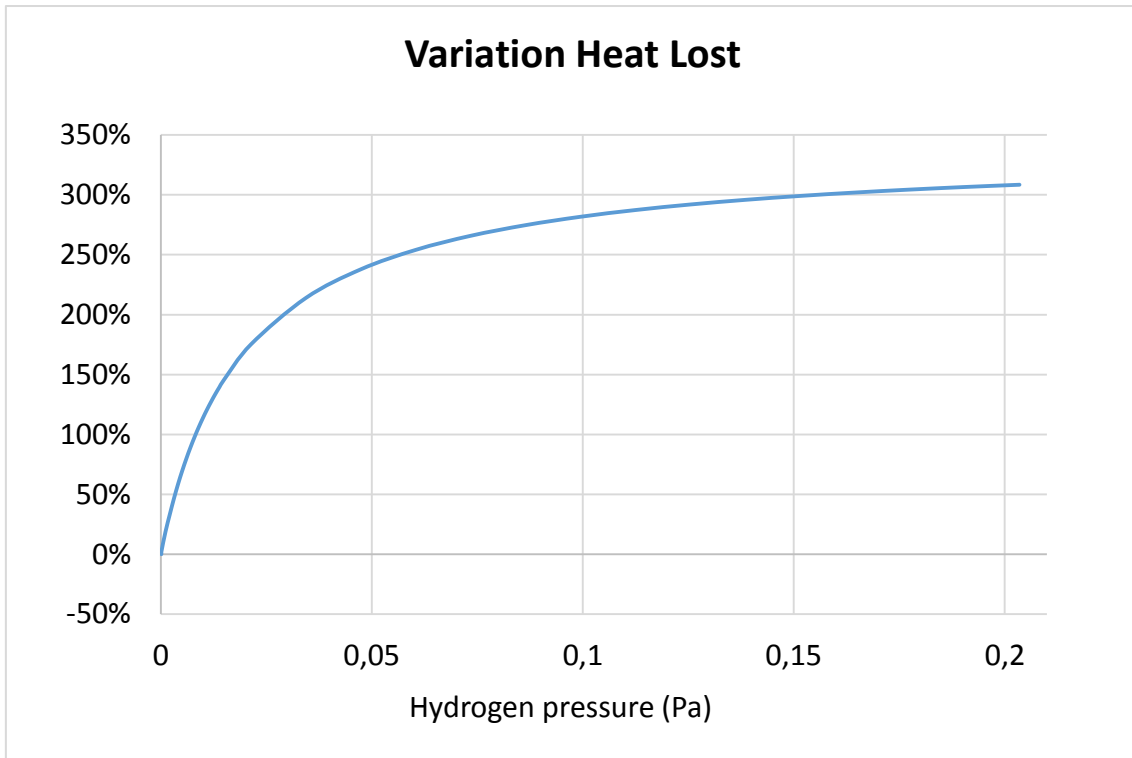
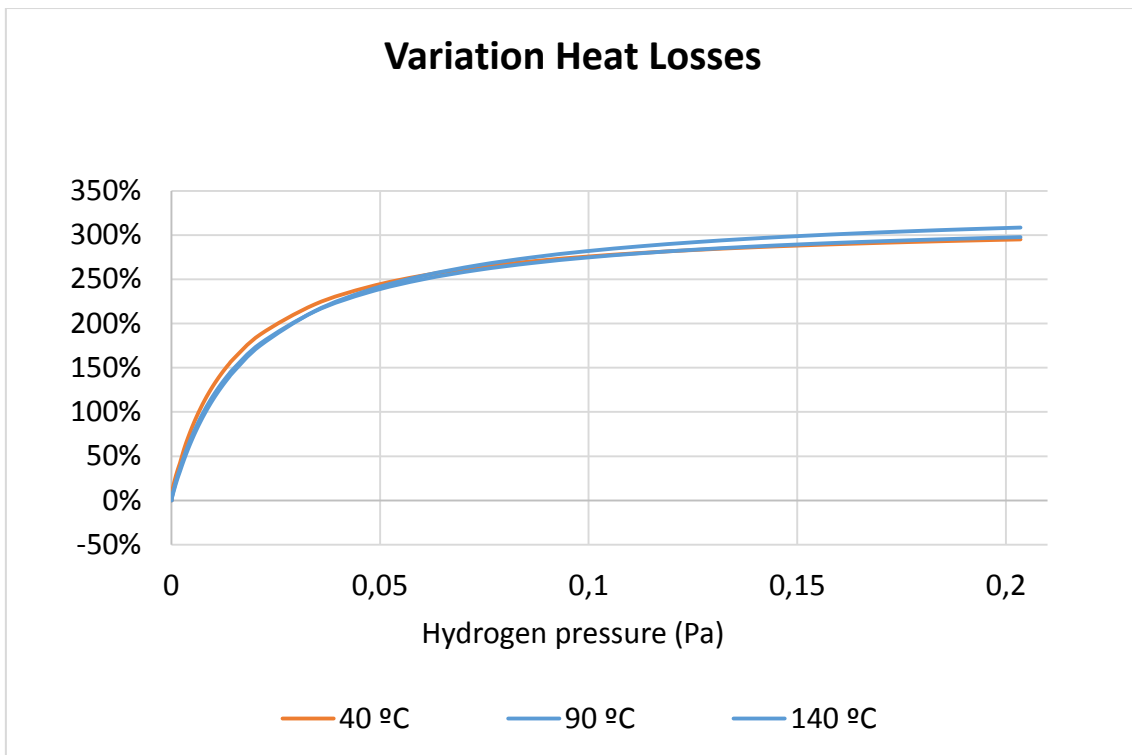
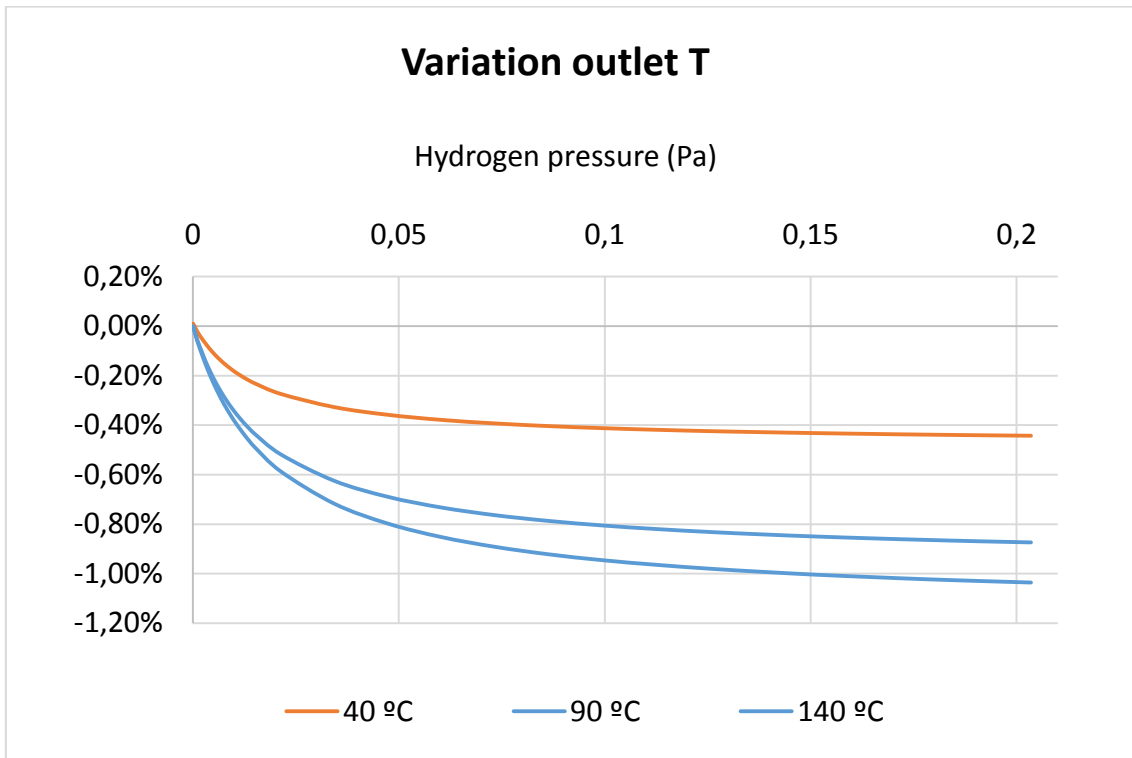


Figure-A 19. Graphs of the results for the heat losses test at 140°C expressed in percentages for different values of hydrogen's pressure.

- Comparing the three cases:



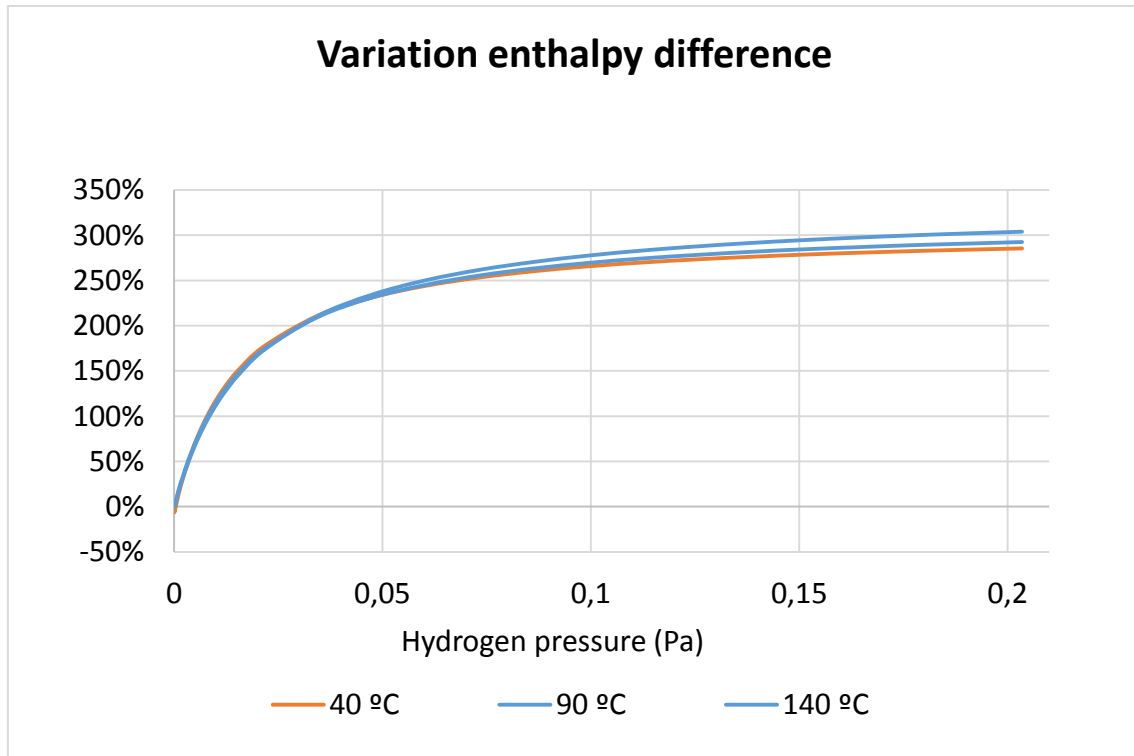
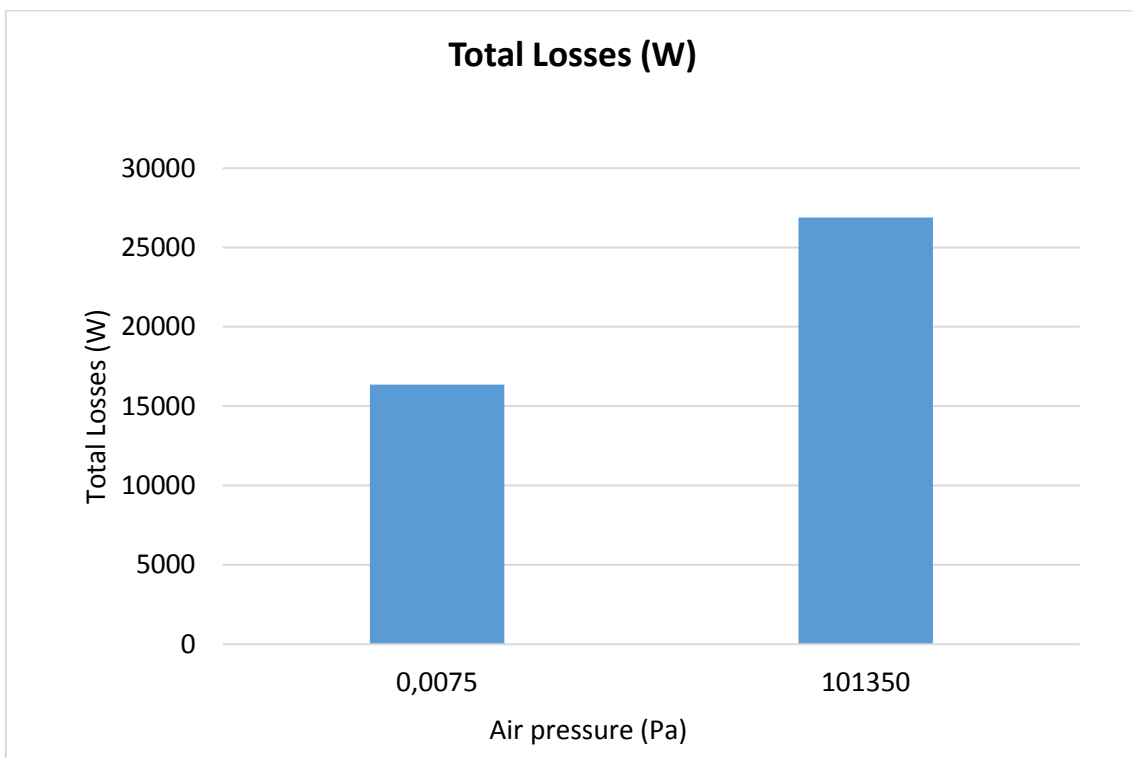
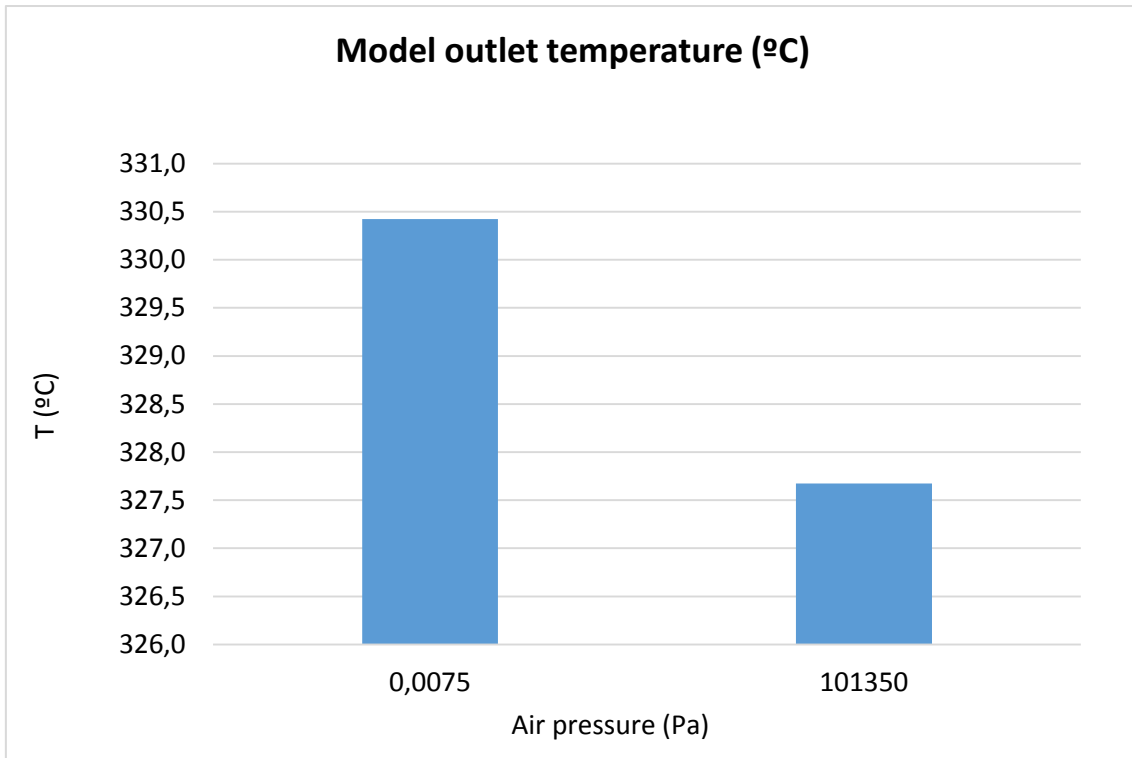


Figure-A 20. Graphs of the results for the heat losses test for the three cases expressed in percentages for different values of hydrogen's pressure.

Infiltration of air

Table A 22. Results of the dynamic efficiency test when air enters the gap between the glass cover and the absorber.

Test	Incidence angle (°)	Inlet Pressure (Pa)	Model Outlet temperature (°C)	Total Losses (W)	Energy (W)	Useful Solar Radiant Power (W)	Model efficiency (%)
1	16,37	0,0075	330,42	16357,62	273524,09	370869,74	73,75%
2	16,37	101350	327,67	26889,54	256697,12	370869,74	69,21%



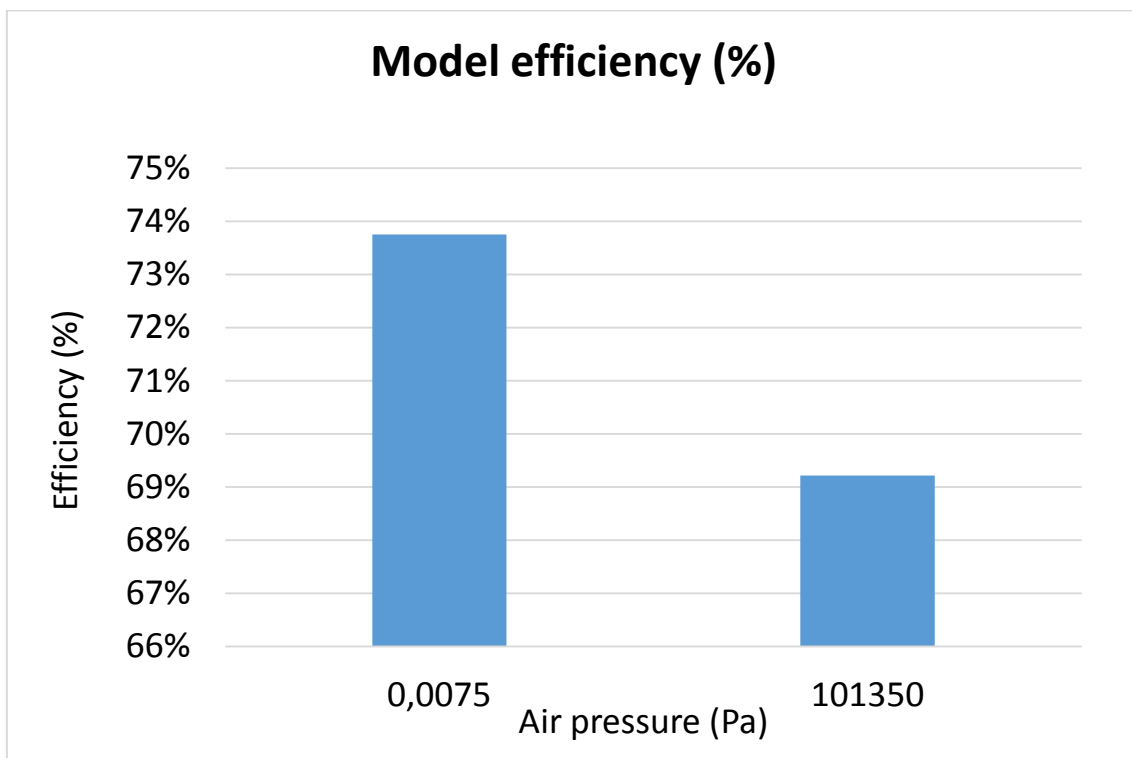
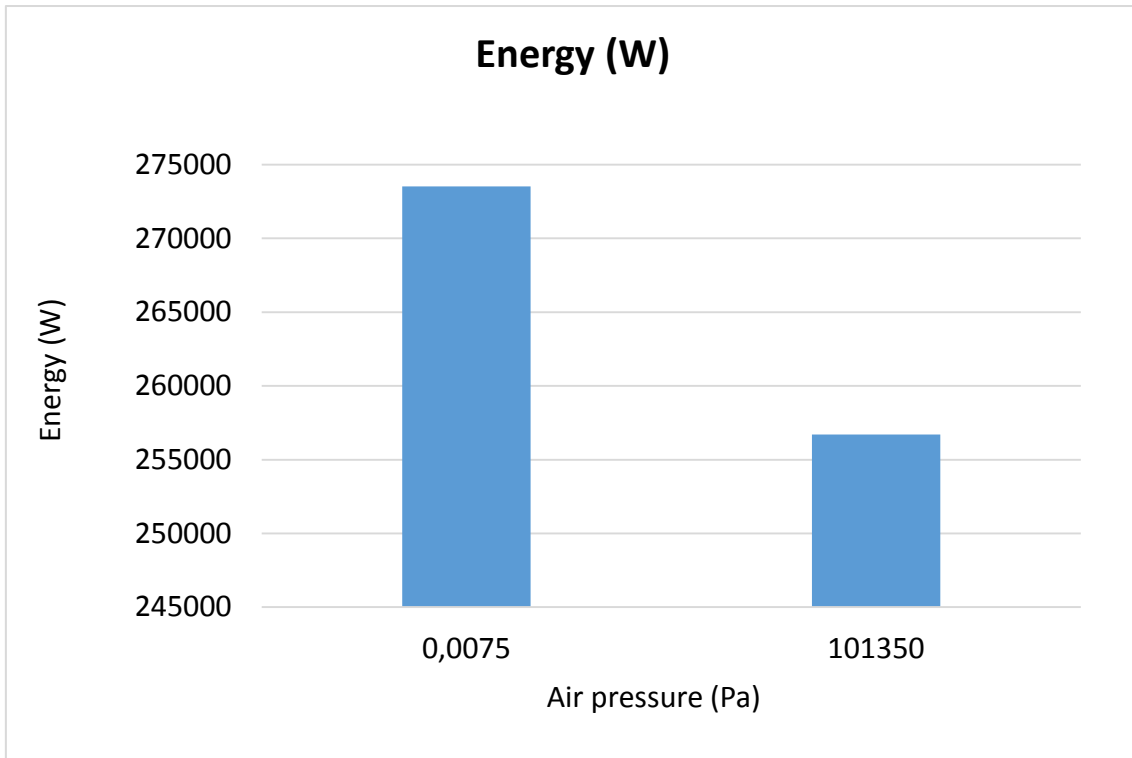


Figure-A 21. Graphs of the results of the dynamic efficiency test when air enters the space between the glass cover and the metal tube.

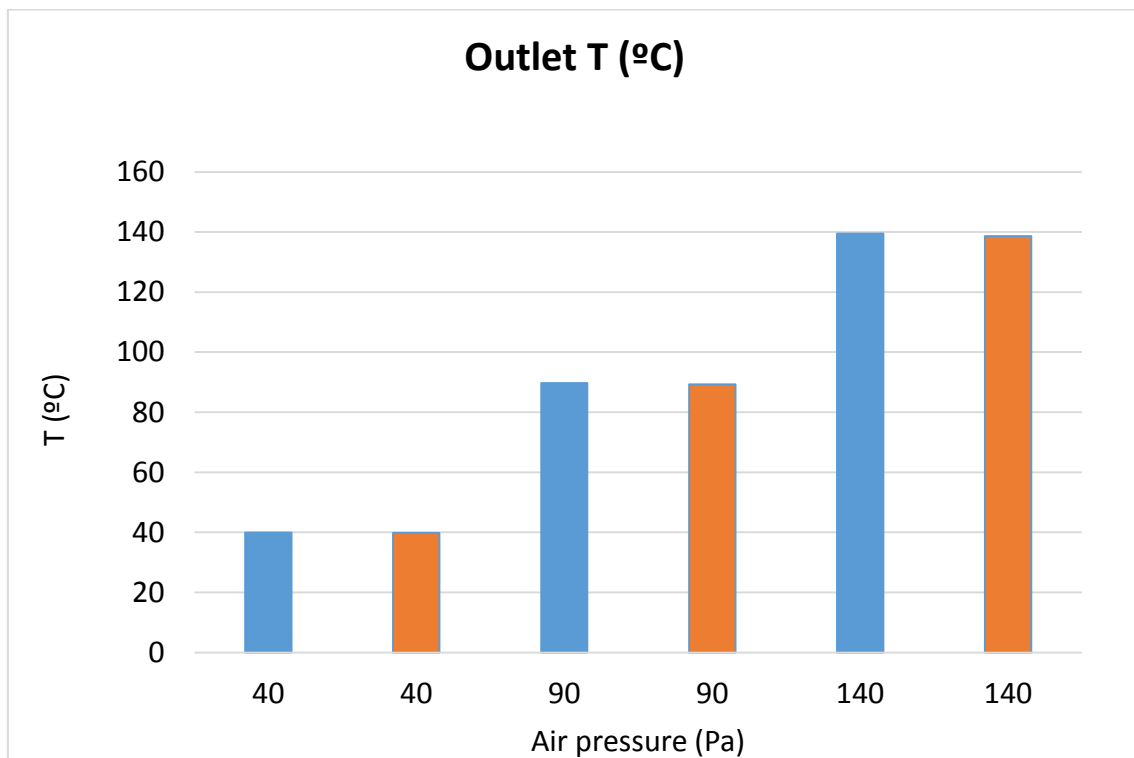
Below it is presented how the variation affects but expressed in percentages.

Table A 23. Results from the dynamic efficiency test when air enters the space between the glass cover and the metal tube expressed in percentages.

Inlet air pressure	Variation Outlet T	Variation Heat Losses	Variation Energy	Variation Efficiency
0,0075	0,00%	0,00%	0,00%	0,00%
101350	-0,83%	64,39%	-6,15%	-6,15%

Table A 24. Results from the heat losses test when air enters the space between the glass cover and the metal tube.

Test	Inlet T (°C)	Air partial pressure (Pa)	Outlet T (°C)	Total Losses (W)	Enthalpy difference (W)
1	40	0,0075	39,94	368,82	364,13
2	40	101350	39,84	917,45	913,19
3	90	0,0075	89,73	1638,78	1656,12
4	90	101350	89,28	4406,02	4424,68
5	140	0,0075	139,53	3041,97	3079,75
6	140	101350	138,67	8616,21	8652,63



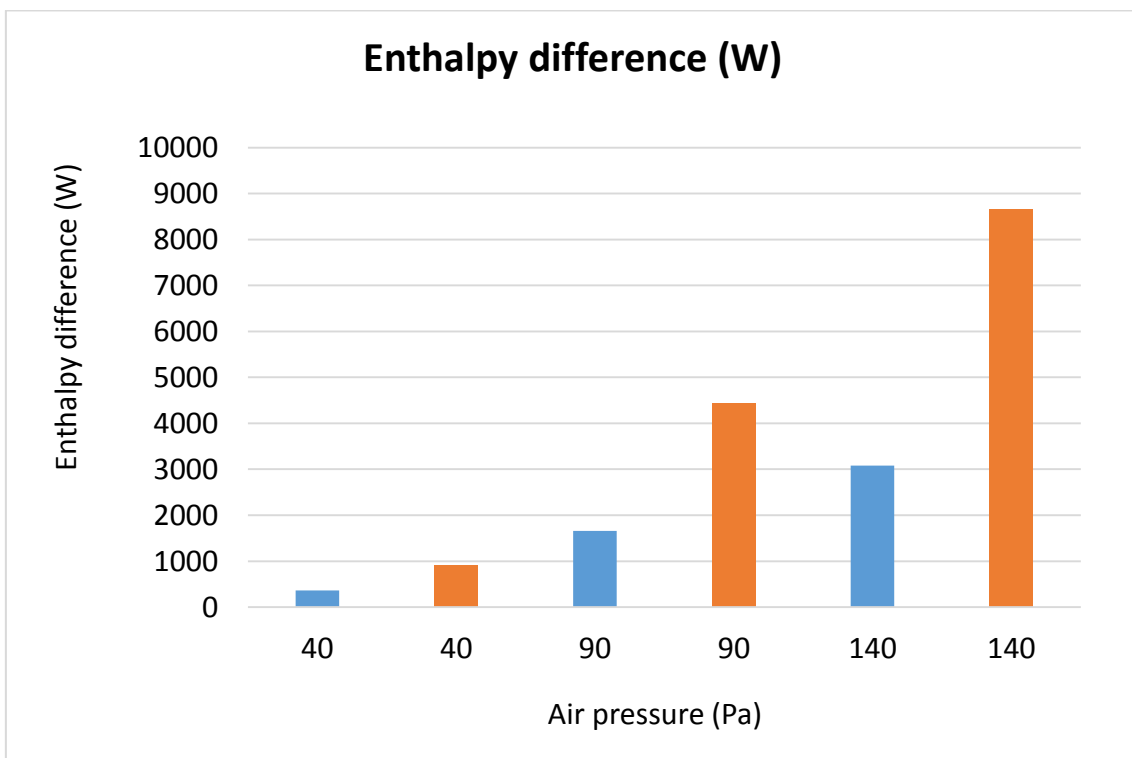
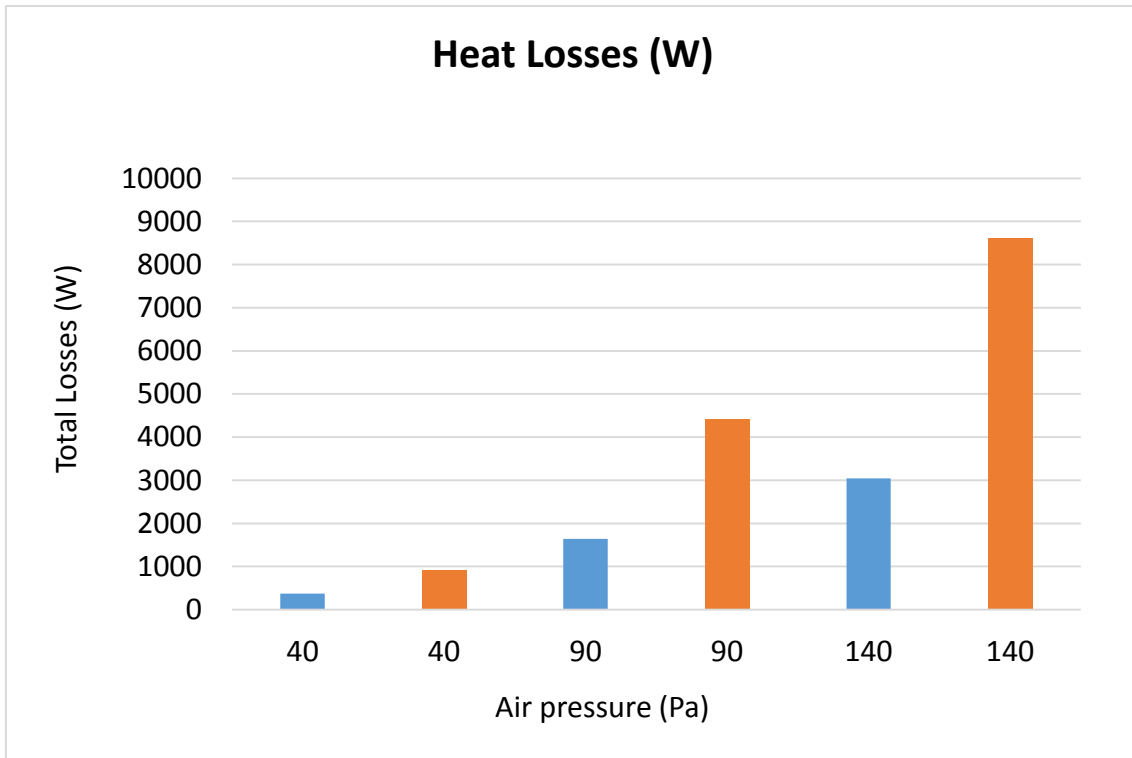


Figure-A 22. Graphs of the results of the heat losses test when air enters the space between the glass cover and the metal tube.

In percentages:

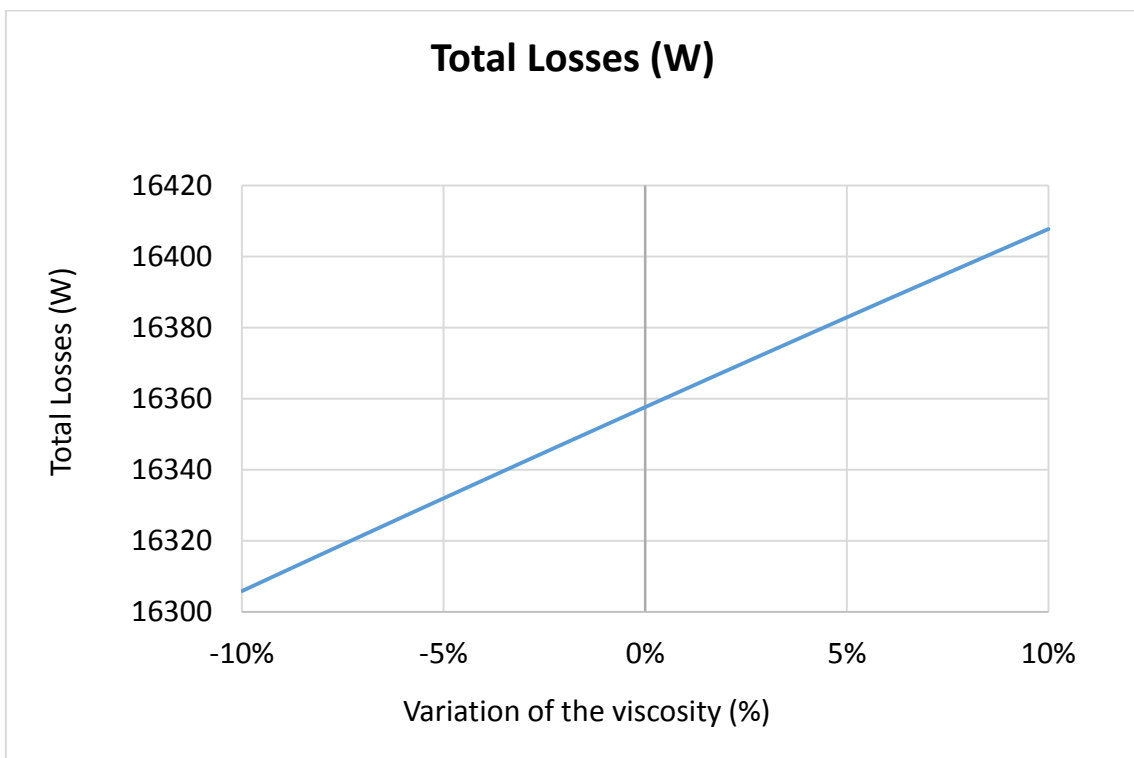
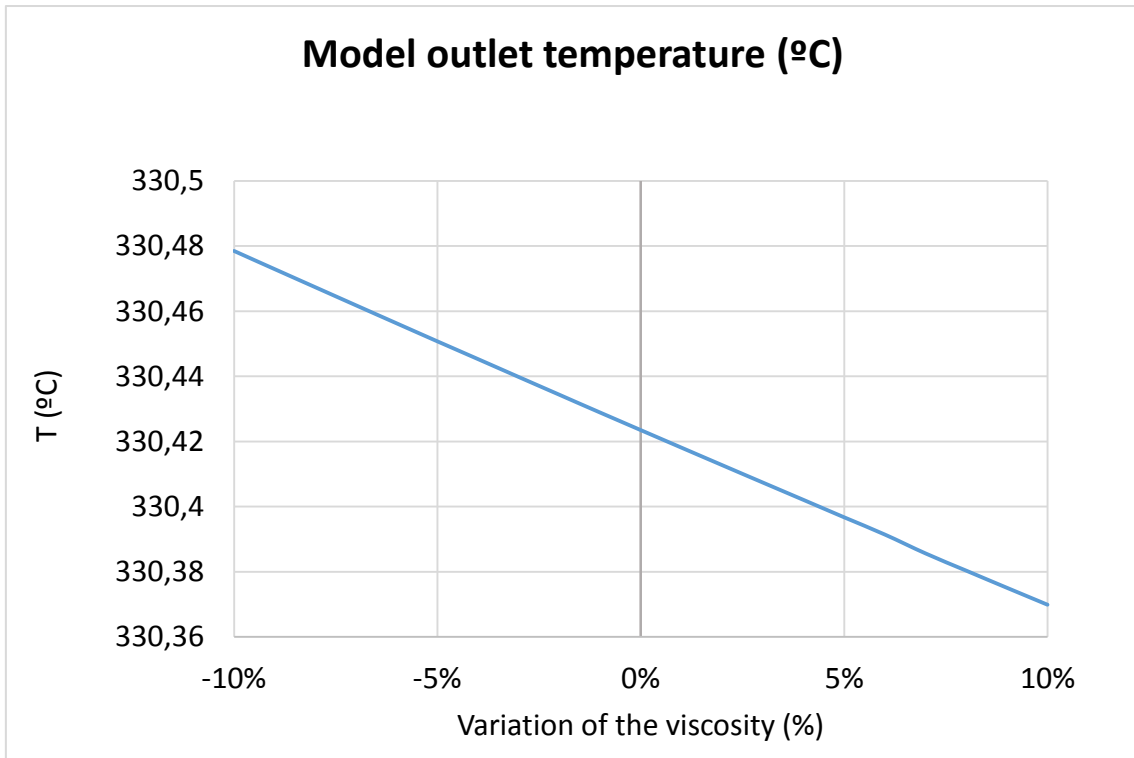
Table A 25. Results from the heat losses test when air enters the space between the glass cover and the metal tube.

Air pressure	Variation Outlet T	Variation Heat Losses	Variation Enthalpy difference
0,0075	0,00%	0,00%	0,00%
101350	-0,23%	148,75%	150,79%
0,0075	0,00%	0,00%	0,00%
101350	-0,50%	168,86%	167,17%
0,0075	0,00%	0,00%	0,00%
101350	-0,62%	183,24%	180,95%

Degradation of the HTF.

Table A 26. Results for the dynamic efficiency test when there is degradation of the HTF.

Test	Incidence angle (°)	Viscosity variation percentage (%)	Model Outlet temperature (°C)	Total Losses (W)	Energy (W)	Useful Solar Radiant Power (W)	Model efficiency (%)
1	16,37	0%	330,42	16357,62	273524,09	370869,74	73,75%
2	16,37	-10%	330,48	16305,85	273859,20	370869,74	73,84%
3	16,37	-9%	330,47	16311,10	273825,12	370869,74	73,83%
4	16,37	-8%	330,47	16316,34	273791,16	370869,74	73,82%
5	16,37	-7%	330,46	16321,56	273757,30	370869,74	73,81%
6	16,37	-6%	330,46	16326,77	273723,67	370869,74	73,81%
7	16,37	-5%	330,45	16331,95	273690,07	370869,74	73,80%
8	16,37	-4%	330,45	16337,12	273656,58	370869,74	73,79%
9	16,37	-3%	330,44	16342,27	273623,28	370869,74	73,78%
10	16,37	-2%	330,43	16347,40	273590,12	370869,74	73,77%
11	16,37	-1%	330,43	16352,52	273557,08	370869,74	73,76%
12	16,37	1%	330,42	16362,70	273491,26	370869,74	73,74%
13	16,37	2%	330,41	16367,77	273458,53	370869,74	73,73%
14	16,37	3%	330,41	16372,82	273425,93	370869,74	73,73%
15	16,37	4%	330,40	16377,85	273393,43	370869,74	73,72%
16	16,37	5%	330,40	16382,87	273361,09	370869,74	73,71%
17	16,37	6%	330,39	16387,88	273328,75	370869,74	73,70%
18	16,37	7%	330,39	16392,84	273293,31	370869,74	73,69%
19	16,37	8%	330,38	16397,82	273261,24	370869,74	73,68%
20	16,37	9%	330,38	16402,77	273229,20	370869,74	73,67%
21	16,37	10%	330,37	16407,72	273197,39	370869,74	73,66%



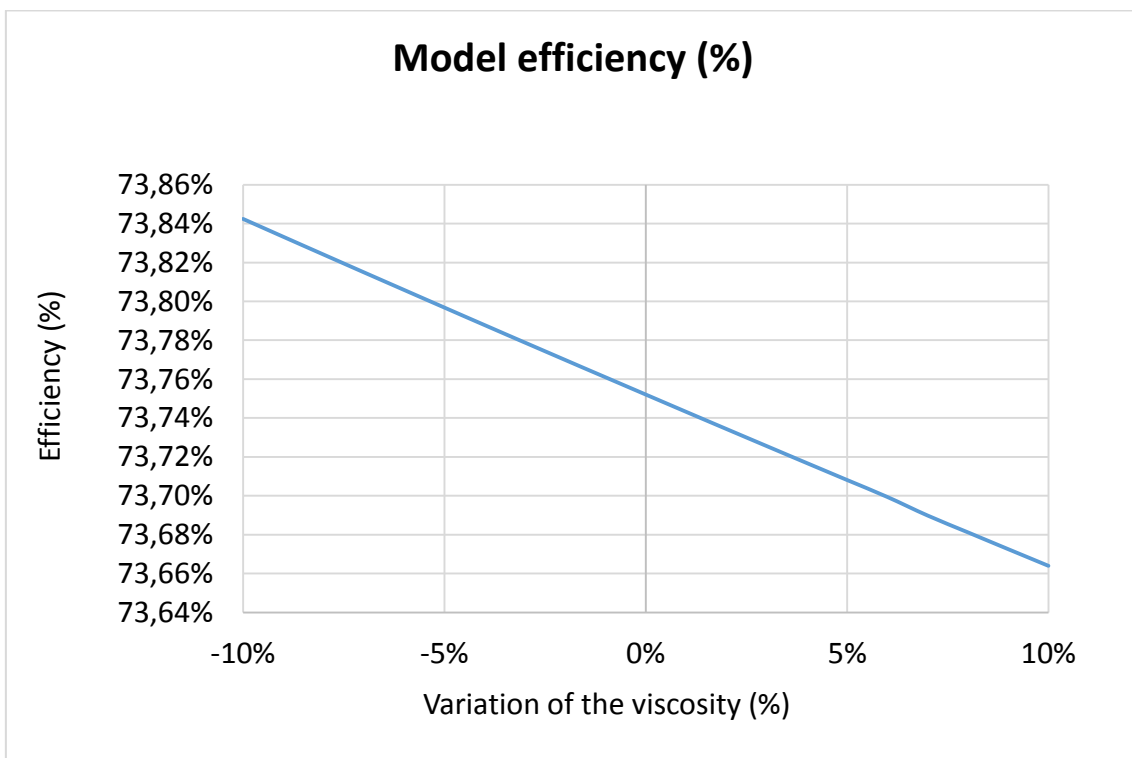
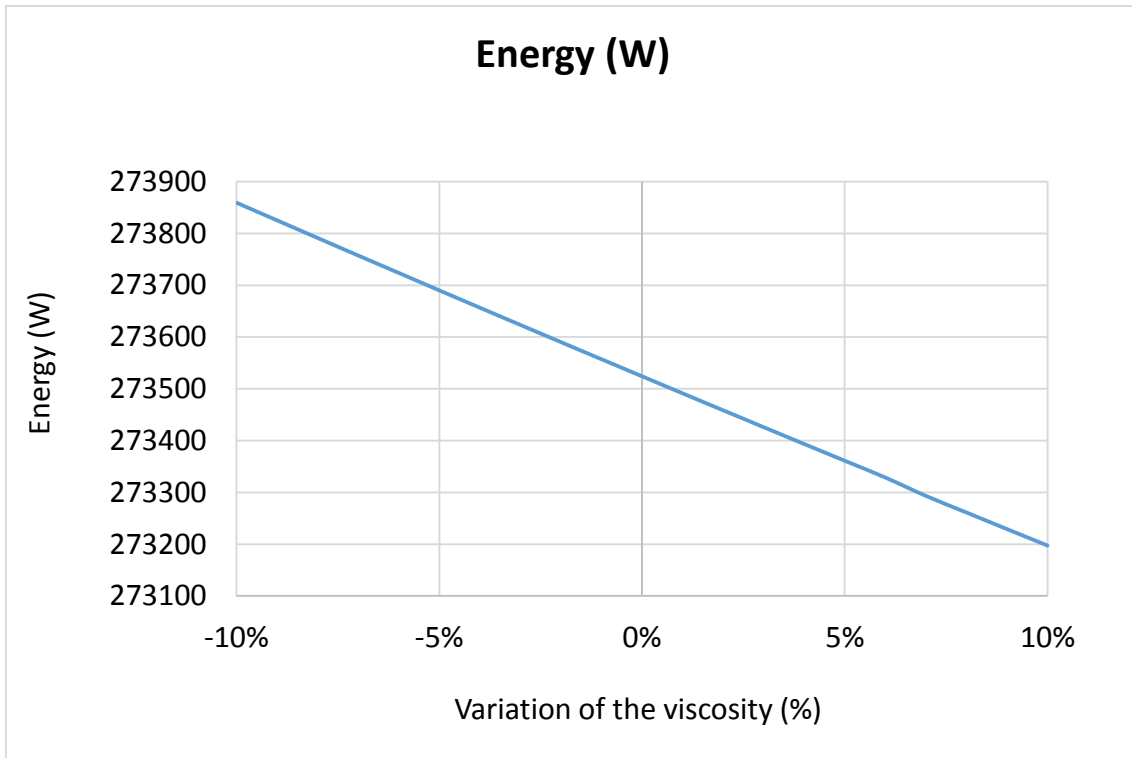
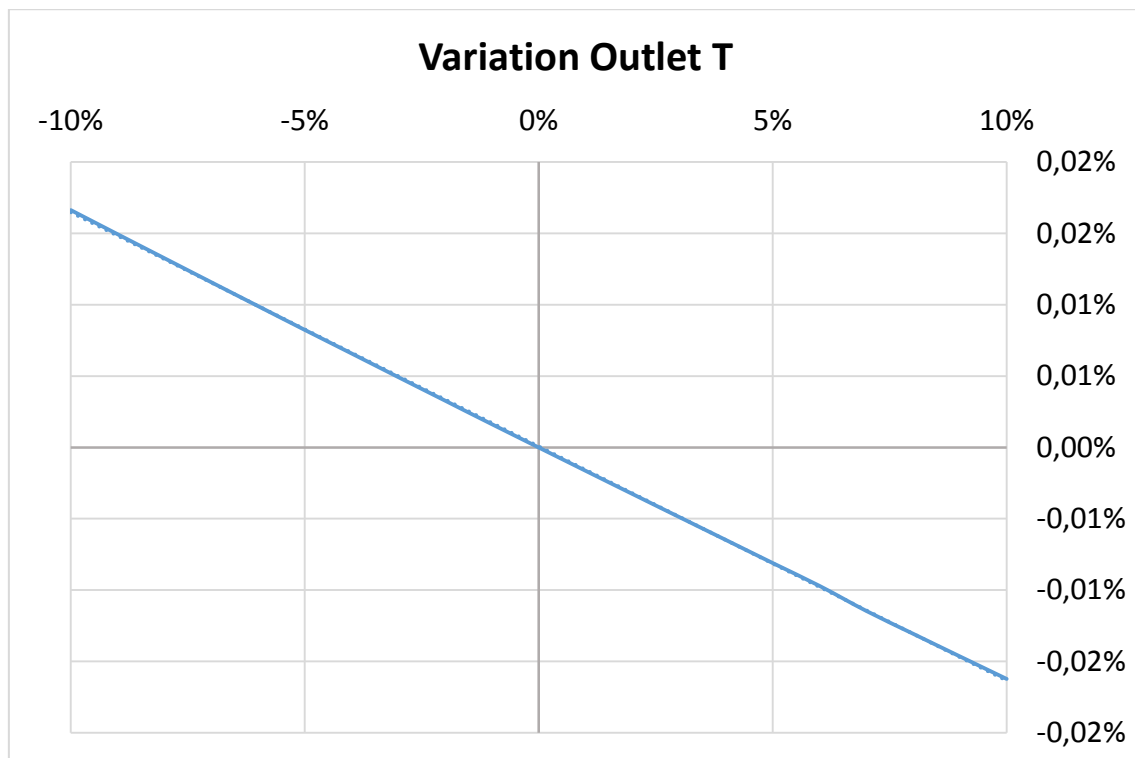


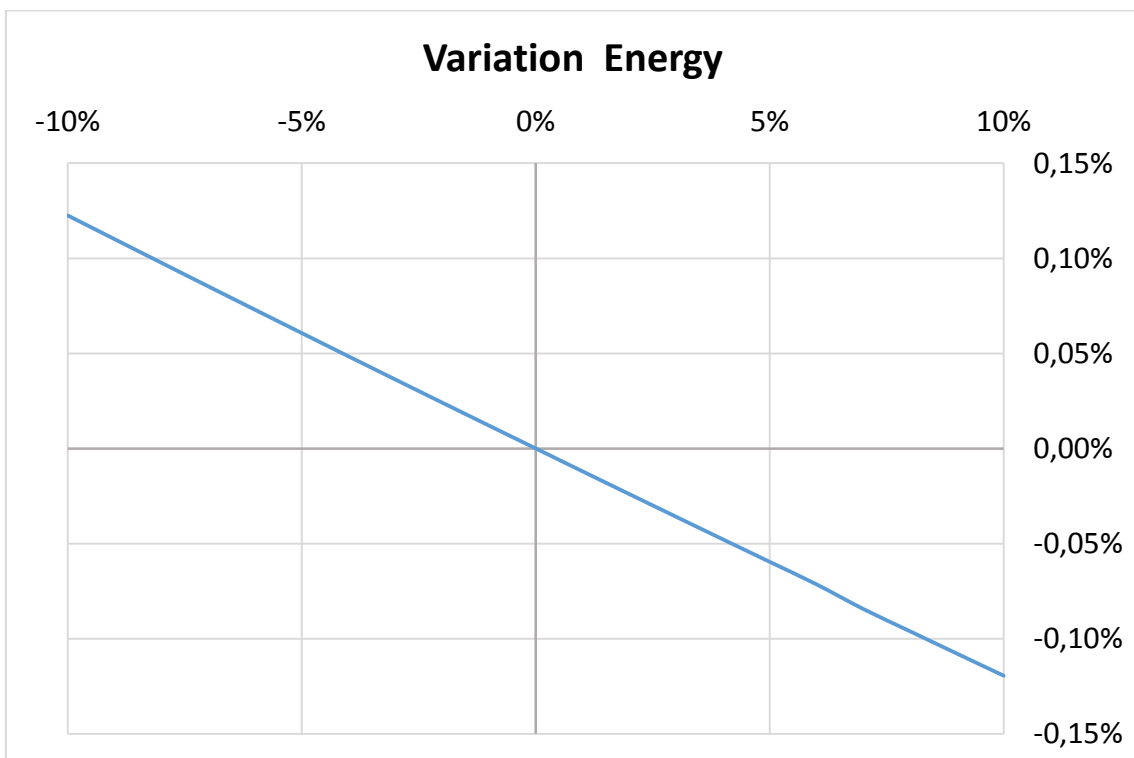
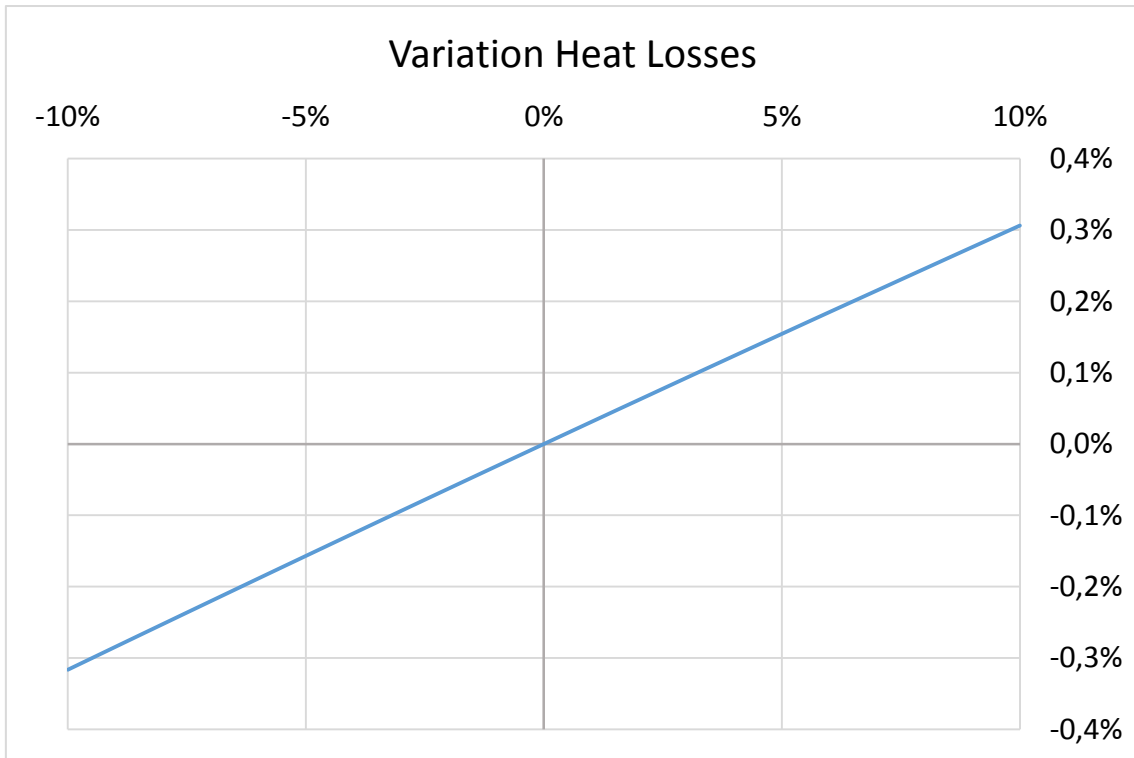
Figure-A 23. Graphs of the results for the dynamic efficiency test when there is degradation of the HTF.

Below it is presented how the variation affects but expressed in percentages.

Table A 27. Results from the dynamic efficiency test expressed in percentages when the HTF degrades.

Variation cinematic viscosity	Variation Outlet T	Variation Heat Losses	Variation Energy	Variation Efficiency
0,00%	0,00%	0,00%	0,00%	0,00%
-10,00%	0,02%	-0,32%	0,12%	0,12%
-9,00%	0,01%	-0,28%	0,11%	0,11%
-8,00%	0,01%	-0,25%	0,10%	0,10%
-7,00%	0,01%	-0,22%	0,09%	0,09%
-6,00%	0,01%	-0,19%	0,07%	0,07%
-5,00%	0,01%	-0,16%	0,06%	0,06%
-4,00%	0,01%	-0,13%	0,05%	0,05%
-3,00%	0,00%	-0,09%	0,04%	0,04%
-2,00%	0,00%	-0,06%	0,02%	0,02%
-1,00%	0,00%	-0,03%	0,01%	0,01%
1,00%	0,00%	0,03%	-0,01%	-0,01%
2,00%	0,00%	0,06%	-0,02%	-0,02%
3,00%	0,00%	0,09%	-0,04%	-0,04%
4,00%	-0,01%	0,12%	-0,05%	-0,05%
5,00%	-0,01%	0,15%	-0,06%	-0,06%
6,00%	-0,01%	0,18%	-0,07%	-0,07%
7,00%	-0,01%	0,22%	-0,08%	-0,08%
8,00%	-0,01%	0,25%	-0,10%	-0,10%
9,00%	-0,01%	0,28%	-0,11%	-0,11%
10,00%	-0,02%	0,31%	-0,12%	-0,12%





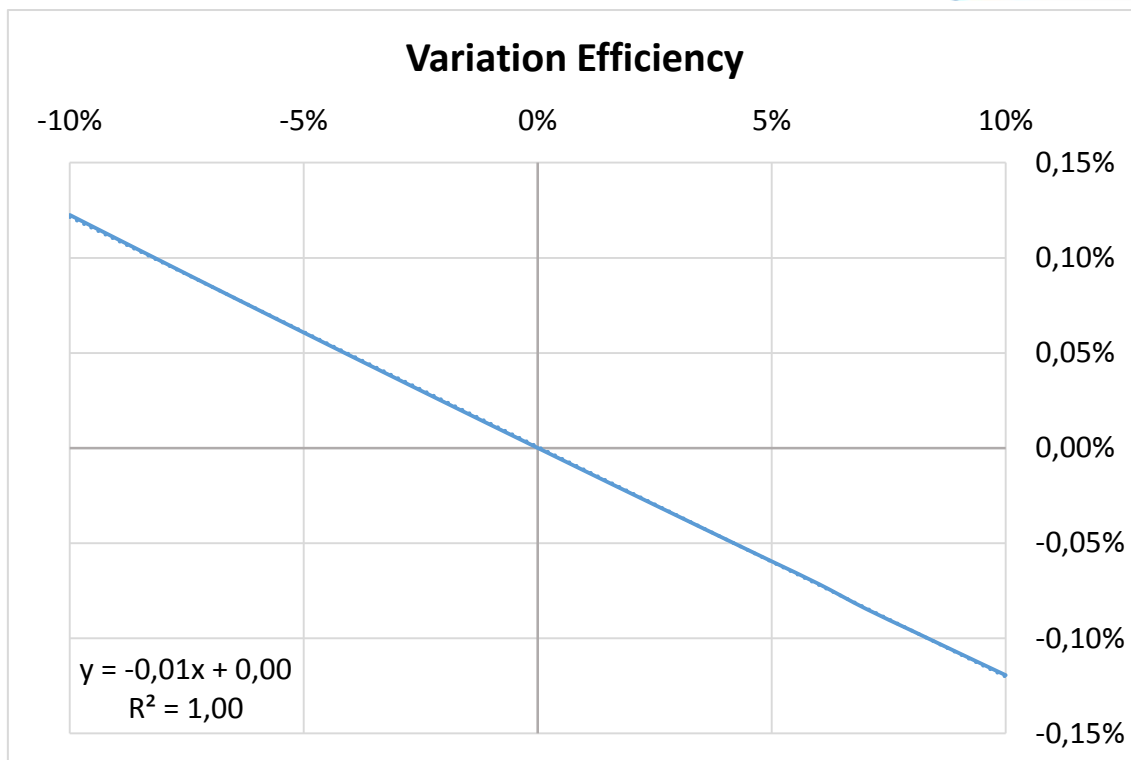


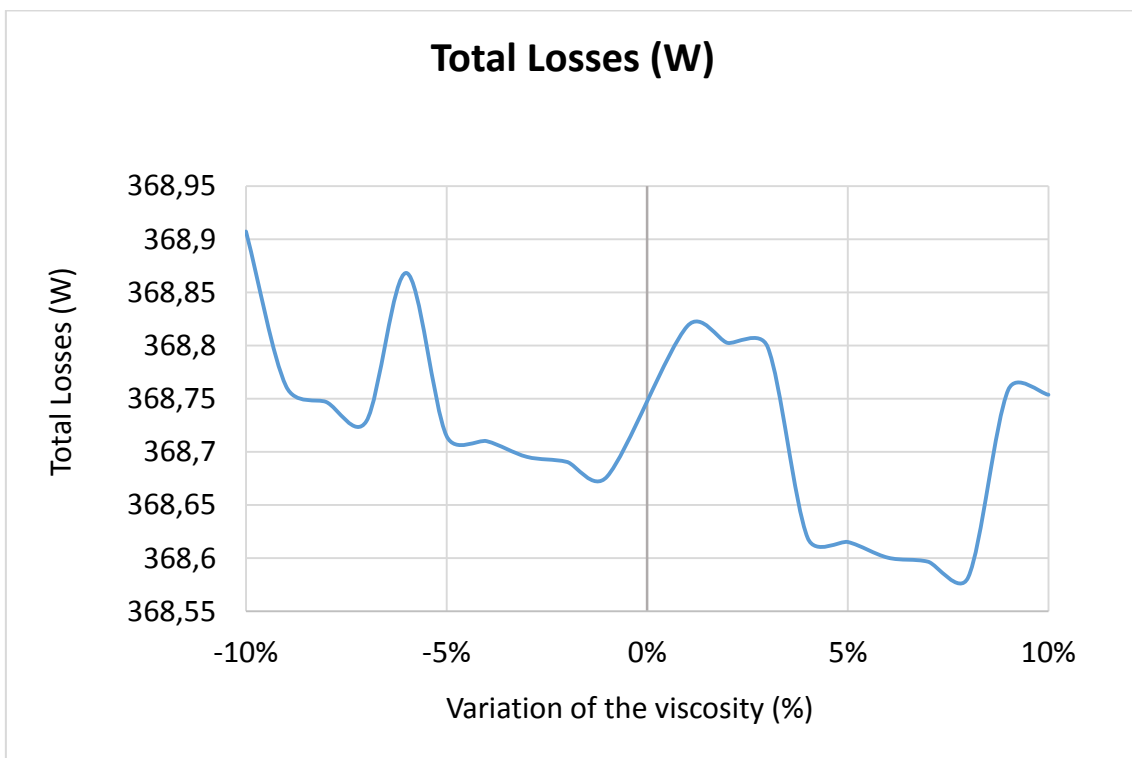
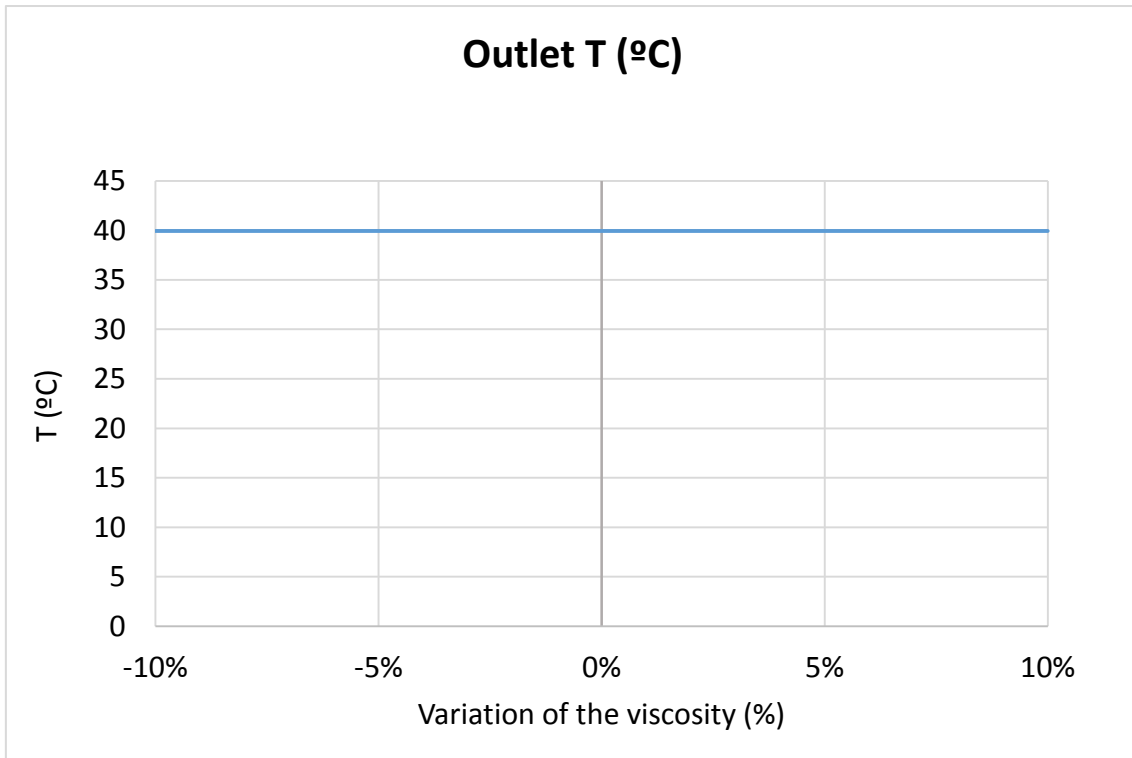
Figure-A 24. Graphs of the results for the dynamic efficiency test expressed in percentages when the HTF degrades.

**

- When the HTF's inlet temperature is 40°C:

Table A 28. Results from the heat losses test at 40°C when HTF degrades.

Test	Inlet T	Viscosity variation percentage (%)	Outlet T (°C)	Total Losses (W)	Enthalpy difference (W)
1	40	0%	39,94	368,82	364,13
2	40	-10%	39,94	368,91	364,13
3	40	-9%	39,94	368,76	364,49
4	40	-8%	39,94	368,75	364,49
5	40	-7%	39,94	368,73	364,13
6	40	-6%	39,94	368,87	364,13
7	40	-5%	39,94	368,71	364,49
8	40	-4%	39,94	368,71	364,49
9	40	-3%	39,94	368,70	364,49
10	40	-2%	39,94	368,69	364,49
11	40	-1%	39,94	368,68	364,49
12	40	1%	39,94	368,82	364,13
13	40	2%	39,94	368,80	364,13
14	40	3%	39,94	368,80	364,13
15	40	4%	39,94	368,62	364,49
16	40	5%	39,94	368,62	364,49
17	40	6%	39,94	368,60	364,49
18	40	7%	39,94	368,60	364,49
19	40	8%	39,94	368,58	364,49
20	40	9%	39,94	368,76	364,13
21	40	10%	39,94	368,75	364,13



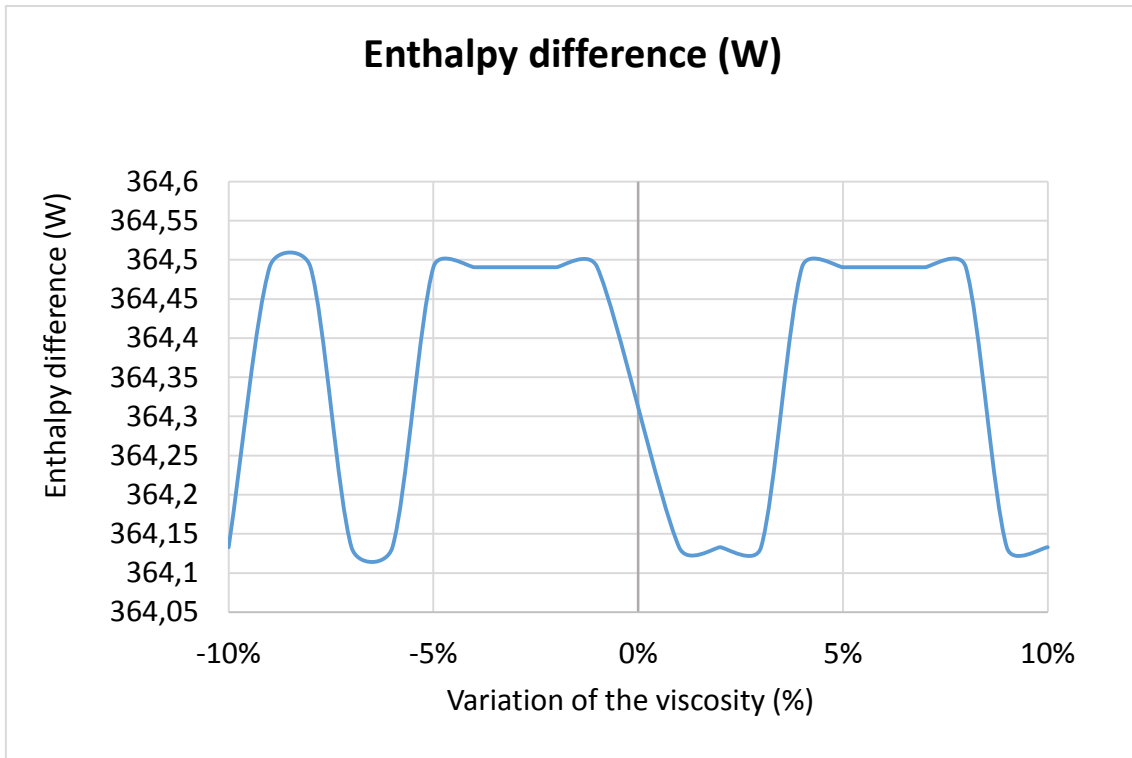
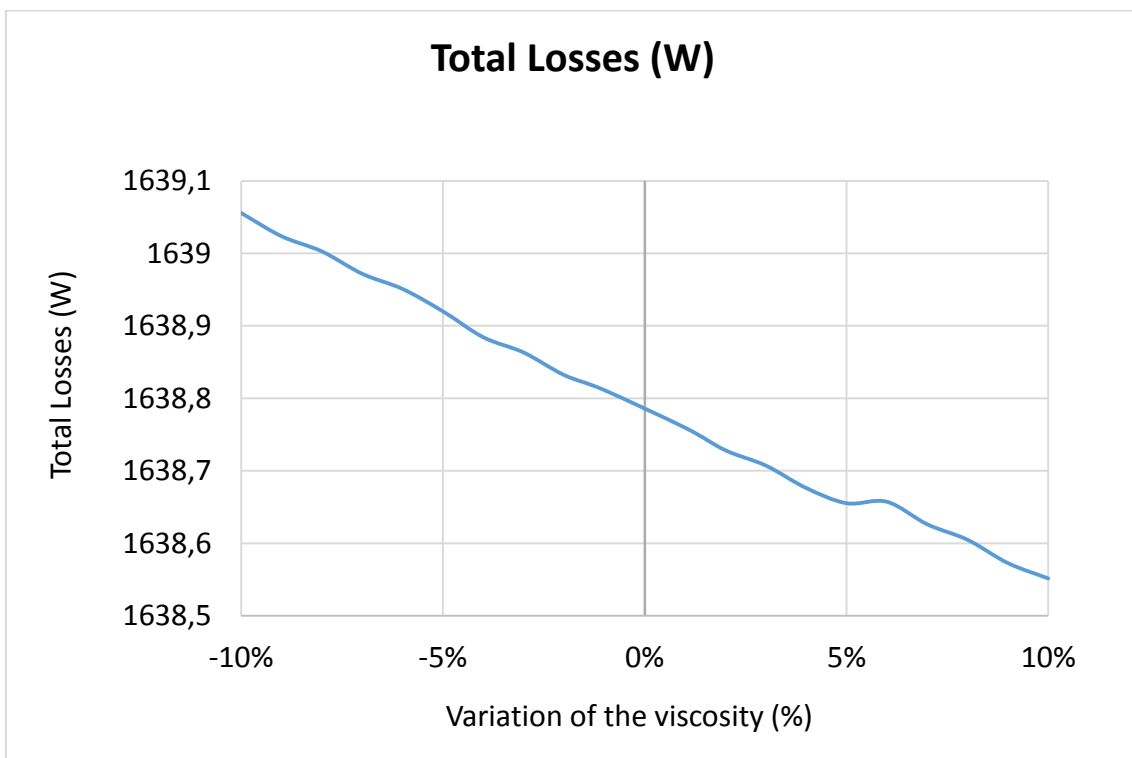
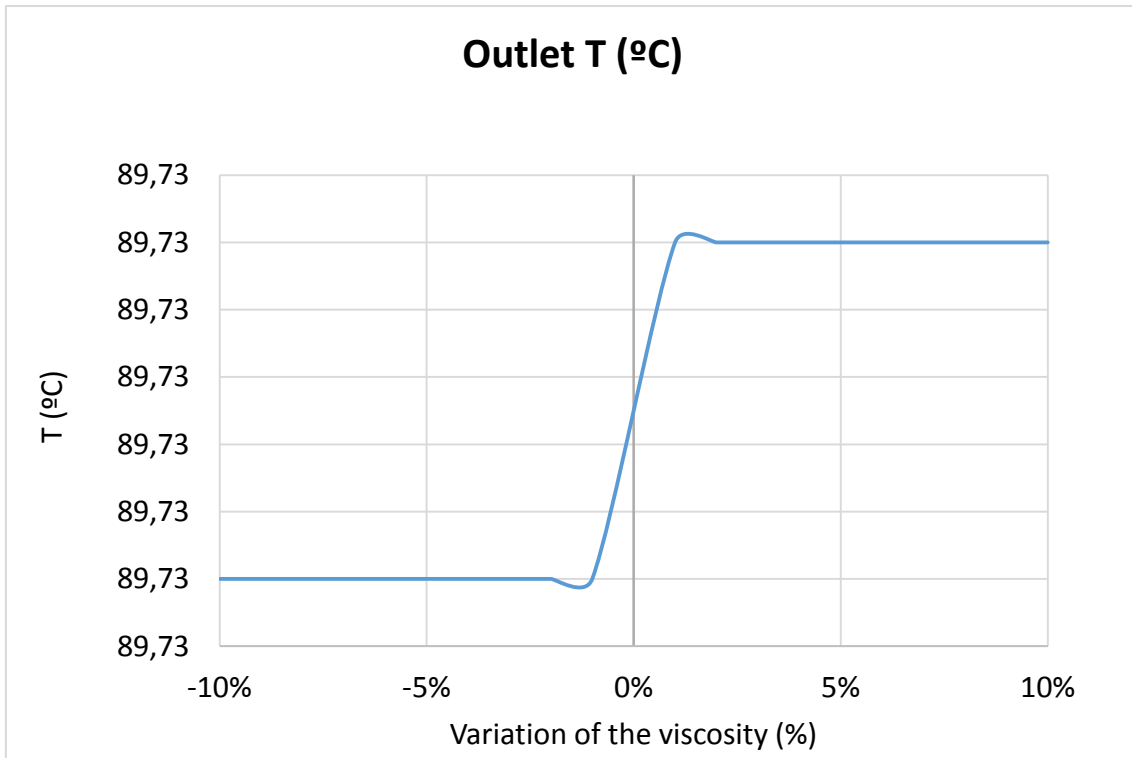


Figure-A 25. Graphs of the results for the heat losses test at 40°C when the HTF degrades.

- When the HTF's inlet temperature is 90°C:

Table A 29. Results from the heat losses test at 90°C when HTF degrades.

Test	Inlet T (°C)	Viscosity variation percentage (%)	Outlet T (°C)	Total Losses (W)	Enthalpy difference (W)
1	90	0%	89,73	1638,78	1656,12
2	90	-10%	89,73	1639,06	1656,12
3	90	-9%	89,73	1639,02	1656,12
4	90	-8%	89,73	1639,00	1656,12
5	90	-7%	89,73	1638,97	1656,12
6	90	-6%	89,73	1638,95	1656,12
7	90	-5%	89,73	1638,92	1656,12
8	90	-4%	89,73	1638,88	1656,12
9	90	-3%	89,73	1638,86	1656,12
10	90	-2%	89,73	1638,83	1656,12
11	90	-1%	89,73	1638,81	1656,12
12	90	1%	89,73	1638,76	1656,12
13	90	2%	89,73	1638,73	1656,12
14	90	3%	89,73	1638,71	1656,12
15	90	4%	89,73	1638,68	1656,12
16	90	5%	89,73	1638,66	1656,12
17	90	6%	89,73	1638,66	1656,12
18	90	7%	89,73	1638,63	1656,12
19	90	8%	89,73	1638,60	1656,12
20	90	9%	89,73	1638,57	1656,12
21	90	10%	89,73	1638,55	1656,12



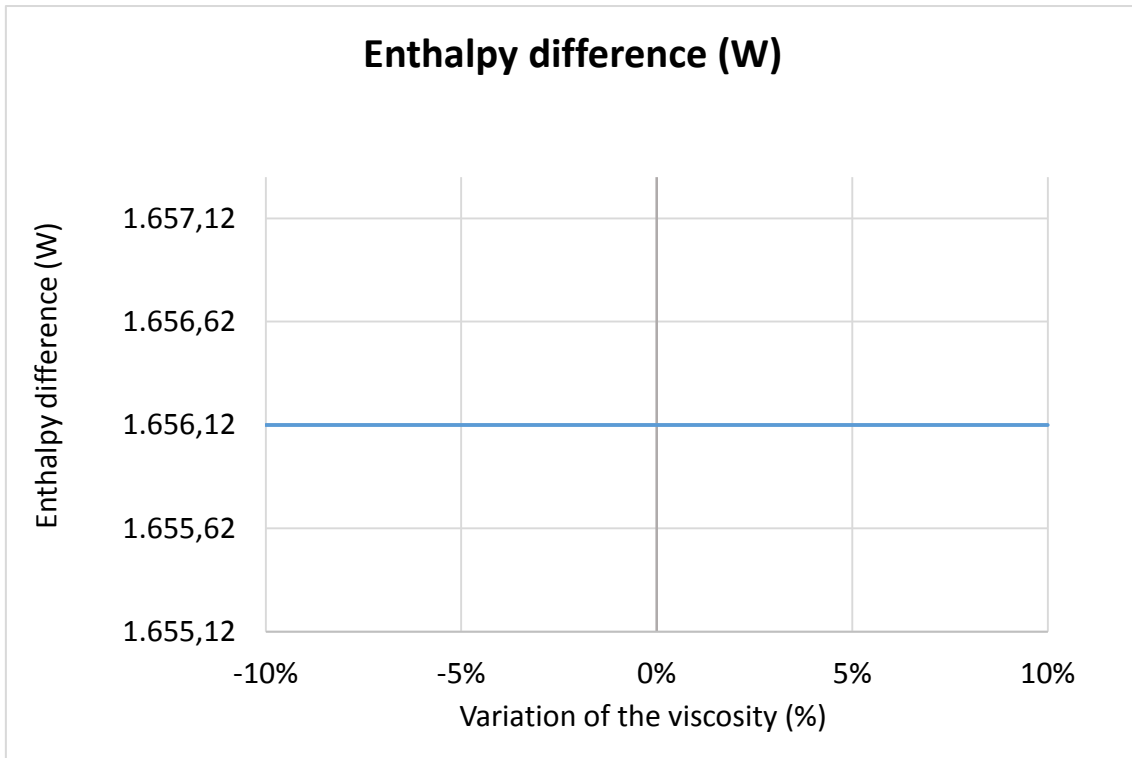
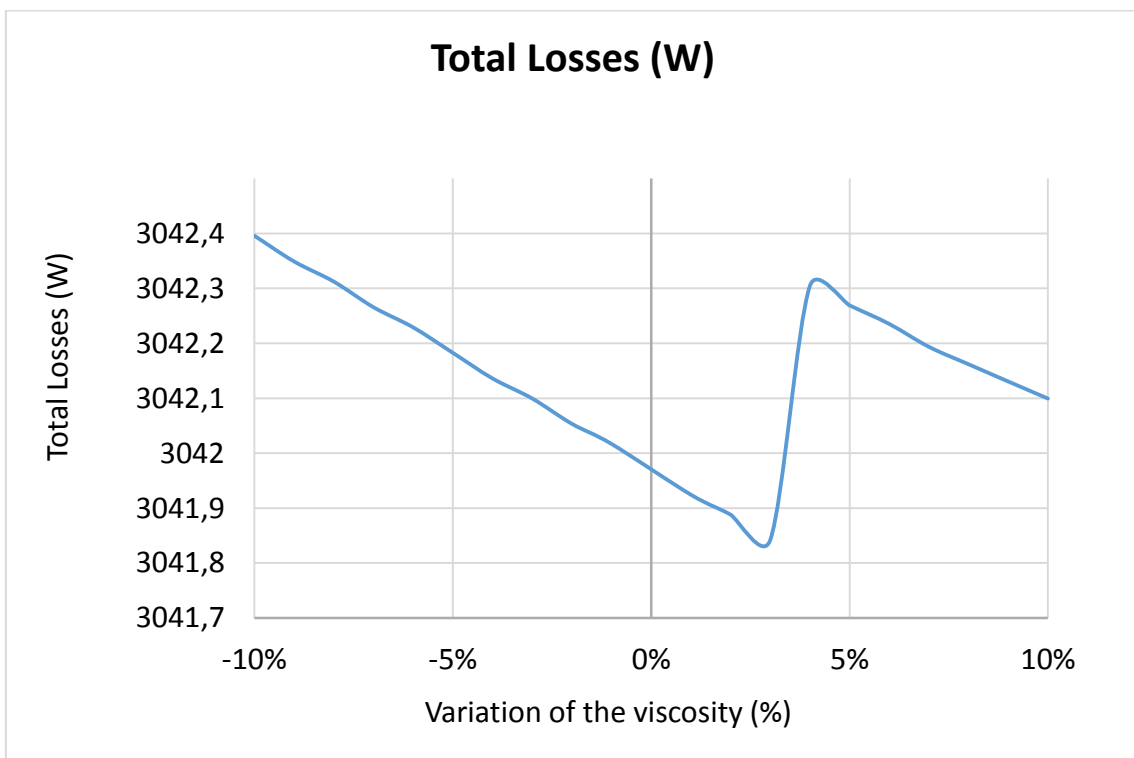
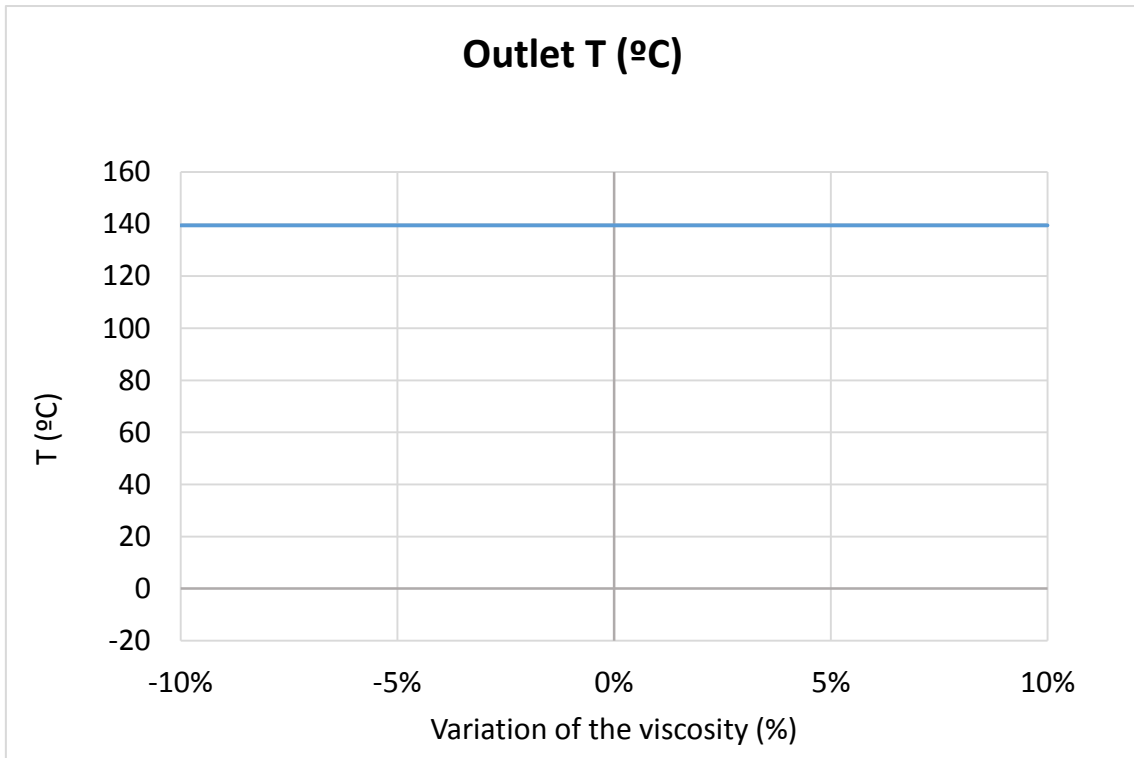


Figure-A 26. Graphs of the results for the heat losses test at 90°C when the HTF degrades.

- When the HTF's inlet temperature is 140°C:

Table A 30. Results from the heat losses test at 140°C when HTF degrades.

Test	Inlet T (°C)	Viscosity variation percentage (%)	Outlet T (°C)	Total Losses (W)	Enthalpy difference (W)
1	140	0%	139,53	3041,97	3079,75
2	140	-10%	139,53	3042,40	3079,75
3	140	-9%	139,53	3042,35	3079,75
4	140	-8%	139,53	3042,31	3079,75
5	140	-7%	139,53	3042,27	3079,75
6	140	-6%	139,53	3042,23	3079,75
7	140	-5%	139,53	3042,18	3079,75
8	140	-4%	139,53	3042,14	3079,75
9	140	-3%	139,53	3042,10	3079,75
10	140	-2%	139,53	3042,05	3079,75
11	140	-1%	139,53	3042,02	3079,75
12	140	1%	139,53	3041,92	3079,75
13	140	2%	139,53	3041,89	3079,75
14	140	3%	139,53	3041,84	3079,75
15	140	4%	139,53	3042,30	3079,75
16	140	5%	139,53	3042,27	3079,75
17	140	6%	139,53	3042,24	3079,75
18	140	7%	139,53	3042,19	3079,75
19	140	8%	139,53	3042,16	3079,75
20	140	9%	139,53	3042,13	3079,75
21	140	10%	139,53	3042,10	3079,75



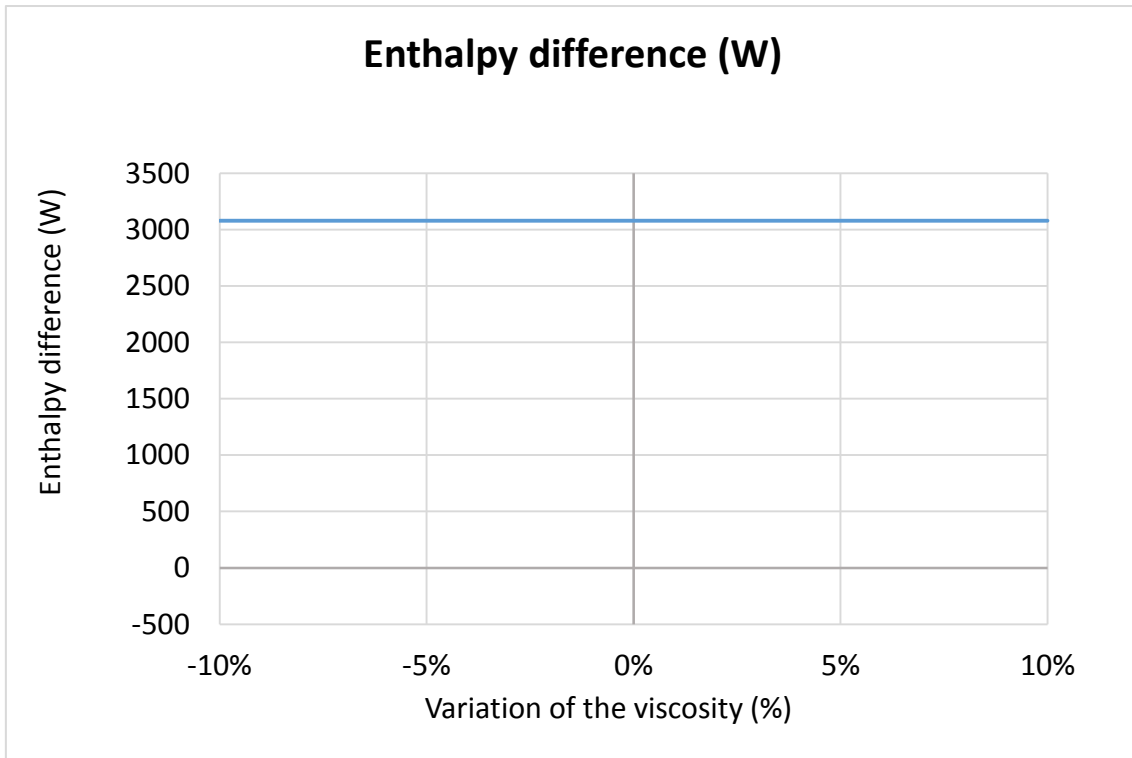
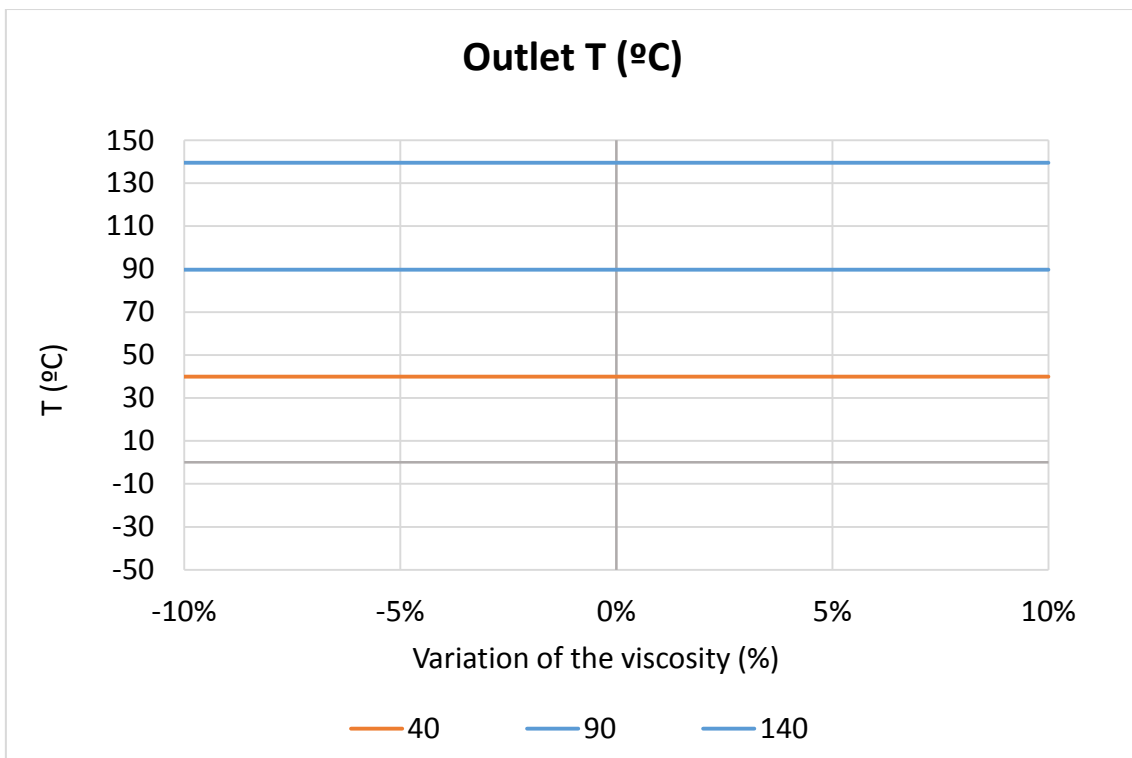


Figure-A 27. Graphs of the results for the heat losses test at 140°C when the HTF degrades.

- Comparing the three cases:



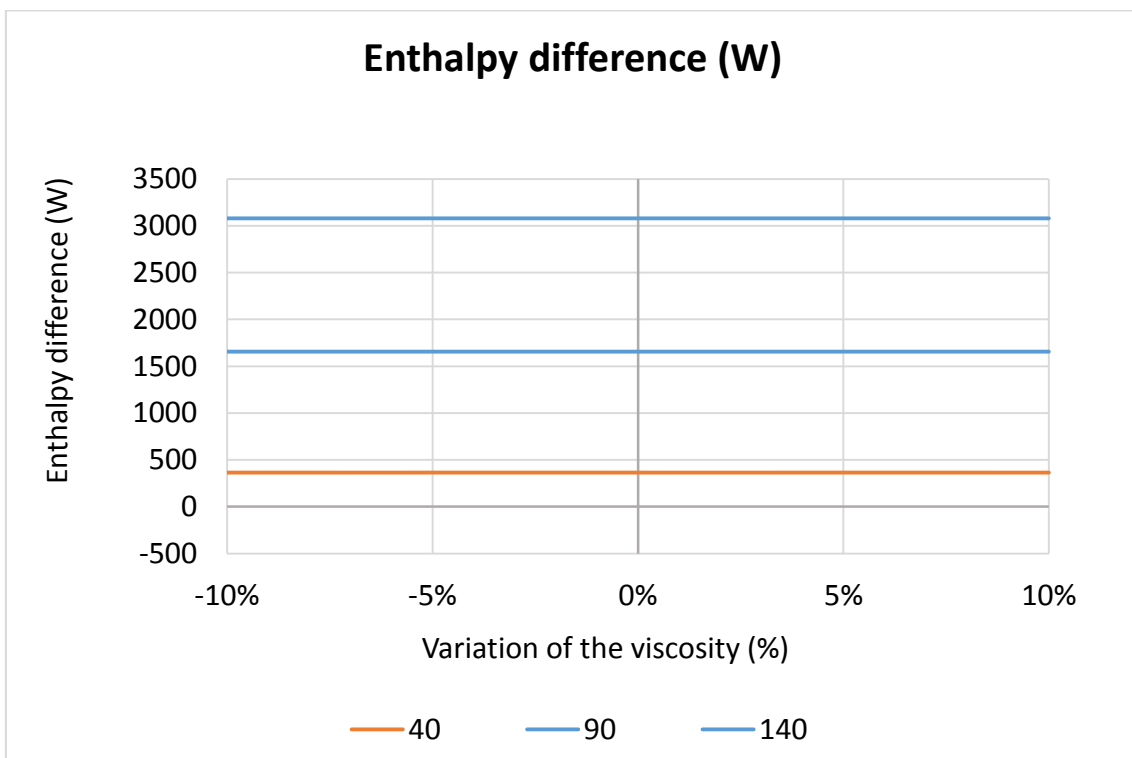
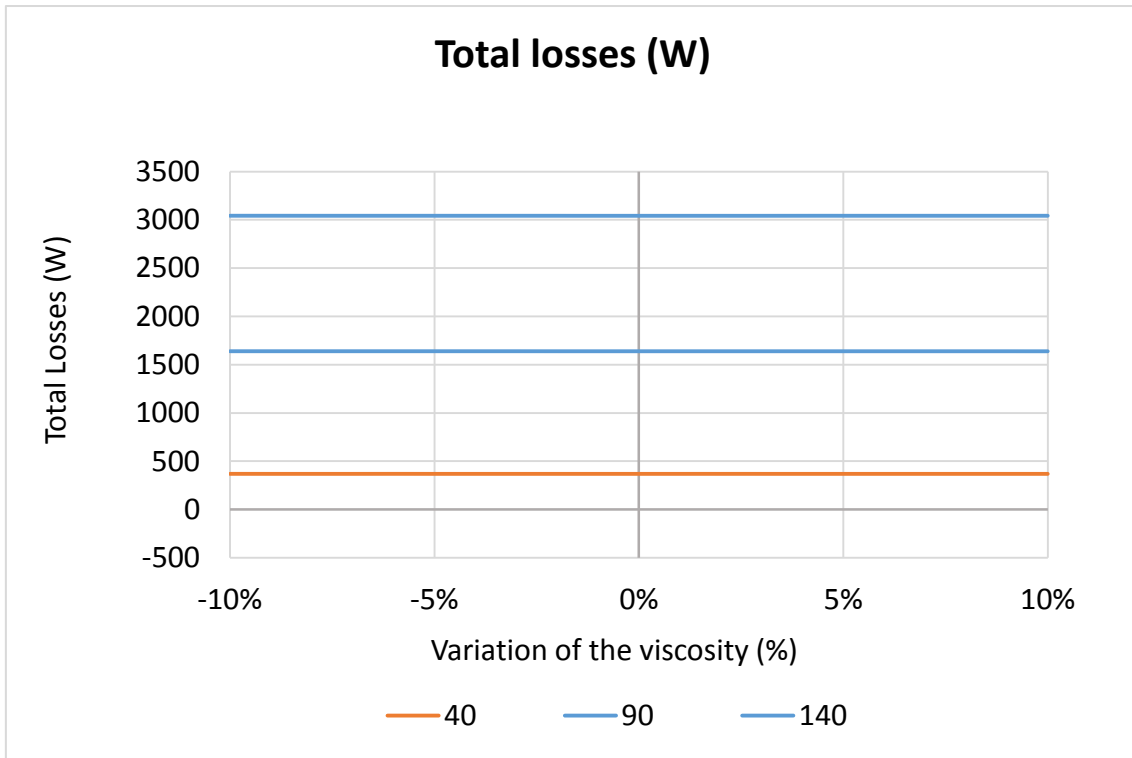
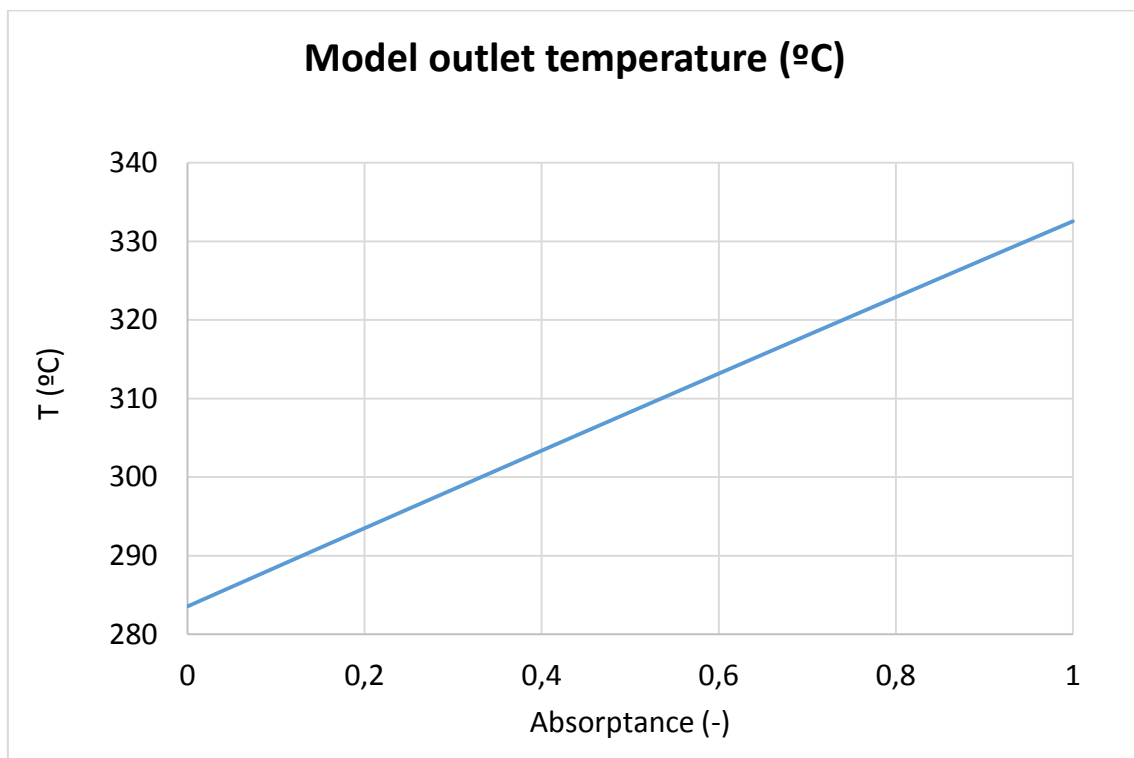


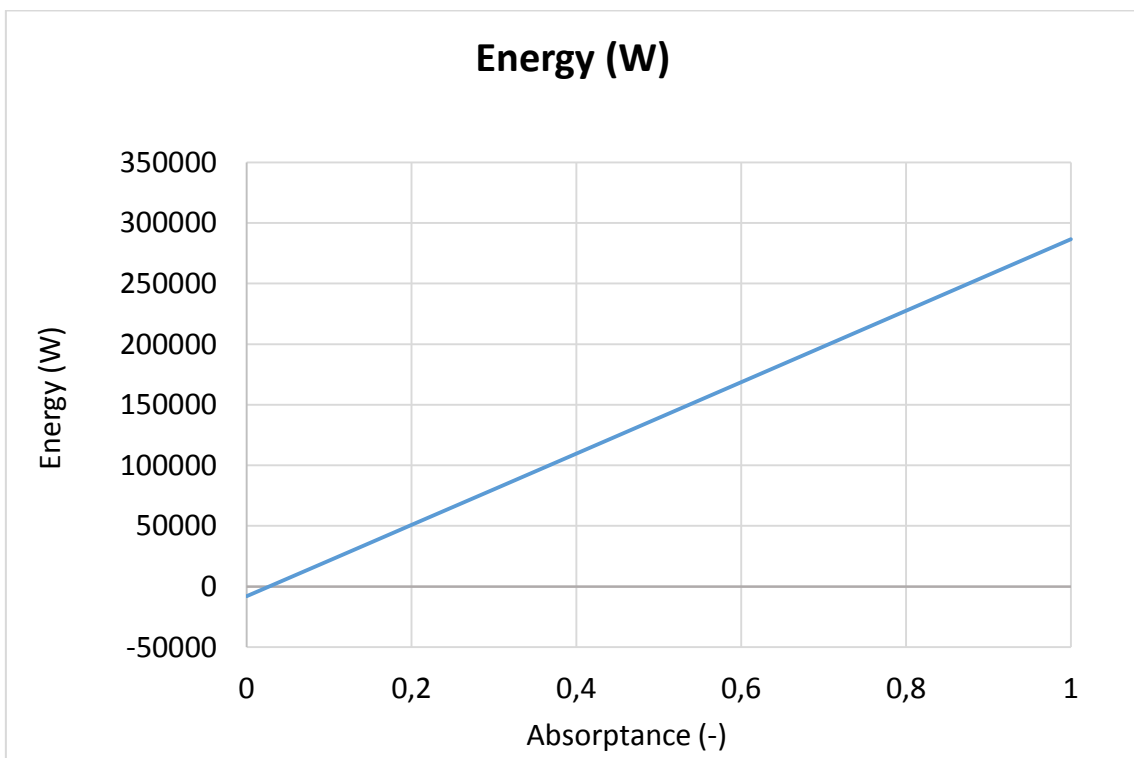
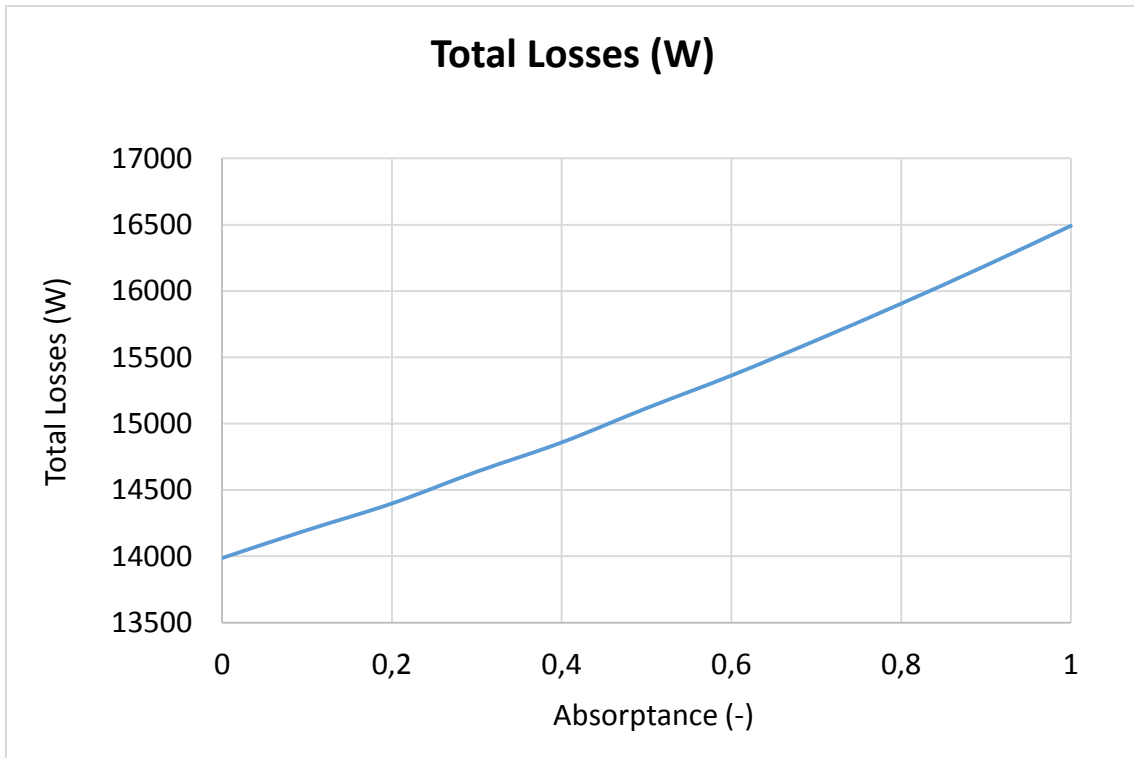
Figure-A 28. Graphs of the results for the heat losses when the HTF degrades.

Absorptance of the absorber tube

Table A 31. Results for the dynamic efficiency test for different values of the absorptance of the metal tube from 0,1 to 1.

Test	Incidence angle (°)	Absorber absorptance (-)	Model Outlet temperature (°C)	Total Losses (W)	Energy (W)	Useful Solar Radiant Power (W)	Model efficiency (%)
1	16,37	0,9557	330,42	16357,62	273524,09	370869,74	73,75%
2	16,37	0	283,55	13986,89	-7941,68	370869,74	-2,14%
3	16,37	0,1	288,53	14197,51	21429,21	370869,74	5,78%
4	16,37	0,2	293,50	14398,06	50870,96	370869,74	13,72%
5	16,37	0,3	298,44	14637,51	80252,55	370869,74	21,64%
6	16,37	0,4	303,37	14858,13	109696,52	370869,74	29,58%
7	16,37	0,5	308,28	15116,49	139163,12	370869,74	37,52%
8	16,37	0,6	313,17	15362,80	168622,62	370869,74	45,47%
9	16,37	0,7	318,05	15628,48	198102,60	370869,74	53,42%
10	16,37	0,8	322,90	15904,92	227585,89	370869,74	61,37%
11	16,37	0,9	327,74	16192,51	257089,68	370869,74	69,32%
12	16,37	1	332,56	16491,51	286600,73	370869,74	77,28%





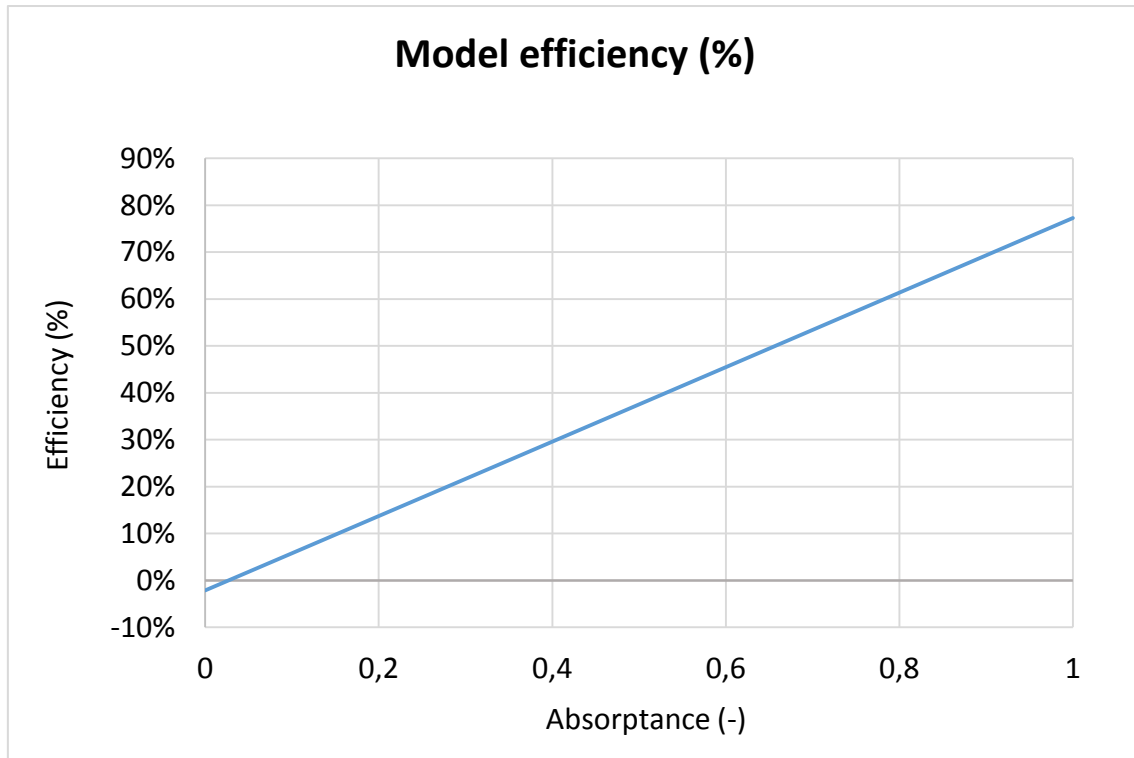
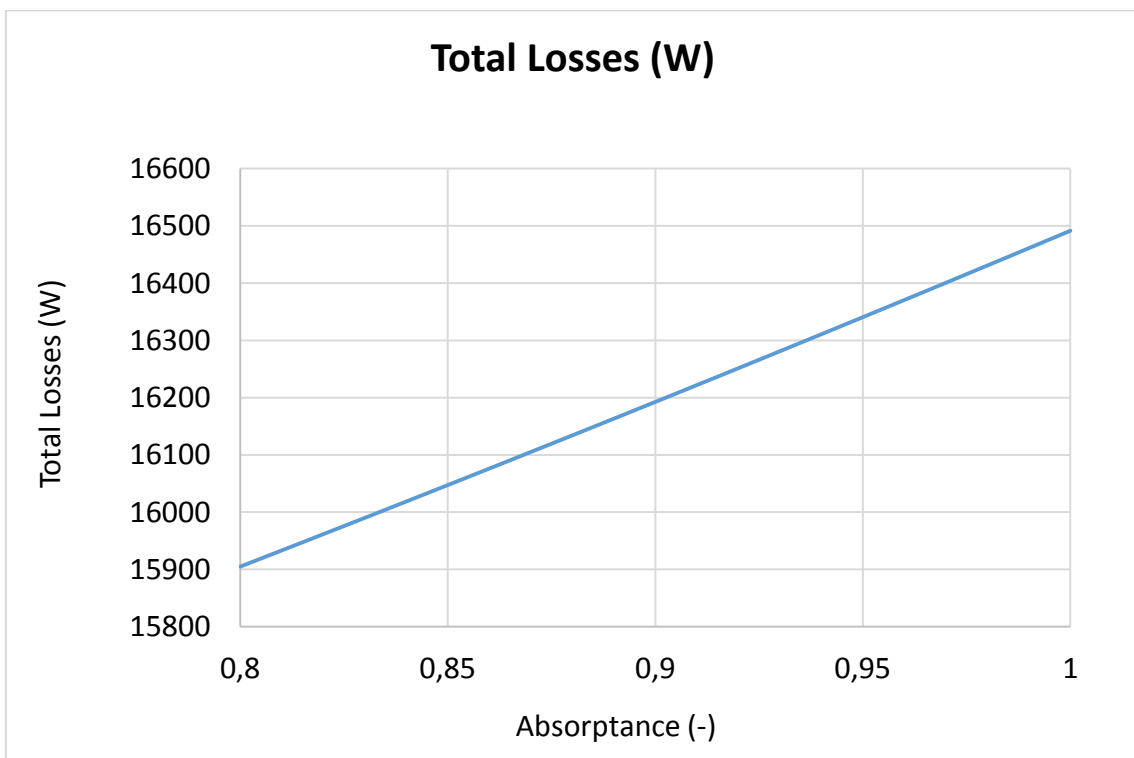
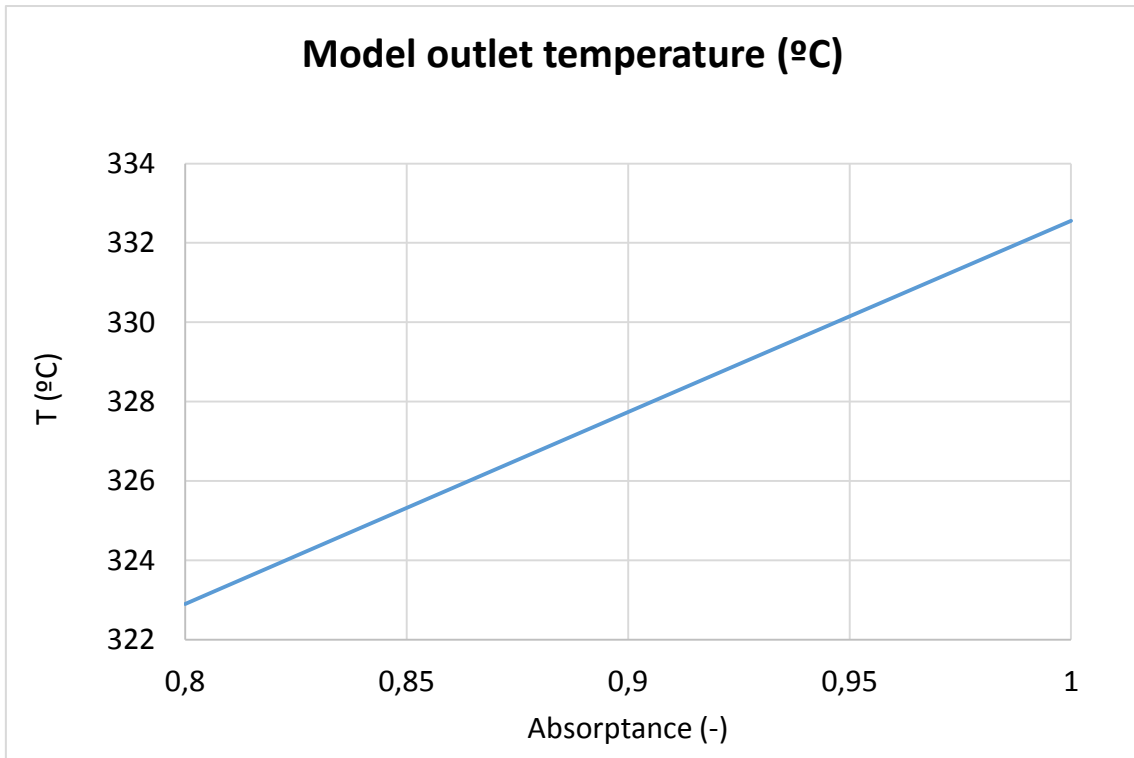


Figure-A 29. Graphs of the results for the dynamic efficiency test when the absorbance of the receive varies from 0,1 to 1.

Table A 32. Results for the dynamic efficiency test for different values of the absorbance of the metal tube from 0,8 to 1.

Test	Incidence angle (°)	Absorber absorbance (-)	Model Outlet temperature (°C)	model delta T (°C)	Total Losses (W)	Energy (W)	Useful Solar Radiant Power (W)	Model efficiency (%)
1	16,37	0,9557	330,42	45,52	16357,62	273524,09	370869,74	73,75%
2	16,37	0,8	322,90	38,00	15904,92	227585,89	370869,74	61,37%
3	16,37	0,81	323,38	38,48	15933,17	230535,76	370869,74	62,16%
4	16,37	0,82	323,87	38,97	15961,54	233485,75	370869,74	62,96%
5	16,37	0,83	324,35	39,45	15990,02	236435,73	370869,74	63,75%
6	16,37	0,84	324,84	39,94	16018,61	239385,96	370869,74	64,55%
7	16,37	0,85	325,32	40,42	16047,31	242336,25	370869,74	65,34%
8	16,37	0,86	325,80	40,90	16076,12	245286,63	370869,74	66,14%
9	16,37	0,87	326,29	41,39	16105,05	248237,26	370869,74	66,93%
10	16,37	0,88	326,77	41,87	16134,09	251187,97	370869,74	67,73%
11	16,37	0,89	327,25	42,35	16163,24	254138,74	370869,74	68,53%
12	16,37	0,9	327,74	42,84	16192,51	257089,68	370869,74	69,32%
13	16,37	0,91	328,22	43,32	16221,89	260040,51	370869,74	70,12%
14	16,37	0,92	328,70	43,80	16251,39	262991,61	370869,74	70,91%
15	16,37	0,93	329,19	44,29	16281,00	265942,86	370869,74	71,71%
16	16,37	0,94	329,67	44,77	16310,71	268890,23	370869,74	72,50%
17	16,37	0,95	330,15	45,25	16340,56	271841,67	370869,74	73,30%
18	16,37	0,96	330,63	45,73	16370,51	274793,33	370869,74	74,09%
19	16,37	0,97	331,11	46,21	16400,59	277745,03	370869,74	74,89%
20	16,37	0,98	331,59	46,69	16430,78	280696,80	370869,74	75,69%
21	16,37	0,99	332,08	47,18	16461,09	283648,78	370869,74	76,48%
22	16,37	1	332,56	47,66	16491,51	286600,73	370869,74	77,28%



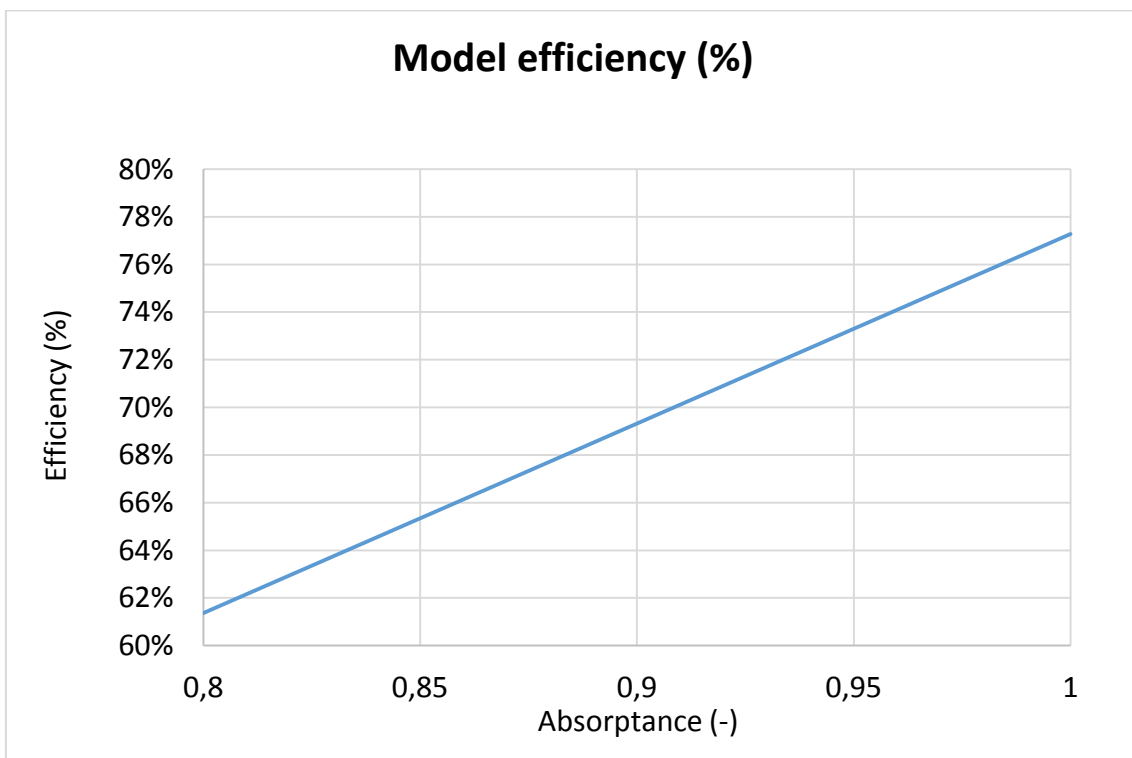
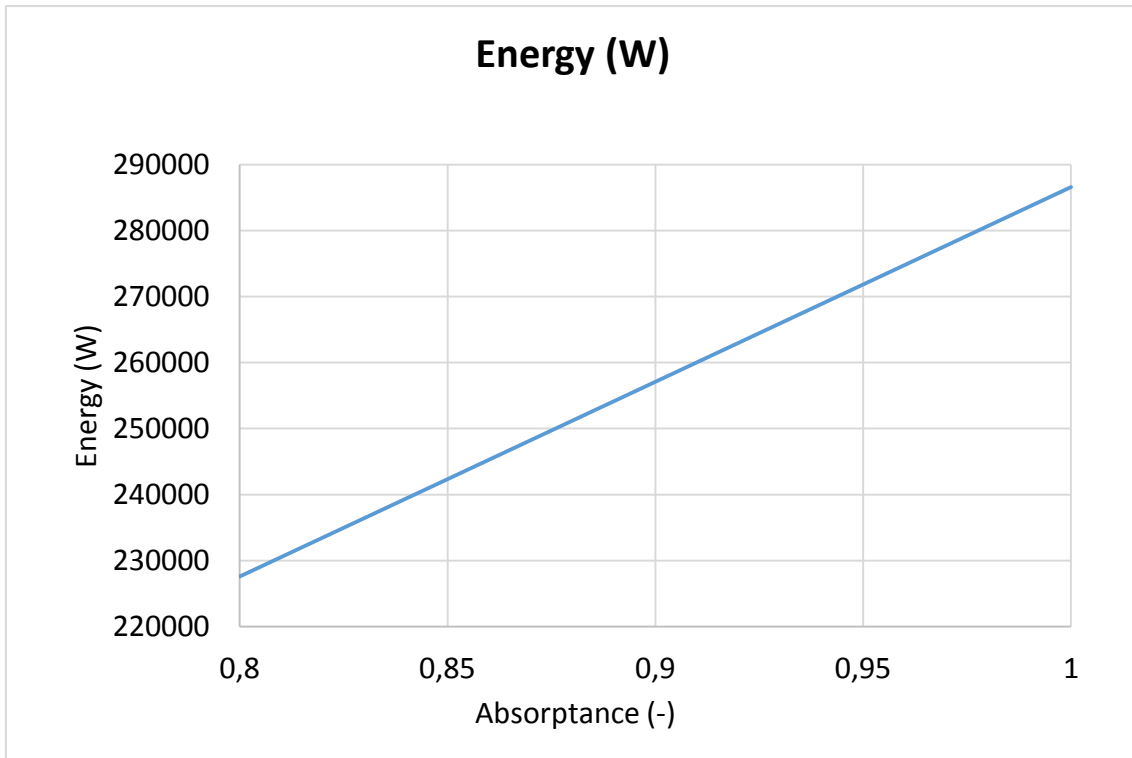
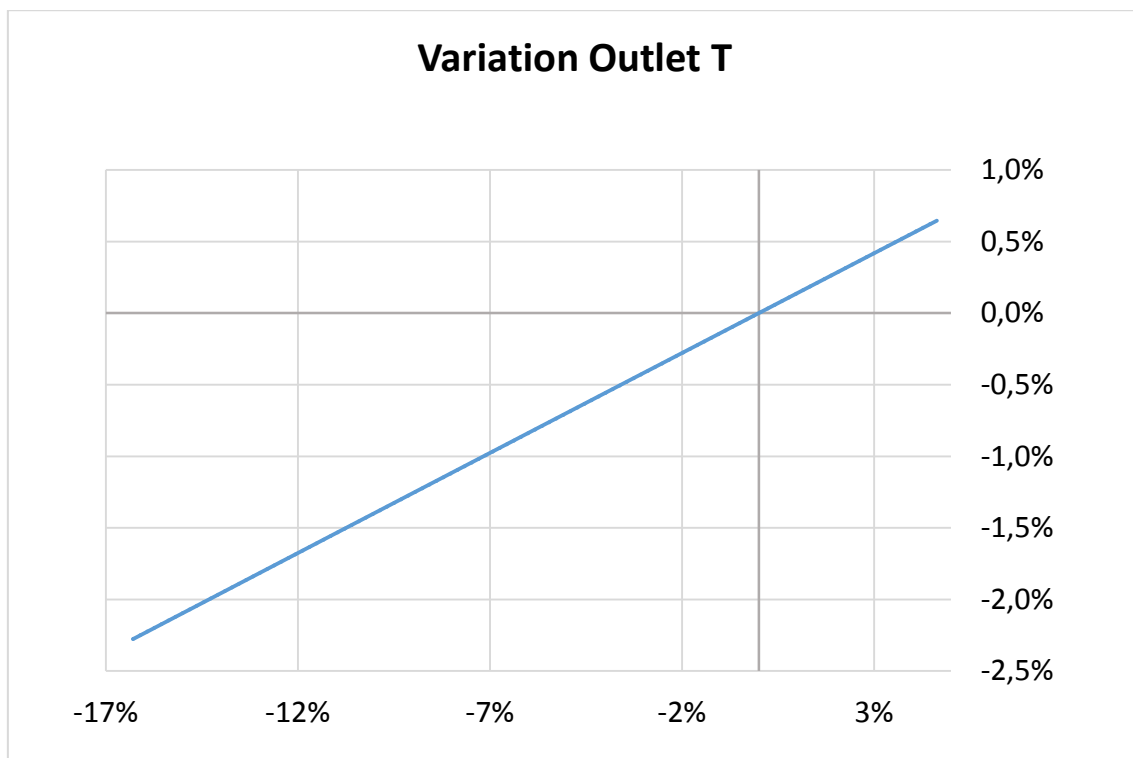
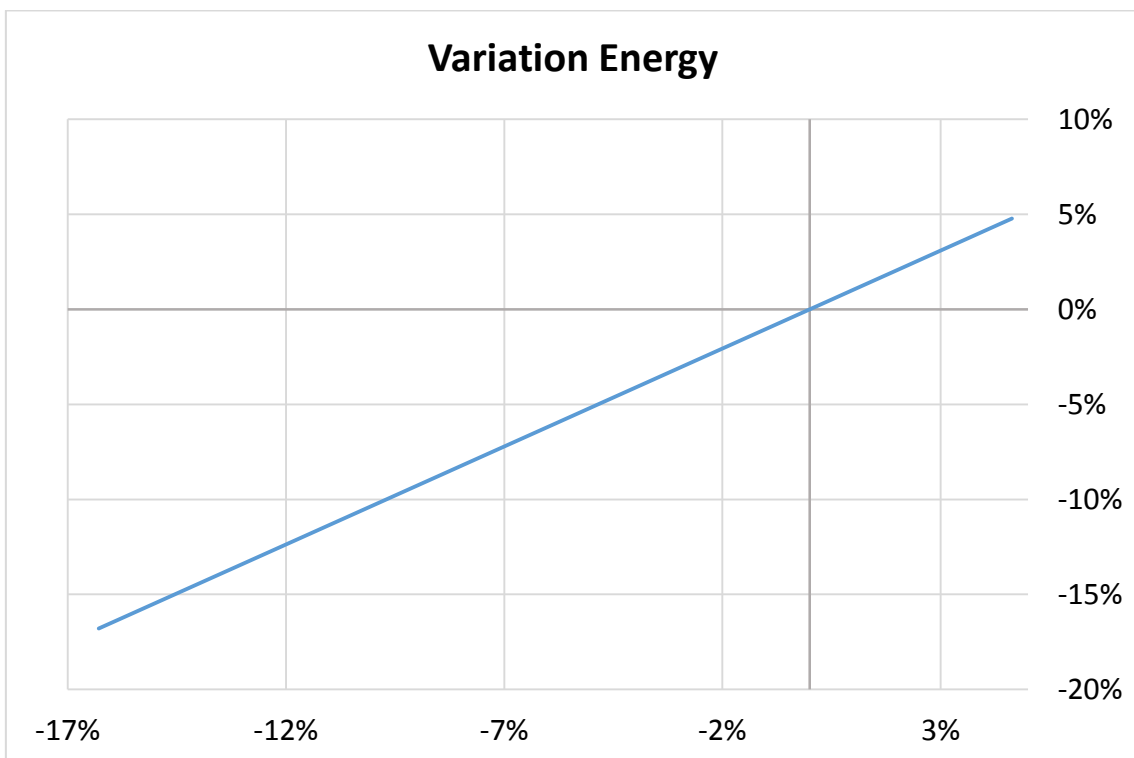
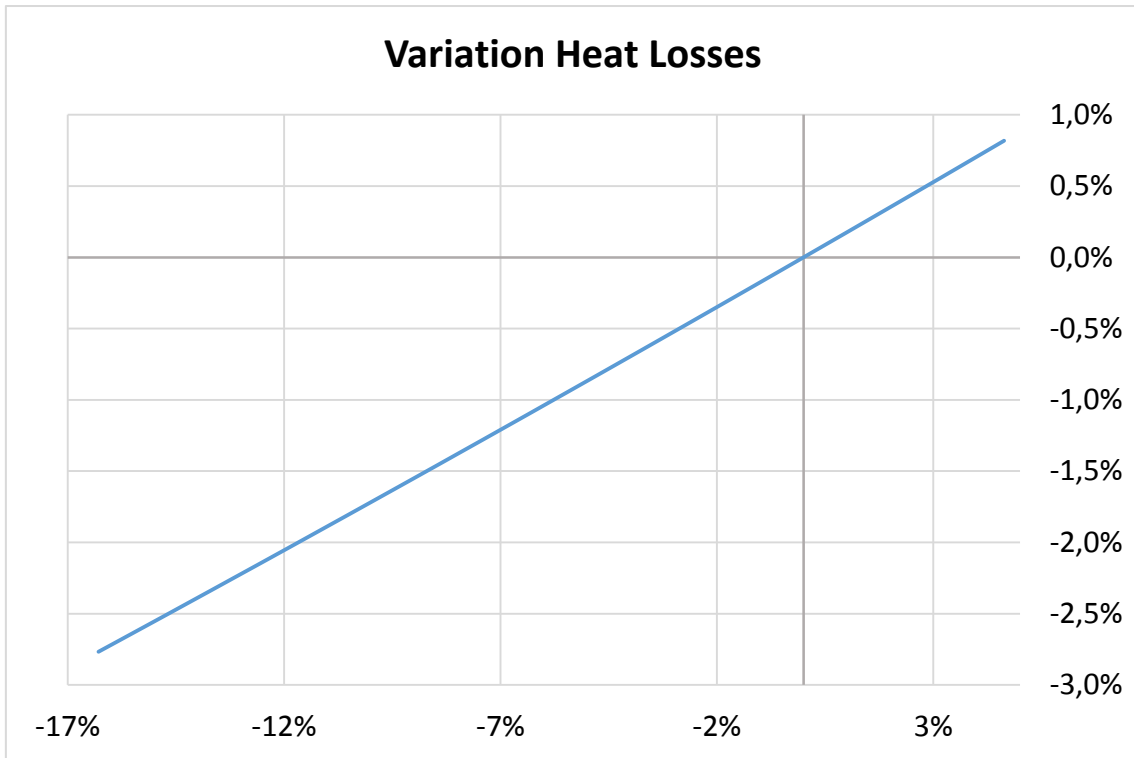


Figure-A 30. Graphs of the results for the dynamic efficiency test when the absorbance of the receive varies from 0,8 to 1.

Table A 33. Results from the dynamic efficiency test expressed in percentages when the absorptance of the receive varies from 0,8 to 1.

Variation Absorber absorptance	Variation Outlet T	Variation Heat Losses	Variation Energy	Variation Efficiency
0,00%	0,00%	0,00%	0,00%	0,00%
-16,29%	-2,28%	-2,77%	-16,79%	-16,79%
-15,25%	-2,13%	-2,59%	-15,72%	-15,72%
-14,20%	-1,98%	-2,42%	-14,64%	-14,64%
-13,15%	-1,84%	-2,25%	-13,56%	-13,56%
-12,11%	-1,69%	-2,07%	-12,48%	-12,48%
-11,06%	-1,54%	-1,90%	-11,40%	-11,40%
-10,01%	-1,40%	-1,72%	-10,32%	-10,32%
-8,97%	-1,25%	-1,54%	-9,24%	-9,24%
-7,92%	-1,11%	-1,37%	-8,17%	-8,17%
-6,87%	-0,96%	-1,19%	-7,09%	-7,09%
-5,83%	-0,81%	-1,01%	-6,01%	-6,01%
-4,78%	-0,67%	-0,83%	-4,93%	-4,93%
-3,74%	-0,52%	-0,65%	-3,85%	-3,85%
-2,69%	-0,37%	-0,47%	-2,77%	-2,77%
-1,64%	-0,23%	-0,29%	-1,69%	-1,69%
-0,60%	-0,08%	-0,10%	-0,62%	-0,62%
0,45%	0,06%	0,08%	0,46%	0,46%
1,50%	0,21%	0,26%	1,54%	1,54%
2,54%	0,35%	0,45%	2,62%	2,62%
3,59%	0,50%	0,63%	3,70%	3,70%
4,64%	0,65%	0,82%	4,78%	4,78%





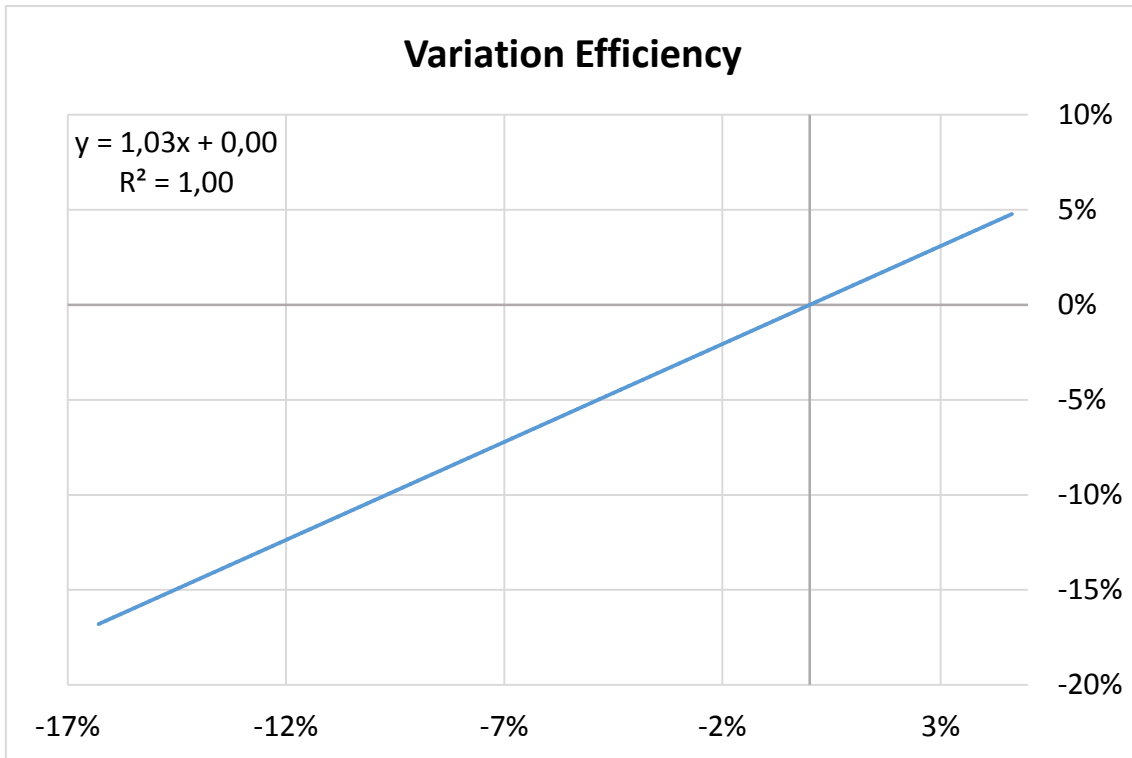
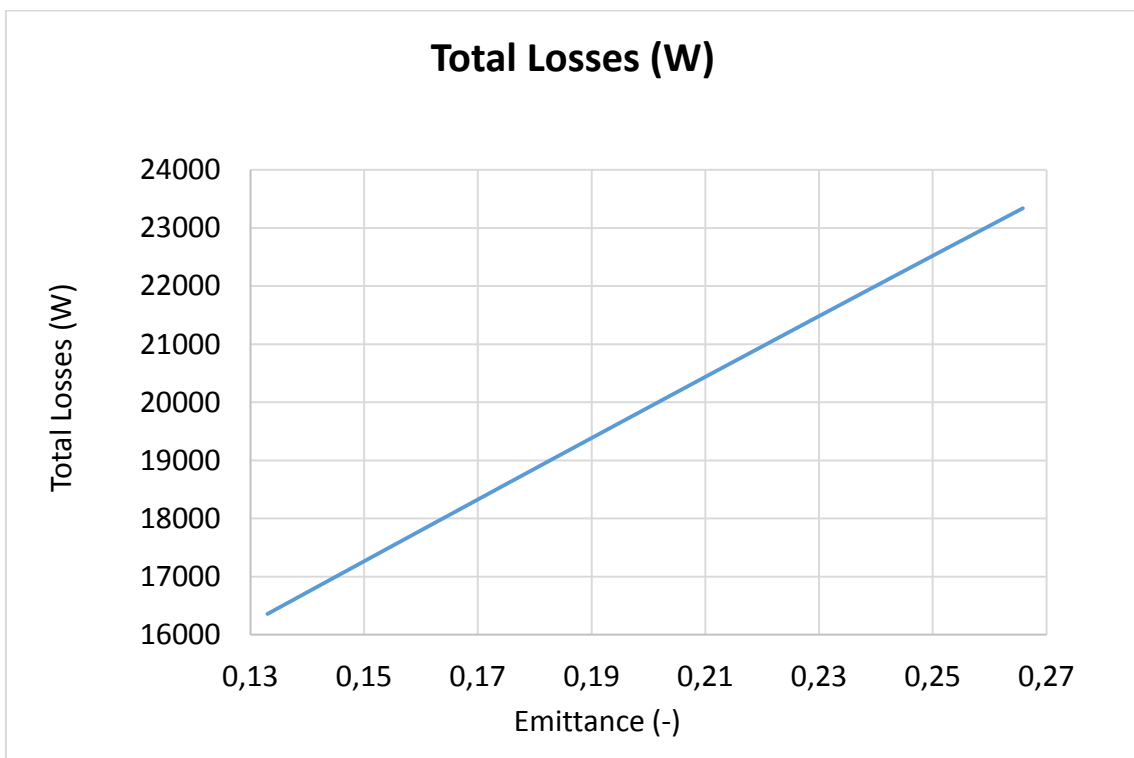
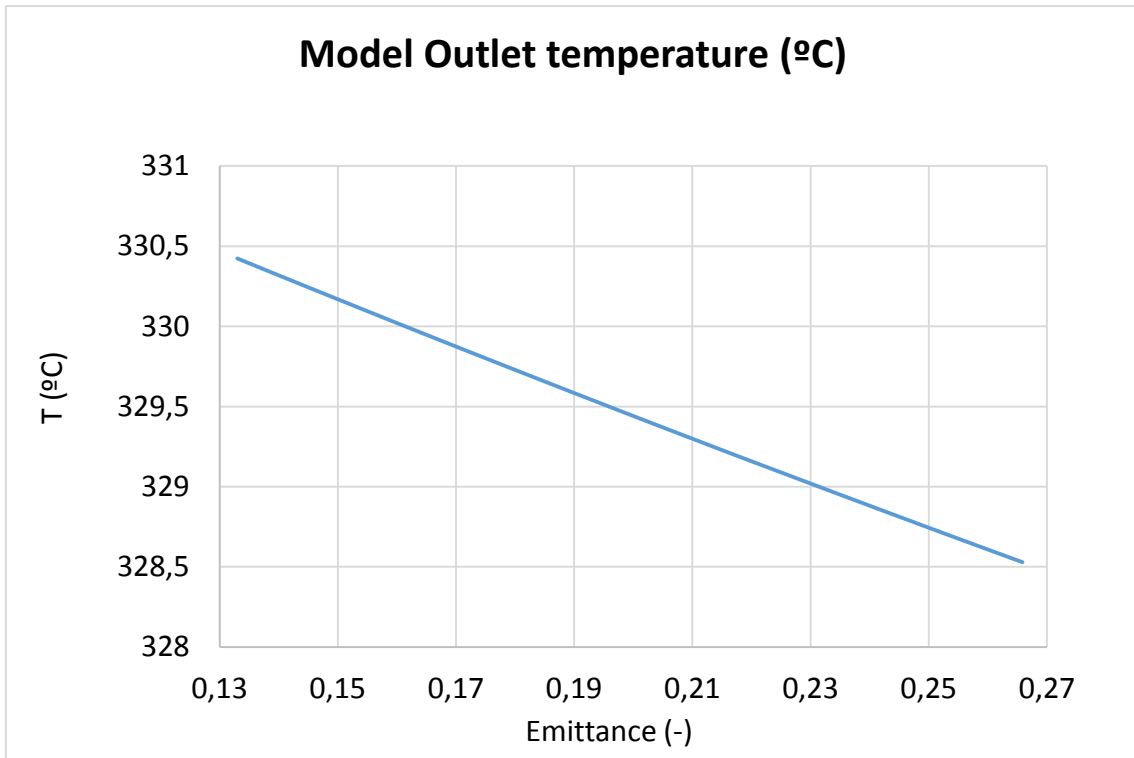


Figure-A 31. Graphs of the results for the dynamic efficiency test expressed in percentages when absorptance of the absorber varies from 0,8 to 1.

Emittance of the absorber tube

Table A 34. Results for the dynamic efficiency test for different values of the emittance of the metal tube.

Test	Incidence angle (°)	Absorber emittance (-)	Model Outlet temperature (°C)	Total Losses (W)	Energy (W)	Useful Solar Radiant Power (W)	Model efficiency (%)
1	16,37	0,13299	330,42	16357,62	273524,09	370869,74	73,75%
2	16,37	0,13963	330,32	16712,48	272911,76	370869,74	73,59%
3	16,37	0,14628	330,22	17066,91	272302,98	370869,74	73,42%
4	16,37	0,15293	330,13	17420,88	271697,69	370869,74	73,26%
5	16,37	0,15957	330,03	17774,35	271095,87	370869,74	73,10%
6	16,37	0,16622	329,93	18127,30	270497,51	370869,74	72,94%
7	16,37	0,17286	329,83	18479,69	269902,58	370869,74	72,78%
8	16,37	0,17950	329,74	18831,49	269311,06	370869,74	72,62%
9	16,37	0,18615	329,64	19182,67	268722,89	370869,74	72,46%
10	16,37	0,19279	329,54	19533,23	268138,19	370869,74	72,30%
11	16,37	0,19944	329,45	19883,11	267556,79	370869,74	72,14%
12	16,37	0,20608	329,35	20232,31	266978,80	370869,74	71,99%
13	16,37	0,21272	329,26	20580,79	266404,03	370869,74	71,83%
14	16,37	0,21936	329,17	20928,55	265832,72	370869,74	71,68%
15	16,37	0,22601	329,08	21275,58	265268,61	370869,74	71,53%
16	16,37	0,23265	328,98	21621,81	264703,77	370869,74	71,37%
17	16,37	0,23929	328,89	21967,25	264142,17	370869,74	71,22%
18	16,37	0,24593	328,80	22311,89	263583,81	370869,74	71,07%
19	16,37	0,25257	328,71	22655,70	263028,60	370869,74	70,92%
20	16,37	0,25922	328,62	22998,66	262476,79	370869,74	70,77%
21	16,37	0,26586	328,53	23340,77	261928,01	370869,74	70,63%



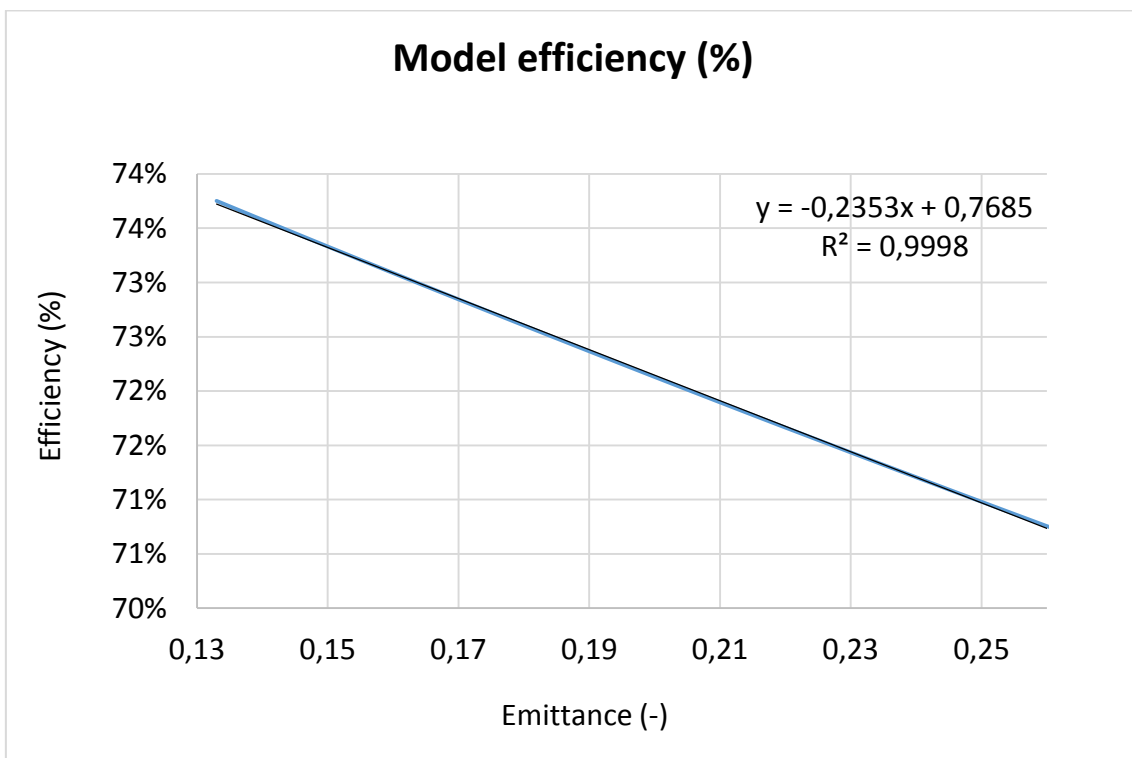
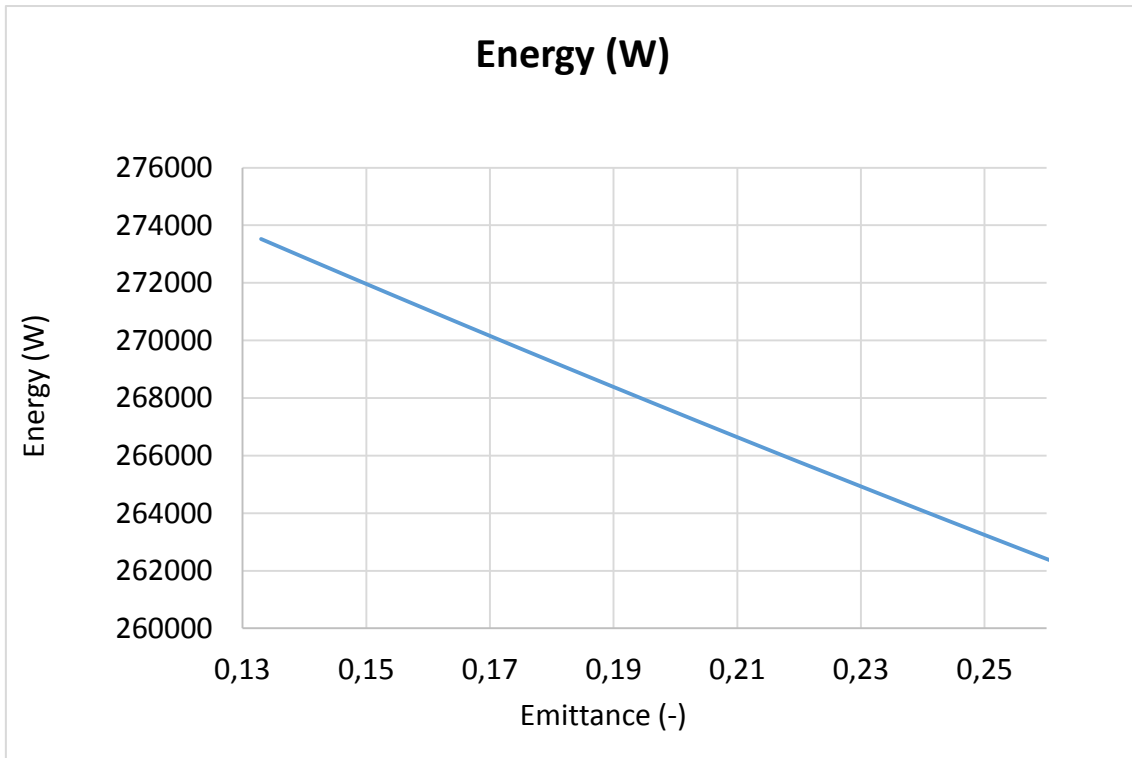
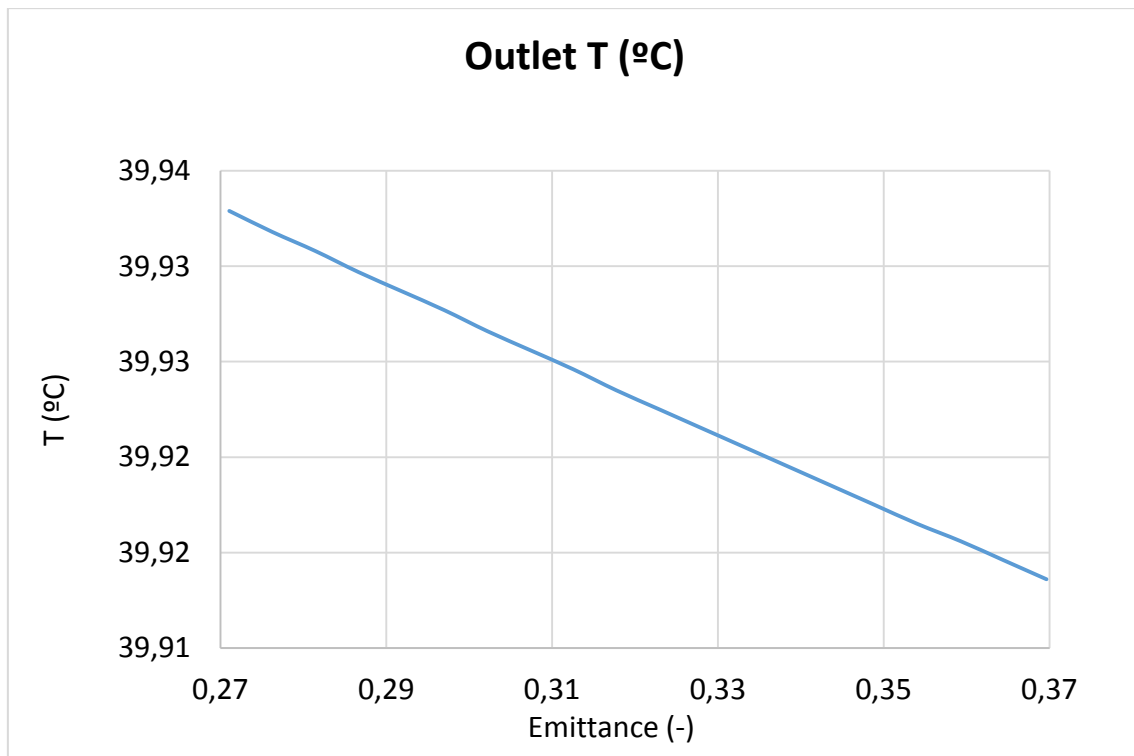


Figure-A 32. Graphs of the results for the dynamic efficiency test when the emittance of the absorber varies.

- When the HTF's inlet temperature is 40°C:

Table A 35. Results from the heat losses test at 40°C for different values of absorber's emittance.

Test	Absorber emittance (-)	Outlet T (°C)	Total Losses (W)	Enthalpy difference (W)
1	0,24641182	39,94	368,82	364,13
2	0,271053	39,93	398,69	394,18
3	0,276242	39,93	404,74	400,62
4	0,281431	39,93	410,93	406,70
5	0,28662	39,93	417,08	412,78
6	0,291809	39,93	423,21	418,86
7	0,296998	39,93	429,32	424,94
8	0,302187	39,93	435,39	431,02
9	0,307376	39,93	441,44	437,10
10	0,312565	39,92	447,46	443,18
11	0,317755	39,92	453,45	449,26
12	0,322944	39,92	459,43	455,34
13	0,328133	39,92	465,37	461,07
14	0,333322	39,92	471,29	467,15
15	0,338512	39,92	477,18	472,87
16	0,343701	39,92	483,05	478,95
17	0,34889	39,92	488,90	484,68
18	0,35408	39,92	494,71	490,40
19	0,359269	39,92	500,51	496,12
20	0,364459	39,91	506,27	502,20
21	0,369648	39,91	512,01	507,93



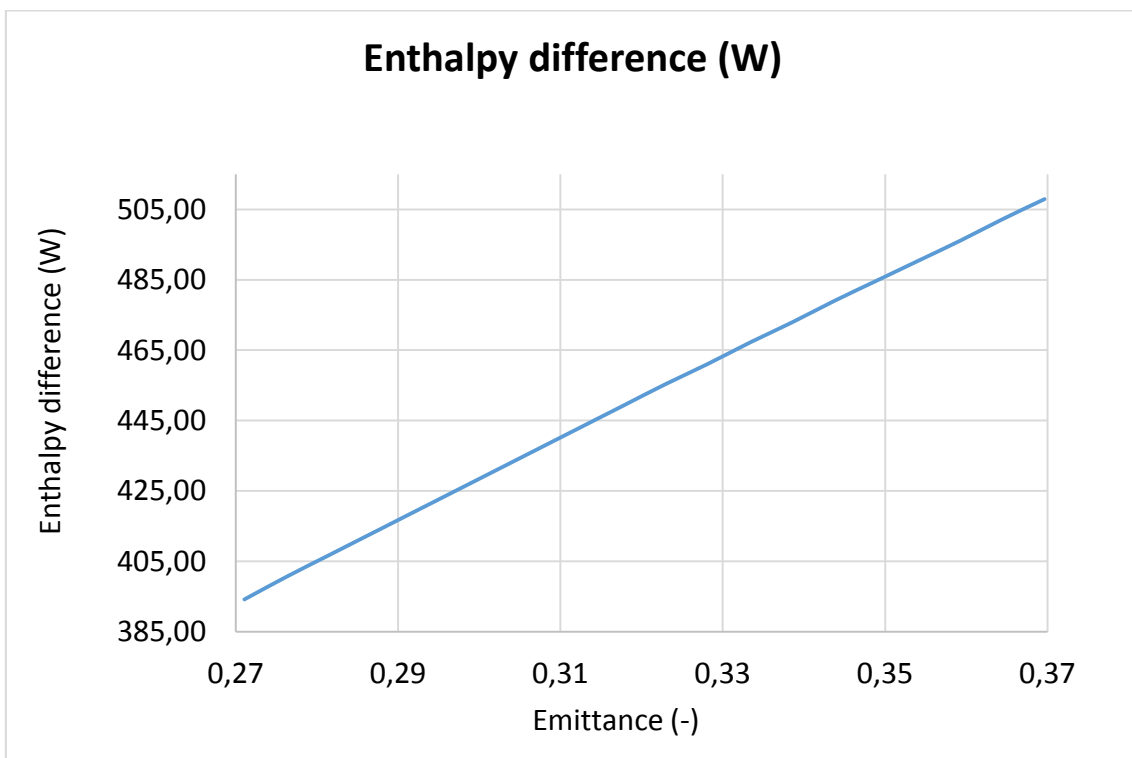
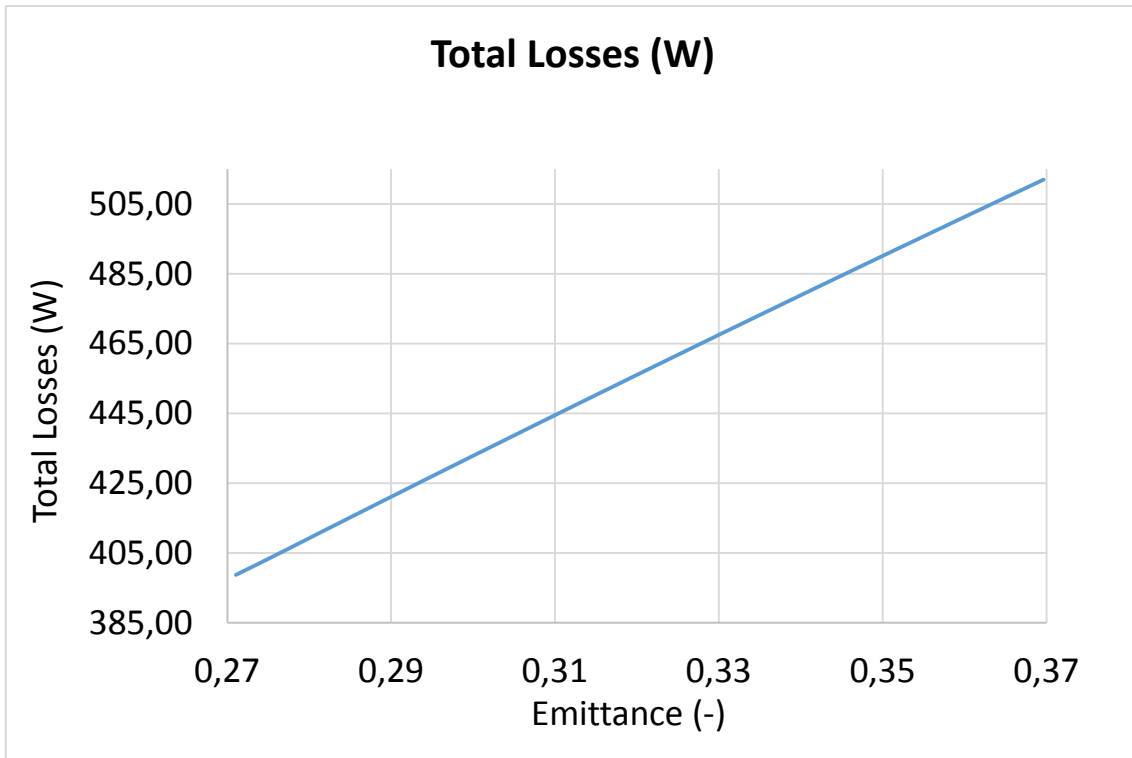
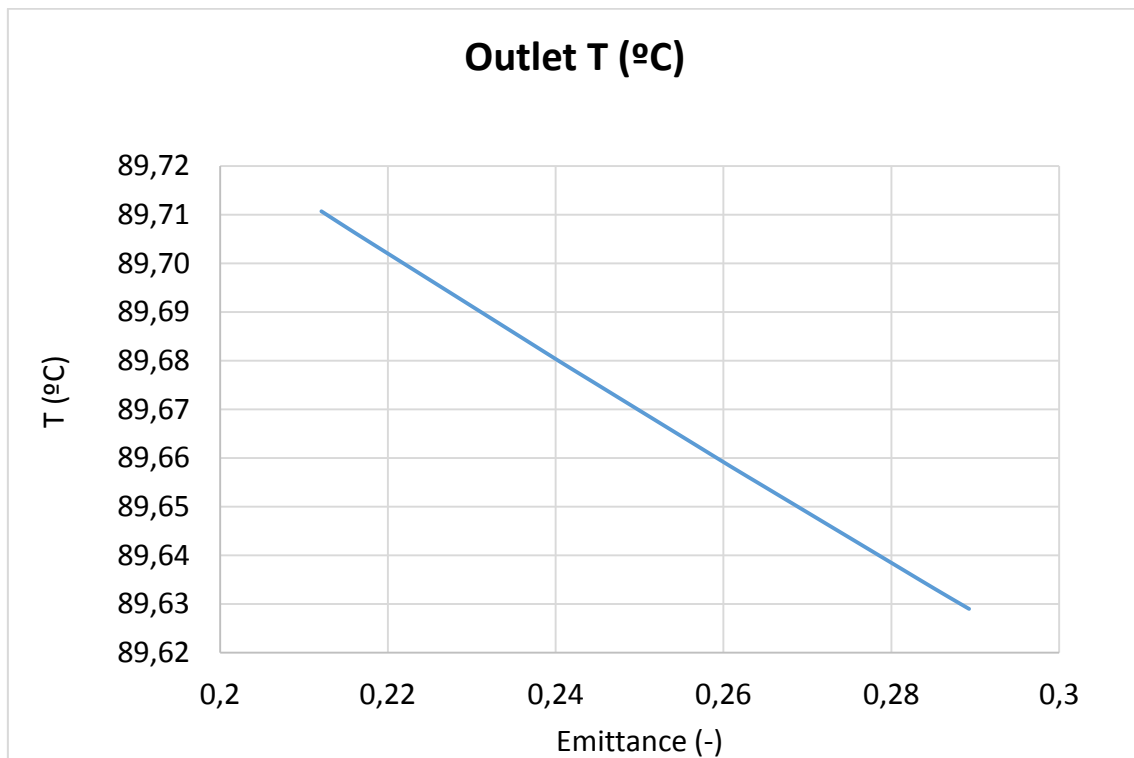


Figure-A 33. Graphs of the results for the heat losses test at 40°C for different values of absorber's emittance.

- When the HTF's inlet temperature is 90°C:

Table A 36. Results from the heat losses test at 90°C for different values of absorber's emittance.

Test	Absorber emittance (-)	Outlet T (°C)	Total Losses (W)	Enthalpy difference (W)
1	0,19280091	89,73	1638,78	1656,12
2	0,212081	89,71	1771,35	1788,47
3	0,216143	89,71	1798,95	1817,09
4	0,220204	89,70	1826,43	1842,13
5	0,224266	89,70	1853,81	1870,74
6	0,228327	89,69	1881,07	1899,36
7	0,232389	89,69	1908,22	1924,40
8	0,236451	89,68	1935,27	1953,01
9	0,240513	89,68	1961,95	1978,05
10	0,244575	89,68	1988,76	2006,67
11	0,248637	89,67	2015,77	2031,70
12	0,252699	89,67	2042,36	2060,32
13	0,256761	89,66	2068,82	2085,36
14	0,260823	89,66	2095,17	2110,40
15	0,264886	89,65	2121,39	2139,01
16	0,268948	89,65	2147,51	2164,05
17	0,273011	89,65	2173,50	2189,09
18	0,277073	89,64	2199,36	2217,70
19	0,281136	89,64	2225,10	2242,74
20	0,285199	89,63	2250,73	2267,78
21	0,289262	89,63	2276,22	2292,82



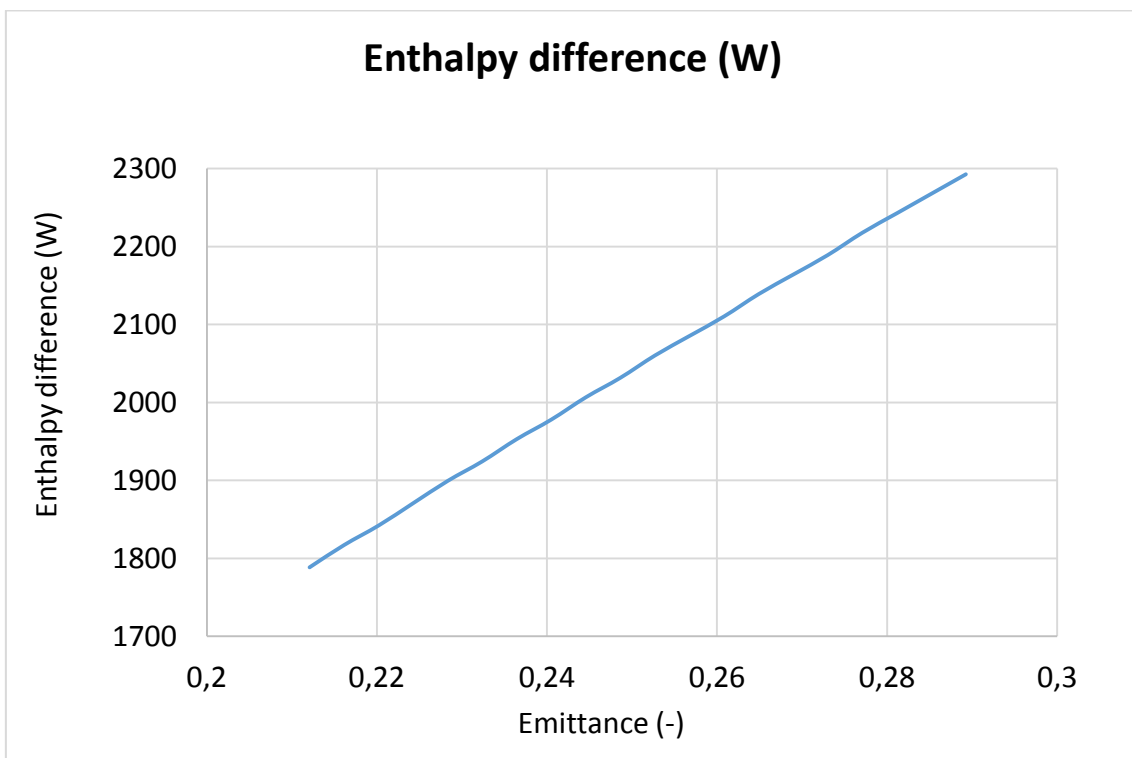
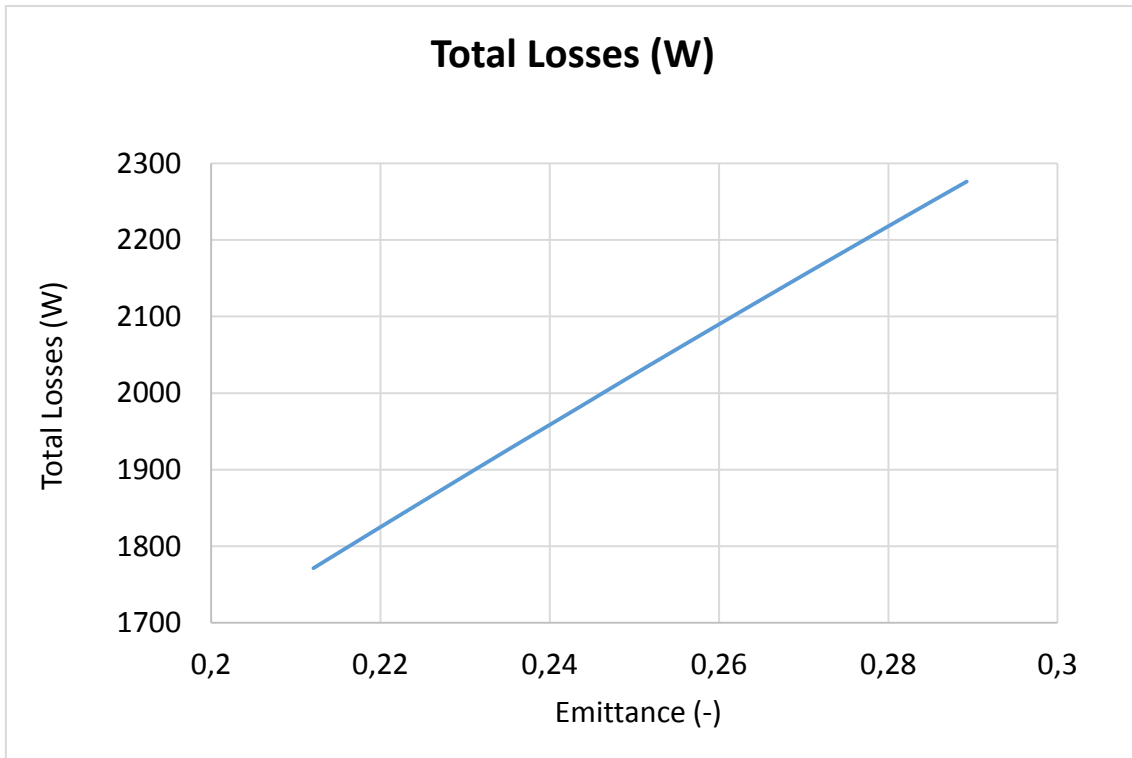
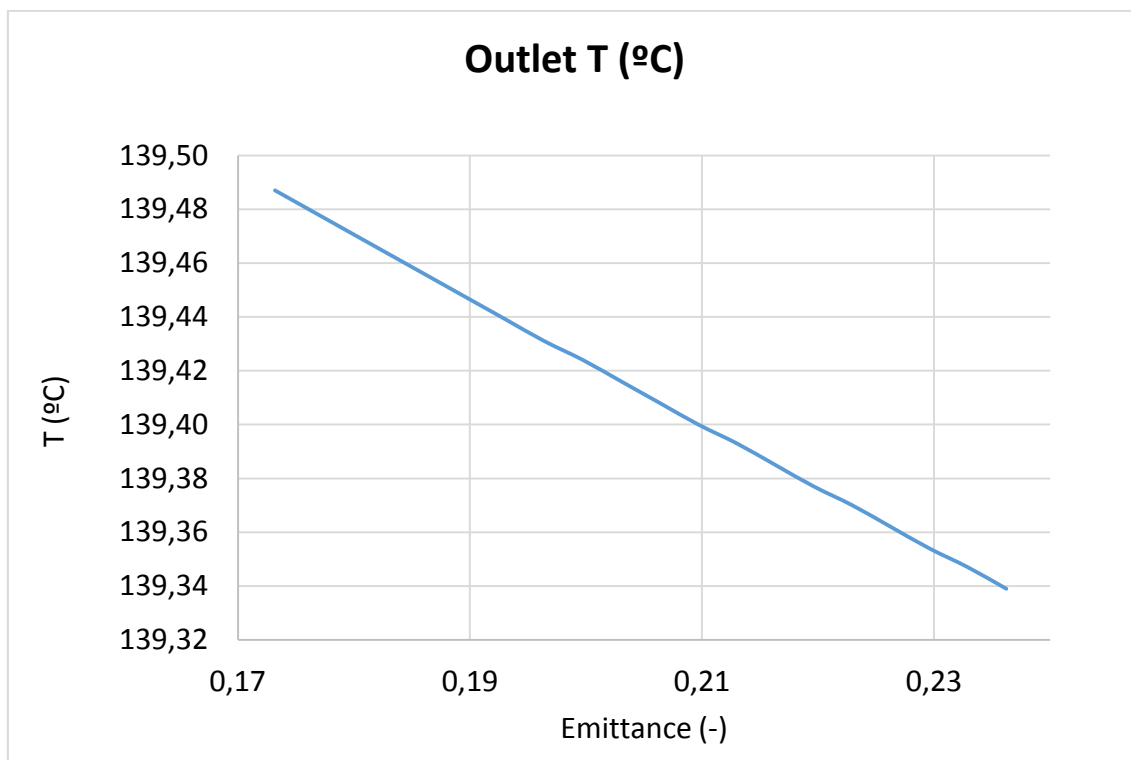


Figure-A 34. Graphs of the results for the heat losses test at 90°C for different values of absorber's emittance.

- When the HTF's inlet temperature is 140°C:

Table A 37. Results from the heat losses test at 140°C for different values of absorber's emittance.

Test	Absorber emittance (-)	Outlet T (°C)	Total Losses (W)	Enthalpy difference (W)
1	0,15744818	139,53	3041,97	3079,75
2	0,173193	139,49	3289,79	3326,56
3	0,17651	139,48	3341,53	3380,21
4	0,179827	139,47	3393,12	3430,29
5	0,183144	139,46	3444,56	3480,37
6	0,186461	139,46	3495,86	3534,02
7	0,189778	139,45	3547,00	3584,10
8	0,193095	139,44	3598,00	3634,17
9	0,196412	139,43	3648,85	3684,25
10	0,19973	139,42	3699,55	3737,91
11	0,203047	139,42	3750,11	3787,98
12	0,206364	139,41	3800,52	3838,06
13	0,209682	139,40	3850,79	3888,14
14	0,212999	139,39	3900,90	3938,21
15	0,216317	139,39	3950,88	3988,29
16	0,219635	139,38	4000,70	4038,37
17	0,222953	139,37	4050,39	4088,45
18	0,22627	139,36	4099,94	4138,52
19	0,229588	139,35	4149,34	4185,02
20	0,232906	139,35	4198,59	4235,10
21	0,236224	139,34	4247,71	4285,18



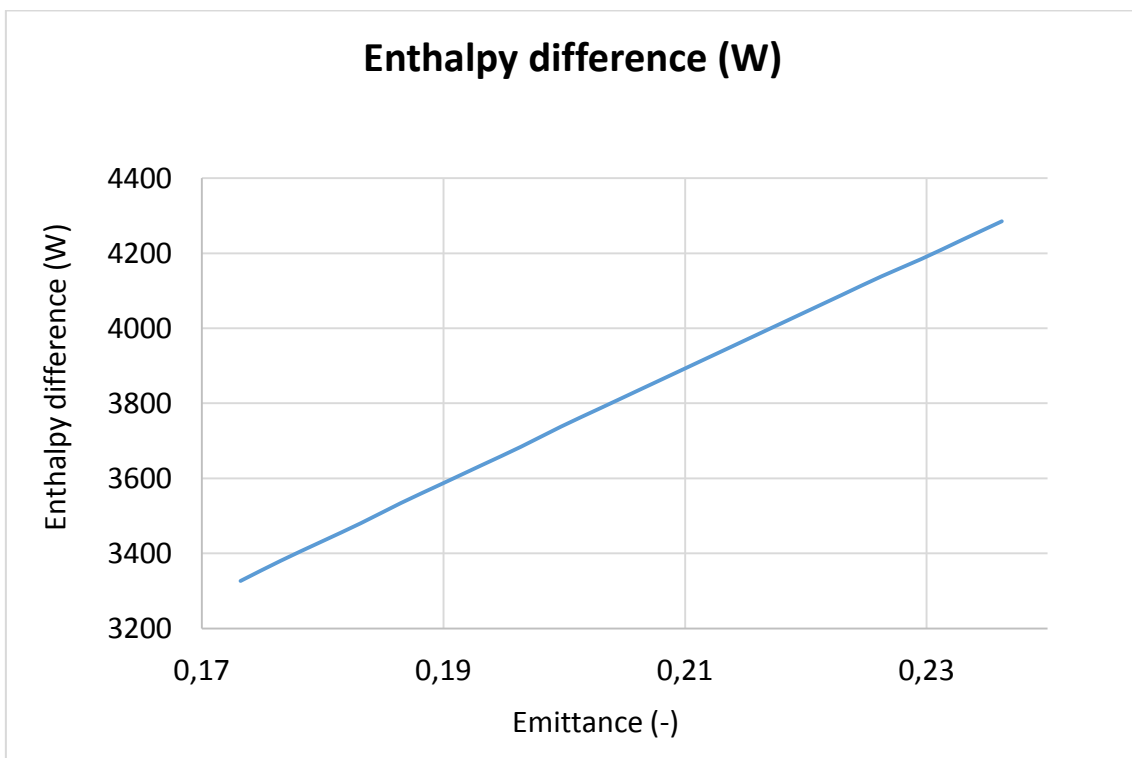
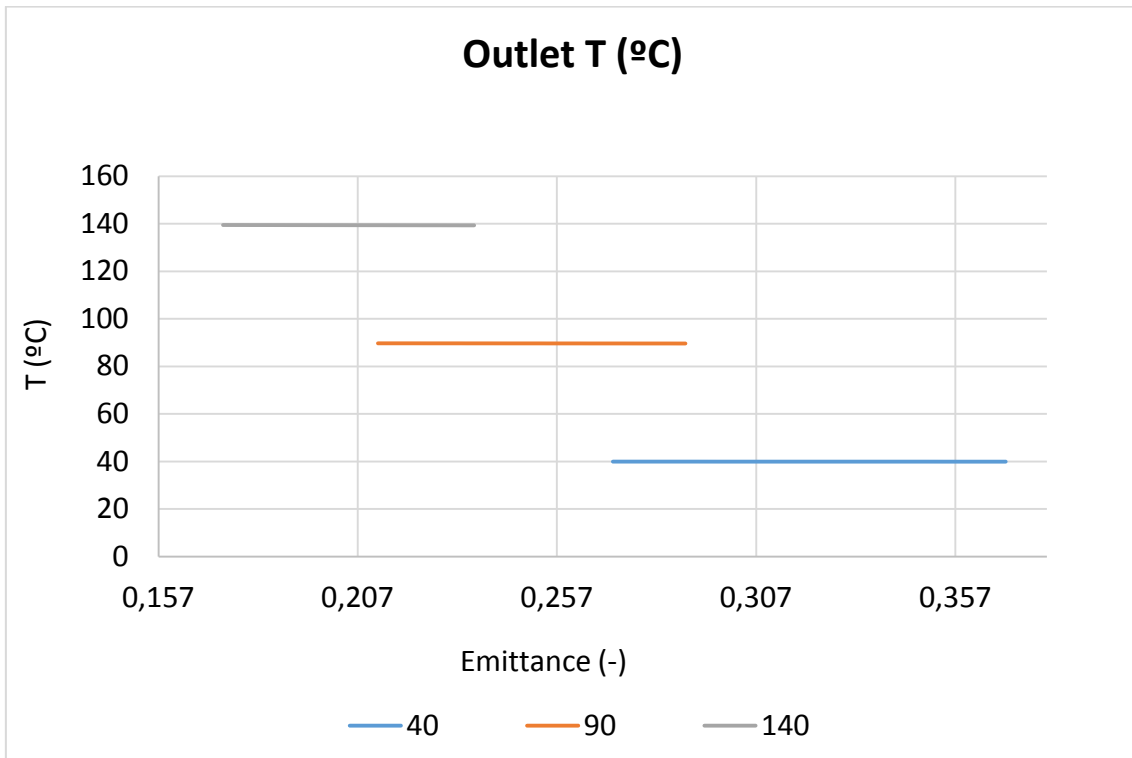


Figure-A 35. Graphs of the results for the heat losses test at 140°C for different values of absorber's emittance.

- Comparing the three cases:



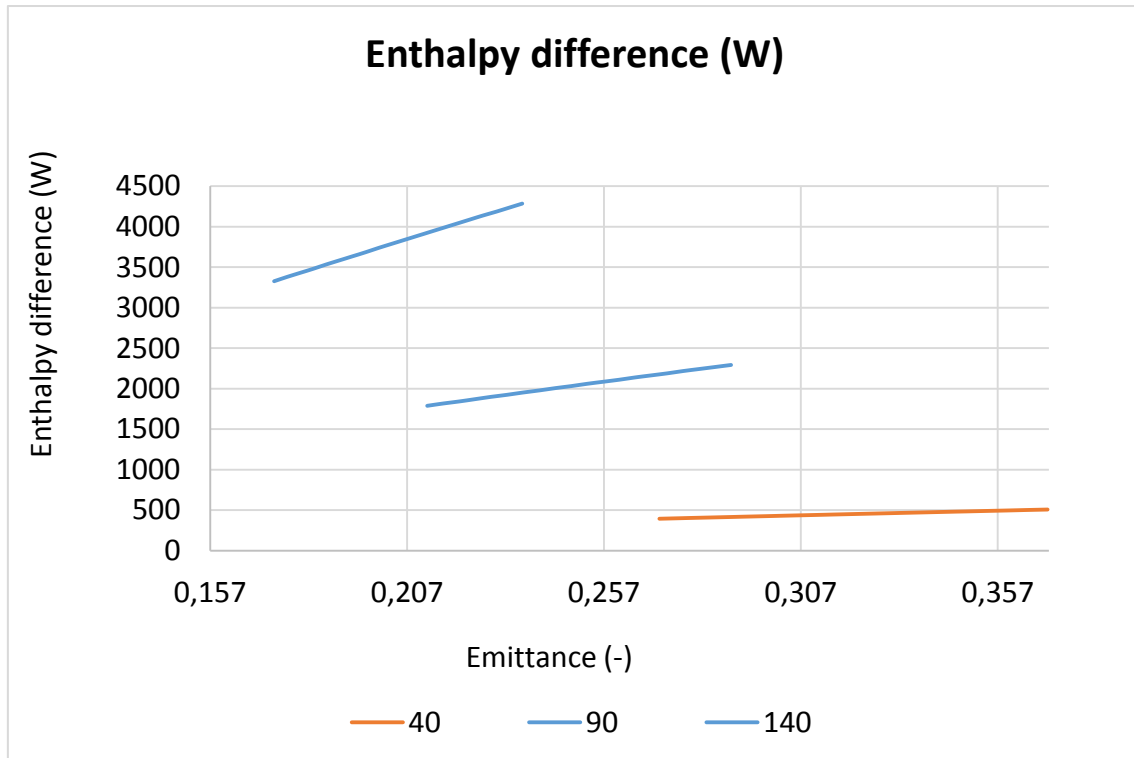


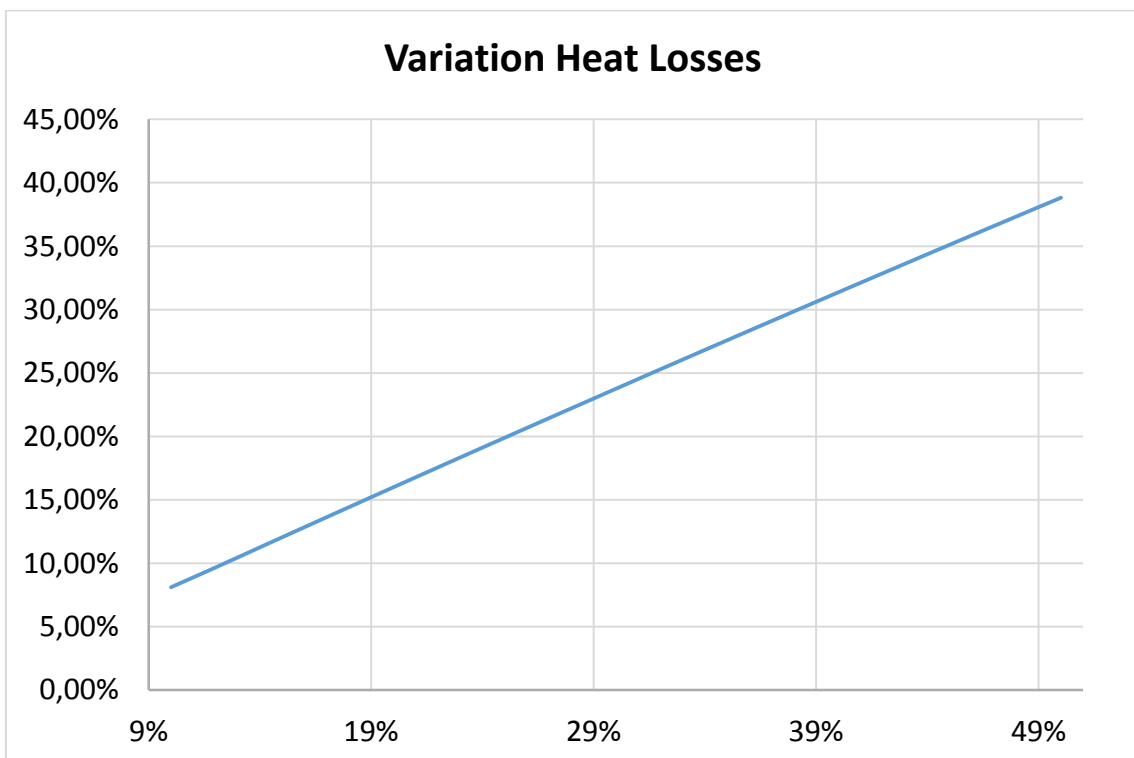
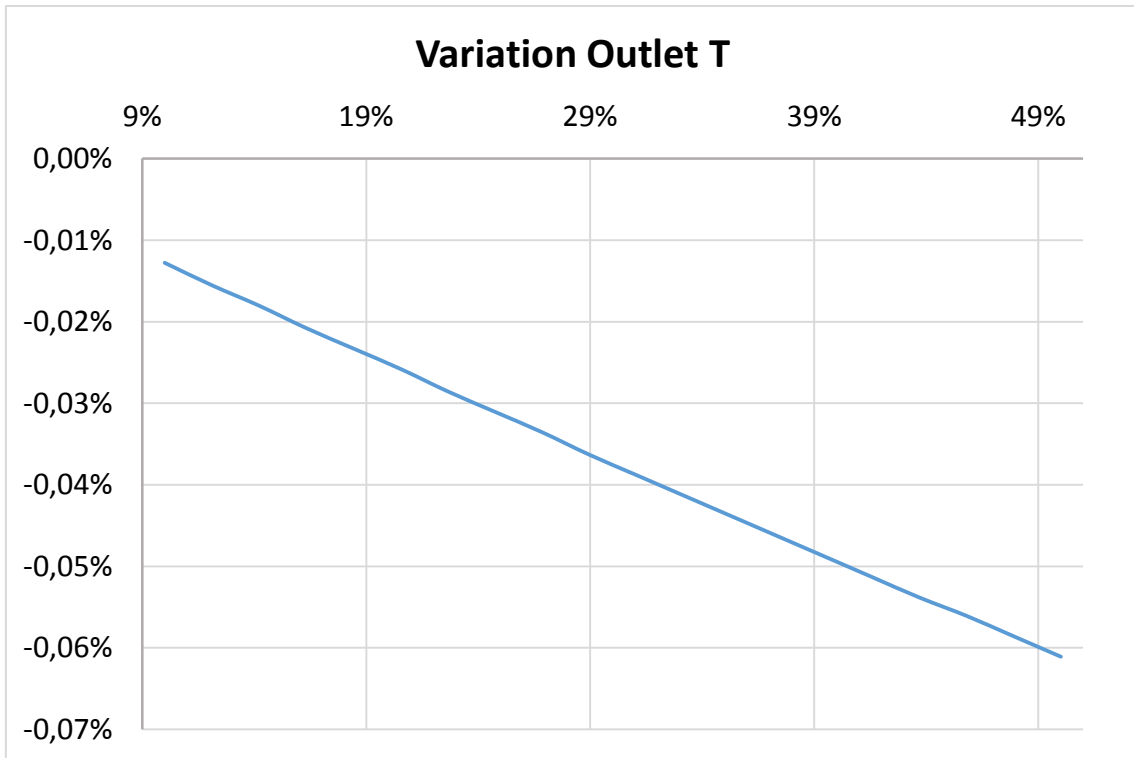
Figure-A 36. Graphs of the results for the heat losses test for different values of absorber's emittance.

Below are presented the same results, but in percentage of the nominal result.

- When the HTF's inlet temperature is 40°C:

Table A 38. Results from the heat losses test at 40°C expressed in percentages for different absorber's emittance.

Variation Absorber emittance	Variation Outlet T	Variation Heat Losses	Variation Enthalpy difference
0,00%	0,00%	0,00%	0,00%
10,00%	-0,01%	8,10%	8,25%
12,11%	-0,02%	9,74%	10,02%
14,21%	-0,02%	11,42%	11,69%
16,32%	-0,02%	13,08%	13,36%
18,42%	-0,02%	14,75%	15,03%
20,53%	-0,03%	16,40%	16,70%
22,63%	-0,03%	18,05%	18,37%
24,74%	-0,03%	19,69%	20,04%
26,85%	-0,03%	21,32%	21,71%
28,95%	-0,04%	22,95%	23,38%
31,06%	-0,04%	24,57%	25,05%
33,16%	-0,04%	26,18%	26,62%
35,27%	-0,04%	27,78%	28,29%
37,38%	-0,05%	29,38%	29,86%
39,48%	-0,05%	30,97%	31,53%
41,59%	-0,05%	32,56%	33,10%
43,69%	-0,05%	34,13%	34,68%
45,80%	-0,06%	35,71%	36,25%
47,91%	-0,06%	37,27%	37,92%
50,01%	-0,06%	38,82%	39,49%



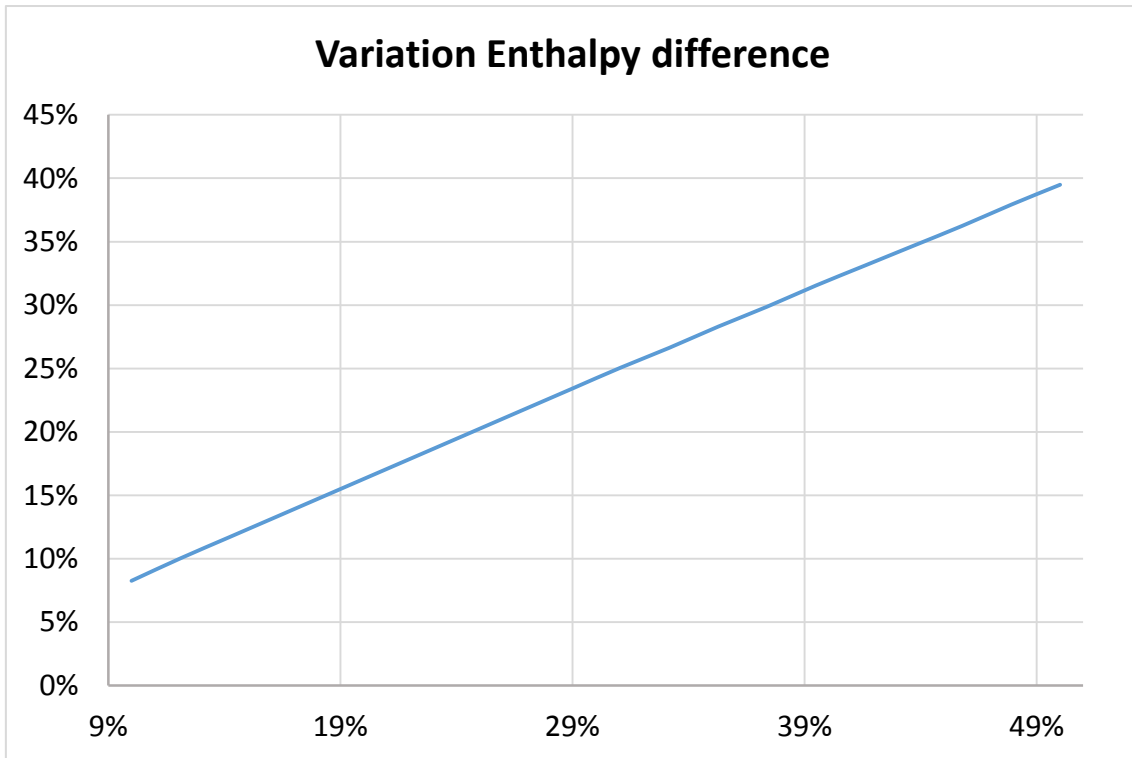
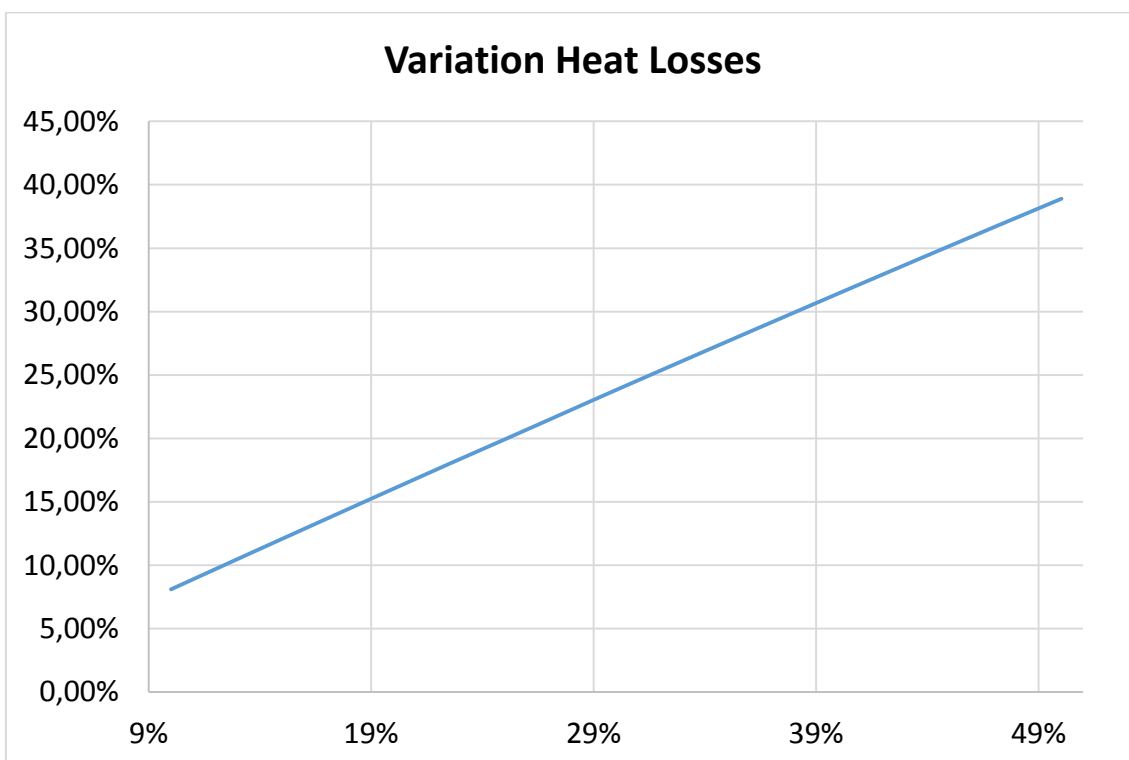
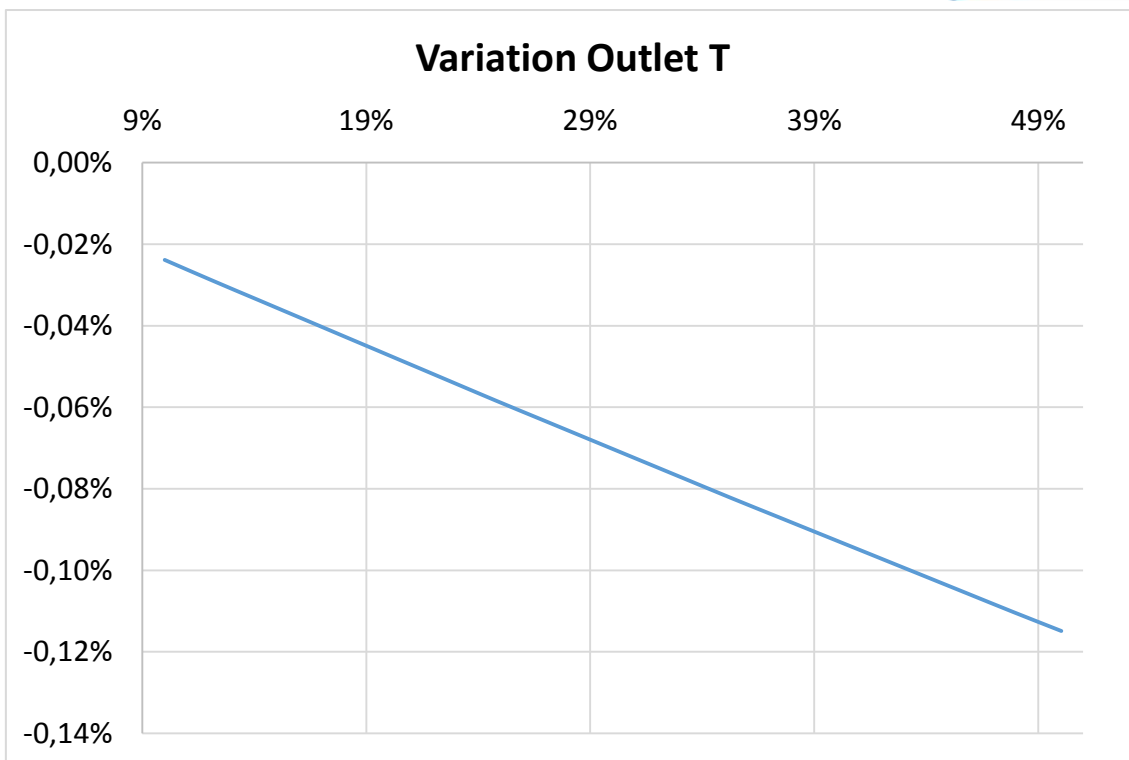


Figure-A 37. Graphs of the results for the heat losses test at 40°C expressed in percentages for different absorber's emittance.

- When the HTF's inlet temperature is 90°C:

Table A 39. Results from the heat losses test at 90°C expressed in percentages for different absorber's emittance.

Variation Absorber emittance	Variation Outlet T	Variation Heat Losses	Variation Enthalpy difference
0,00%	0,00%	0,00%	0,00%
10,00%	-0,02%	8,09%	7,99%
12,11%	-0,03%	9,77%	9,72%
14,21%	-0,03%	11,45%	11,23%
16,32%	-0,04%	13,12%	12,96%
18,43%	-0,04%	14,78%	14,69%
20,53%	-0,05%	16,44%	16,20%
22,64%	-0,05%	18,09%	17,93%
24,75%	-0,06%	19,72%	19,44%
26,85%	-0,06%	21,36%	21,17%
28,96%	-0,07%	23,00%	22,68%
31,07%	-0,07%	24,63%	24,41%
33,17%	-0,08%	26,24%	25,92%
35,28%	-0,08%	27,85%	27,43%
37,39%	-0,09%	29,45%	29,16%
39,50%	-0,09%	31,04%	30,67%
41,60%	-0,10%	32,63%	32,18%
43,71%	-0,10%	34,21%	33,91%
45,82%	-0,11%	35,78%	35,42%
47,92%	-0,11%	37,34%	36,93%
50,03%	-0,11%	38,90%	38,44%



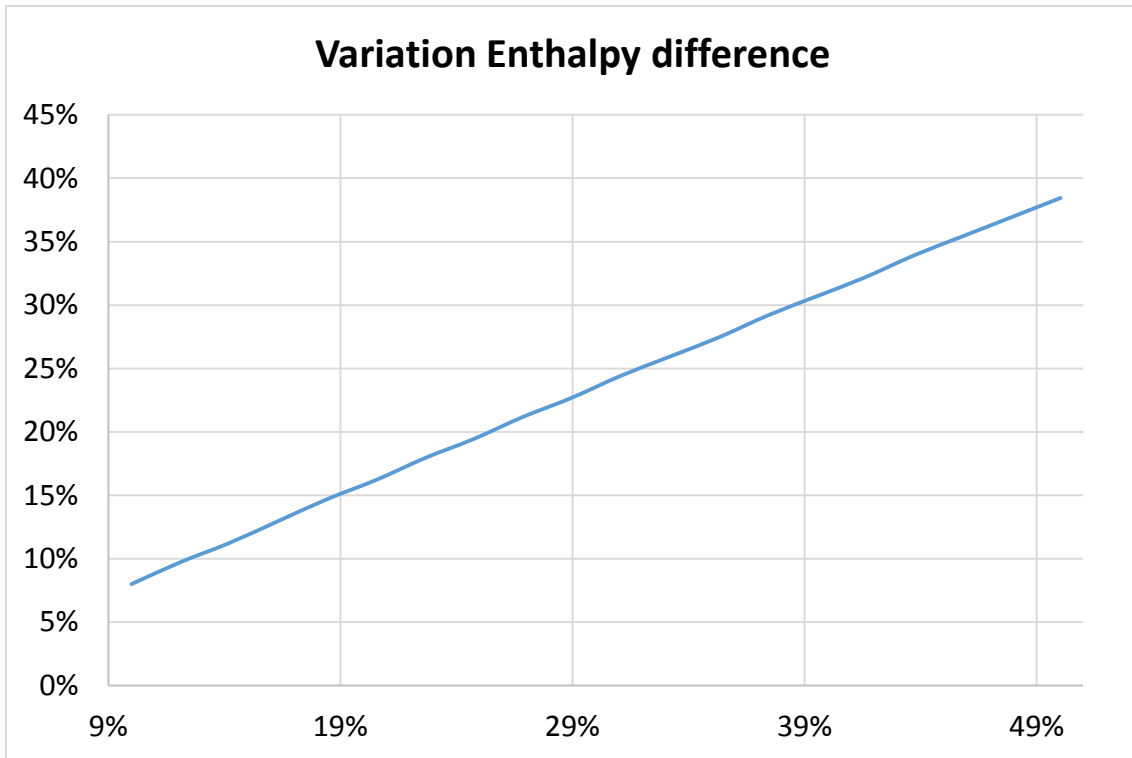
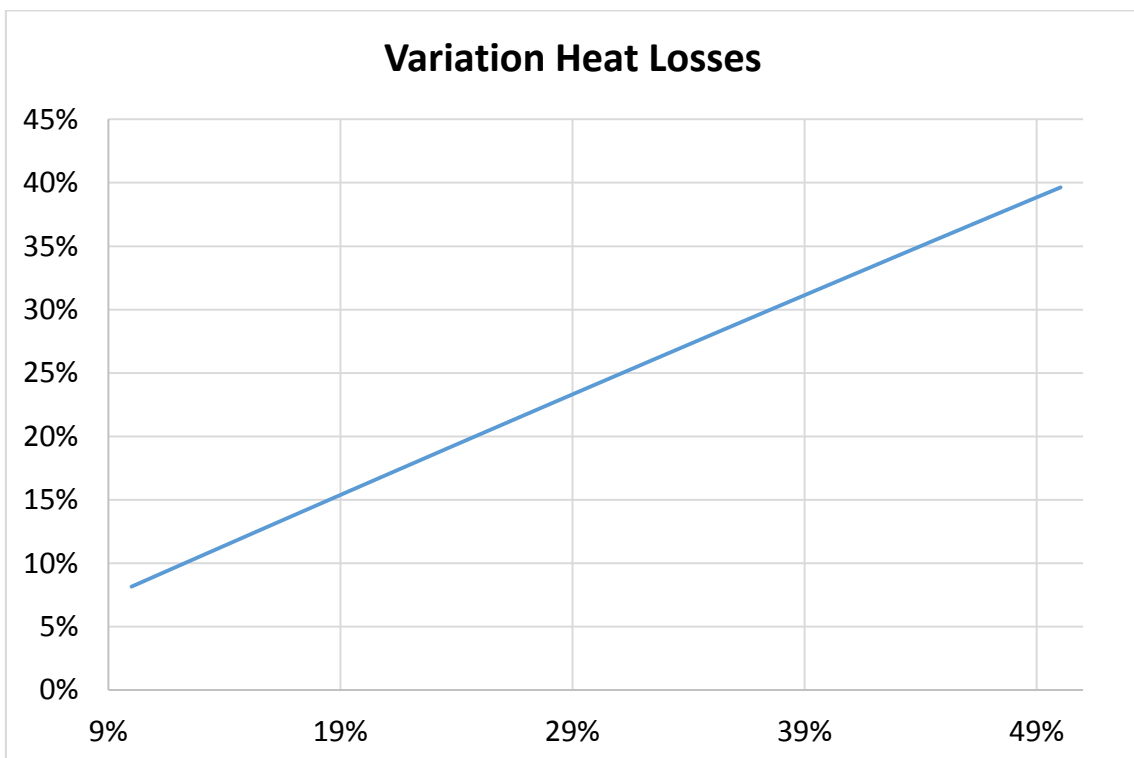
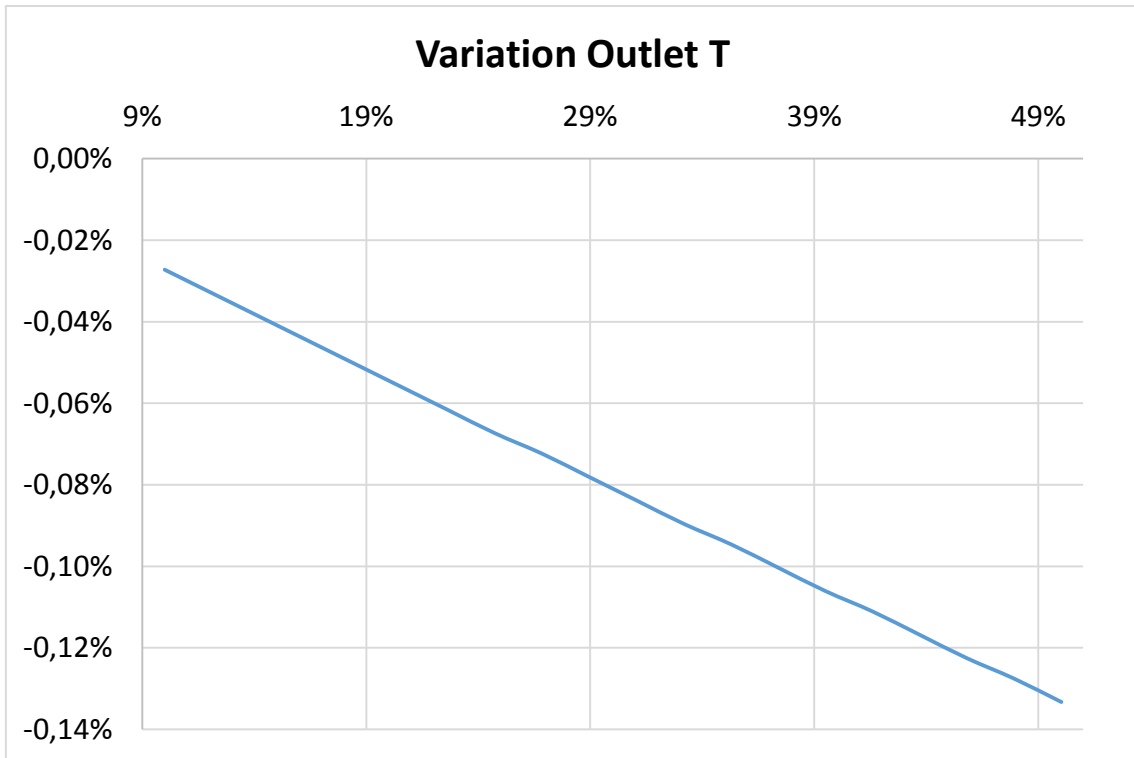


Figure-A 38. Graphs of the results for the heat losses test at 90°C expressed in percentages for different absorber's emittance.

- When the HTF's inlet temperature is 140°C:

Table A 40. Results from the heat losses test at 140°C expressed in percentages for different absorber's emittance.

Variation Absorber emittance	Variation Outlet T	Variation Heat Losses	Variation Enthalpy difference
0,00%	0,00%	0,00%	0,00%
10,00%	-0,03%	8,15%	8,01%
12,11%	-0,03%	9,85%	9,76%
14,21%	-0,04%	11,54%	11,38%
16,32%	-0,04%	13,23%	13,01%
18,43%	-0,05%	14,92%	14,75%
20,53%	-0,06%	16,60%	16,38%
22,64%	-0,06%	18,28%	18,00%
24,75%	-0,07%	19,95%	19,63%
26,85%	-0,07%	21,62%	21,37%
28,96%	-0,08%	23,28%	23,00%
31,07%	-0,08%	24,94%	24,62%
33,18%	-0,09%	26,59%	26,25%
35,28%	-0,09%	28,24%	27,87%
37,39%	-0,10%	29,88%	29,50%
39,50%	-0,11%	31,52%	31,13%
41,60%	-0,11%	33,15%	32,75%
43,71%	-0,12%	34,78%	34,38%
45,82%	-0,12%	36,40%	35,89%
47,93%	-0,13%	38,02%	37,51%
50,03%	-0,13%	39,64%	39,14%



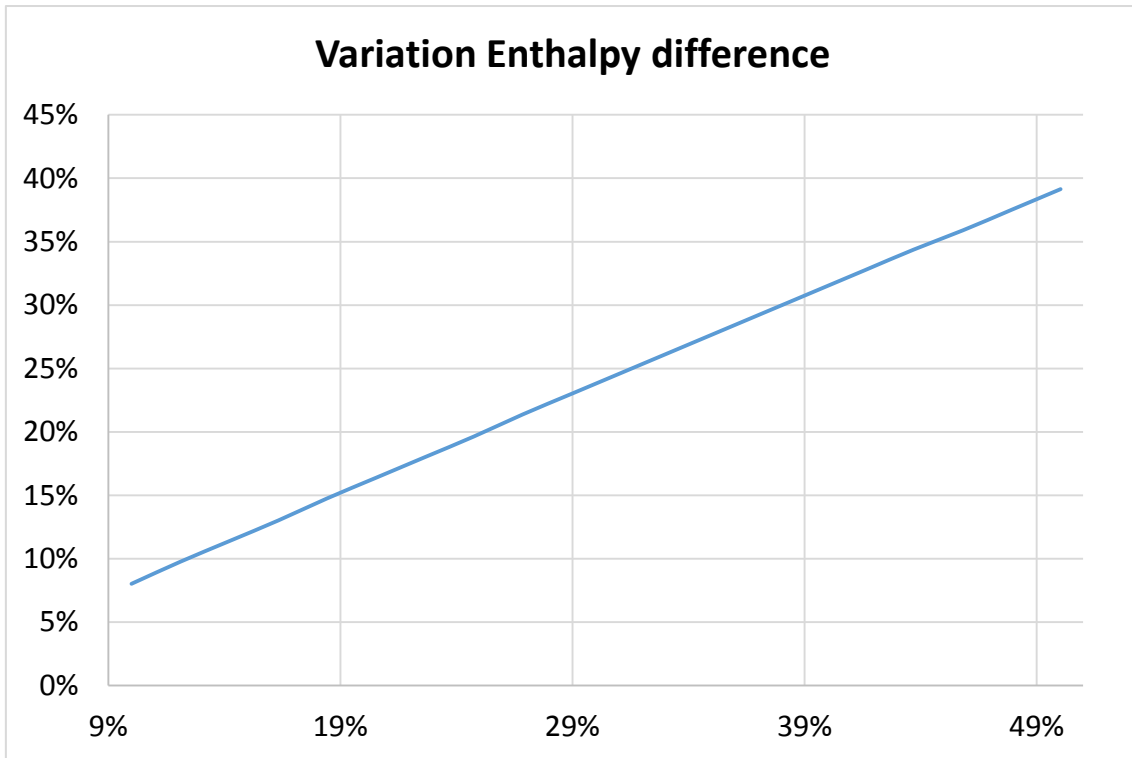
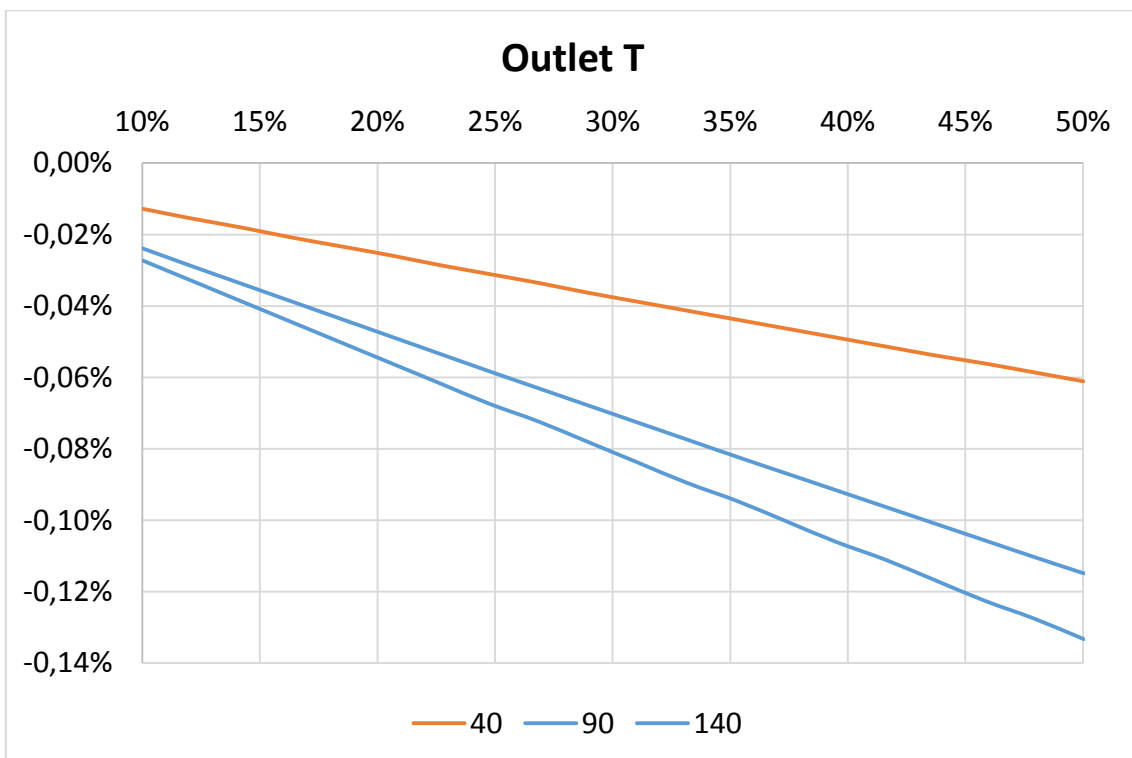


Figure-A 39. Graphs of the results for the heat losses test at 140°C expressed in percentages for different absorber's emittance.

- Comparing the three cases:



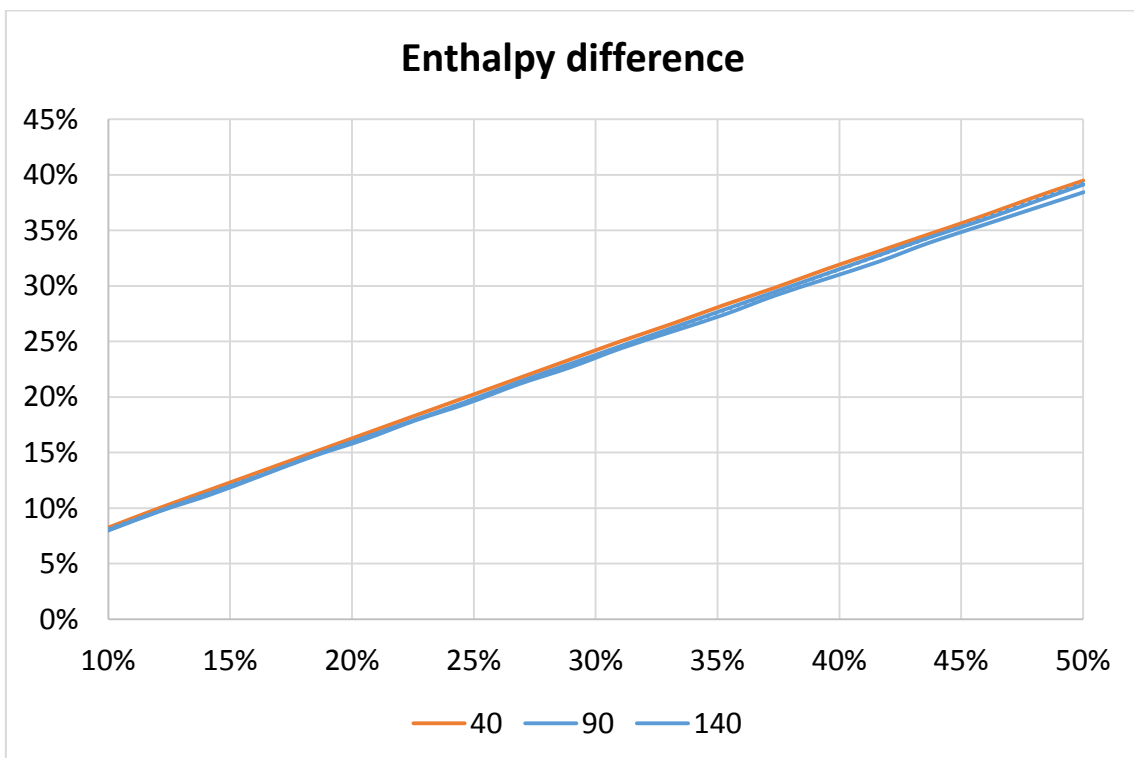
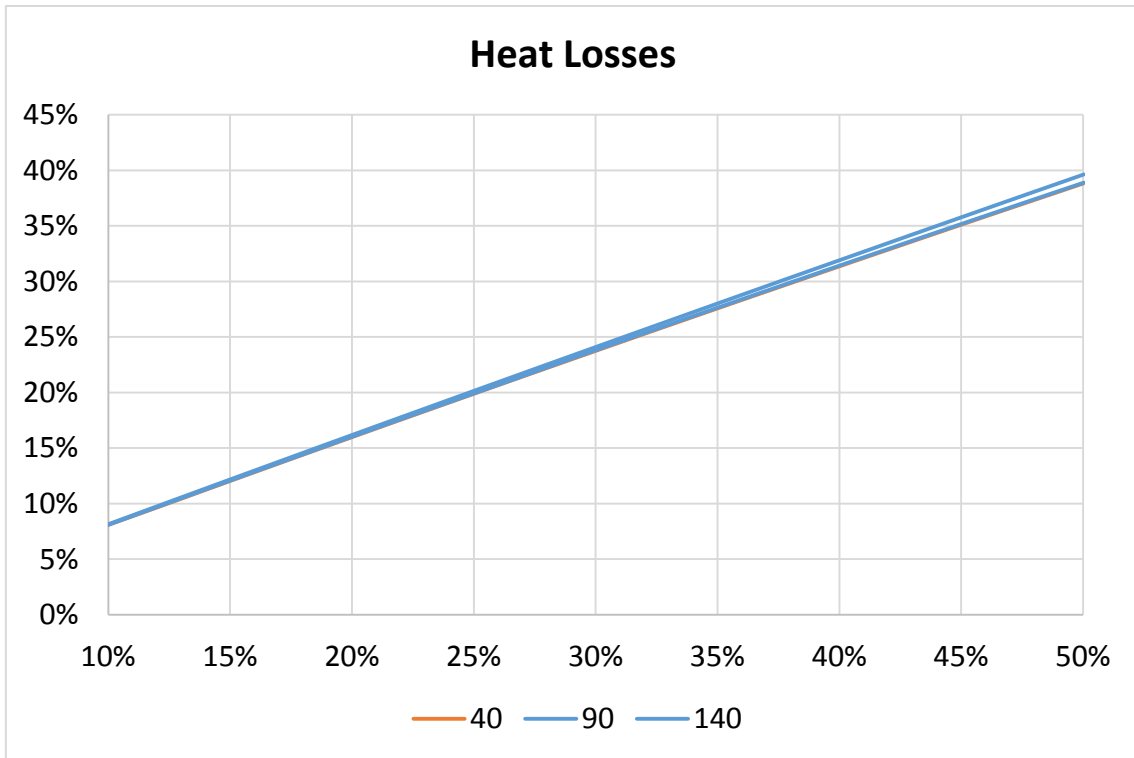
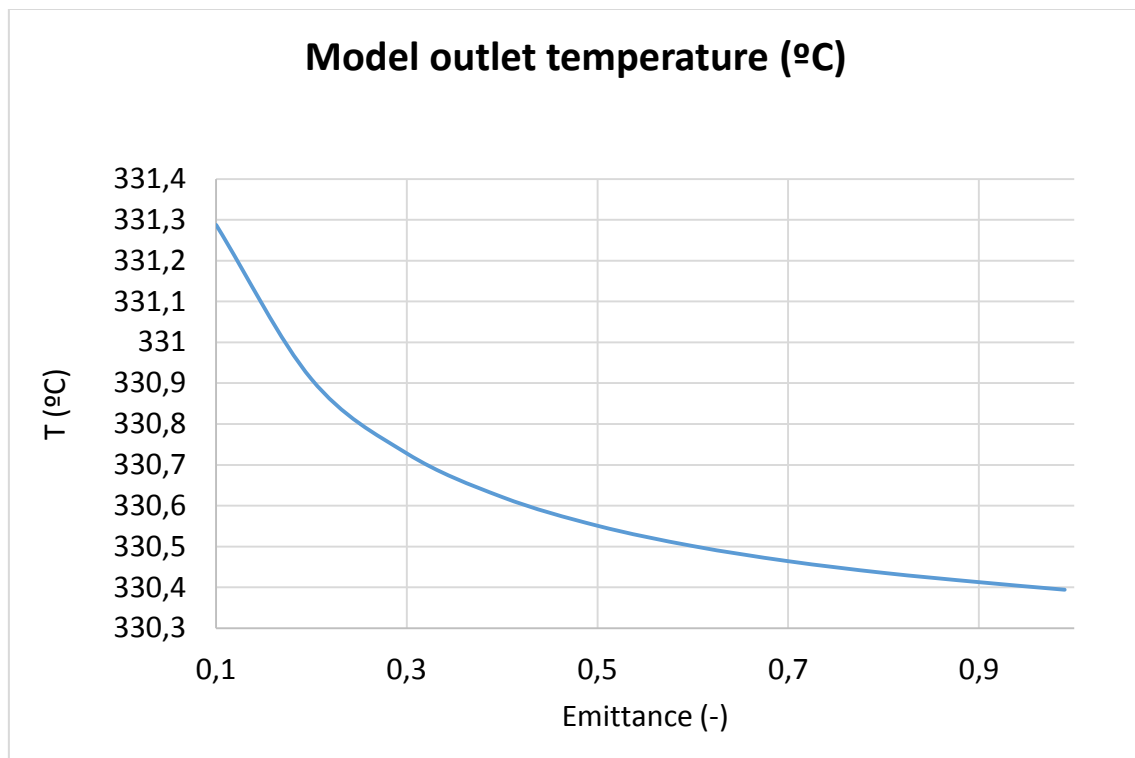


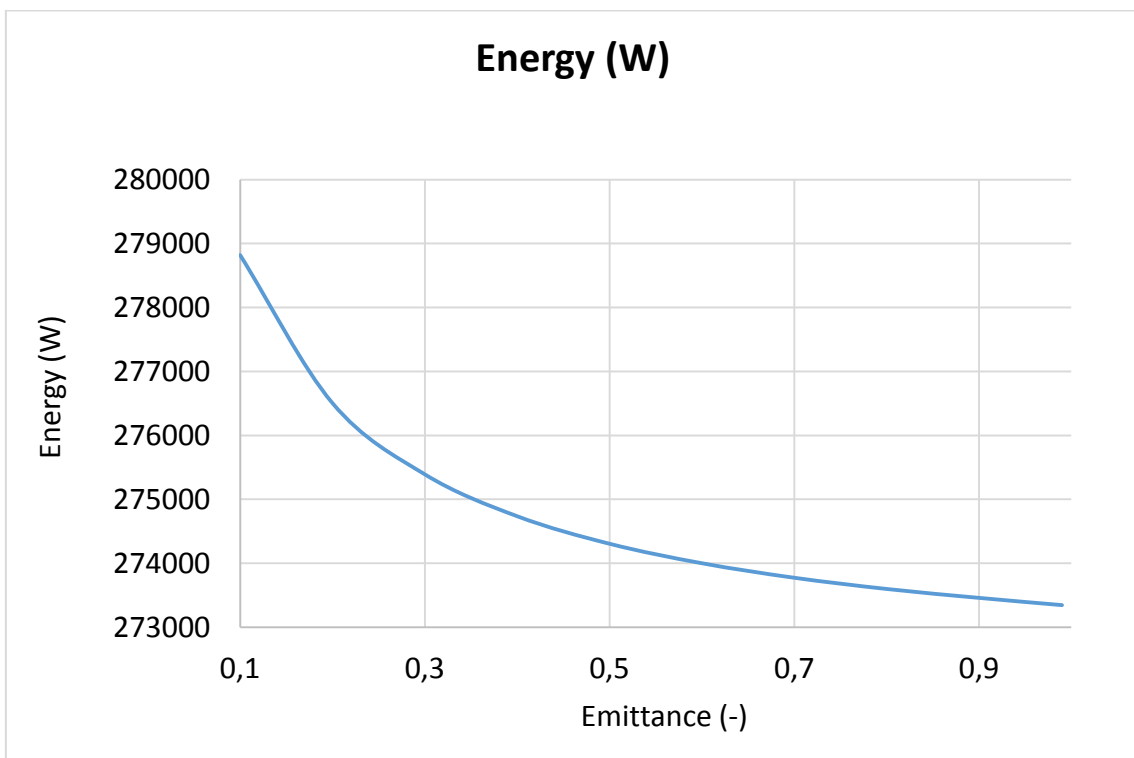
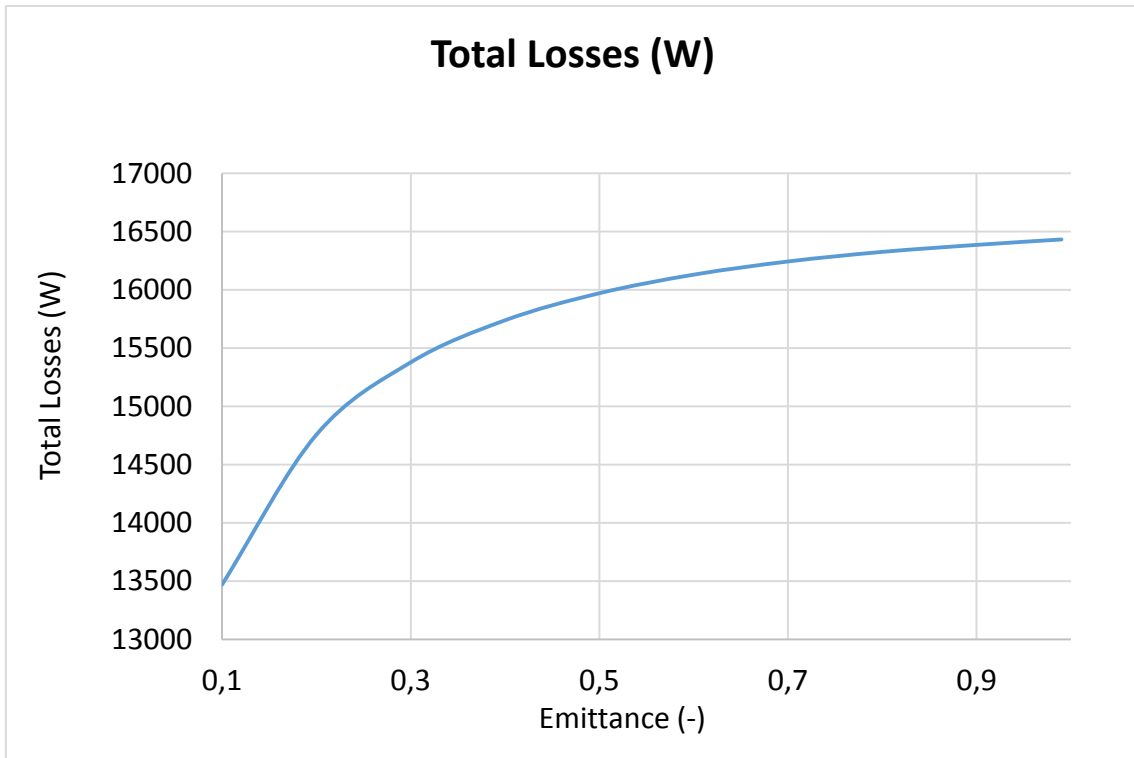
Figure-A 40. Graphs of the results for the heat losses test expressed in percentages for different absorber's emittance.

Emittance of the glass cover

Table A 41. Results for the dynamic efficiency test for different values of the emittance of the glass cover.

Test	Incidence angle (°)	Glass emittance (-)	Model outlet temperature (°C)	Total Losses (W)	Energy (W)	Useful Solar Radiant Power (W)	Model efficiency (%)
1	16,37	0,85	330,42	16357,62	273524,09	370869,74	73,7521%
2	16,37	0,1	331,29	13471,55	278818,80	370869,74	75,1797%
3	16,37	0,2	330,91	14757,32	276503,19	370869,74	74,5553%
4	16,37	0,3	330,73	15377,87	275389,47	370869,74	74,2550%
5	16,37	0,4	330,62	15738,64	274734,86	370869,74	74,0785%
6	16,37	0,5	330,55	15970,70	274304,33	370869,74	73,9624%
7	16,37	0,6	330,50	16129,90	273999,66	370869,74	73,8803%
8	16,37	0,7	330,46	16242,97	273772,85	370869,74	73,8191%
9	16,37	0,8	330,44	16325,37	273597,58	370869,74	73,7719%
10	16,37	0,9	330,41	16385,37	273458,11	370869,74	73,7343%
11	16,37	0,99	330,39	16432,11	273344,47	370869,74	73,7036%





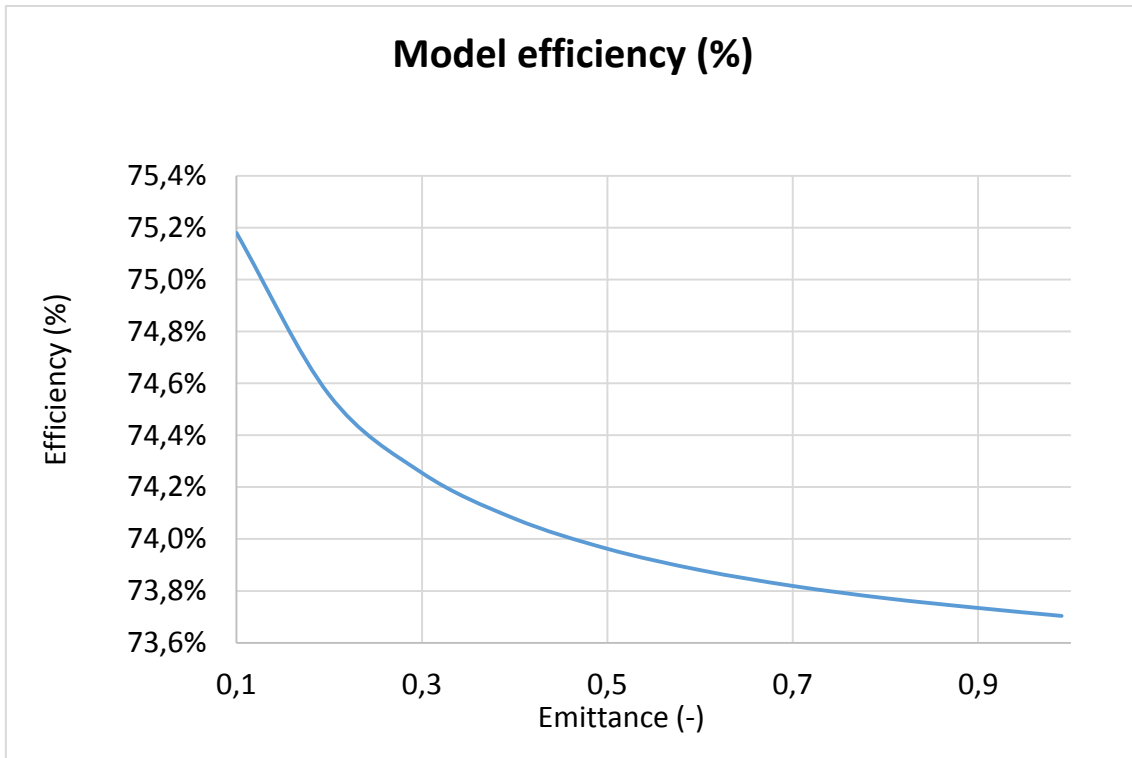
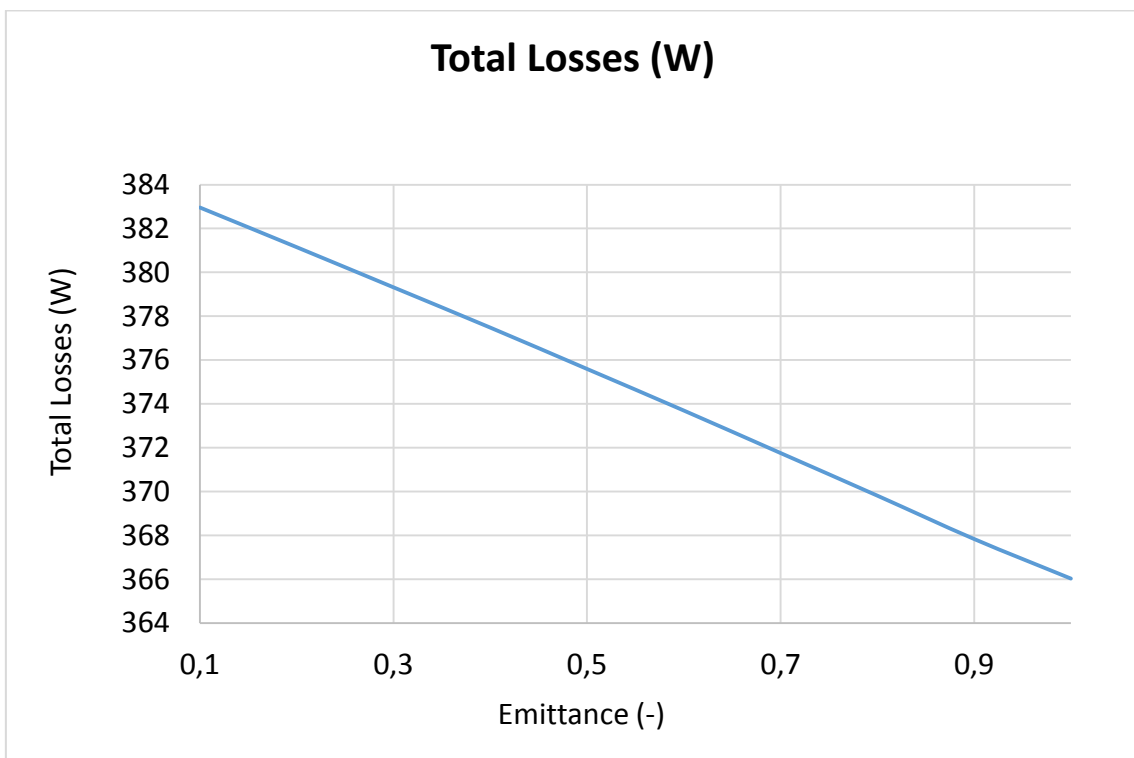
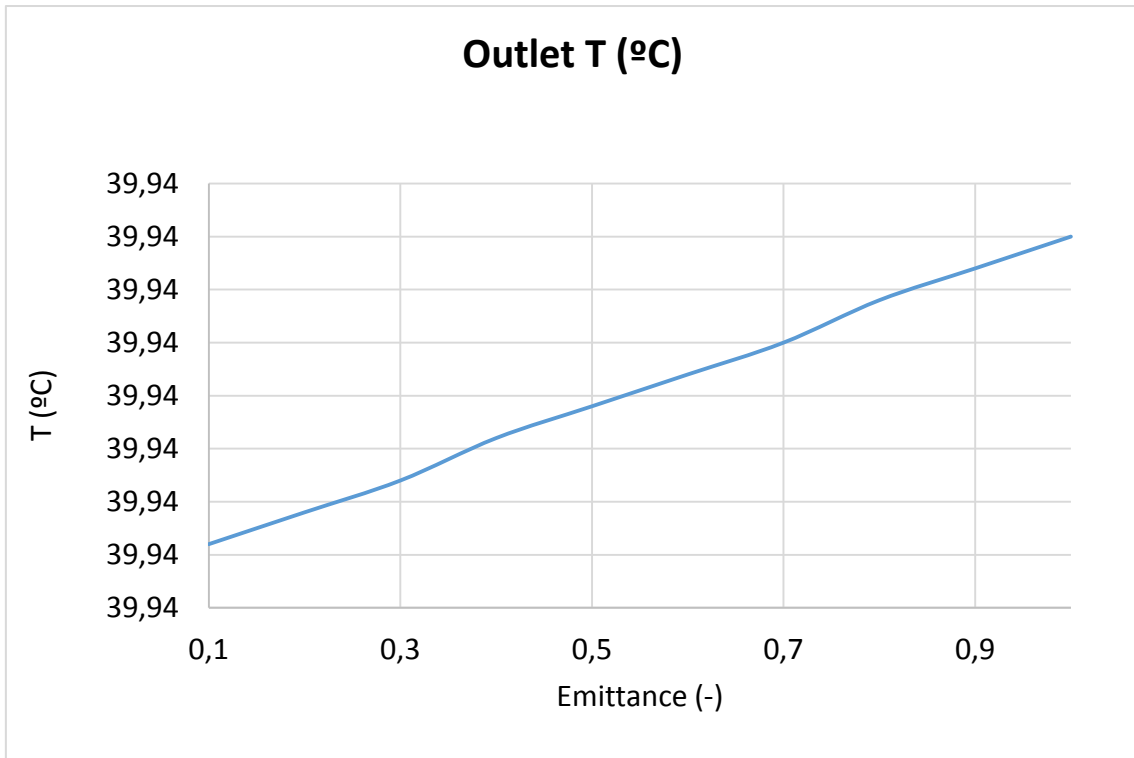


Figure-A 41. Graphs of the results for the dynamic efficiency test when the emittance of the glass cover varies.

- When the HTF's inlet temperature is 40°C:

Table A 42. Results from the heat losses test at 40°C for different values of glass cover's emittance.

Test	Glass emittance (-)	Outlet T (°C)	Total Losses (W)	Enthalpy difference (W)
1	0,85	39,94	368,82	364,13
2	0,1	39,94	382,96	378,44
3	0,2	39,94	381,15	376,29
4	0,3	39,94	379,32	374,51
5	0,4	39,94	377,48	372,72
6	0,5	39,94	375,59	370,93
7	0,6	39,94	373,69	369,14
8	0,7	39,94	371,75	366,99
9	0,8	39,94	369,81	365,21
10	0,9	39,94	367,83	363,06
11	1	39,94	366,03	361,27



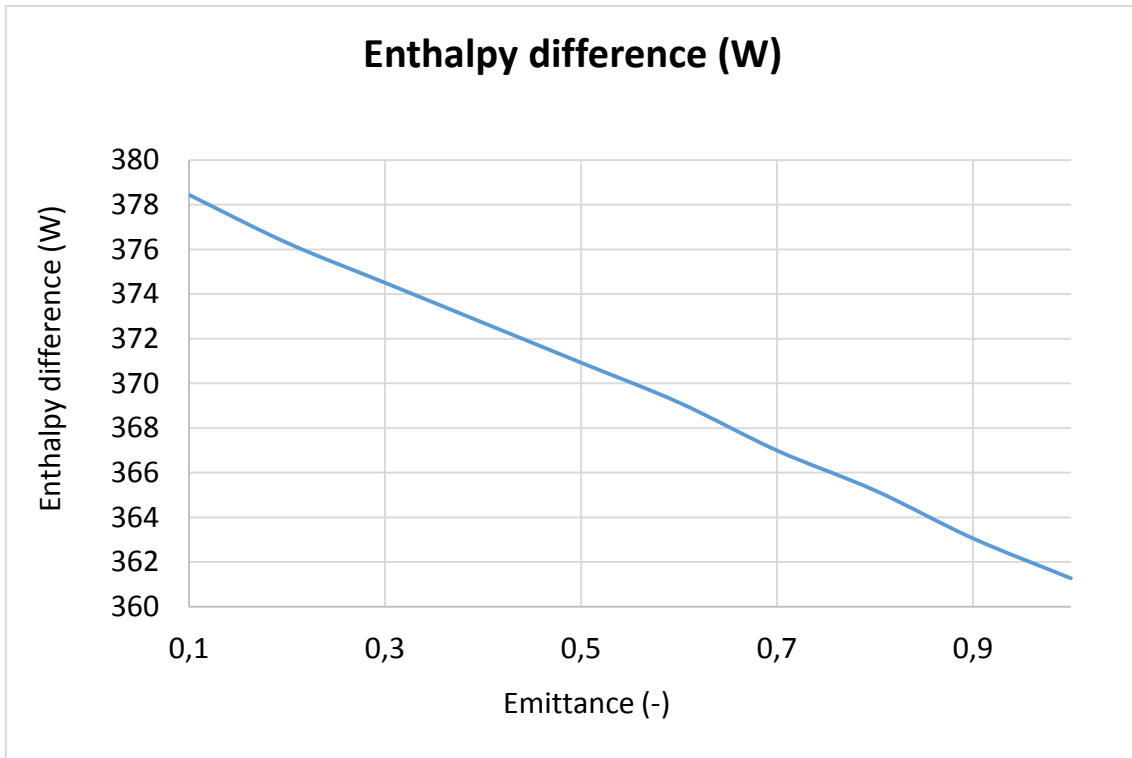
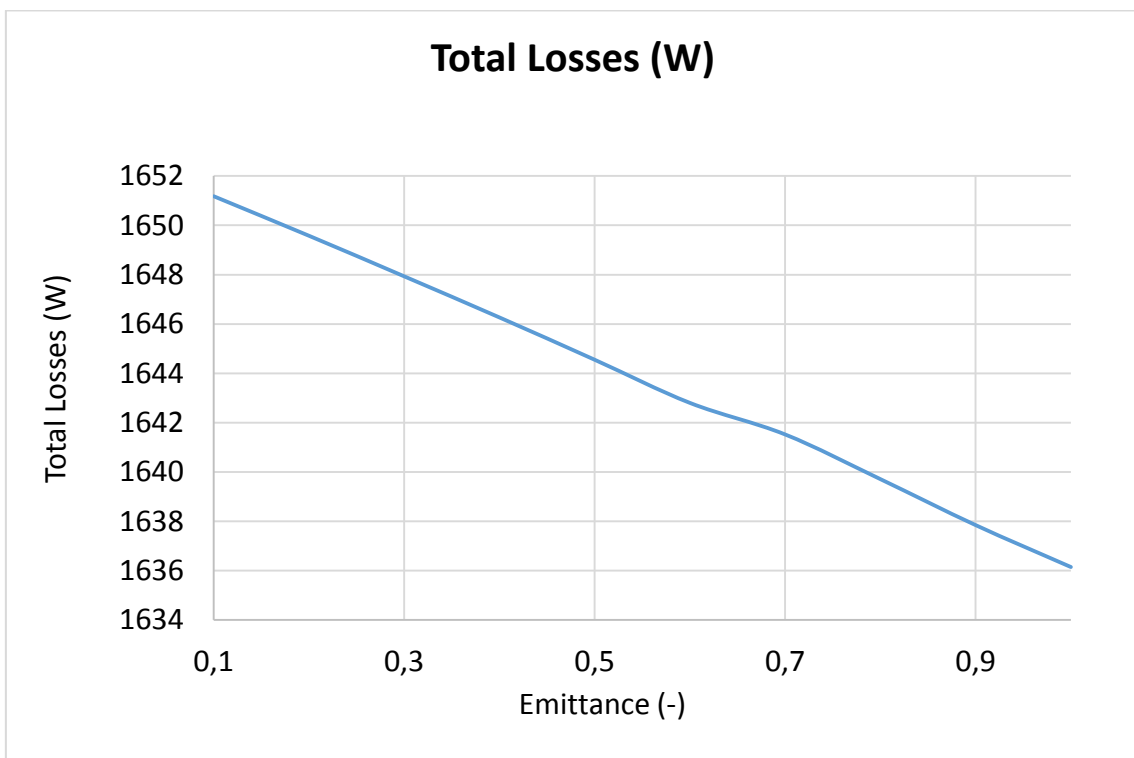
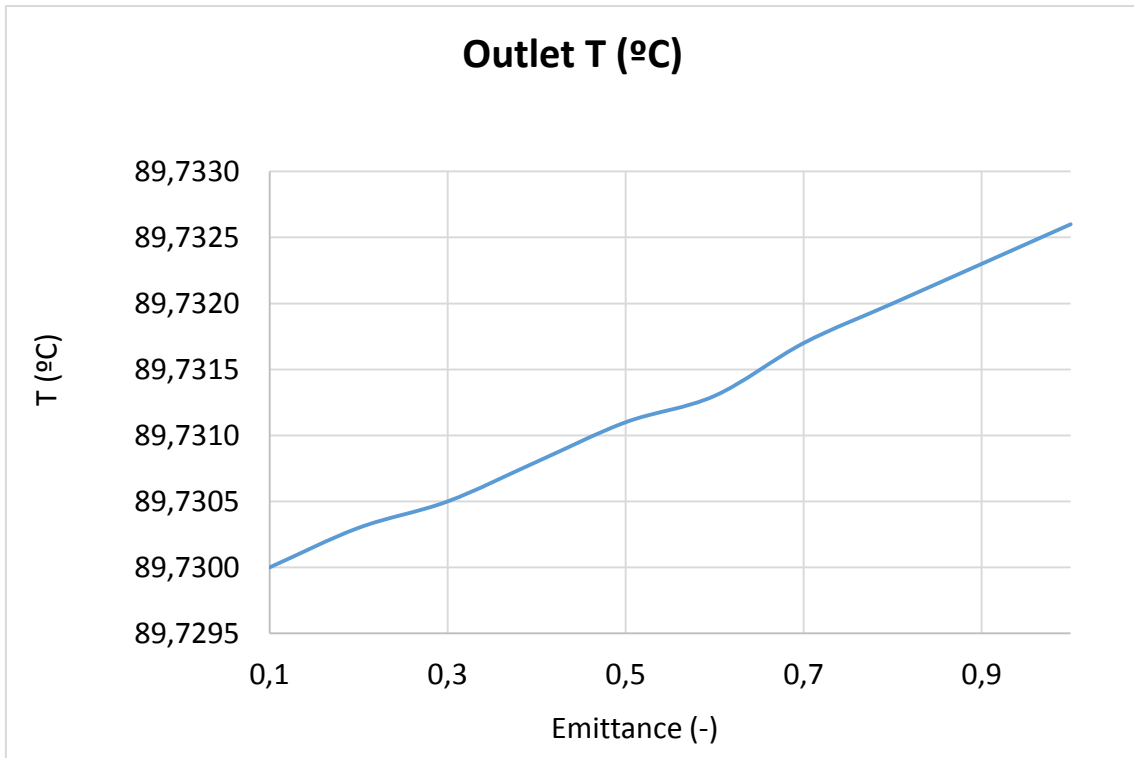


Figure-A 42. Graphs of the results for the heat losses test at 40°C for different values of glass cover's emittance.

- When the HTF's inlet temperature is 90°C:

Table A 43. Results from the heat losses test at 90°C for different values of glass cover's emittance.

Test	Glass emittance (-)	Outlet T (°C)	Total Losses (W)	Enthalpy difference (W)
1	0,85	89,73	1638,78	1656,12
2	0,1	89,73	1651,18	1670,43
3	0,2	89,73	1649,58	1666,86
4	0,3	89,73	1647,93	1666,86
5	0,4	89,73	1646,27	1663,28
6	0,5	89,73	1644,55	1663,28
7	0,6	89,73	1642,80	1659,70
8	0,7	89,73	1641,52	1659,70
9	0,8	89,73	1639,71	1656,12
10	0,9	89,73	1637,85	1656,12
11	1	89,73	1636,15	1652,55



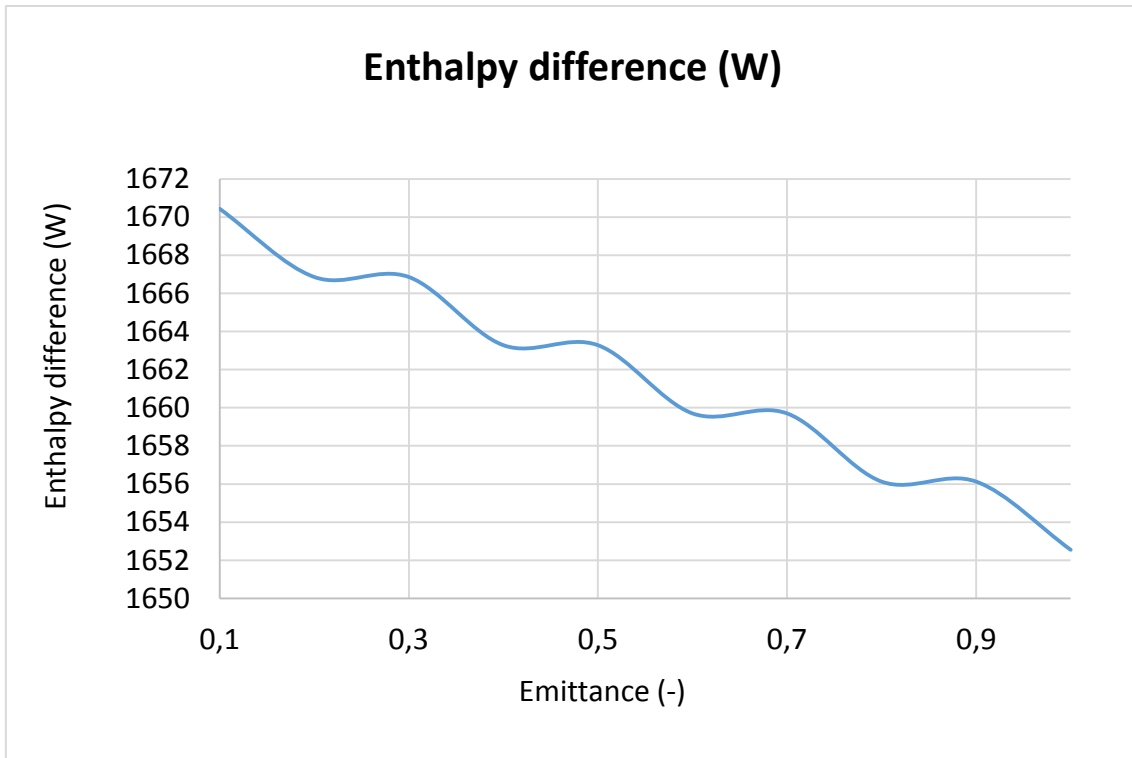
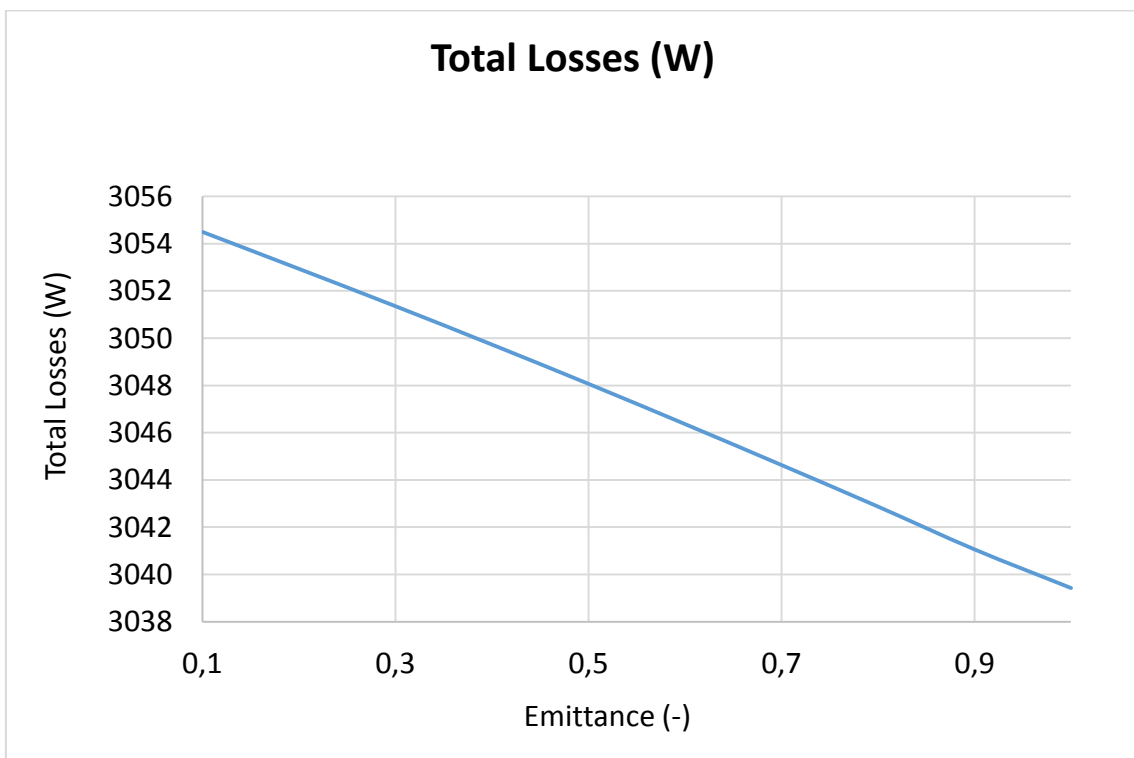
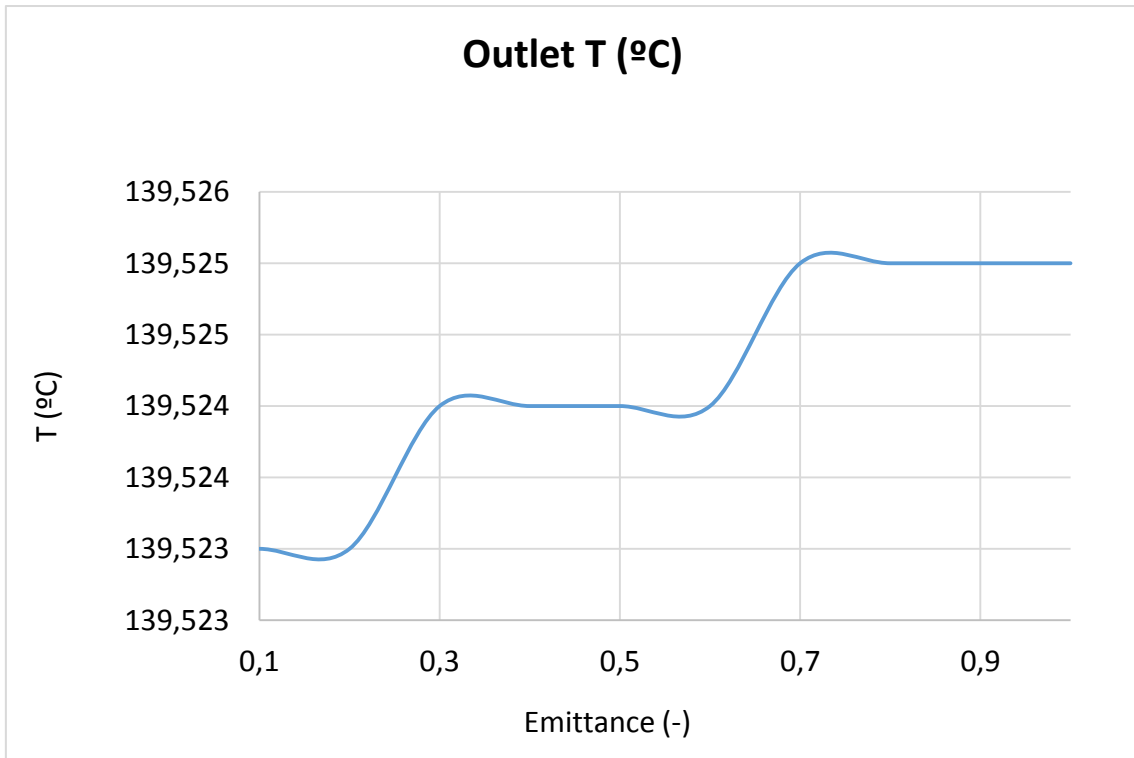


Figure-A 43. Graphs of the results for the heat losses test at 90°C for different values of glass cover's emittance.

- When the HTF's inlet temperature is 140°C:

Table A 44. Results from the heat losses test at 140°C for different values of glass cover's emittance.

Test	Glass emittance (-)	Outlet T (°C)	Total Losses (W)	Enthalpy difference (W)
1	0,85	139,525	3041,97	3079,75
2	0,1	139,523	3054,50	3090,48
3	0,2	139,523	3052,93	3090,48
4	0,3	139,524	3051,35	3086,90
5	0,4	139,524	3049,73	3086,90
6	0,5	139,524	3048,07	3083,33
7	0,6	139,524	3046,36	3083,33
8	0,7	139,525	3044,63	3079,75
9	0,8	139,525	3042,87	3079,75
10	0,9	139,525	3041,06	3079,75
11	1	139,525	3039,43	3076,17



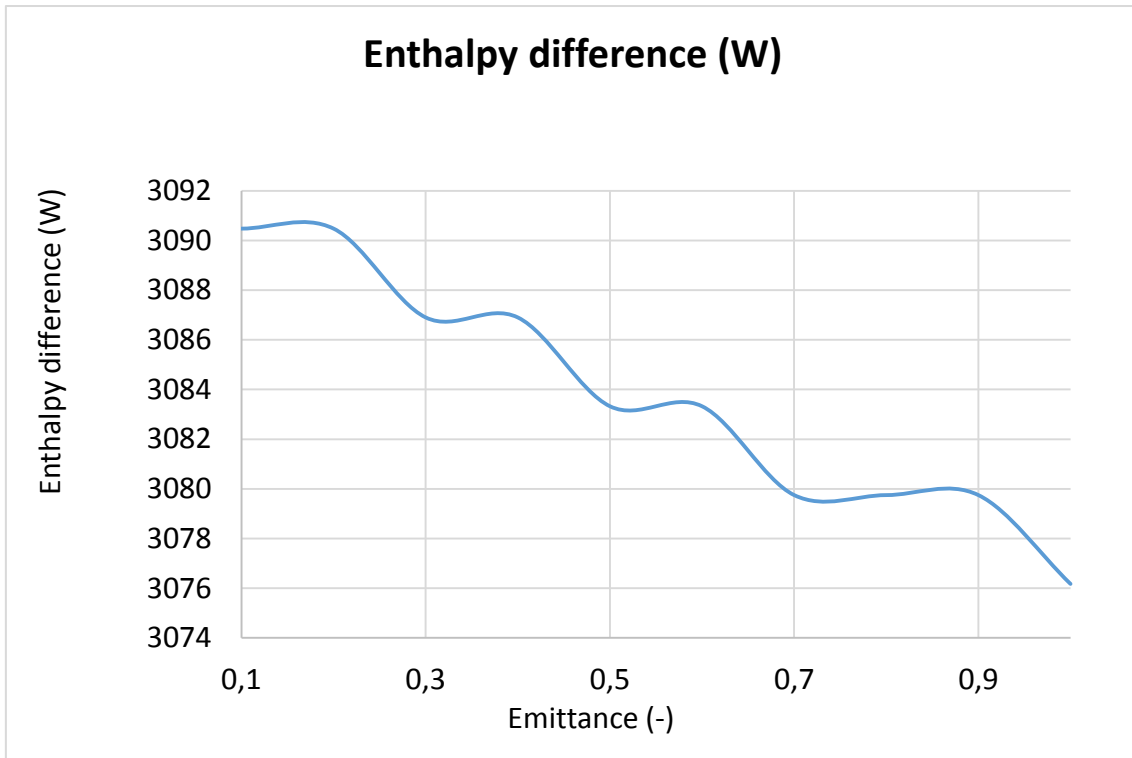
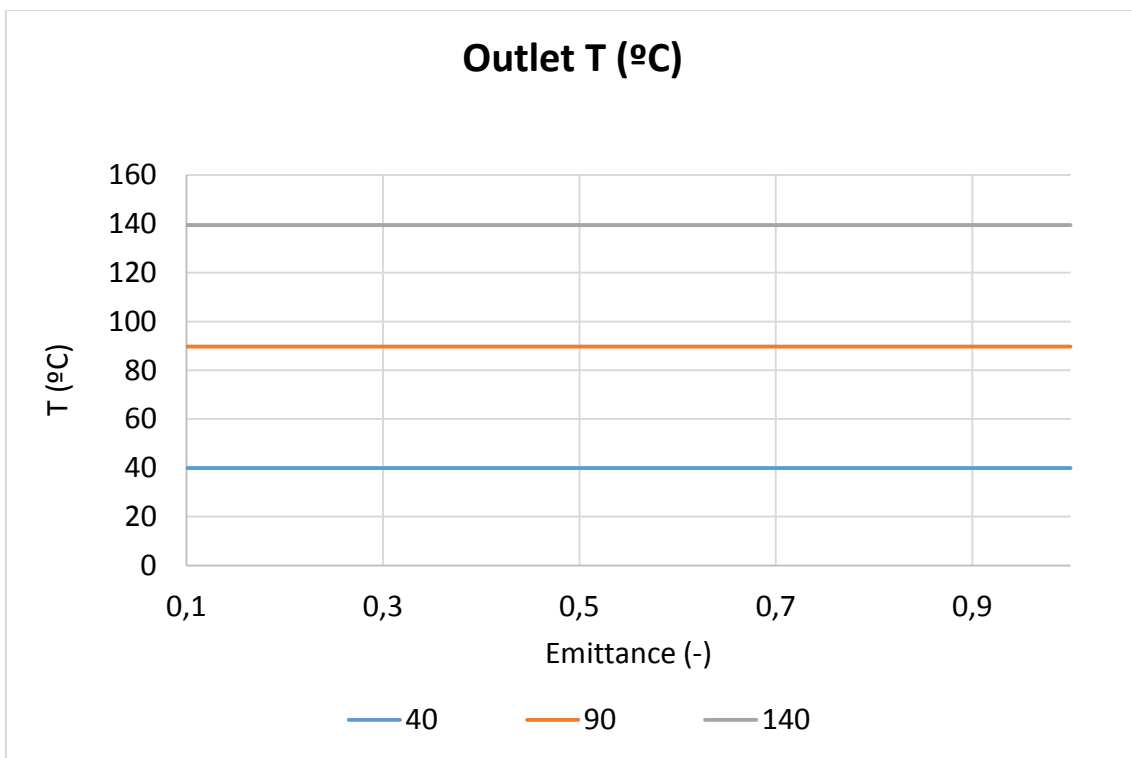


Figure-A 44. Graphs of the results for the heat losses test at 140°C for different values of glass cover's emittance.

- Comparing the three cases:



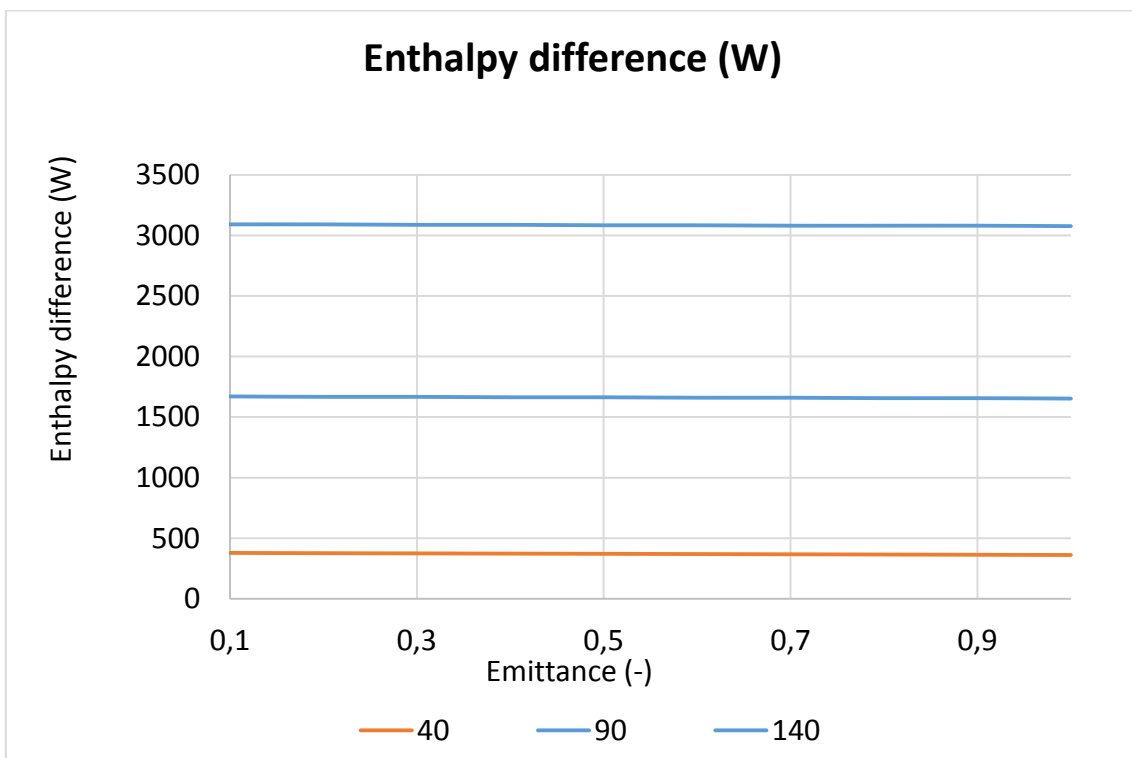
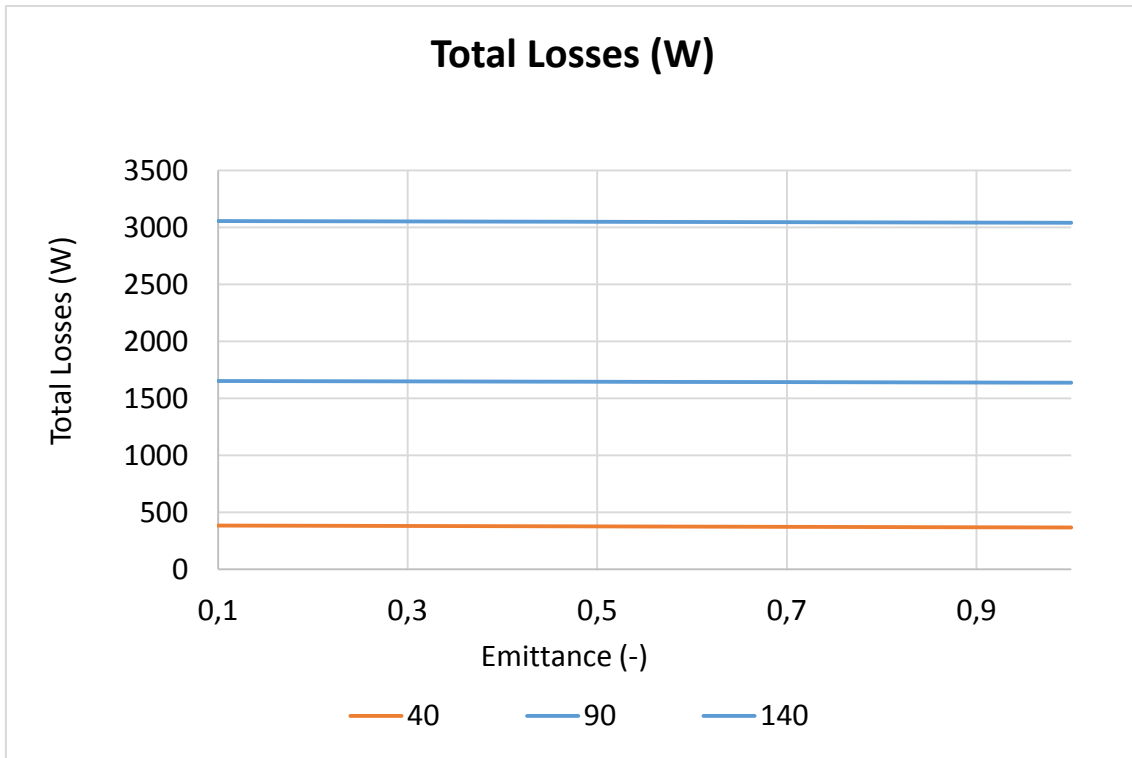
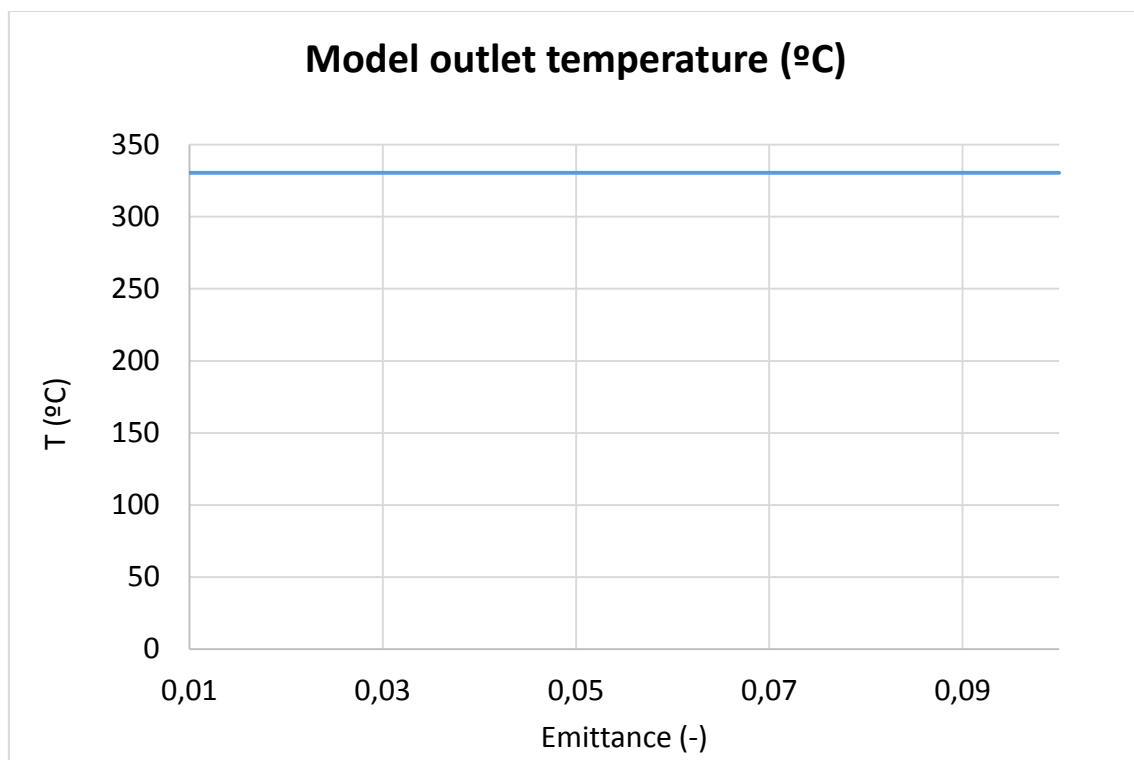


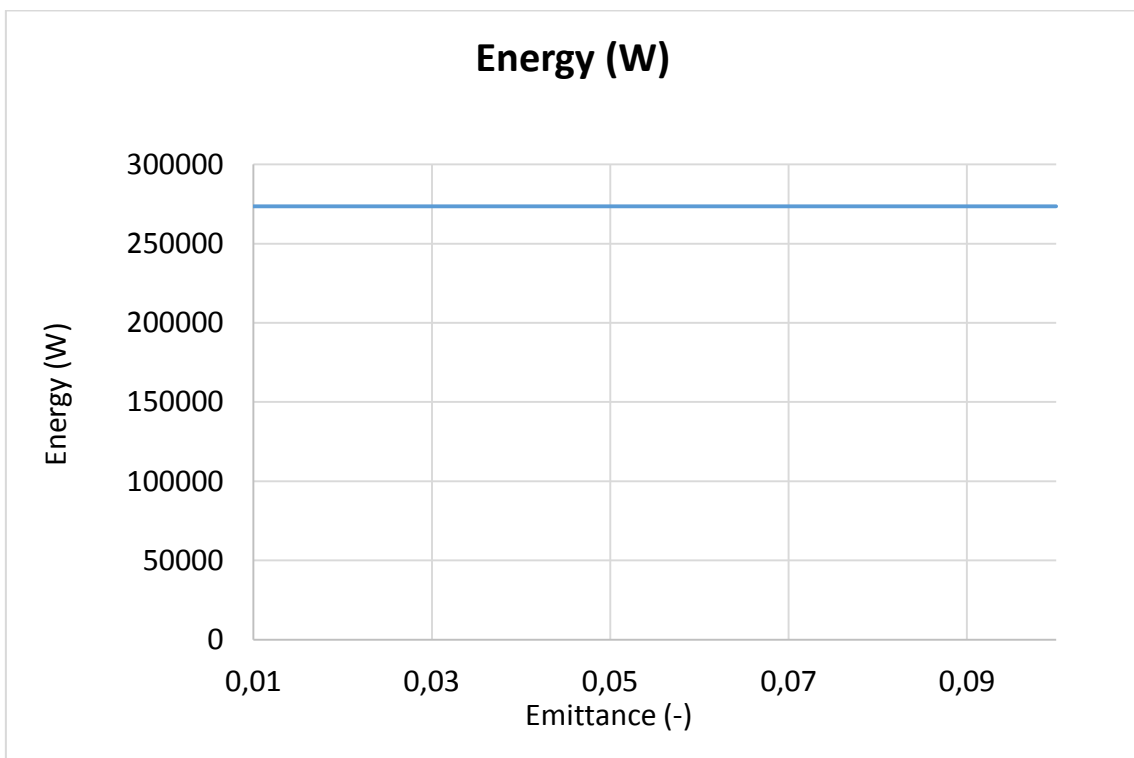
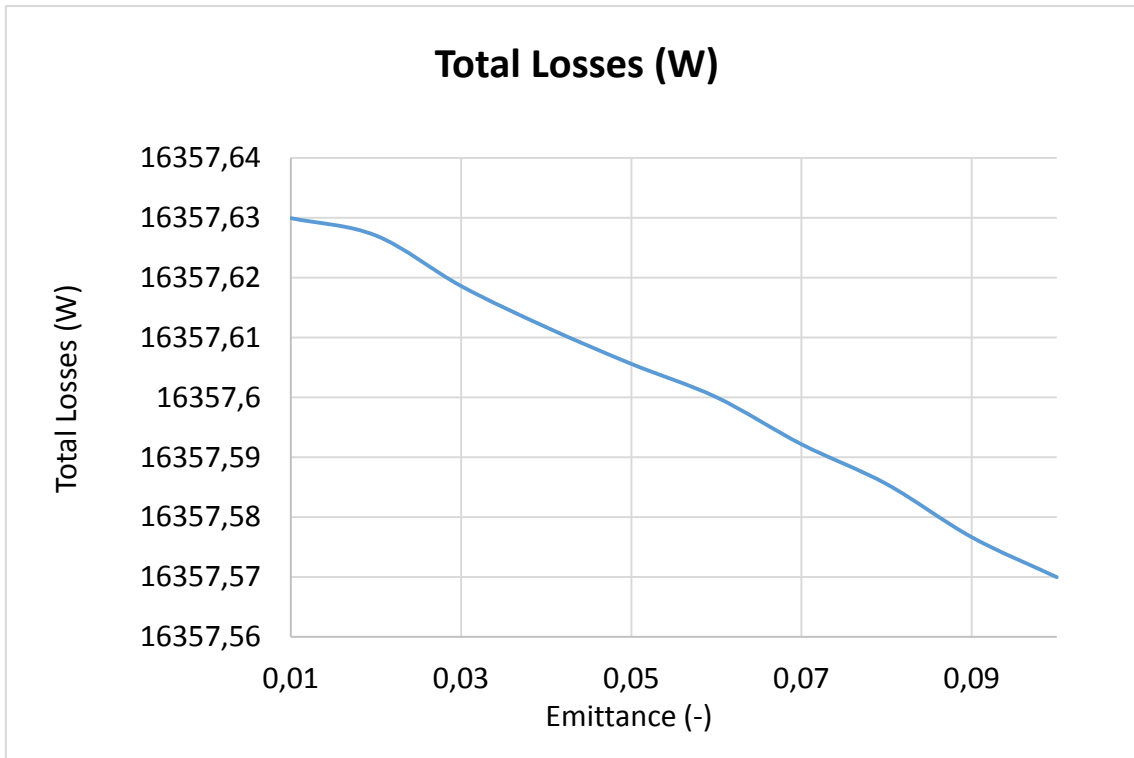
Figure-A 45. Graphs of the results for the heat losses for different values of glass cover's emittance.

Emittance of the shield

Table A 45. Results for the dynamic efficiency test for different values of the emittance of the shield.

Test	Incidence angle (°)	Shield emittance (-)	Model outlet temperature (°C)	Total Losses (W)	Energy (W)	Useful Solar Radiant Power (W)	Model efficiency (%)
1	16,37	0,03	330,42	16357,62	273524,09	370869,74	73,75%
2	16,37	0,01	330,42	16357,63	273524,09	370869,74	73,75%
3	16,37	0,02	330,42	16357,63	273524,09	370869,74	73,75%
4	16,37	0,03	330,42	16357,67	273524,09	370869,74	73,75%
5	16,37	0,04	330,42	16357,61	273524,09	370869,74	73,75%
6	16,37	0,05	330,42	16357,61	273524,09	370869,74	73,75%
7	16,37	0,06	330,42	16357,60	273524,09	370869,74	73,75%
8	16,37	0,07	330,42	16357,59	273524,09	370869,74	73,75%
9	16,37	0,08	330,42	16357,59	273524,09	370869,74	73,75%
10	16,37	0,09	330,42	16357,58	273524,09	370869,74	73,75%
11	16,37	0,1	330,42	16357,57	273524,09	370869,74	73,75%





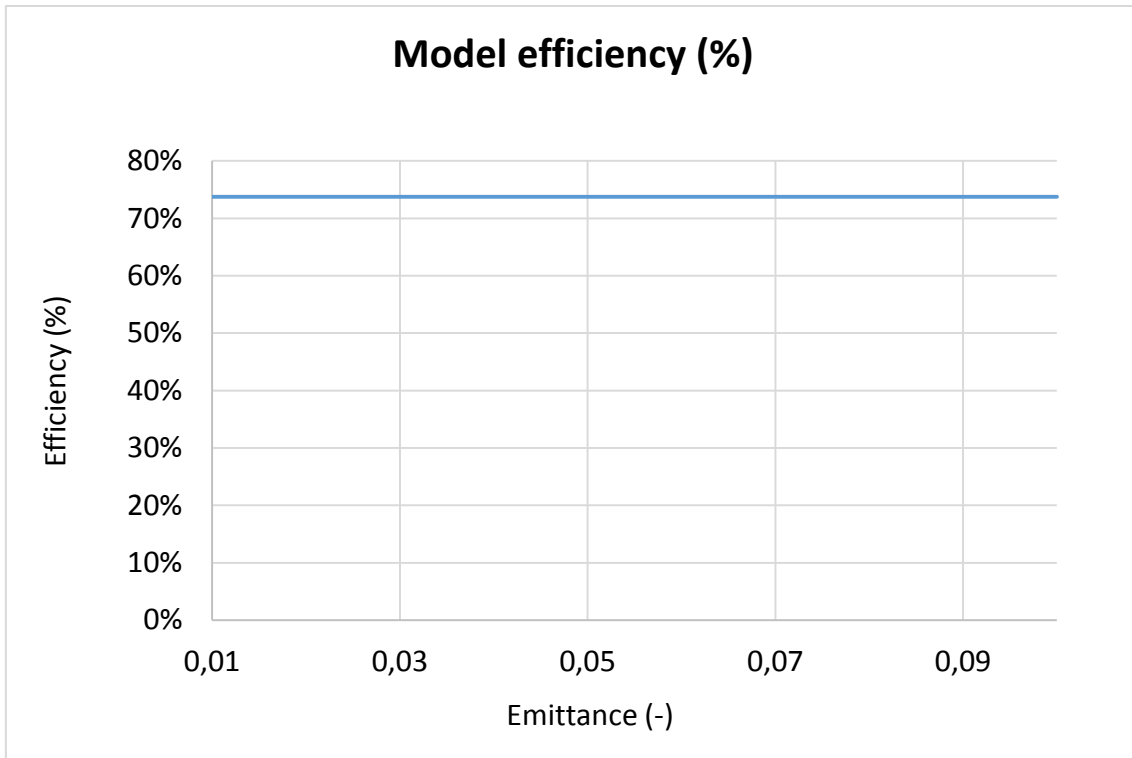
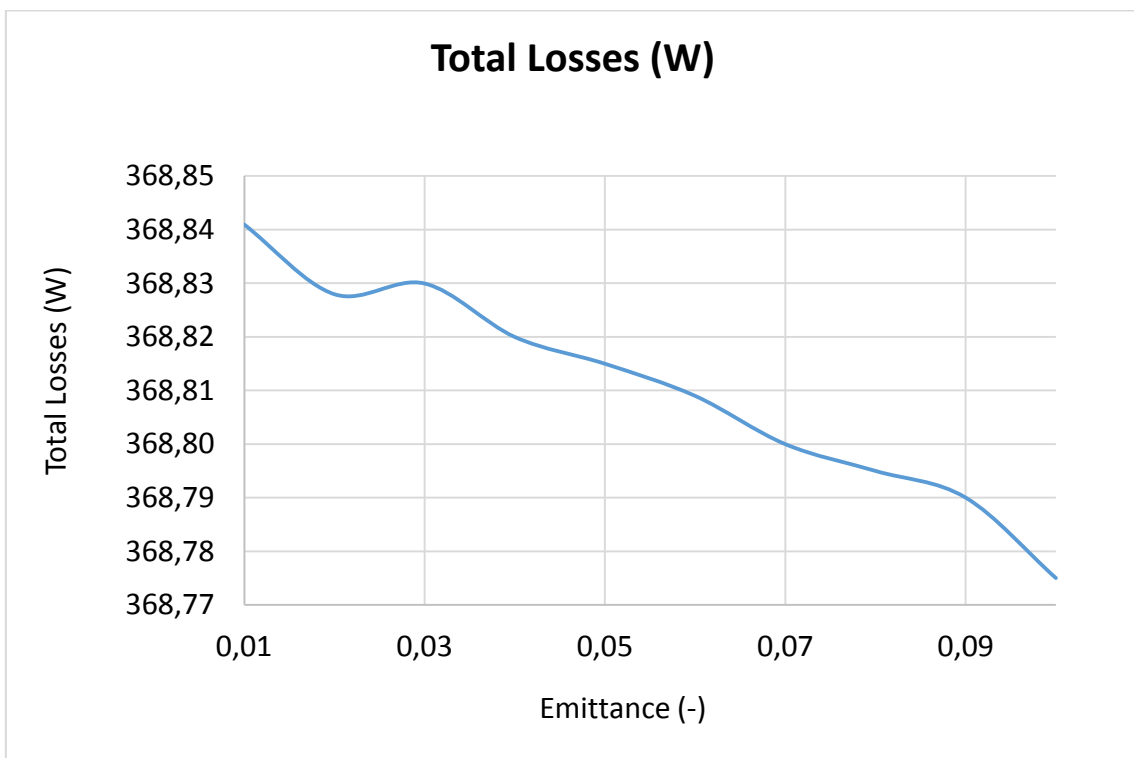
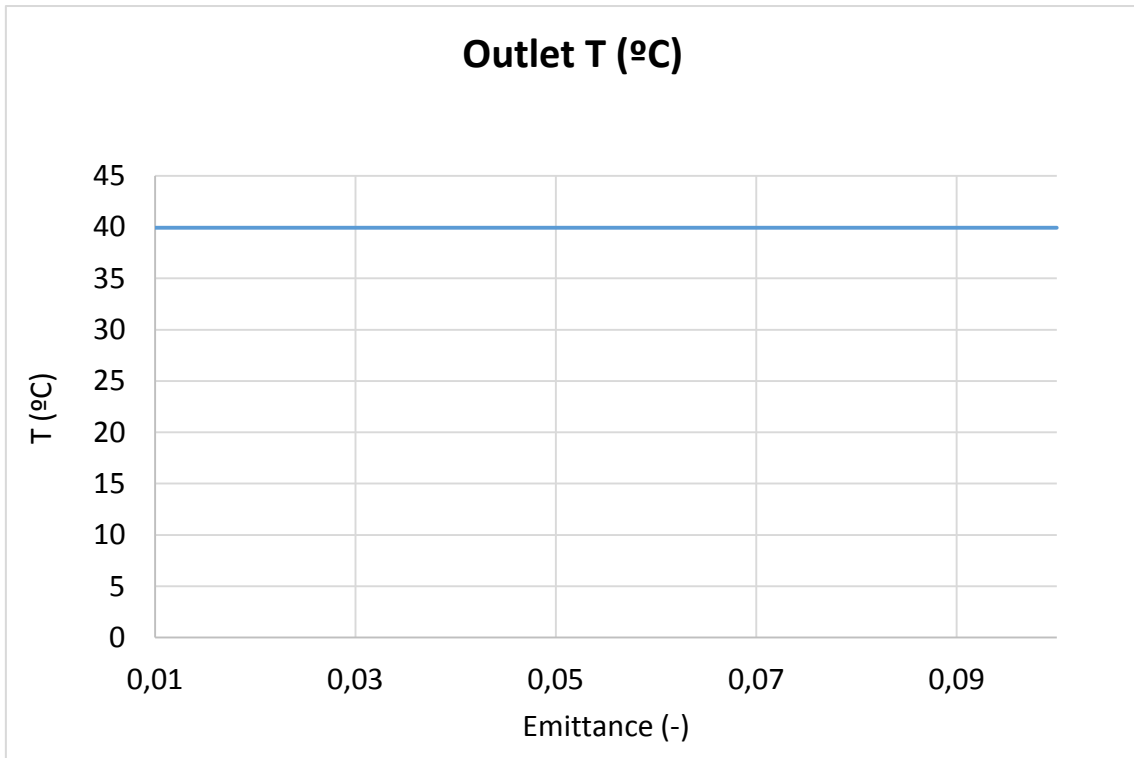


Figure-A 46. Graphs of the results for the dynamic efficiency test when the emittance of the shield varies.

- When the HTF's inlet temperature is 40°C:

Table A 46. Results from the heat losses test at 40°C for different values of shield's emittance.

Test	Glass emittance (-)	Outlet T (°C)	Total Losses (W)	Enthalpy difference (W)
1	0,03	39,94	368,82	364,13
2	0,01	39,94	368,84	364,13
3	0,02	39,94	368,83	364,13
4	0,03	39,94	368,83	364,13
5	0,04	39,94	368,82	364,13
6	0,05	39,94	368,81	364,13
7	0,06	39,94	368,81	364,13
8	0,07	39,94	368,80	364,13
9	0,08	39,94	368,79	364,13
10	0,09	39,94	368,79	364,13
11	0,1	39,94	368,78	364,13



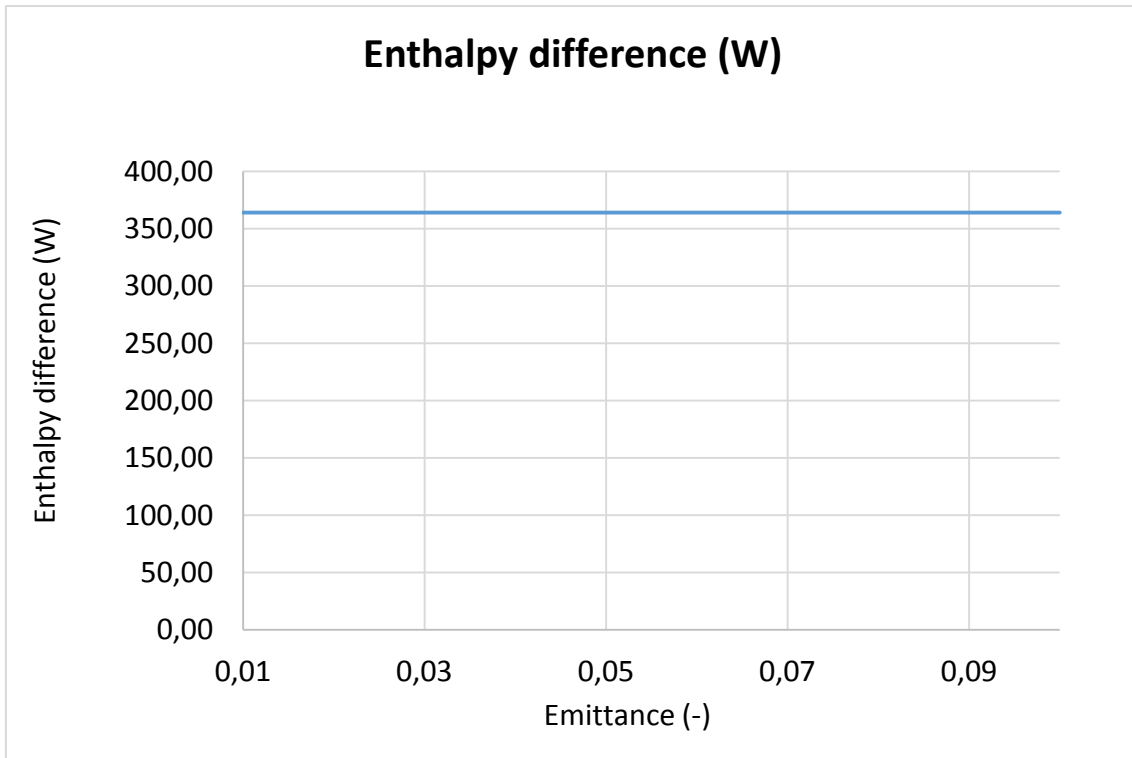
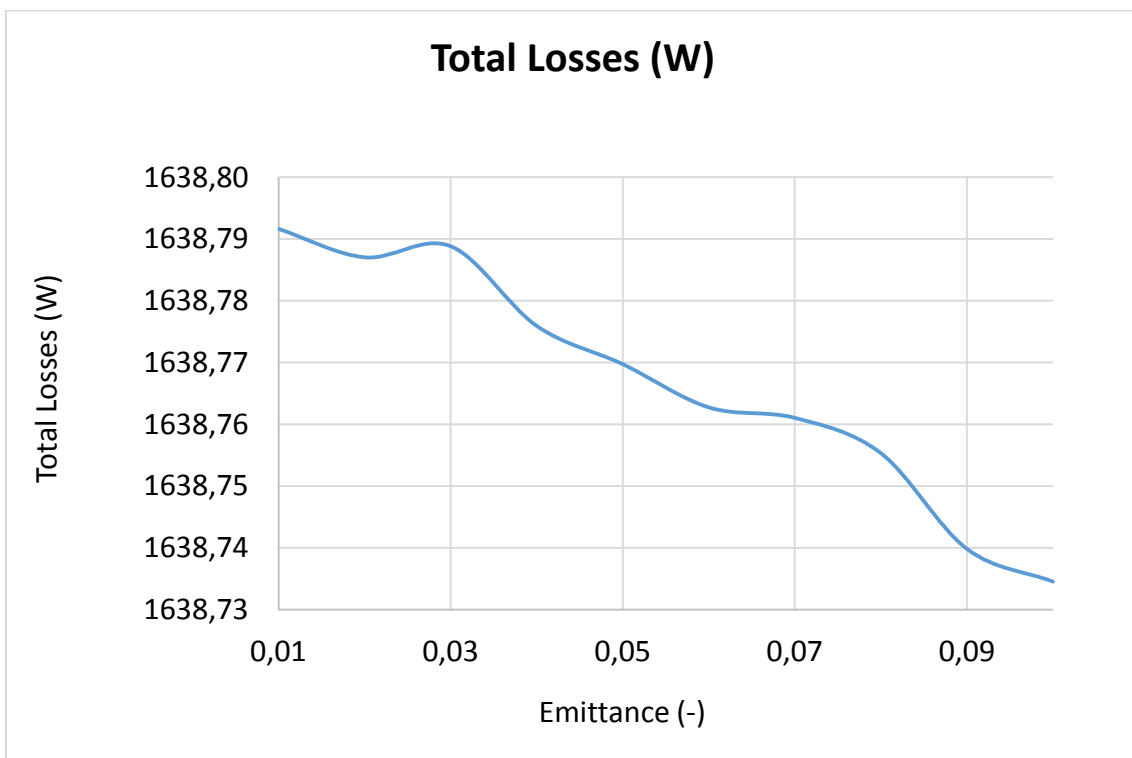
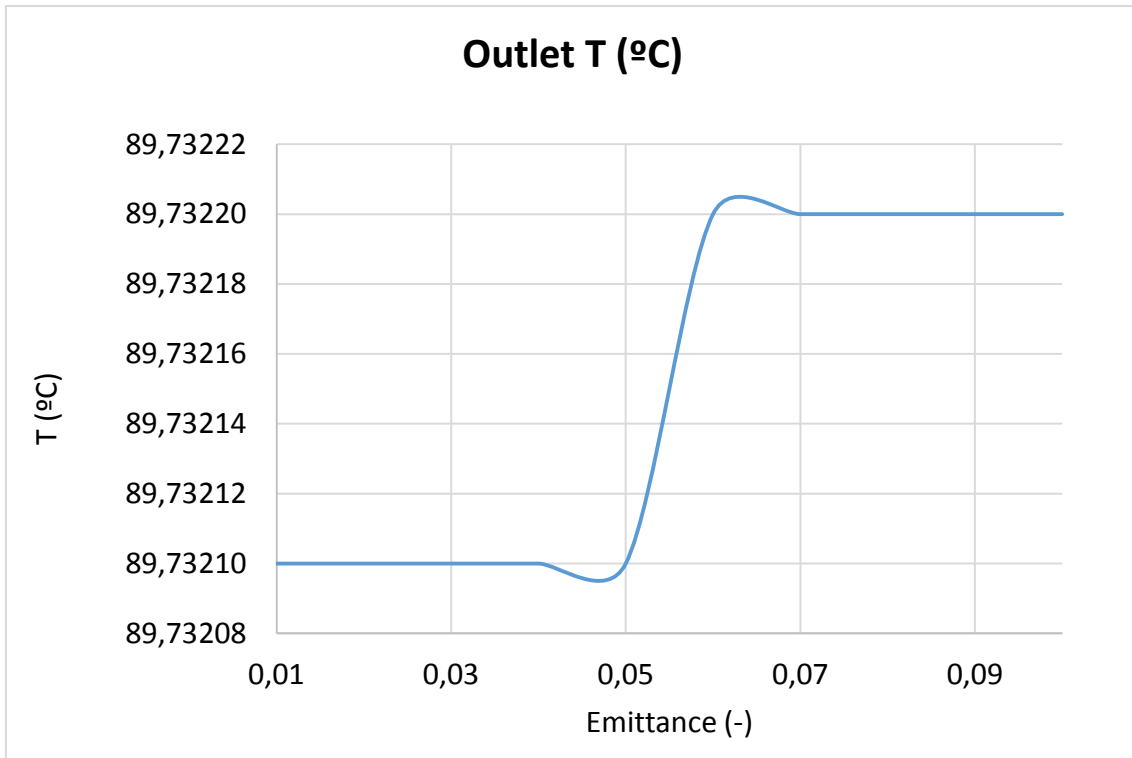


Figure-A 47. Graphs of the results for the heat losses test at 40°C for different values of shield's emittance.

- When the HTF's inlet temperature is 90°C:

Table A 47. Results from the heat losses test at 90°C for different values of shield's emittance.

Test	Glass emittance (-)	Outlet T (°C)	Total Losses (W)	Enthalpy difference (W)
1	0,03	89,73	1638,78	1656,12
2	0,01	89,73	1638,79	1656,12
3	0,02	89,73	1638,79	1656,12
4	0,03	89,73	1638,79	1656,12
5	0,04	89,73	1638,78	1656,12
6	0,05	89,73	1638,77	1656,12
7	0,06	89,73	1638,76	1656,12
8	0,07	89,73	1638,76	1656,12
9	0,08	89,73	1638,76	1656,12
10	0,09	89,73	1638,74	1656,12
11	0,1	89,73	1638,73	1656,12



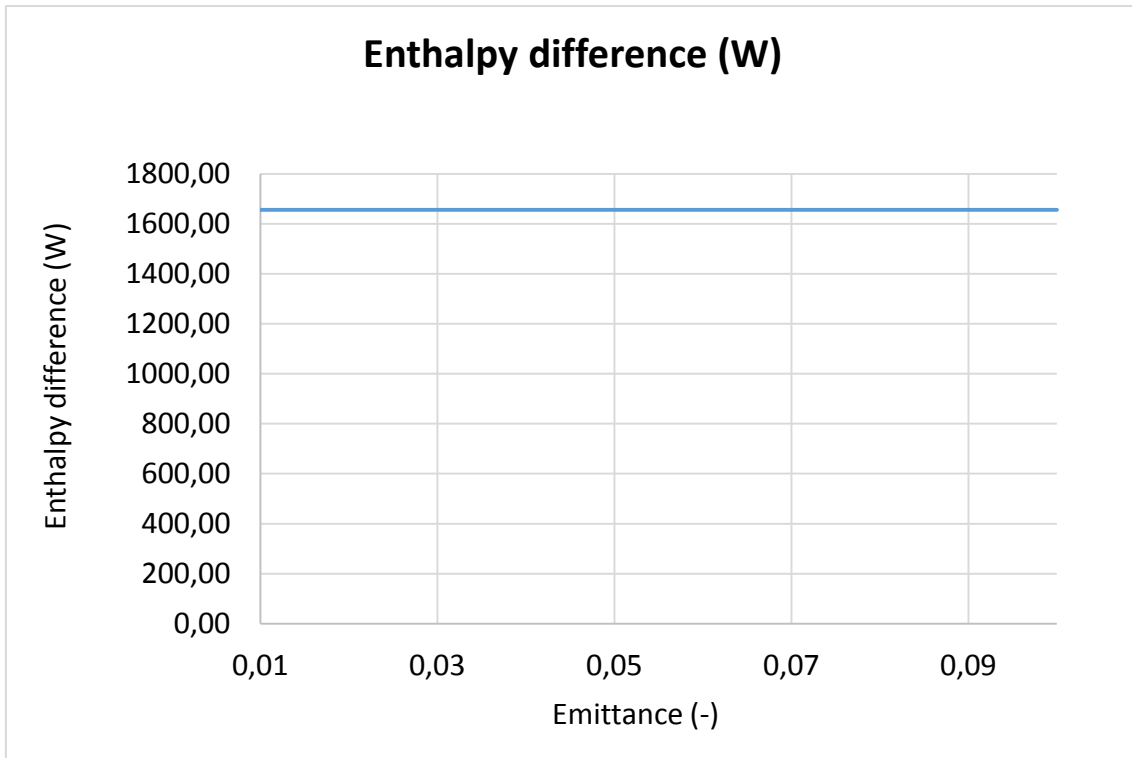
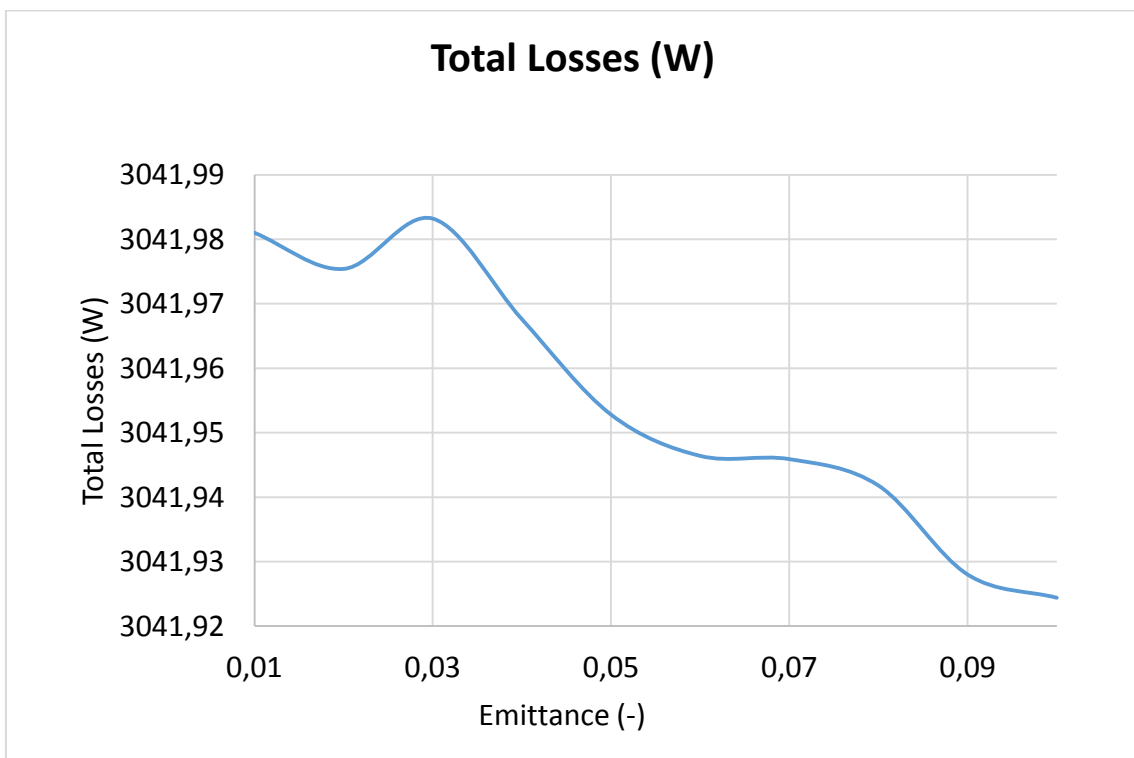
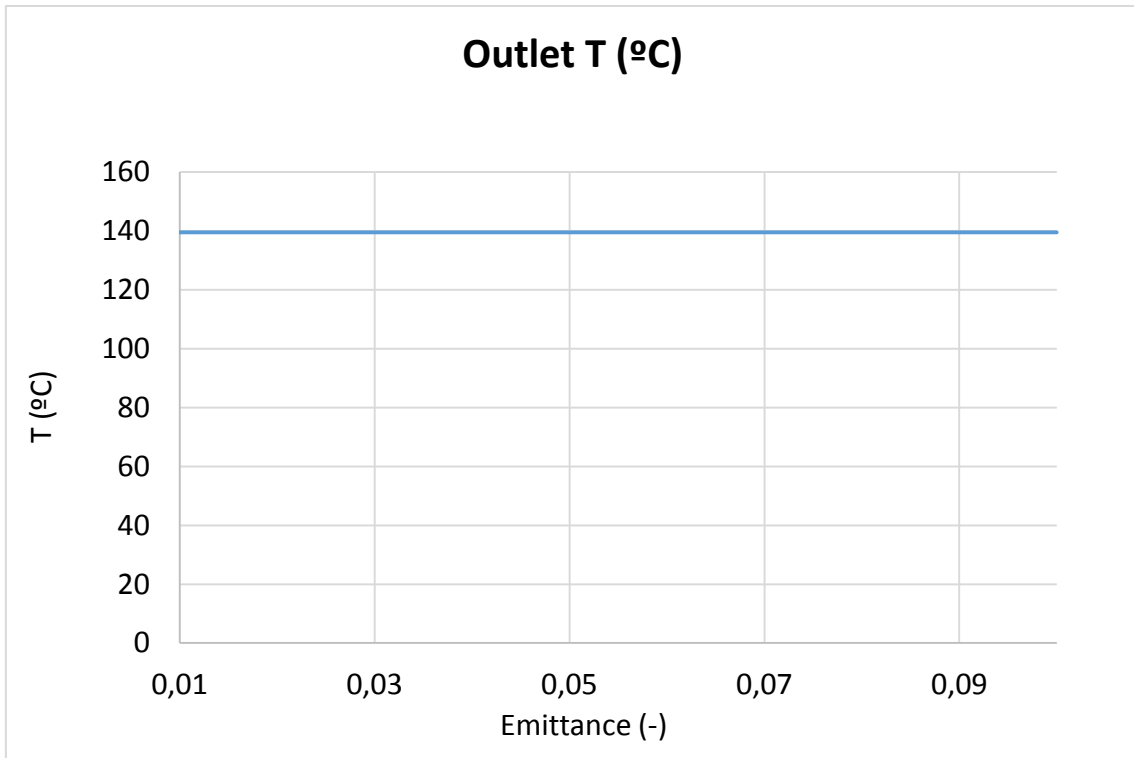


Figure-A 48. Graphs of the results for the heat losses test at 90°C for different values of shield's emittance.

- When the HTF's inlet temperature is 140°C:

Table A 48. Results from the heat losses test at 140°C for different values of shield's emittance.

Test	Glass emittance (-)	Outlet T (°C)	Total Losses (W)	Enthalpy difference (W)
1	0,03	139,53	3041,97	3079,75
2	0,01	139,53	3041,98	3079,75
3	0,02	139,53	3041,98	3079,75
4	0,03	139,53	3041,98	3079,75
5	0,04	139,53	3041,97	3079,75
6	0,05	139,53	3041,95	3079,75
7	0,06	139,53	3041,95	3079,75
8	0,07	139,53	3041,95	3079,75
9	0,08	139,53	3041,94	3079,75
10	0,09	139,53	3041,93	3079,75
11	0,1	139,53	3041,92	3079,75



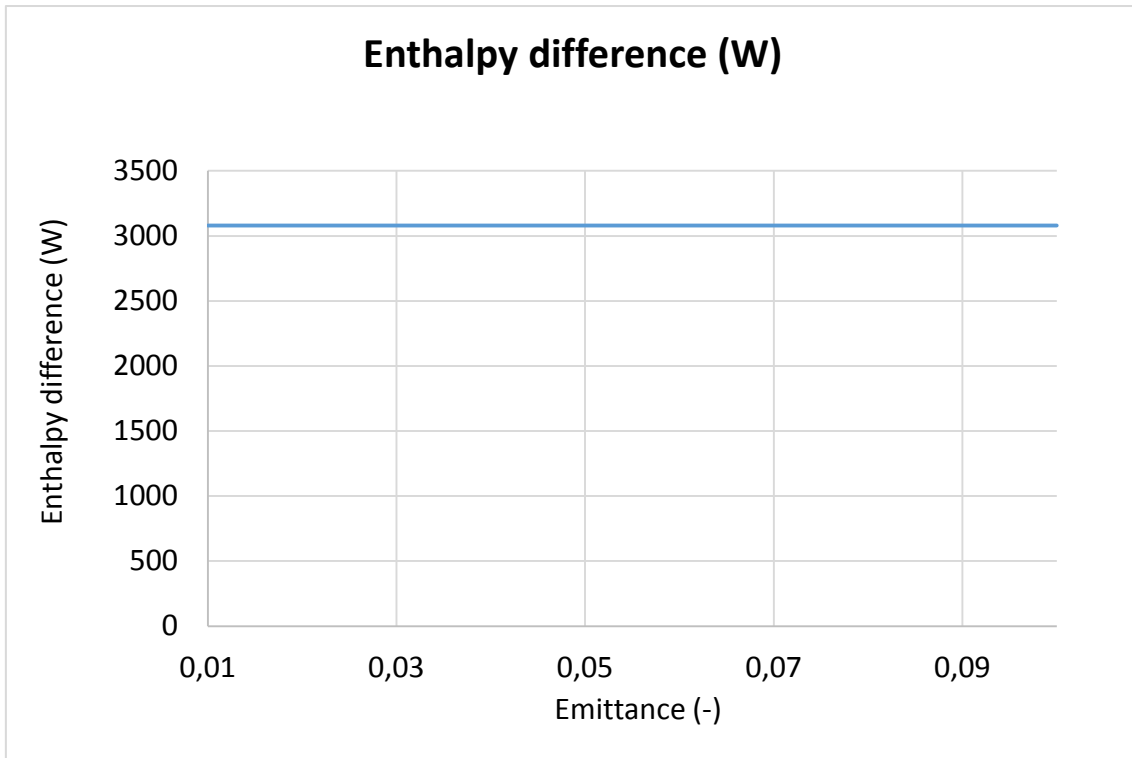
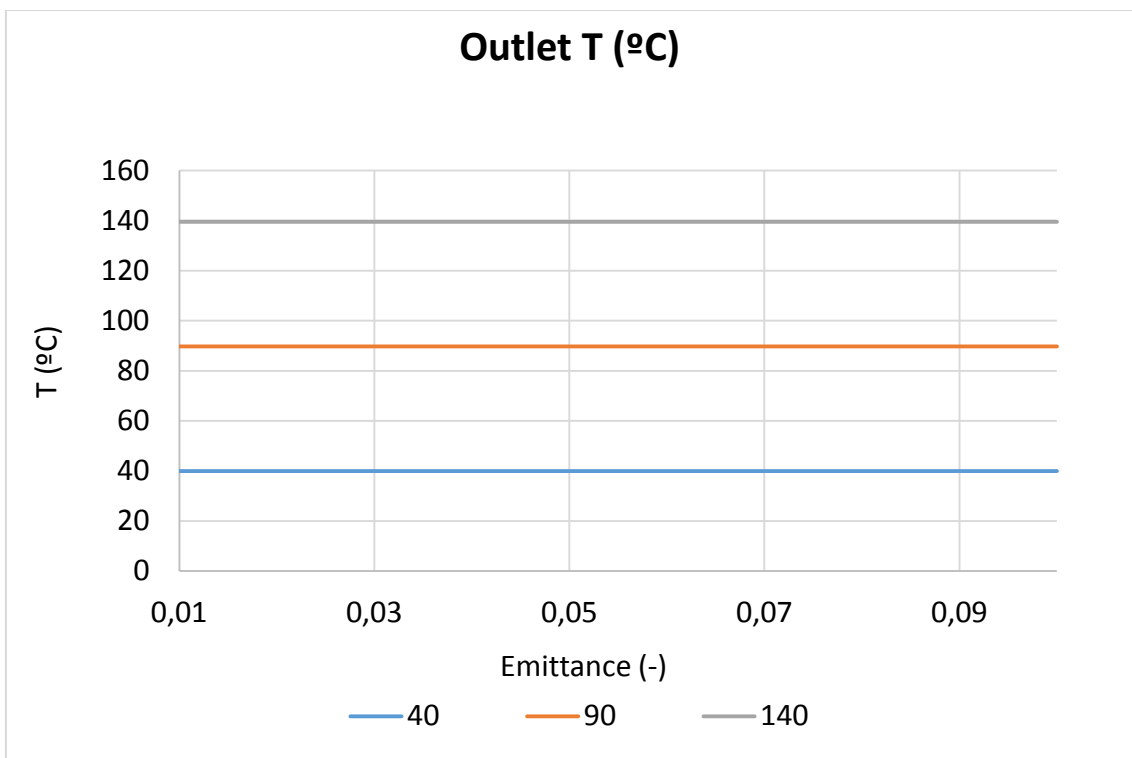


Figure-A 49. Graphs of the results for the heat losses test at 140°C for different values of shield's emittance.

- Comparing the three cases:



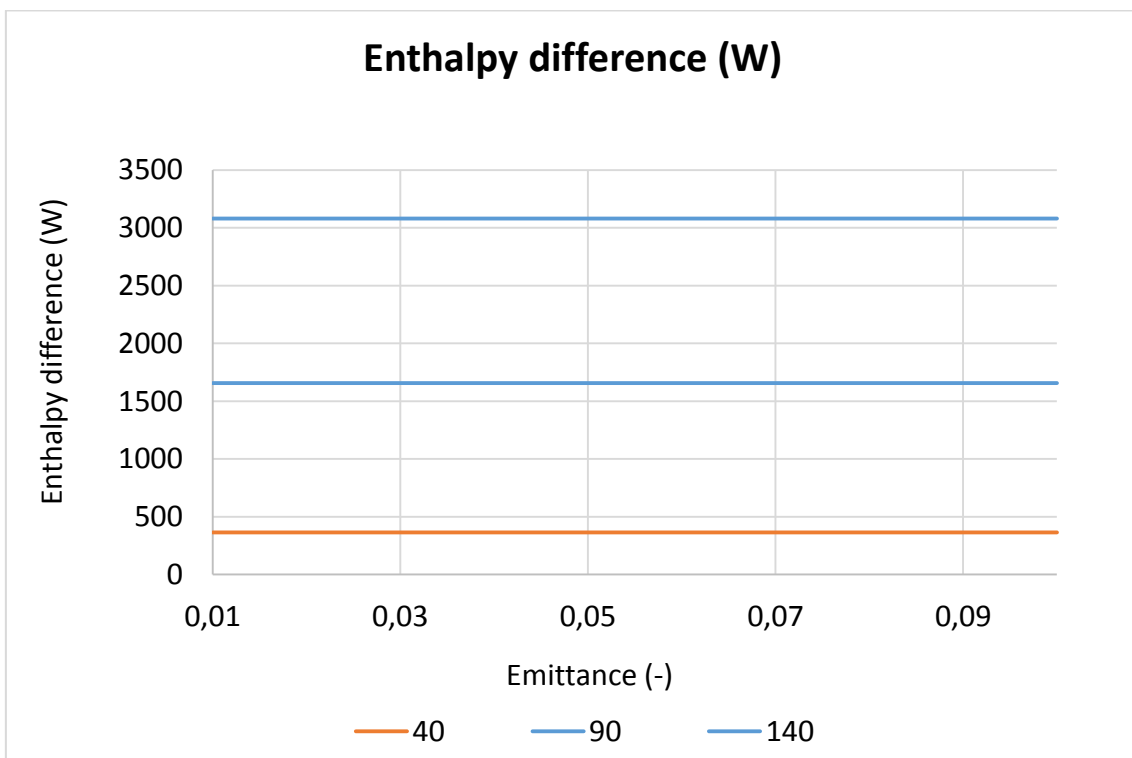
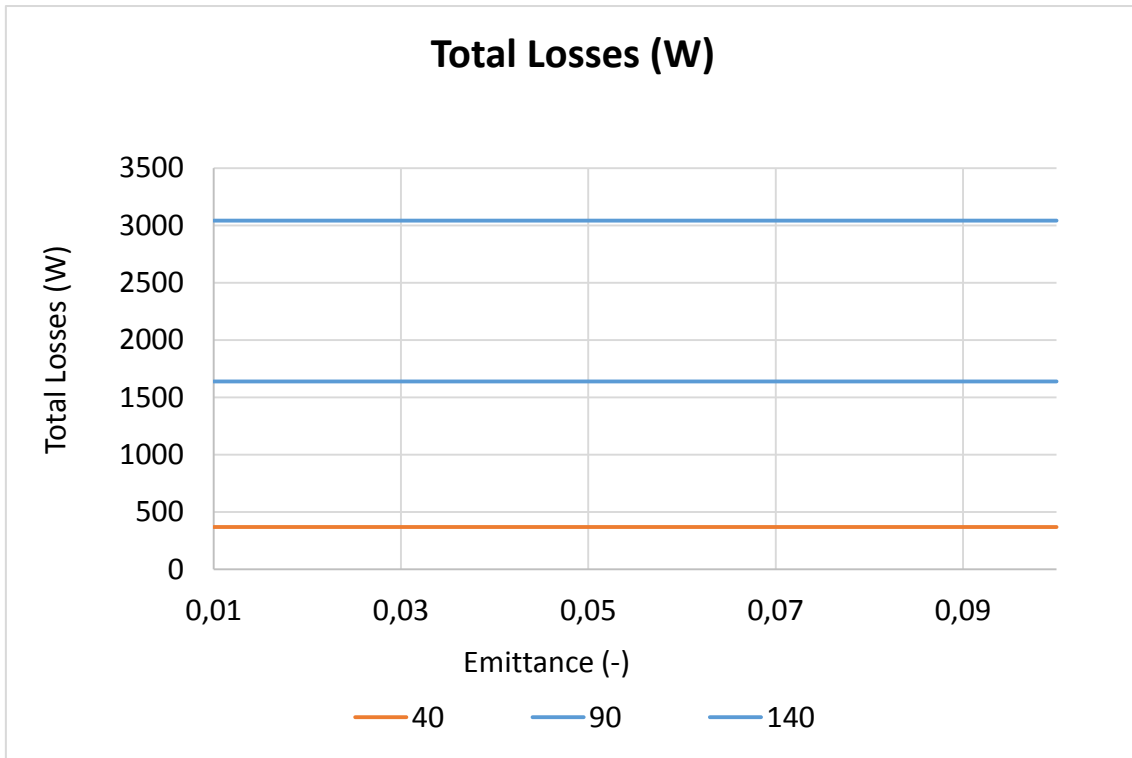
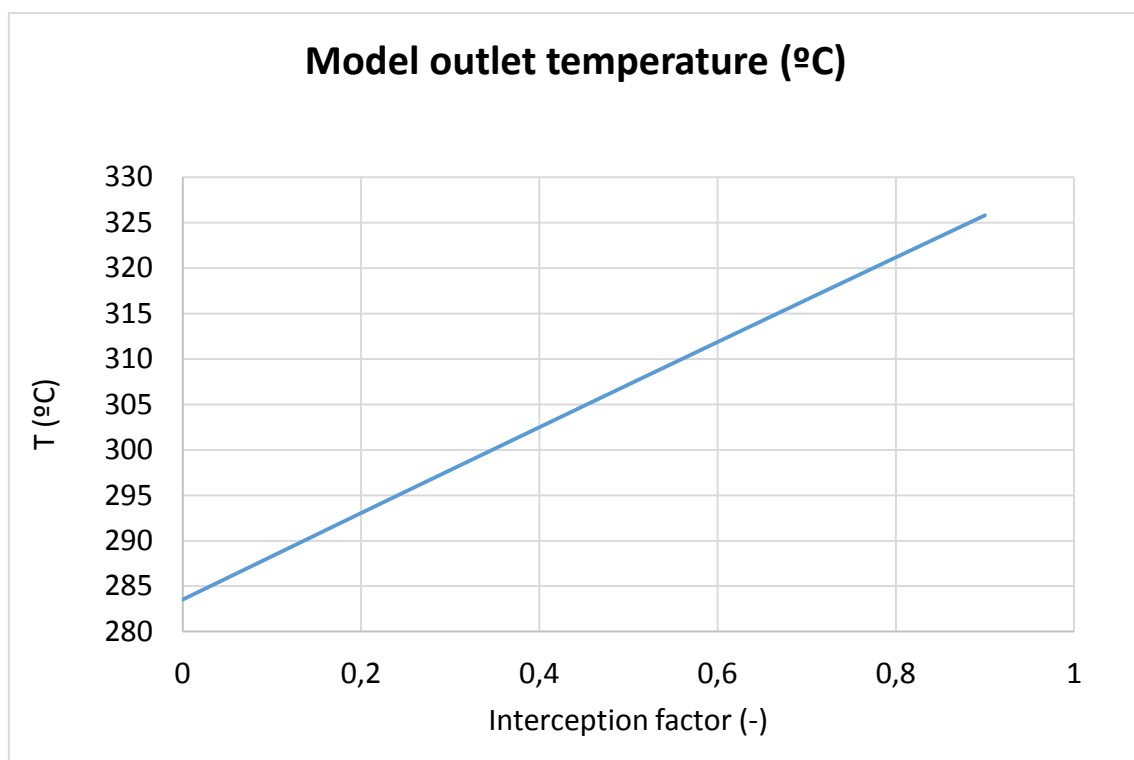


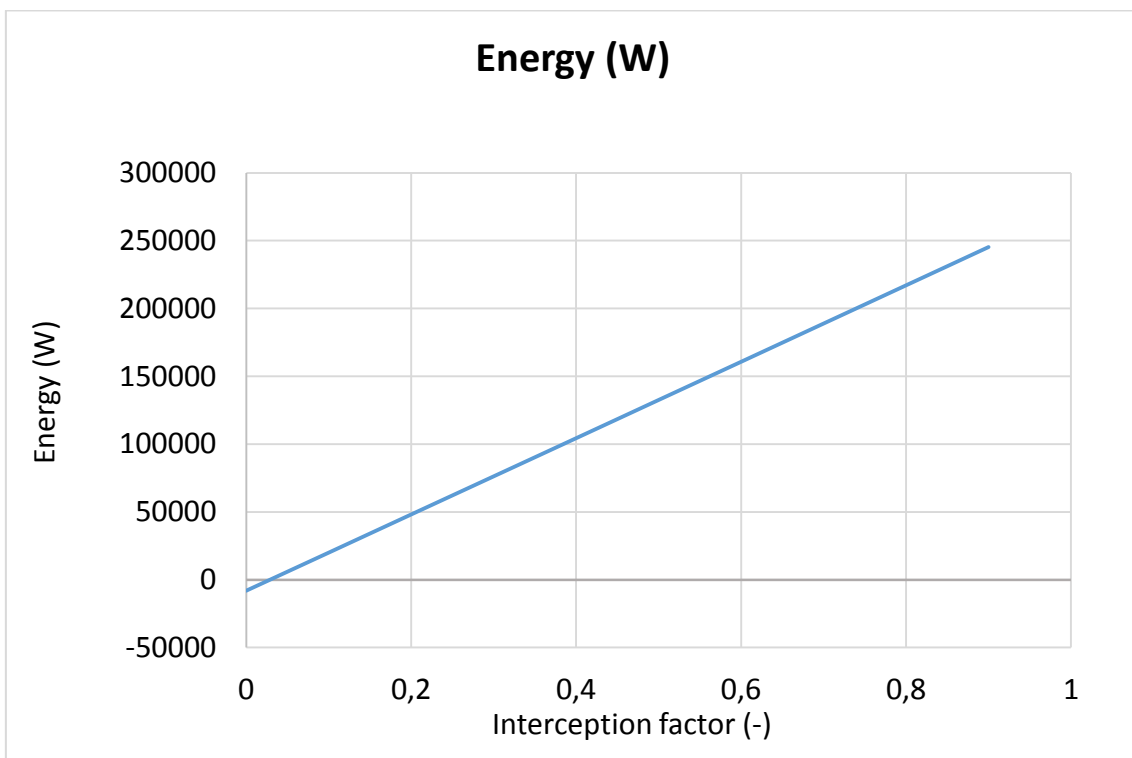
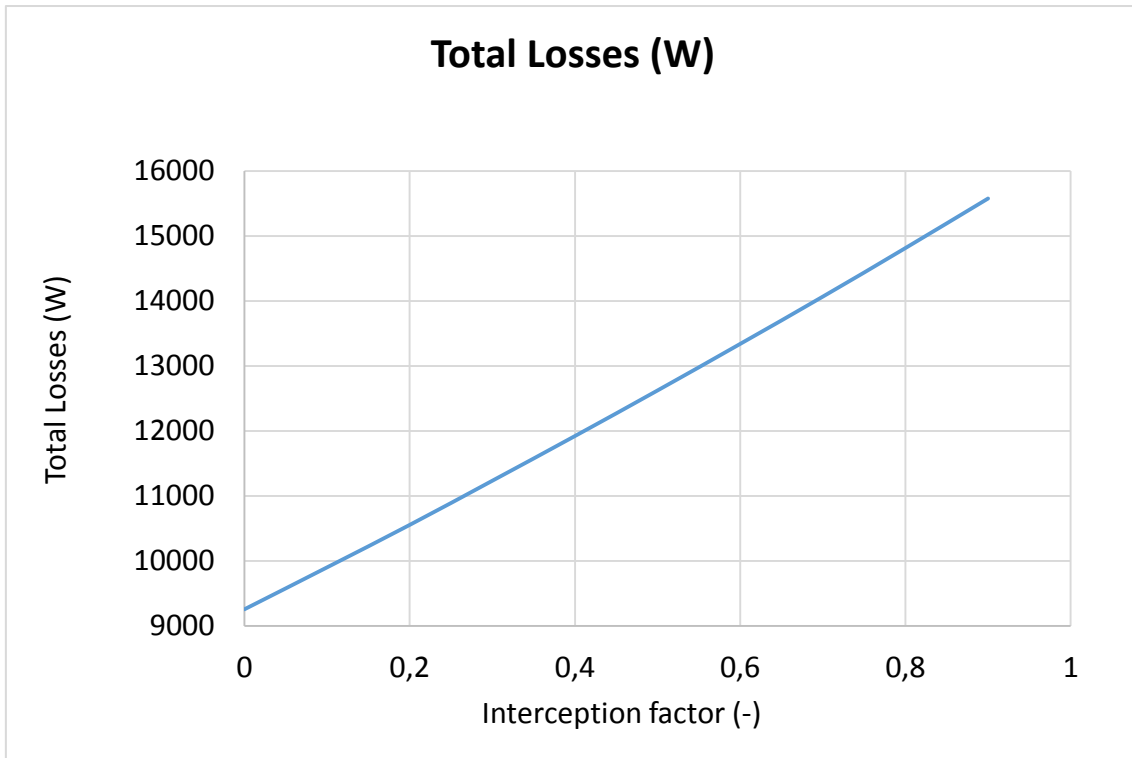
Figure-A 50. Graphs of the results for the heat losses test for different values of shield's emittance.

Interception factor

Table A 49. Results for the dynamic efficiency test when the interception factor of the collector varies from 0 to 1.

Test	Incidence angle (°)	Interception Factor (-)	Model outlet temperature (°C)	Total Losses (W)	Energy (W)	Useful Solar Radiant Power (W)	Model efficiency (%)
1	16,372	1	330,42	16357,62	273524,09	370869,74	73,75%
2	16,372	0	283,52	9255,13	-8107,98	370869,74	-2,19%
3	16,372	0,1	288,29	9900,73	19976,37	370869,74	5,39%
4	16,372	0,2	293,04	10554,26	48129,50	370869,74	12,98%
5	16,372	0,3	297,77	11234,26	76229,81	370869,74	20,55%
6	16,372	0,4	302,48	11922,38	104362,82	370869,74	28,14%
7	16,372	0,5	307,18	12624,42	132551,10	370869,74	35,74%
8	16,372	0,6	311,86	13340,77	160707,52	370869,74	43,33%
9	16,372	0,7	316,53	14068,65	188905,69	370869,74	50,94%
10	16,372	0,8	321,18	14816,17	217096,32	370869,74	58,54%
11	16,372	0,9	325,81	15579,11	245306,55	370869,74	66,14%





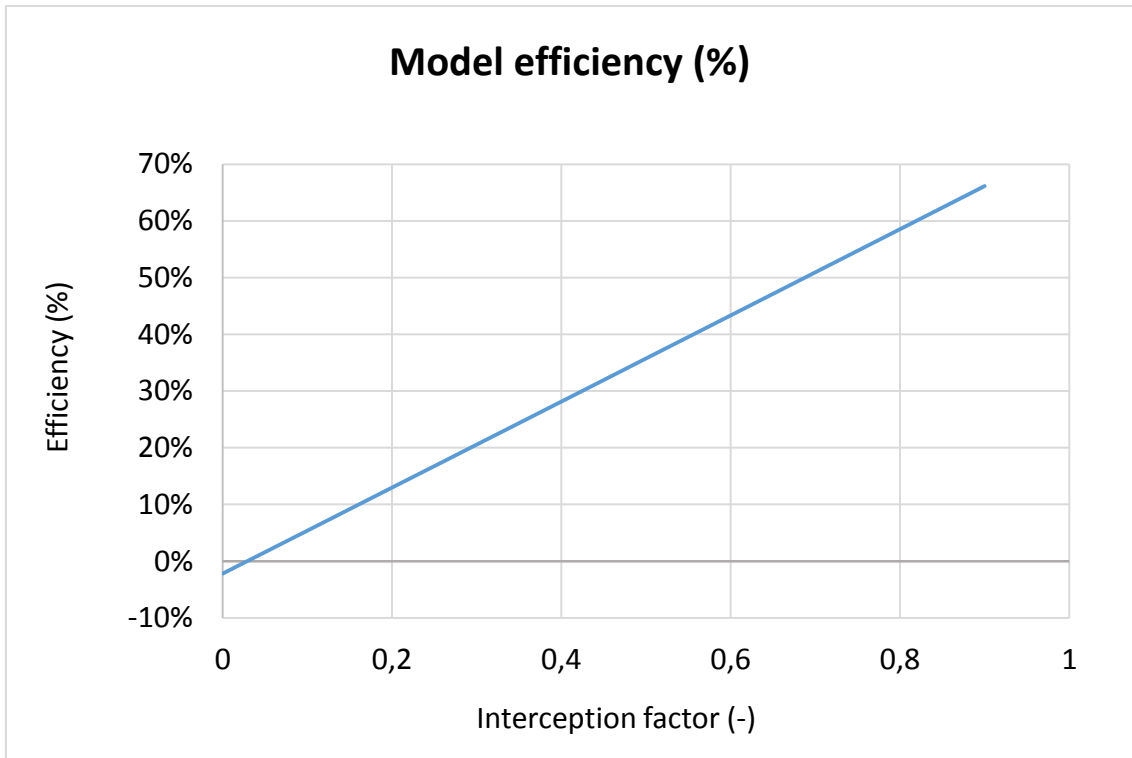
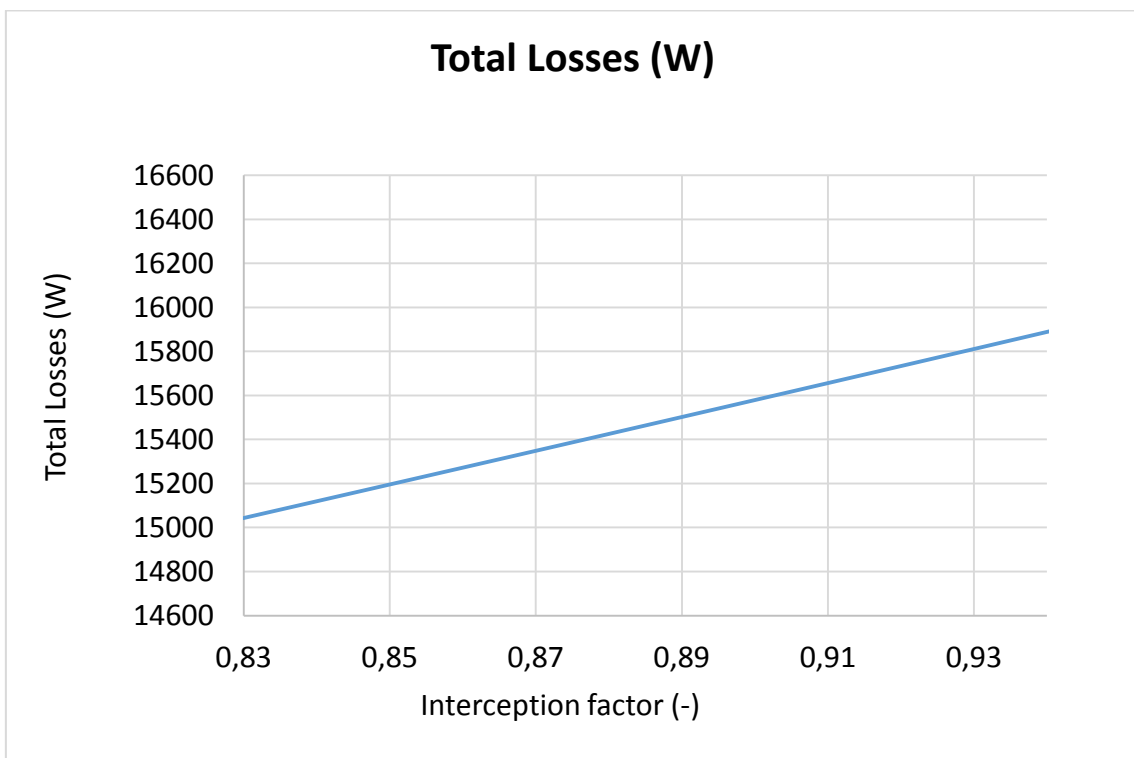
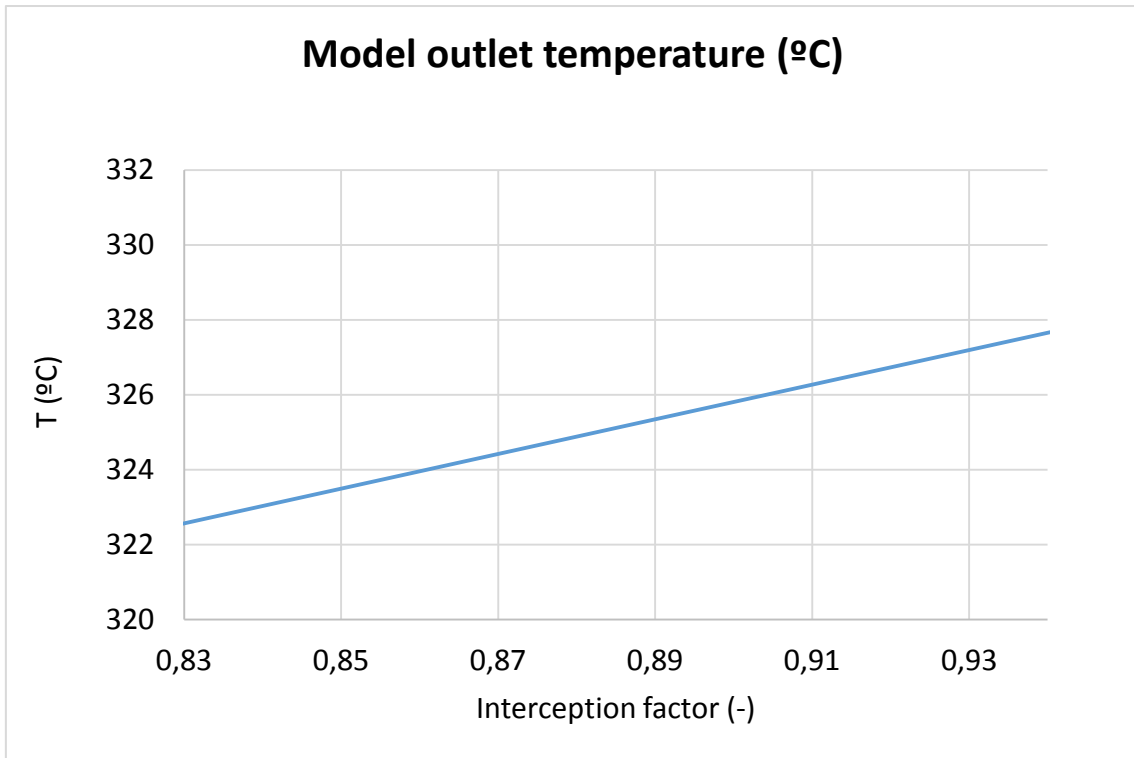


Figure-A 51. Graphs of the results for the dynamic efficiency test when the interception factor of the collector varies from 0 to 1.

Table A 50. Results for the dynamic efficiency test when the interception factor of the collector varies from 0,8 to 1.

Test	Incidence angle (°)	Interception Factor (-)	Model outlet temperature (°C)	Total Losses (W)	Energy (W)	Useful Solar Radiant Power (W)	Model efficiency (%)
1	16,37	1	330,42	16357,62	273524,09	370869,74	73,75%
2	16,37	0,8	321,18	14816,17	217096,32	370869,74	58,54%
3	16,37	0,82	322,10	14967,53	222737,46	370869,74	60,06%
4	16,37	0,84	323,03	15119,49	228379,01	370869,74	61,58%
5	16,37	0,86	323,96	15272,08	234021,05	370869,74	63,10%
6	16,37	0,88	324,88	15425,28	239663,57	370869,74	64,62%
7	16,37	0,9	325,81	15579,11	245306,55	370869,74	66,14%
8	16,37	0,92	326,73	15733,57	250949,95	370869,74	67,67%
9	16,37	0,94	327,66	15888,64	256593,94	370869,74	69,19%
10	16,37	0,96	328,58	16044,34	262238,09	370869,74	70,71%
11	16,37	0,98	329,50	16200,66	267878,88	370869,74	72,23%



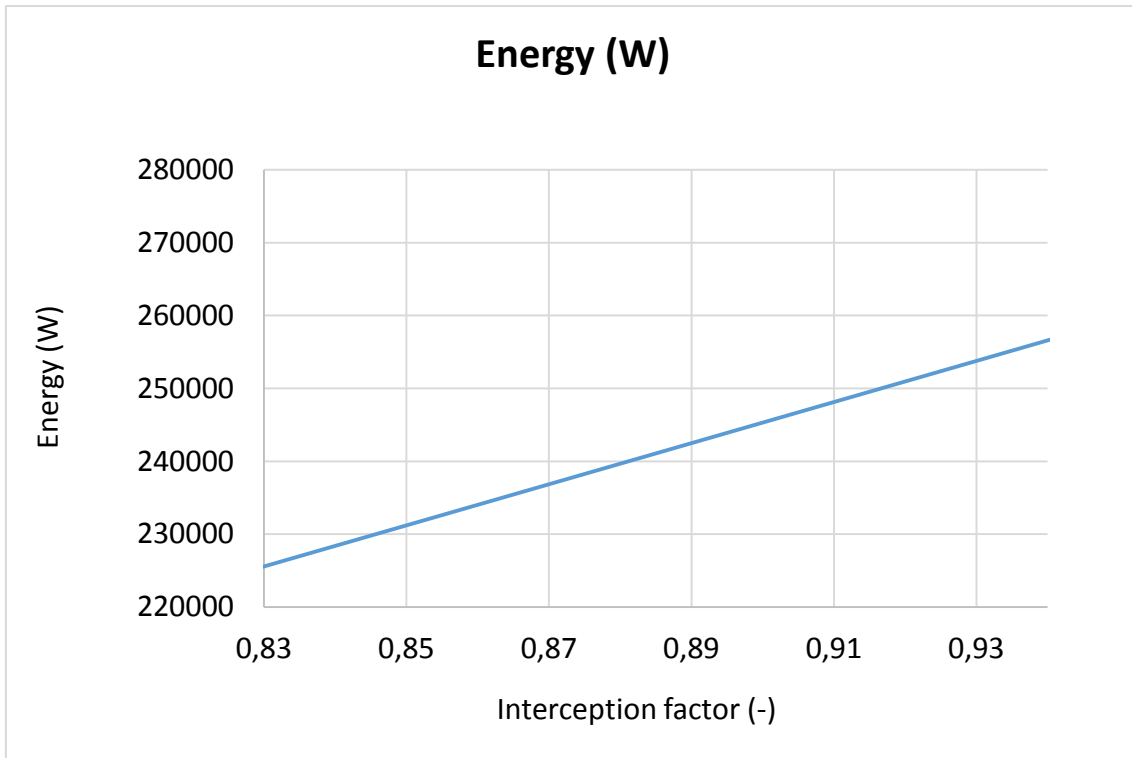
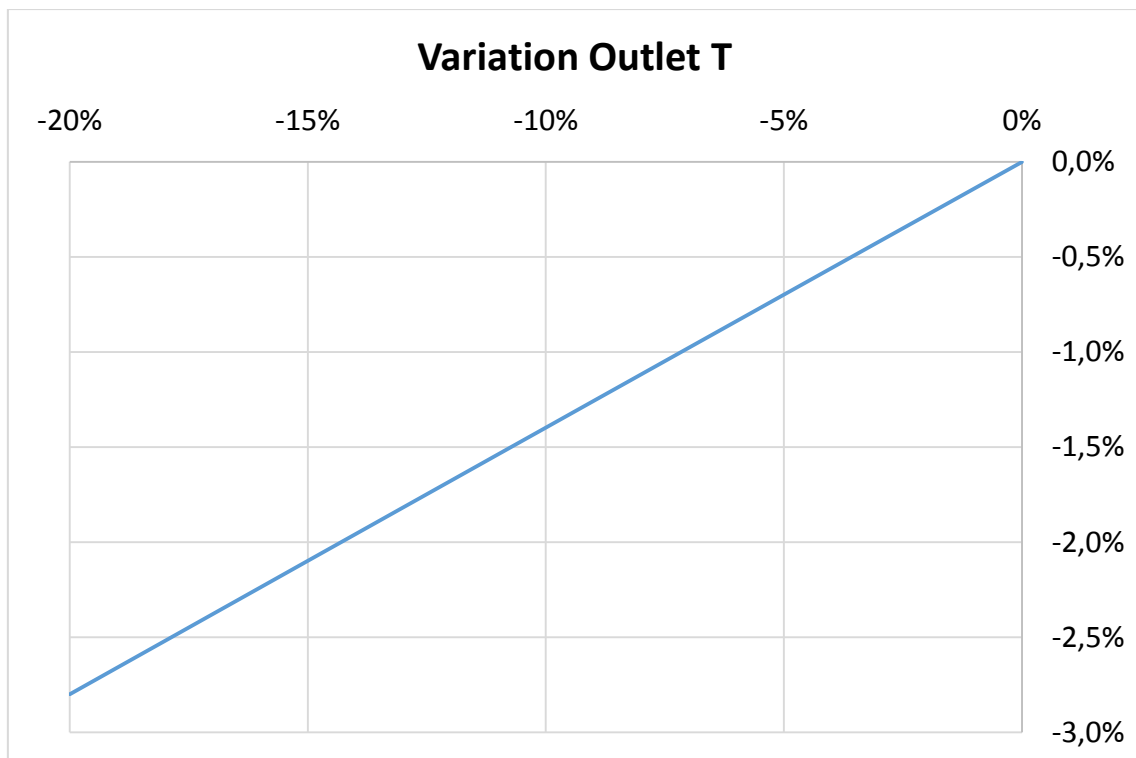
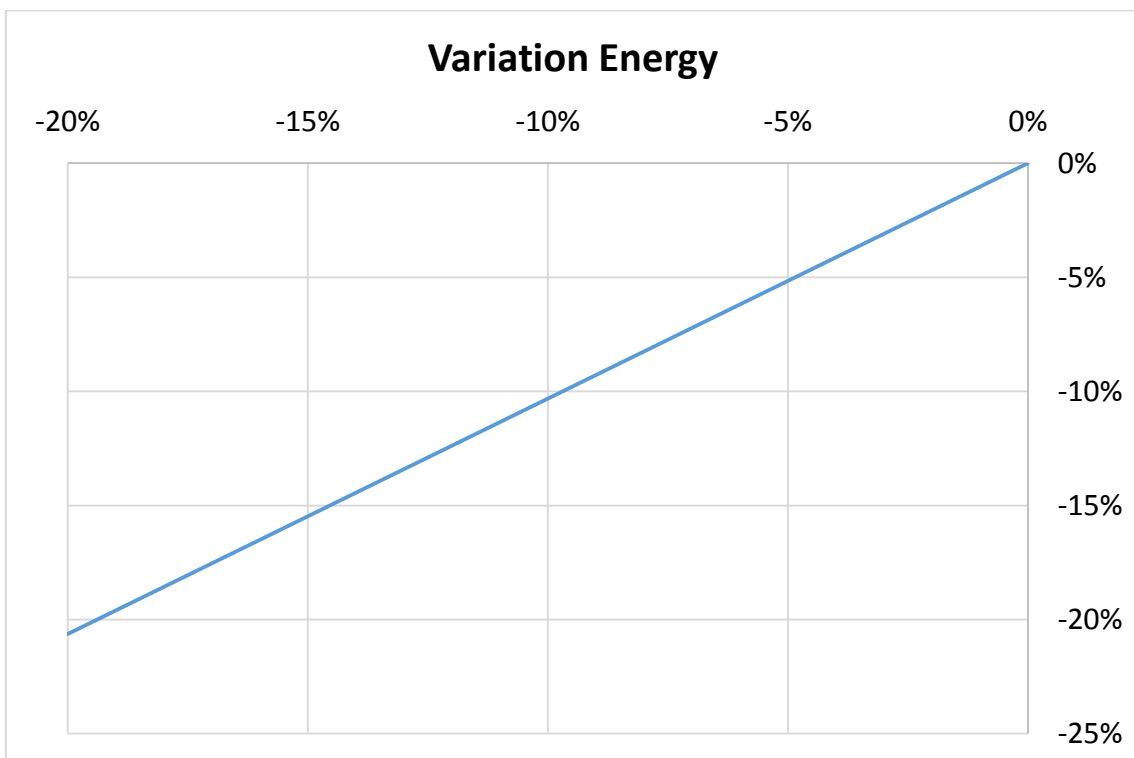
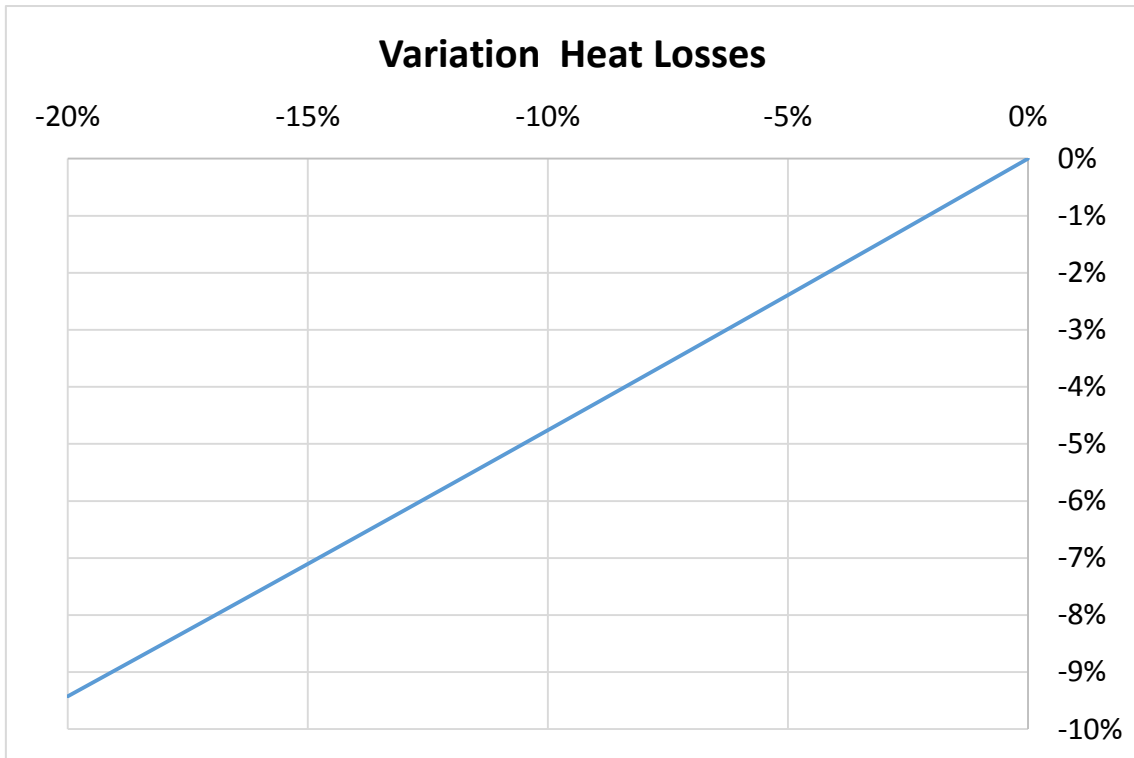


Figure-A 52. Graphs of the results for the dynamic efficiency test when the interception factor of the collector varies from 0,8 to 1.

Table A 51. Results from the dynamic efficiency test expressed in percentages when the interception factor of the collector varies from 0,8 to 1.

Variation Interception factor	Variation Outlet T	Variation Heat Losses	Variation Energy	Variation Efficiency
0,00%	0,00%	0,00%	0,00%	0,00%
-20,00%	-2,80%	-9,42%	-20,63%	-20,63%
-18,00%	-2,52%	-8,50%	-18,57%	-18,57%
-16,00%	-2,24%	-7,57%	-16,50%	-16,50%
-14,00%	-1,96%	-6,64%	-14,44%	-14,44%
-12,00%	-1,68%	-5,70%	-12,38%	-12,38%
-10,00%	-1,40%	-4,76%	-10,32%	-10,32%
-8,00%	-1,12%	-3,82%	-8,25%	-8,25%
-6,00%	-0,84%	-2,87%	-6,19%	-6,19%
-4,00%	-0,56%	-1,92%	-4,13%	-4,13%
-2,00%	-0,28%	-0,96%	-2,06%	-2,06%





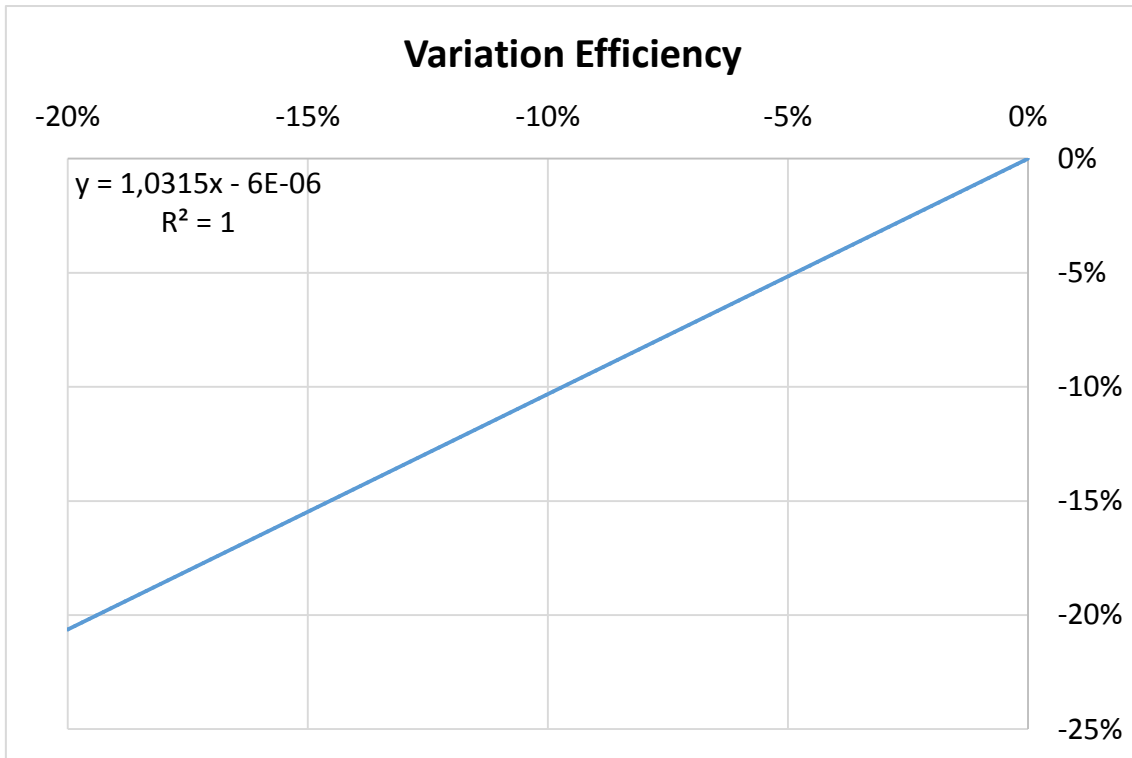


Figure-A 53. Graphs of the results for the dynamic efficiency test expressed in percentages when the interception factor of the collector varies from 0,8 to 1.